UNIVERSITÀ DELLA CALABRIA

UNIVERSITA' DELLA CALABRIA

Dipartimento di Ingegneria Civile

Dottorato di Ricerca in

Ingegneria Civile e Industriale

CICLO

XXXII

NEW ONE-LINE MODEL FOR SHORELINE EVOLUTION AT BEACHES COMPOSED OF NOT COHESIVE GRAINS OF ANY SIZE

Settore Scientifico Disciplinare ICAR/02

Coordinatore: Ch.mo Prof. Ing. Franco FURGIUELE

Supervisori/Tutors: Ch.mo Prof. Ing. Giuseppe Roberto TOMASICCHIO

Ch.mo Prof. Ing. Ferdinando FREGA

Dottorando: Ing. Antonio Francone

PREFACE

The present thesis is submitted as part of the requirements for obtaining a Ph.D. degree from the University of Calabria. The study has been conducted at the University of Calabria, Department of Civil Engineering, under supervision of Prof. Giuseppe Roberto Tomasicchio and Prof. Ferdinando Frega. Ph.D. grant of 3 years has been financed by Regione Calabria.

ABSTRACT

Over recent decades, efforts have been made to find robust methods for predicting shoreline evolution near to the coastal structures. This requires a rigorous understanding of the key coastal processes that drive sediment transport, and how they are impacted by the presence of structures. Once this understanding is reached, a method for predicting morphological shoreline evolution is required. In this context, numerical modelling plays an important role.

A new one-line model for shoreline evolution at beaches composed of not cohesive grains of any size is proposed: the General Shoreline beach (GSb). GSb model is based on the one-line theory, for which it is assumed that the equilibrium beach profile remains unchanged (Dean, 1990), thereby allowing beach change to be described uniquely in terms of the shoreline position. The longshore sediment transport rate is estimated by means of a general formula/procedure (Tomasicchio et al., 1994; Lamberti and Tomasicchio, 1997; Tomasicchio et al., 2013; Tomasicchio et al., 2015) combining an energy flux approach with an empirical/statistical relationship between the wave-induced forcing and the number of moving units.

The uniqueness of the proposed new one-line model consists in the possibility to simulate beach change, including the effects of coastal structures (i.e. groynes, detached breakwaters), at a mound composed of not cohesive grains of any size, from sand to rock units.

Despite other existing models, the GSb model presents a calibration factor, K_{GSb} solely and it has been calibrated and verified against field and laboratory data on sandy and mixed beach (sand and gravel) referring to simple groyne and detached breakwater (Ming and Chiew, 2000; Hamilton et al., 2001; Martin-Grandes et al., 2009; Medellin et al., 2018;). Optimal values of K_{GSb}, valid for different types of not cohesive grains and coastal structures, have been reported.

It is showed that the GSb model can be considered a reliable engineering tool to conduct morphodynamics studies. A demo version of the GSb model, for Mac and Windows systems, has been released for the scientific community and is available at www.scacr.eu.

AKNOWLEDGMENTS

I am grateful to my supervisor Prof. Giuseppe Roberto Tomasicchio for his encouragement, precious ideas, recommendations and patience during my research activities. I would also like to express my sincere gratitude to my co-supervisor Professor Ferdinando Frega for his help and good suggestions.

Many thanks to Felice D'Alessandro and Samuele De Bartolo for their precious advices and continuous encouragements.

I would like to gratefully thank to David Simmonds for providing me the placement opportunity at the University of Plymouth, where I have benefited from the experience of many experts of the COAST group. Thanks also for providing me the data of the field experiment conducted at Milford on Sea. I also would like to gratefully thank Professor Alessandro Antonini (TUD, Netherlands) for his support and hospitality received before and during my period at Plymouth.

Thanks to Alec Torres-Freyermuth and Gabriela Medellín for providing me the data of the field experiment conducted at Sisal (Mexico).

I am appreciative to my friends from University of Calabria and EUMER Lab, thanks for accompanying me in this experience.

Thanks to my family, my girlfriend, and all friends that have provided encouragement during these three years. My sacrifices and goals are for you.

Table of Contents

1 INTRODUCTION

1.1 Background

Presently, more than 200 million people worldwide live in the low-elevation coastal zone (at less than 5 m elevations from the sea). More than 37 million people and 19 million homes have been added to coastal areas during the last three decades (NOOA, 2017). 180 million people visit the coast each year (Field et al., 2001). As a result, the coastal zone has become an attractive place with social, political and economic interest. In many nations, where tourism is central to the economy, coasts offer recreational activities attracting tourist. However, the rapid development and use of the coastal zone causes adverse effects on the beach equilibrium leading to severe erosion and sometimes consequently beach disappearance.

Coastal erosion may be caused by the variations in sediment transport due to natural and anthropogenic factors. Due to the complicated behaviour of the coast, the beach morphodynamics cannot be described by simple formulae. The evaluation of coastline change represents a fundamental aspect for sustainable management of coastal zones, and accurate design of coastal protection measures must be performed. The choice of a measure for the coastal protection is not immediate: hard measures (i.e. groynes, detached breakwaters, submerged breakwaters, jetties, seawalls) or soft measures (i.e. beach nourishment) can be applied.

Over many decades, researchers and engineers inspired by coastal sediment phenomena have conducted field and laboratory experiments to learn more about coastal processes and sediment dynamics. Their efforts have resulted in a wealth of papers and documents published in journals, conference and symposium proceedings over the last 50 years (Van Rijn et al., 2013). The understanding of the physical processes governing the morphodynamic and the rapid advance in computation technology have increased the interest in developing numerical models. Sophisticated models to reproduce the coastline evolution were developed. Given the complexity of the processes, which cannot be fully represented by deterministic formulae, and the high uncertainty in wave and sediment transport data (Kamphuis, 1999), numerous runs are necessary for sensitivity analysis and model calibration making prohibitive the practical use of such sophisticated models (Dabees, 2000). In this context, one-line models demonstrated practical capability in predicting coastline change, and to assist in the selection of the most appropriate protection design in the planning of projects located in the nearshore zone (Guner

et al., 2011). However, no one-line model suitable for estimation of coastline change for various type of coastal mound (e.g. sandy, gravel, cobble, mixed beaches, etc.) is available.

1.2 Aim of the thesis

The aim of the present thesis is to develop and propose a novel morphodynamic model to simulate shoreline evolution at sand, gravel, cobbles, shingle, and rock beaches under the spatial and temporal changes in longshore sediment transport: the General Shoreline beach (GSb).

The thesis work proves the model to simulate shoreline change, including the influence of coastal structures (i.e. groynes, detached breakwaters). In particular, it is showed that simulations can be performed for wide spatial extents and short and long-time intervals (from 1 hour till years).

1.3 Thesis structure

The present thesis is composed of eight chapters, including the introduction and conclusions. The content of each chapter is described below.

Chapter 1 introduces the research topic and the aim of the present work.

Chapter 2 provides, after a brief introduction of the coastal environment, an overview of the shoreline detection methods and the causes producing the shoreline changes. The main characteristics of the sediment composing the coasts are presented with particular attention to the mechanism governing the transport of sediments in both longshore and cross-shore direction. A general review of the relationships for the computation of the longshore and cross-shore sediment transport is presented. The concept of equilibrium beach profile is introduced and discussed.

Chapter 3 presents a review of the mathematical models for coastline evolution. The conceptual model and formulations of the three main categories of numerical beach modelling are discussed: planform (one-line and multi-line models), beach profile and three-dimensional modelling. The numerical methods to solve the model equations of the planform and beach profile models are presented.

Chapter 4 describes the most popular one-line models for the prediction of the long-term coastline changes. The differences and similarities between them are discussed.

Chapter 5 introduces the main assumptions of the proposed numerical model, General Shoreline beach (GSb). The fundamental equations of the GSb model, the longshore sediment formula used to compute the sediment transport rate, the calculation of the wave characteristics,

the equilibrium beach profile, the boundary conditions, and the permeability of the structures are described.

Chapter 6 presents the sensitivity analysis of the proposed numerical model, GSb, performed by the analysis of the coastline change in presence of single groyne and detached breakwater varying: the offshore wave direction, the boundary conditions, the grains size, the permeability factor, and the calibration parameter. Simulations of coastal change were also performed in case of multiple groynes and multiple detached breakwaters. The sensitivity of coastline response varying the GSb input parameters is discussed.

Chapter 7 presents the calibration and verification of the GSb model, performed against field and laboratory experiments. Numerical simulations are performed for different beach and coastal structures configurations (i.e., temporary groynes for sandy and mixed beaches, detached breakwaters).

Chapter 8 summarizes the conclusions of the present work.

2 LITERATURE REVIEW

2.1 Coastal zone

The coastal zone is the dynamic area between terrestrial and marine environments, modelled by a variety of marine processes. Figure 2.1 shows a coastal zone where four main areas are defined: backshore, foreshore, nearshore, and offshore. The backshore is the landward part of the shore modelled primarily from the aeolian processes. The foreshore is the seaward part of the shore, and it is comprised between the high-water elevation and the low-water elevation. The foreshore is the portion of the shore where wave-energy is dissipated on the land. The nearshore and offshore are seaward of the low-water line. The beach scarp is the upper portion of the foreshore normally exposed to wave uprush. The berm crest is the transition area between the foreshore and backshore. The nearly horizontal part is the berm, which forms from the deposition of lower-foreshore sediment that is transported over the berm crest (Dingler, 2005).

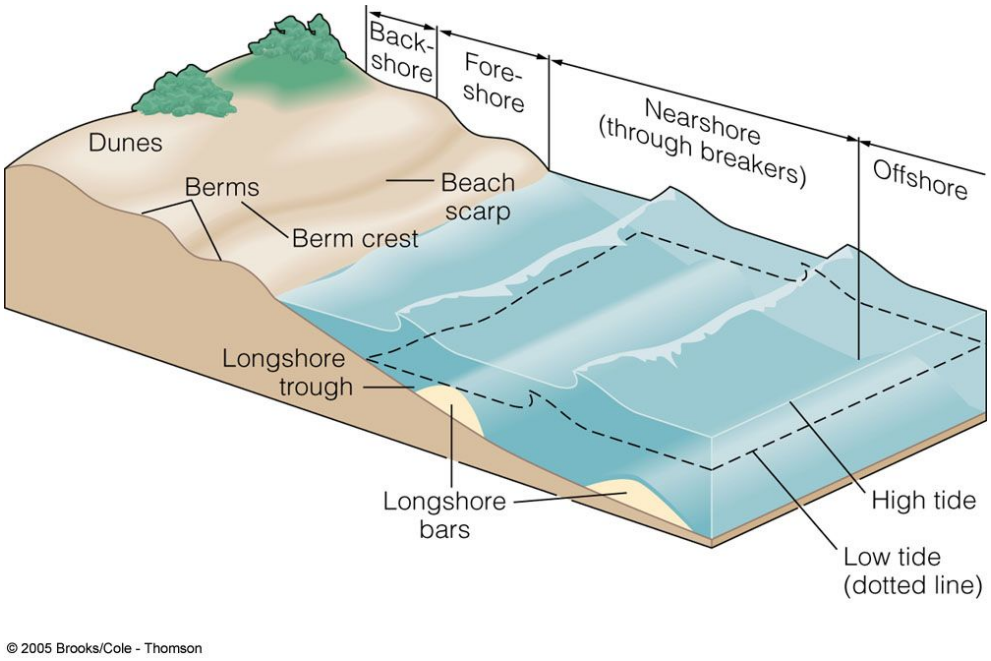

Figure 2.1 - Sketch of a typical coastal zone, terminology and zonation (http://ksuweb.kennesaw.edu/)

The foreshore is composed of two zones: a surf zone and a swash zone (Figure 2.2). The surf zone is the area where the waves approaching the coastline break dissipating most of the energy. The swash zone is the region where the beach is covered and uncovered by water with moves as water level vary, extending from the limits of run-up and run-down (CIRIA, 1996).

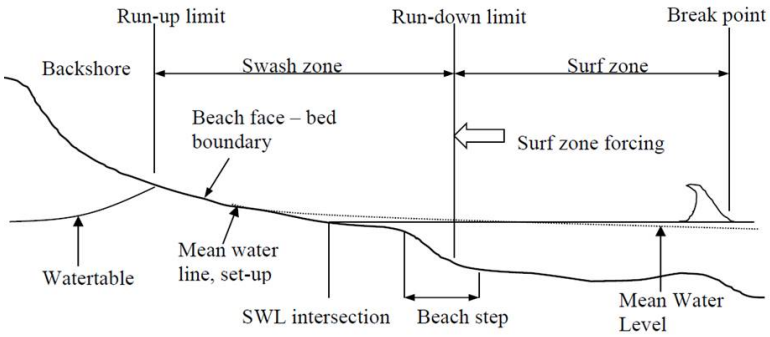

Figure 2.2 -Definition sketch of the nearshore littoral area (Elfrink and Baldock, 2002)

2.2 Shoreline detection

The study of coastal evolution represents one of the main activities in coastal engineering. A definition of the shoreline must be given in order to evaluate its evolution correctly. A shoreline is defined as the line of contact between the land and water (Dolan et al., 1980). Accurate monitoring of the shoreline evolution is necessary for understanding coastal processes (Natesan, 2009). The correct evaluation of shoreline change can be crucial for the coastal environment protection and design of coastal infrastructures (Trinder and Liu, 2018). The simple theoretical definition of the shoreline is not reflected in practice due to the coastal dynamics and the wide variety of indicators that can be based on geomorphologic aspect, tidal level, or in the configuration of the vegetation (Faye, 2010).

Various shoreline indicators are reported in different papers (Pajak and Leatherman, 2002; Leatherman, 2003; Ruggiero et al., 2003; Hess, 2003). The key shoreline indicators can be divided into two categories: the first one based on discernible coastal features and the second one based on a tidal datum. The first category of indicators is described in Boak and Turner (2005), where a study of the shoreline definitions with extensive references was performed. The most commonly used indicators are shown in (Figure 2.3).

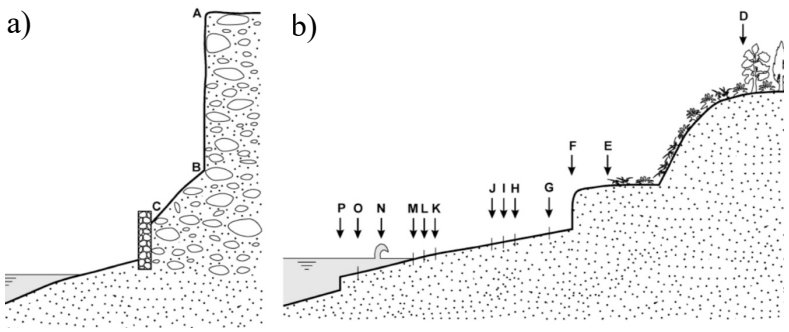

Figure 2.3 - Positions of the commonly used shoreline indicators (Boak and Turner, 2005)

Figure 2.3a shows the indicators:

A = cliff top;

B = base of cliff;

C = landward edge of shore protection structure.

Figure 3b shows the indicators:

D = seaward stable dune vegetation line;

E = seaward dune vegetation line;

F = erosion scarp;

G = storm line;

H = an old high tide water level;

I = previous high tide high water level;

J = mean high water level (datum referenced);

K = wet/ dry line or runup maxima;

L = groundwater exit point;

M = instantaneous water line;

N = shorebreak maximum intensity;

O = mean lower low water line (datum referenced);

P = beach toe or crest of beach step.

Figure 2.4 shows an example of visually discernible indicators identified on a beach sited at Duranbah Beach, New South Wales, Australia.

Figure 2.4 - Example of visibly discernible shoreline indicator features, Duranbah Beach, New South Wales, Australia. (Boak and Turner, 2005)

The National Ocean Service (NOS) defines a shoreline at the Mean High Water Line (MHWL), and MHWL is defined as a datum where the surface elevation is determined by averaging the heights of the water to equal interval of time, (Graham et al., 2003) usually hourly.

For the second category of shoreline indicators, based on a tidal datum, it is necessary to introduce the elevations of various tidal datums at control tide stations defined by the National Ocean Survey (NOS) based on 19 years of data. The 19-years period is known as a tidal epoch because it constitutes a full cycle of the tidal variations. The tidal datum is referred only at the location where the tidal information is obtained and cannot be extended into areas having different topographic features (Shalowitz, 1962; Maloney and Ausness, 1974).

Figure 2.5 shows the standard tidal datums determined by NOS as:

- *Mean higher high water (MHHW)*: the arithmetic mean of the higher-high-water heights of a mixed tide over a specific 19-years tidal epoch;
- *Mean high water (MHW)*: the arithmetic mean of the high-water heights over a specific 19-years tidal epoch; for a semidiurnal or mixed tide, the two high waters of each tidal day are included in the mean.
- *Mean sea level (MSL)*: the arithmetic mean of hourly water elevations over a specific 19-years tidal epoch.
- *Mean low water (MLW)*: the arithmetic mean of the low-water heights over a specific 19-years tidal epoch; for a semidiurnal or mixed tide, the two low waters of each tidal day are included in the mean.
- *Mean lower low water (MLLW)*: the arithmetic mean of the lower-low-water heights of a mixed tide over a specific 19-years tidal epoch.

If an average wave height can be estimated for the study site, then a mean swash elevation (MSE) can be estimated for any reach of shore.

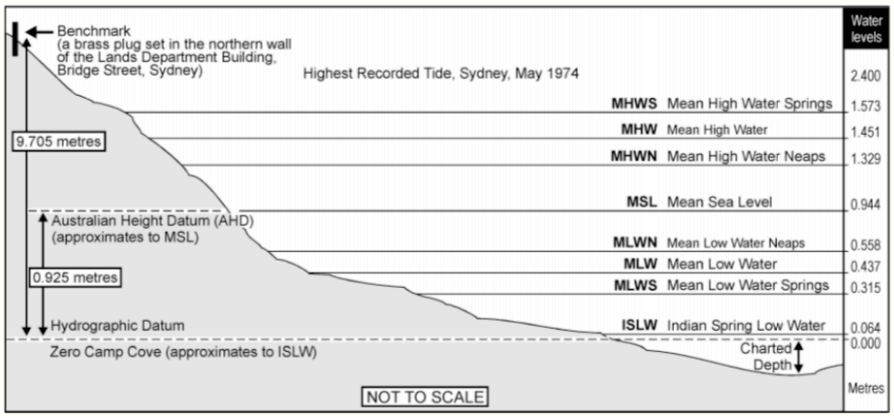

Figure 2.5 - Tidal datums used along the New South Wales coastline, Australia (Boak and Turner, 2005)

A tidal datum-based shoreline indicator is determined by the intersection of the coastal profile with a specific tidal elevation of a particular area (Figure 2.6).

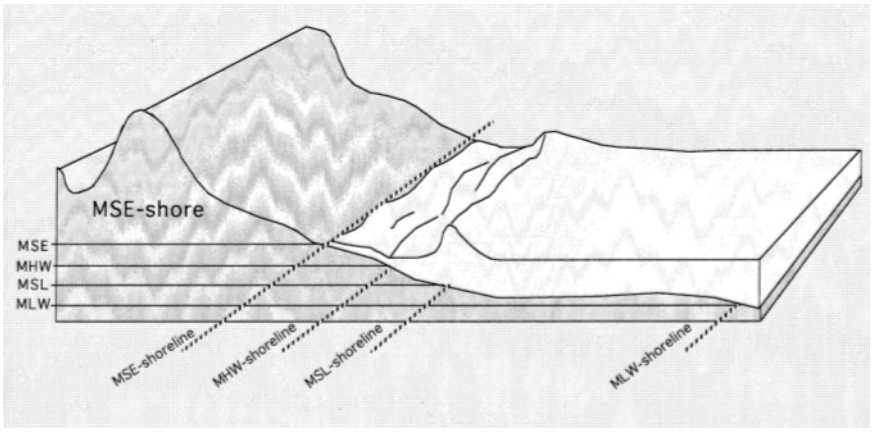

Figure 2.6 - Sketch illustrating the relationship between four tidal datums and the corresponding shoreline position (Oertel, 2005)

Most coastal researchers use the MHW because this shoreline indicator is visible in the field and can be interpreted from images (Leatherman, 2003). It represents the line of permanent emersion of the land area.

In the evaluation of the shoreline position, it is important to consider the slope of the shore profile; in fact, considering a cross-shore profile for a steeply and gently sloping shore and given a constant vertical tidal range, the horizontal spreads of water across a gently sloping surface is considerably greater than across a steeply sloping surface (Figure 2.7). Considering a typical beach with slope comprised between 1 and 3°, 1 m rise in water level may cause a landward shift in the shoreline position up to 188 m (Oertel, 2005).

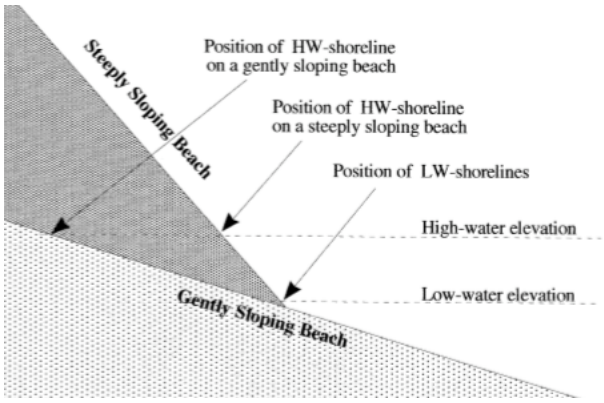

Figure 2.7 - Sketch of the shoreline position in case of steeply and gently sloping shore (Oertel, 2005)

A recent methodology to detect the shoreline is based on the application of image processing techniques to extract shoreline indicators from digital and satellite images (Figure 2.8). A literature review of image processing methods for shoreline detection in remote sensing was presented by Toure et al. (2019). An open-source software toolkit able to obtain time-series of shoreline position at any erodible coastline worldwide from 30+ years satellite imagery has been developed by Vos et al. (2019a). Example applications and accuracy of the resulting satellite-derived shorelines are discussed in (Vos et al., 2019b).

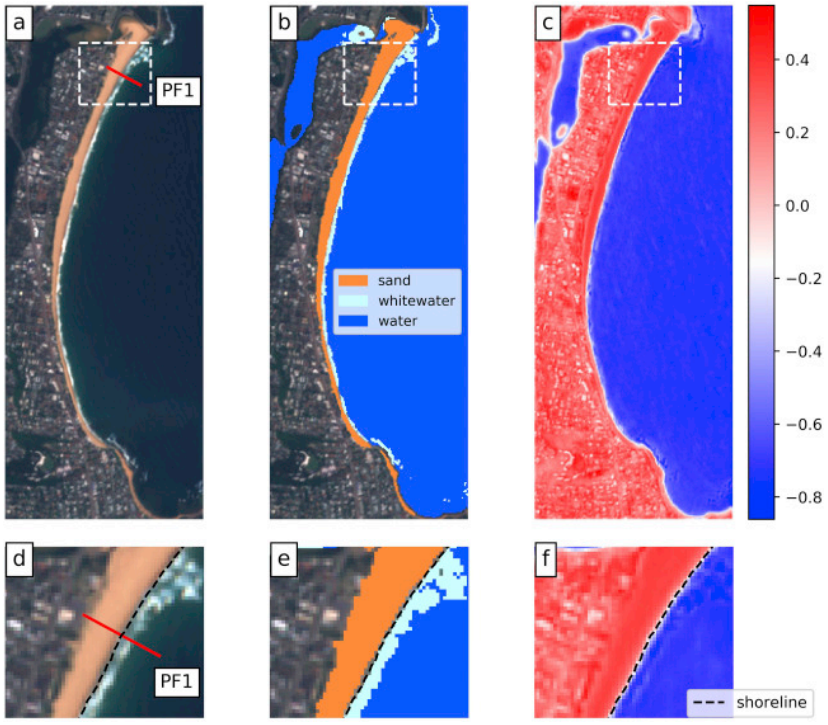

Figure 2.8 - a) Example region of interest within RGB image located at Narrabeen-Collaroy in southeast Australia, Sentinel-2. b) Output of image classification where each pixel has been labelled with one of three classes: 'sand', 'white-water' and 'water'. c) Single colour band image of the Modified Normalized Difference Water Index (MNDWI) pixel values. d), e) and f) Insets showing the detected shoreline, respectively on the RGB image, classified image and MNDWI image. (Vos et al., 2019

2.3 Causes of shoreline changes

The shore management guidelines (Mangor et al., 2017) describe the three main processes of shoreline change as:

- changes in the cross-shore profile occurring as a result of combined effect of storm surge and storm waves. The combination of these effects produces a strong offshore sediment transport and the consequently beach profile change. The cross-shore profile change can happen without a change in the volume of the beach, as illustrated in Figure 2.9;
- changes in volume of the active coastal profile occurring as a result of the gradient in the littoral drift in the direction of the net transport. This process continues up to the sediment is available for erosion. During extreme events the gradient in the littoral transport can become very large causing the major changes in the beach volume. This type of process is only reversed if additional sediment is supplied.
- sea level rise causes a general setback of the shoreline position occurring as a result of adaptation of the coastal profile to a new equilibrium shape under the higher mean sea level. This process happens on a large time scale.

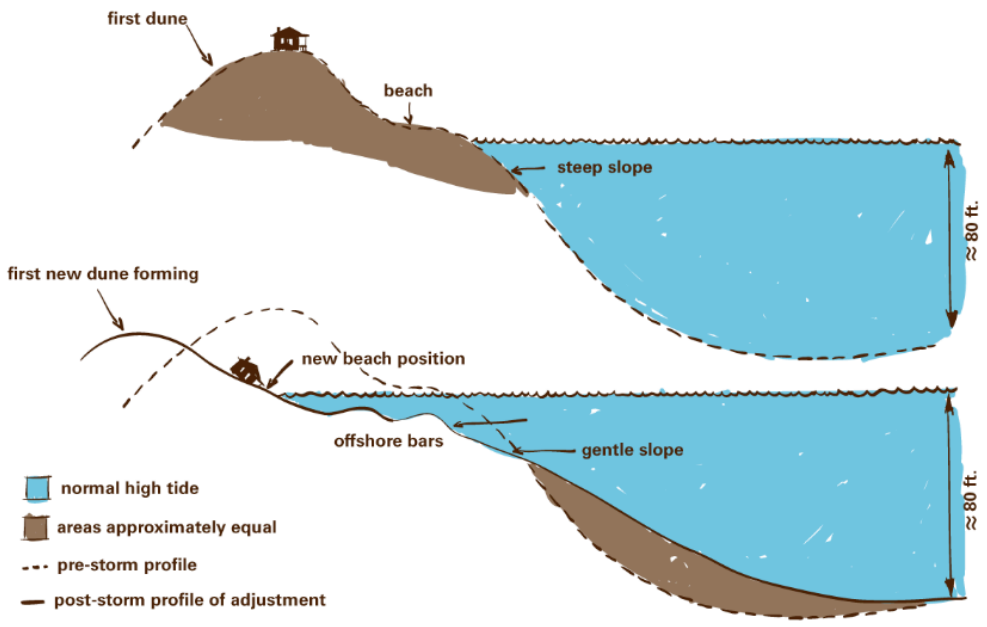

Figure 2.9 - Typical response of a beach to a storm event (www. fcit.usf.edu)

A combination of the three described processes determines the change in the shoreline position.

2.4 Sediment characteristics

A beach can be composed of grains of sand, gravel, pebbles, cobbles, or rock. The main characteristic of sediment is the size of the particles. The range of grain sizes composing a coast covers about five orders of magnitude, from sand particles to rock units (Figure 2.10).

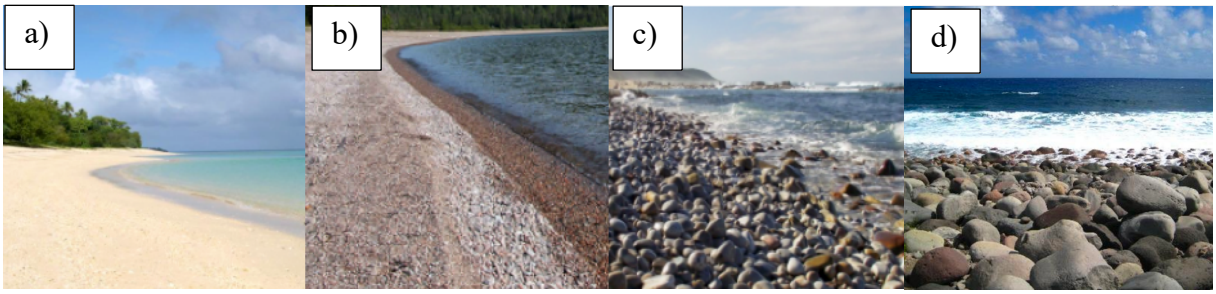

Figure 2.10 – Beach characterized by units of: a) sand, b) gravel, c) cobbles, d) rock

The particles size is defined in terms of diameter. The classification of sediment as sand, gravel, shingle, cobbles, rock, etc., is arbitrary, and many schemes have been proposed in relation to the sediment sizes (Figure 2.11).

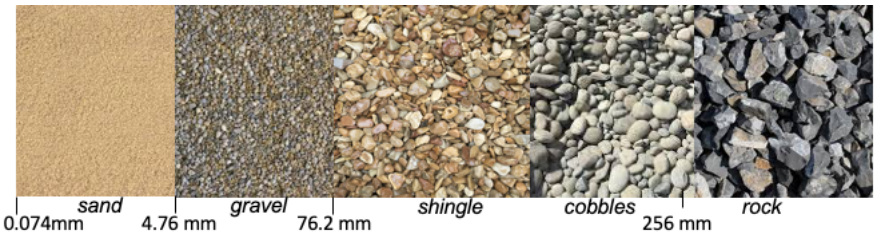

Figure 2.11 – ASTM sediment classification (USACE, 2003a) in relation to the sediment size

Coastal engineers adopt two classification systems:

- the Modified Wentworth Classification generally used in geology;
- the Unified Soils Classification or the ASTM Classification.

In the Coastal Engineering Manual (CEM)(USACE, 2003a), both systems are reported, where the corresponding size in mm and Phi (ϕ) are listed (Table 2.1). ϕ is calculated as suggested by Krumbein and Sloss (1963):

$$\phi = -log_2(D/D_0) \qquad (2.1)$$

where D = diameter of the particle in millimetres and D_0 = is a reference diameter equal to 1 mm.

Rearranging Equation (2.1) diameter D can be calculated as:

$$D = D_0 2^{-\phi} \qquad (2.2)$$

Table 2.1 - Sediment Particle Sizes, ASTM and Wentworth classification. (USACE, 2003a)

ASTM (Unified) Classification	U.S. Std. Sieve	Size in mm	Phi Size	Wentworth Classification
Boulder		4096.	-12.0	
		1024.	-10.0	Boulder
	12 in. (300 mm)	256.	-8.0	
Cobble		128.	-7.0	Large Cobble
		107.64	-6.75	
		90.51	-6.5	Small Cobble
	3 in. (75 mm)	76.11	-6.25	
		64.00	-6.0	
		53.82	-5.75	
		45.26	-5.5	Very Large Pebble
Coarse Gravel		38.05	-5.25	
		32.00	-5.0	
		26.91	-4.75	
		22.63	-4.5	Large Pebble
	3/4 in. (19 mm)	19.03	-4.25	
		16.00	-4.0	
		13.45	-3.75	
		11.31	-3.5	Medium Pebble
		9.51	-3.25	
Fine Gravel	2.5	8.00	-3.0	
	3	6.73	-2.75	
	3.5	5.66	-2.5	Small Pebble
	4 (4.75 mm)	4.76	-2.25	
	5	4.00	-2.0	
Coarse Sand	6	3.36	-1.75	
	7	2.83	-1.5	Granule
	8	2.38	-1.25	
	10 (2.0 mm)	2.00	-1.0	
	12	1.68	-0.75	
	14	1.41	-0.5	Very Coarse Sand
	16	1.19	-0.25	
	18	1.00	0.0	
Medium Sand	20	0.84	0.25	
	25	0.71	0.5	Coarse Sand
	30	0.59	0.75	
	35	0.50	1.0	
	40 (0.425 mm)	0.420	1.25	
	45	0.354	1.5	Medium Sand
	50	0.297	1.75	
	60	0.250	2.0	
	70	0.210	2.25	
Fine Sand	80	0.177	2.5	Fine Sand
	100	0.149	2.75	
	120	0.125	3.0	
	140	0.105	3.25	
	170	0.088	3.5	Very Fine Sand
	200 (0.075 mm)	0.074	3.75	
	230	0.0625	4.0	
	270	0.0526	4.25	
	325	0.0442	4.5	Coarse Silt
	400	0.0372	4.75	
		0.0312	5.0	
		0.0156	6.0	Medium Silt
		0.0078	7.0	Fine Silt
		0.0039	8.0	Very Fine Silt
		0.00195	9.0	Coarse Clay
		0.00098	10.0	Medium Clay
		0.00049	11.0	Fine Clay
		0.00024	12.0	
		0.00012	13.0	Colloids
		0.000061	14.0	

All samples of beach contain grains having a range of sediment sizes. A characterization of the sample can be done using a simple grain diameter as measure of the central tendency of the distribution. The median grain diameter D_{50} is the characteristic most often used. The definition of D_{50} is that half particles in the sample have a larger diameter and half have a smaller. This quantity is easily obtained graphically, if the sample is sorted by sieving. Other size fractions are similarly indicated. For example, D_{90} is the diameter for which 90 percent of the sample has a smaller diameter.

Another common measure of the central tendency of a sediment sample is the mean grain size, M_φ. Several formulas have been proposed to compute M_φ (Otto, 1939; Inman, 1952; Folk and Ward, 1957; McCammon, 1962). These formulas are averages of 2, 3, 5, or more percentiles of the phi frequency distribution. Following Folk (1974):

$$M_\varphi = \frac{(\varphi_{16} + \varphi_{50} + \varphi_{84})}{3} \qquad (2.3)$$

where M_φ = estimated grain size of the sample in phi units.

The median and mean grain sizes are usually quite similar for most beach sediments (USACE, 2003a).

Ternary diagrams are useful techniques for scientific analysis of systems characterized by different components. One of the most commonly used classifications of sediment is the Shepard ternary classification (Shepard, 1954). It considers the sand, silt and clay fractions with the identification of 10 sediment classes (Figure 2.12a).

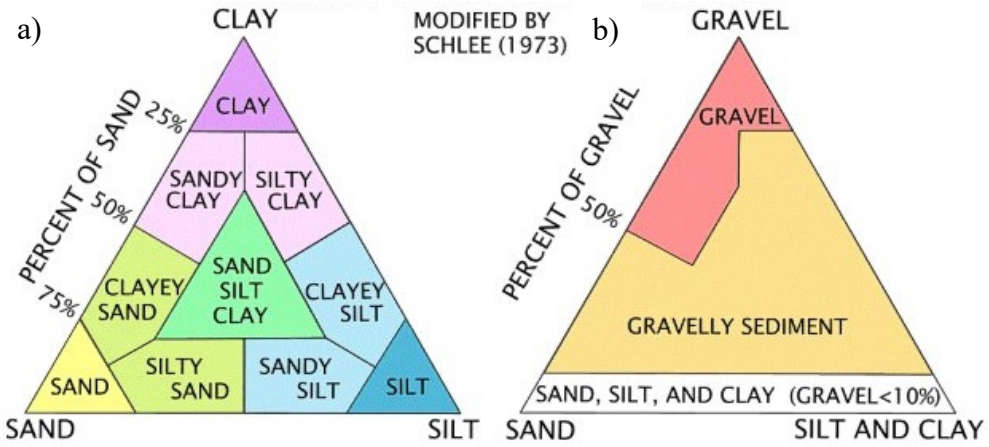

Figure 2.12 - Shephard's (1954) sediment classification system modified by Schlee (1973) with sand, silt, and clay size fractions based on Wentworth (1922) grade scale

This scheme, however, does not allow for sediments with significant amounts of gravel. Therefore, Shepard's classification scheme was subsequently modified by the addition of a second ternary diagram to account for the gravel fraction (Figure 2.12b) (Schlee, 1973).

The classification proposed by Folk (1954, 1974) consists of two triangular diagrams where the proportions of gravel, sand, and mud (Figure 2.13a) and the proportions of sand, silt, and clay are plotted (Figure 2.13b) defining in total 25 categories and using the term mud (defined as silt plus clay).

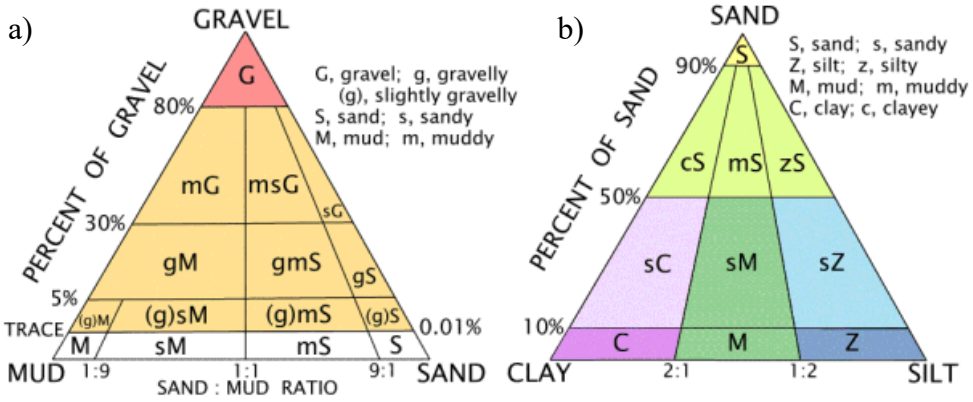

Figure 2.13 - Folk's sediment classification system (Folk, 1954)

2.5 Longshore transport formulae

Longshore transport is defined as the movement of water and sediment parallel to the coastline (Bascom, 1964; Lincoln et al., 1998) (Figure 2.14). Longshore transport of sediments controls the shoreline change occurring over several years or decades (Gravens and Rosati, 1994).

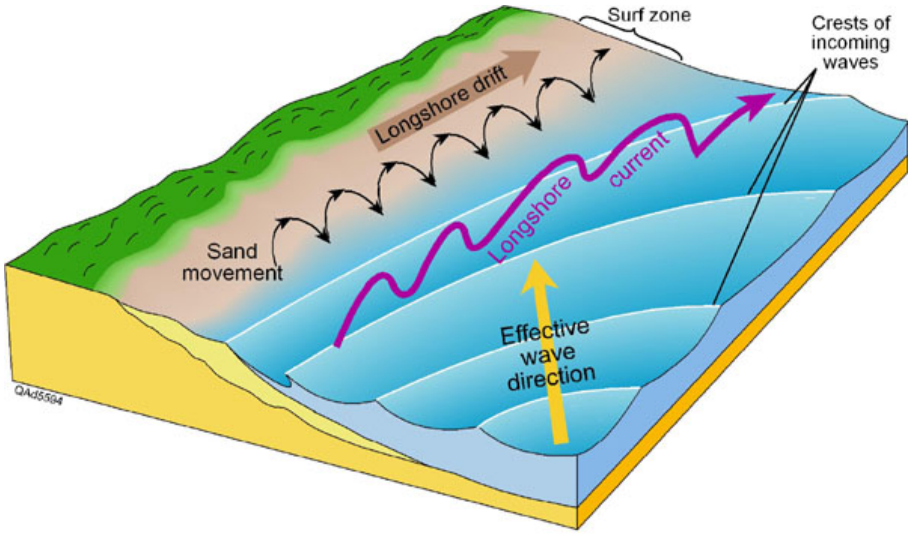

Figure 2.14 – Definition sketch of the longshore current and transport (http://www.geol.wwu.edu)

The main parameters for the description of the transport of the sediments along a shoreline are:

- the wave characteristics;
- the current conditions;
- the water-level conditions (i.e. tide, storm surge and wave set-up);

- the bathymetry of the area;
- the sediment characteristics of the beach;
- the sources and sinks of sediment, (e.g rivers, eroding coasts, etc.).

Sediment transport along the coastline occurs in several modes (Figure 2.15):

- *bedload transport*, referred to sediment transport by rolling and saltating grains in close contact with the seabed. Bedload transport is dominated by the flow velocity when is above the critical velocity for setting bed particles in motion (in the order of 0.2 - 0.4 m/s for sandy sediments), but insufficient for bringing sediment particles in suspension. Detailed information is presented by Van Rijn (1993).
- *suspended load,* referred to sediment transport occurring when the value of the bed-shear velocity exceeds the particle fall velocity.

It is not clear which of these mechanisms predominates for various wave conditions, sediment types, and locations on the profile (Dean and Darlymple, 2004).

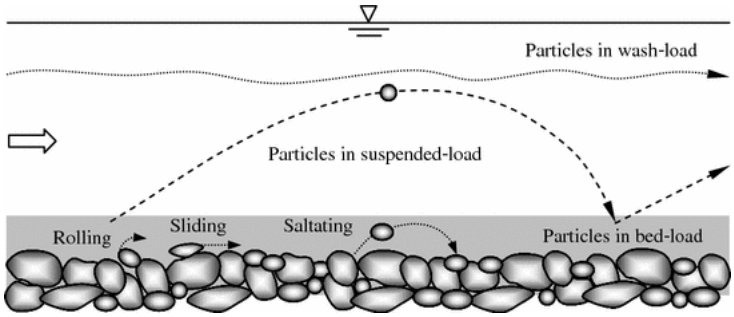

Figure 2.15 – Modes of sediment transport (Dey, 2014)

The sediment movement occurs in a three-dimensional pattern. The artificial separation of the total transport into components parallel and perpendicular to the shore is done as a convenience leading to a simpler understanding of a very complex environment (Seymour, 2005).

Depending on the wave direction approaching the coast, sediment transport, Q_l, occurs in two directions. By convention, the transport is positive to the right of an observer looking seaward from the beach, and negative if sediment transport is toward the left. The net transport, Q_{l_net}, is the sum of the positive and negative components, and the gross transport, Q_{l_gross}, is the sum of the drift magnitudes.

The transport rate can be defined as the volume of sand passing a point on the shore in a unit time (Watts, 1953), or as the immersed weight of sand passing per unit time (Inman and

Bagnold, 1963). The longshore transport in units of volume or weight can be estimated by the integral of the transport rate over time (USACE, 2003b).

The net longshore sediment transport rate, Q_{l_net}, is the time average transport given by:

$$Q_{l\_net} = \frac{1}{T_0}\int_0^{T_0} Q_l(t)dt \qquad (2.4)$$

The gross longshore sediment transport rate, Q_{l_gross}, is given by:

$$Q_{l\_gross} = \frac{1}{T_0}\int_0^{T_0} |Q_l(t)|dt \qquad (2.5)$$

where T_0 =length of the record, and Q_l = longshore transport.

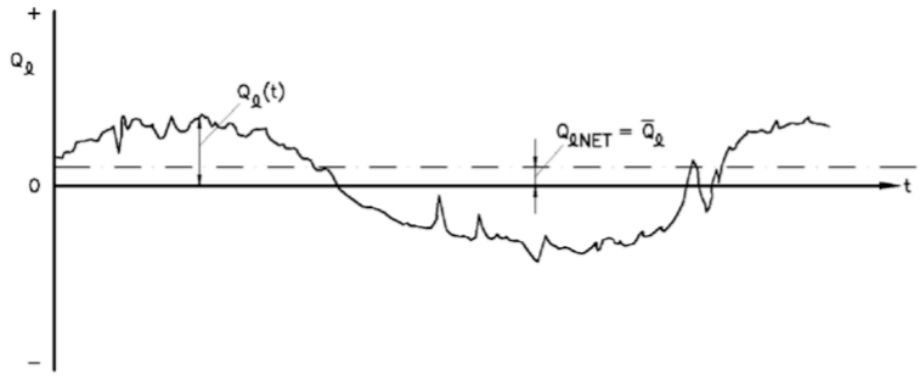

Figure 2.16 - Longshore transport definitions (USACE, 2003b)

Estimate of net and gross longshore transport is important in coastal engineering because it can be a support to the design of coastal protection measures. Gradients in the net transport of a coast section indicate if there is erosion or accretion. The gross transport is important for backfilling of channels across the littoral drift zone (Mangor, 2004).

The measure of the longshore transport is difficult in the field and in the laboratory because it is a mixture of suspended and bedload transport. Instruments have been developed to measure suspended sediment concentrations at a point, but no satisfactory method of measuring bedload has yet been demonstrated (Seymour, 2005). The total longshore sediment transport rate in the surf zone can be measured with a method note as “impoundment” that consist in deploying a temporary groyne. The efficiency of this method for the longshore transport calculation was highlighted from Bodge (1986), Bodge and Dean (1987), and Wang and Kraus (1999).

2.5.1 Energetics and Traction approaches

Sediment transport models reflect two distinct approaches: an energetics approach and a traction approach. The former includes models by Inman and Bagnold (1963), Thornton (1973), Komar (1971, 1977), Bowen (1981), and Bailard and Inman (1981), while the latter include models by Bijker (1971), Swart (1977), and Madsen and Grant (1976). In both cases, these approaches are based on adaptation of stream flow sediment transport models.

The energetics approach is based on the stream transport model developed by Bagnold (1963, 1966). Bagnold, comparing the stream to a machine, defined the sediment transport efficiency as the ratio of the rate of energy expended in transporting either the bedload or the suspended load, divided by the total rate of energy production of the stream.

The generally applied CERC formula (1973, 1984) for the longshore transport relates the longshore transport to the longshore current caused by the breaking waves, without using this current explicitely.

Traction type models use a formulation which relates the sediment transport to the current taking the wave influence into consideration. It is explicitely assumed that the waves itself do not transport material. As long as the direction of the wave propagation is not close to the current direction this assumption gives no problems.

Inman and Bagnold's model (1963) is currently the most widely accepted and is equivalent in form to the equation recommended by CERC (1973, 1984). Inman and Bagnold's model linearly relates the total spatially integrated immersed weight longshore transport rate, I_b, to the longshore component of wave energy flux per unit length of beach, P_l. Consequently, the energetics approach is also termed energy flux approach.

Eaton (1951) was the first to suggest the relationship between longshore transport and the wave characteristics at breaking point, based on energy flux approach, with the assumption that the longshore transport rate depends on the longshore component of wave energy. The formulation proposed by Eaton (1951) and Komar and Inman (1970), Inman and Bagnold (1963), Van Hijum and Pilarczyk (1982), CERC (1984), Kamphuis et al. (1986), Walton and Bruno (1989), Chadwick (1989), Van der Meer (1990), Kamphuis (1991), Vrijling et al. (1991), Van der Meer and Veldman (1992), Van Rijn (2002), Bayram et al. (2007), Tomasicchio et al. (2013), Mil-Homens et al. (2013), Van Rijn (2014) are described in the following in a chronological order.

2.5.2 Eaton (1951) and Komar e Inman (1970)

The most popular formulations to determinate the longshore transport rate are based on energy flux model, with the assumption that the longshore transport rate depends on the longshore component of wave energy.

As said, Eaton (1951) was the first to suggest the relationship between longshore transport and the wave characteristics at breaking point, based on energy flux approach. In Figure 2.17, circumference sectors represent two orthogonal of wave-front that rotate due to refraction, dl their distance, P energy flux per unit length, dx the x horizontal projection of dl and ϑ the inclination of P. Assuming $dx = 1$, dl can be written as $dl = dx\ cos\vartheta = cos\vartheta$.

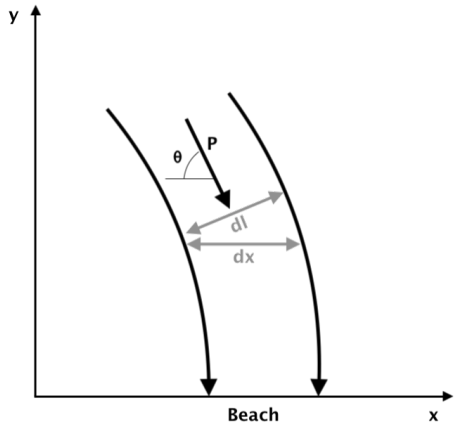

Figure 2.17 - Flux of energy between two orthogonal waves.

The horizontal projection of P is:

$$P_l = P\ dl\ sin\vartheta = P\ cos\vartheta\ sin\vartheta \qquad (2.6)$$

The flux of energy can also be written as $P = \bar{E}\ c_g$, where c_g = wave group celerity and $\bar{E}$ represents the sum of kinetic and potential energy, $\bar{E} = \frac{1}{8}\rho g H^2$ (with ρ = water density, g = gravitational acceleration and H = wave height) and $\frac{1}{2} sin2\vartheta\ = sin\vartheta\ cos\vartheta$, Equation (2.6) can be written as:

$$P_l = \frac{\rho g}{16}\ H^2\ c_g\ sin2\vartheta \qquad (2.7)$$

At the breaker line, Equation (2.7) can be written in function of significant wave height as below:

$$P_{ls} = \frac{\rho g}{16} {H_{sb}}^2 \, c_{gb} \, sin2\vartheta_b \qquad (2.8)$$

Komar and Inman (1970) found the relationship between weight of immersed material, I_l, and longshore energy, P_{ls}, given by:

$$I_l = K \, P_{ls} \qquad (2.9)$$

K coefficient was determined by linear regression on field measurements of sediment transport obtained at Silver Strand, California, and El Moreno, Mexico. Komar and Inman (1970) obtained a value of $K = 0.77$, using the root mean square wave height, H_{rms}.
I_l can also be written as:

$$I_l = (\rho_s - \rho) \, g \, n \, Q_l \qquad (2.10)$$

where ρ_s = mass density of sediment, ρ = water density, n = porosity = volume solids/total volume (0.4 about), Q_l = longshore sediment transport.

Combining Equation (2.8), Equation (2.9), Equation (2.10), Q_l can be written as:

$$Q_l = \frac{K}{(\rho_s - \rho) g n} \, P_{ls} \qquad (2.11)$$

2.5.3 Inman and Bagnold (1963)

Inman and Bagnold (1963) proposed a model based on the energetic approach. The immersed weight longshore sediment transport rate, I_l, was related to combined effect of waves and currents:

$$I_l = K \frac{(EC_n)_b}{u_{mb}} V_l \qquad (2.12)$$

where *K* is a non-dimensional empirical coefficient. Komar and Inman (1970) and Kraus et al. (1982) performed sand tracer experiments determining a value of $K = 0.28$ and $K = 0.21$ respectively, E = wave energy, C_n = wave group celerity, with the subscript *b* for the breaking

condition, u_{mb} = maximum horizontal orbital velocity of the waves at the breaker zone, and V_l = mid-surf longshore current velocity given as:

$$V_l = 1.17\sqrt{gH_b}\,sin\,\vartheta_b \qquad (2.13)$$

with g = gravitational acceleration, H_b= breaking wave height and ϑ_b = breaking wave angle with respect to the shoreline.

2.5.4 Van Hijum and Pilarczyk (1982)

Van Hijum and Pilarczyk (1982) proposed a formula valid for gravel beaches. Equation (2.14) has been obtained from the dimensional analysis on the experimental data conducted by van Hijum (1976) and van Hijum and Pilarczyk (1982) at Delft Hydraulics where the longshore sediment transport Q_l can be calculated as following:

$$\frac{Q_l}{gD_{90}T_s} = 7.1210^{-4}\frac{H_s(cos\,\theta)^{1/2}}{D_{90}}\left[\frac{H_s(cos\,\theta)^{1/2}}{D_{90}} - 8.3\right]\frac{sin\,\theta}{tanh\left(\frac{2\pi h}{L}\right)} \qquad (2.14)$$

where D_{90} = 90% representative grain diameter, T_s = significant wave period, H_s = significant wave height, θ = wave angle, L = wavelength, and h = water depth. According to van Wellen et al. (2000), Equation (2.14) introduces unwanted complications by using wave parameters measured at an offshore location and at the toe of the structure.

2.5.5 CERC (USACE, 1984)

Based on Komar and Inman's (1970) transport relationship, the energetics based CERC formula (USACE, 1984) was presented in the Shore Protection Manual (SPM) becoming one of the most commonly used methods for calculating the longshore transport rate (LSTR). The LSTR, Q_l, is calculated on the base of energy flux model from the empirical equation relating longshore energy flux in the breaker zone:

$$Q_l = \frac{K}{(\rho_s - \rho)g(1-n)}\frac{\rho g}{16}H_b^2 c_{gb}\,sin\,2\theta_b \qquad (2.15)$$

where K = dimensionless empirical constant depending on the grain size of the sediment and the wave characteristics in the surf zone, ρ_s= sediment density, ρ = water density, n = porosity factor (0.4), H_b= breaking wave height, c_{gb} = wave group celerity at breaking, θ_b = breaking wave angle.

The SPM (USACE, 1984) indicates the K values in case of significant wave height K_{Hs} = 0.39 and in case of root mean squares wave height K_{Hrms} = 0.92. Although the sediment transport predictions followed a clear correlation with observations, there was considerable scatter, which may suggest that K is a function of some other physical parameters. Several other studies attempted to find a more robust value or formulation for K.

The CERC formula (USACE, 1984) does not consider the effect of the sediment size. Dean et al. (1982) studied the relationship between the K coefficient and the sediment size (Figure 2.18).

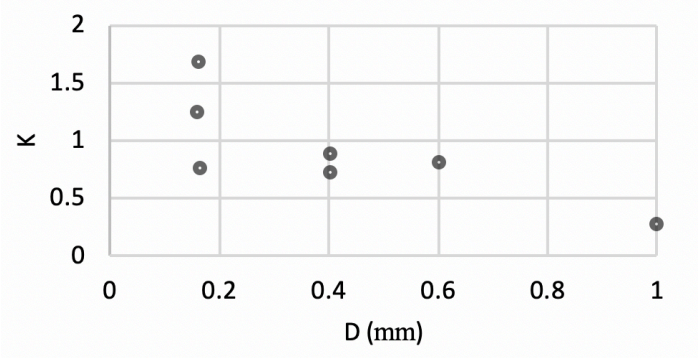

Figure 2.18 - Variation in K-parameter with grain size D (from Dean et al. (1982))

Kamphuis and Readshaw (1978) found that the K parameter can be related to the type of breaking:

$$K = 0.7\xi_b \qquad (2.16)$$

where ξ_b = Iribarren number given as:

$$\xi_b = \frac{m}{\sqrt{\frac{H_b}{L_o}}} \qquad (2.17)$$

with m = beach slope, L_o = wavelength at the deep water.

Ozhan (1982) based on laboratory experiments proposed a relation finding that *K* parameter is a function of the wave steepness calculated at deep water:

$$K \cong \frac{0.007}{\left(\frac{H_o}{L_o}\right)} \qquad (2.18)$$

with H_o = wave height at deep water.

Bailard (1984) calibrated the *K* parameter using field and laboratory data. The proposed equation calculates *K* as:

$$K = 0.05 + 2.6\, sin^2(2\theta_b) + 0.007 \frac{u_{mb}}{w_f} \qquad (2.19)$$

where u_{mb} = maximum horizontal orbital velocity of the waves evaluated at the breaker zone and w_f= fall speed of the sediment. The equation is considered valid for 2.5 < w_f < 20.5 cm/s, 0.2 < θ_b < 15° and 33 < u_{mb} < 283 cm/s

Del Valle et al. (1993) proposed the following equation:

$$K = 1.4e^{-2.5D_{50}} \qquad (2.20)$$

where D_{50} = median grain size expressed in *mm*. The equation is considered valid for 0.40<D_{50}<*1.5* mm.

Finally, Mil-Homens et al. (2013) proposed the following relationship to determine K:

$$K = \left[2232.7\left(\frac{H_b}{L_o}\right)^{1.45} + 4.505\right]^{-1} \qquad (2.21)$$

The relationship is considered valid for 0.001 < H_b/L_o < *0.1*

2.5.6 Kamphuis et al. (1986)

Kamphuis et al. (1986) proposed an empirical formula including the beach slope and the sediment grain size. The longshore transport, Q_l, is given as:

$$Q_l = 1.28 \frac{m\, H_{sb}^{3.5}}{D_{50}} sin(2\theta_b) \qquad (2.22)$$

with H_{sb} = significant breaking wave height, m = beach slope, D_{50} = median sediment grain size expressed in meters, and θ_b =breaking wave angle.

2.5.7 Walton and Bruno (1989)

Walton and Bruno (1989) used the breaker wave height and longshore velocity to calculate the longshore transport, Q_l, as:

$$Q_l = \frac{K}{(\rho_s - \rho) g (1-n)} \frac{\rho\, g\, H_b\, W\, V\, C_f}{0.78 \left(5\, \frac{\pi}{2}\right) \left(\frac{V}{V_0}\right)} \qquad (2.23)$$

where K = non dimensional empirical constant, ρ_s= sediment density, ρ = water density, H_b= breaking wave height, n = porosity factor (0.4), W = surf zone width, V = mean longshore velocity, C_f = friction coefficient dependent on bottom water particle excursion and bottom roughness, $\left(\frac{V}{V_0}\right)$ = the theoretical dimensionless longshore velocity for Longuet-Higgins, (1970).

2.5.8 Chadwick (1989)

Chadwick (1989) proposed a formula on the base of the data set at the beach of Shoreham (West Sussex, England):

$$Q_l = 0.0013 (g D_{90}^2 T_s) W (W - 8.3)\, sin\, \theta_b \qquad (2.24)$$

with D_{90} = 90% representative grain diameter, ϑ_b = breaking wave angle, T_s = significant wave period, and

$$W = \frac{H_{sb} \sqrt{cos\, \theta_b}}{D_{90}} \qquad (2.25)$$

where H_{sb} = significant breaking wave height.

Equation (2.24) can be applied within the limits $H_s/\Delta D_{n50} > 10$ (for rock/ gravel beaches).

2.5.9 Van der Meer (1990)

Van der Meer (1990) re-analysed the van Hijum and Pilarczyk (1982) formula in order to make it more practical:

$$Q_l = 0.0012 g D_{50} T_p H_s \sqrt{cos\,\theta_b} \left(\frac{H_s \sqrt{cos\,\theta_b}}{D_{50}} - 11 \right) sin\,\theta_b \qquad (2.26)$$

where D_{50} = median grain size, T_p = peak period, H_s= significant wave height at the toe of the structure, and θ_b= breaking wave angle.

2.5.10 Kamphuis (1991)

Kamphuis (1991) developed a formula based on an extensive data set, mainly comprising small scale laboratory data at sandy beaches taking into account the wave period:

$$Q_l = 2.27\, H_{sb}^2 T_p^{1.5} m^{0.75} D_{50}^{-0.25}\, sin^{0.6}(2\theta_b) \qquad (2.27)$$

with H_{sb} = significant breaking wave height, T_p = peak wave period, m = beach slope near the breaking point, D_{50} = median grain size, and θ_b = breaking wave angle.

Wang et al. (1998) found that the Kamphuis (1991) formula predicted consistently lower total longshore transport rates than those predicted by the CERC formula (USACE, 1984). Also, Miller (1998) found that the Kamphuis model gave predictions an order of magnitude lower than the CERC formula for storm conditions with breaker height of nearly 4 m. The formula proposed by Kamphuis (1991) over-predicts transport for gravel beaches because it does not include a critical shear stress, assuming that particles move even for small conditions, which is true for sand but not for gravel (Kamphuis, 2010).

2.5.11 Vrijling et al. (1991)

Vrijling et al. (1991) adopted a probabilistic approach to calculate the longshore transport (LT) at a reshaping type berm breakwater over its total lifetime. In that case the start or onset of LT is extremely important. They used the data of the tests performed by van der Meer and Veldman (1992) and the data by Burcharth and Frigaard (1987), but not the extended series described in Burcharth and Frigaard (1988). Based on all data points they come to a formula for berm breakwaters:

$$Q_l = 0 \; for \; N_s T_p^* < 100 \qquad (2.28)$$

$$Q_l = 0.000048\left(N_s T_p^* - 105\right)^2 \qquad (2.29)$$

where $N_s = H_s/\Delta D_{50}$ stability number, H_s = significant wave height, Δ = relative mass density of the unit = $(\rho_s - \rho)/\rho$, T_p^* = dimensionless wave period related to the nominal diameter:

$$T_p^* = T_p\sqrt{g/D_{50}} \qquad (2.30)$$

where T_p= peak period and D_{50}= median grain size.

2.5.12 Van der Meer and Veldman (1992)

Van der Meer and Veldman (1992) specified that Equation (2.26) proposed by Van der Meer (1990) should only be applied within the limit of stability number *Ns* = 12–27, i.e. fairly large gravel in prototype. Equation (2.26) shows a dependency on the grain diameter. For small grain sizes (gravel/sandy beaches) it reduces to:

$$Q_l = 0.0012\pi H_s c \; sin\, 2\theta_b \qquad (2.31)$$

where H_s= significant wave height at the toe of the structure, c = wave celerity, and θ_b= breaking wave angle.

2.5.13 Van Rijn (2002)

Van Rijn (2002) proposed a simplified equation for sand transport after an analysis of the longshore process of various field data sets (USA and Netherlands). The simplified formula is:

$$Q_l = 42 \; K_{swell} K_{grain} K_{slope} (H_{sb})^{2.5} V_{eff,L} \qquad (2.32)$$

with $K_{swell} = T_{swell}/T_{ref}$ swell correction factor for swell waves; $K_{grain} = d_{50,ref}/d_{50}$= particle size correction factor ($d_{50,ref} = 0.2\; mm$), with $K_{grain,min} = 0.1$ for $d_{50} > 2\; mm$; $K_{slope} = (\tan\beta/\tan\beta_{ref})^{0.5}$ = bed slope correction factor ($K_{slope,max} = 1.25$, $K_{slope,min} = 0.75$); $\tan\beta$ = actual bed slope, $\tan\beta_{ref} = 0.01$; the overall profile slope is defined as the slope between the waterline and the 8 m depth contour; H_{sb} = significant breaking wave height;

$V_{eff,L} = \left[\left(V_{wave,L}\right)^2 + \left(V_{tide,L}\right)^2\right]^{0.5}$ = effective longshore velocity at mid surf zone for tidal velocity and wave-induced in the same direction. $V_{wave,L} = 0.3(gH_{sb})^{0.5}\sin(2\theta_b)$ = wave-induced longshore velocity in mid surf zone (incl. wind effect), H_{sb}= significant breaking wave height, θ_b =breaking wave angle, $V_{tide,L}$ = longshore velocity in mid surf zone due to tidal forcing (=0 m/s for non-tidal cases, 0.1 m/s for micro-tidal, 0.3 m/s for meso-tidal and 0.5 m/s for macro-tidal cases).

2.5.14 Bayram et al. (2007)

Bayram et al. (2007) presented a predictive formula for the LT derived from both field and laboratory data at sandy beaches; it was developed from principles of sediment transport physics assuming that breaking waves mobilize the sediment, which is subsequently moved by a mean current:

$$Q_l = \frac{\varepsilon}{(\rho_s - \rho)(1-n)gw_s} F\bar{V} \qquad (2.33)$$

with ε = transport coefficient which expresses the efficiency of the waves in keeping sand grains in suspension, ρ_s= sediment density, ρ = water density, n = porosity factor, w_s = fall speed determined using high-quality field and laboratory data or theoretically, $\bar{V}$ = mean longshore current velocity over the surf zone, F = wave-energy flux given by:

$$F = E_b c_{gb} \cos\theta_b \qquad (2.34)$$

where E_b = wave energy at breaking, c_{gb} = wave group celerity at breaking, θ_b = breaking wave angle.

Bayram et al. (2007) estimated the coefficient ε by performing a dimensional and error analysis, which led to the following transport coefficient:

$$\varepsilon = \left(9 + 4\frac{H_{sb}}{w_s T_p}\right)10^{-5} \qquad (2.35)$$

where T_p= peak period.

2.5.15 Tomasicchio et al. (2013)

A General Longshore Transport (GLT) model was proposed relating longshore transport due to oblique wave attacks to the mobility level of the units composing the coastal structure (Lamberti and Tomasicchio, 1997). It combines an energy flux approach with an empirical/statistical relationship between the wave induced forcing and the number of moving units. The main assumption of GLT model is that movements statistics is affected by obliquity only through an appropriate mobility index and that the units move during up- and down-rush with the same obliquity of breaking and reflected waves at the breaker depth (Tomasicchio et al., 1994; Lamberti and Tomasicchio, 1997).

It is assumed that a particle will pass through a certain control section in a small time interval Δt if and only if it is removed from an updrift area of extension equal to the longitudinal component of the displacement length, $l_d \sin\theta_d$, where l_d is the displacement length and θ_d is its obliquity (Figure 2.19).

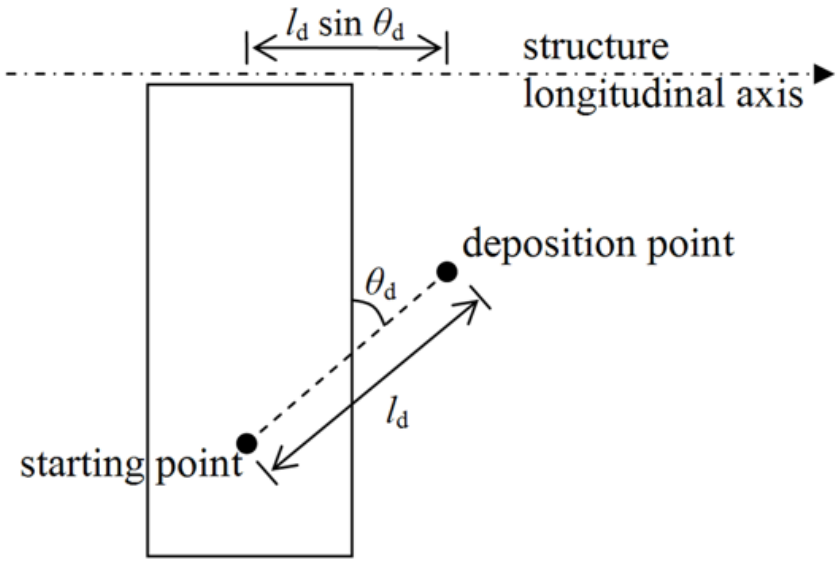

Figure 2.19 - Definition sketch for the GLT model (Tomasicchio et al., 2013)

This process description is particularly true when considering the wave obliquity, the up-rush and related longshore transport (LT) at the swash zone. Assuming that the displacement obliquity is equal to the characteristic wave obliquity at breaking ($\theta_d = \theta_{k,b}$), and that a number N_{od} of particles removed from a nominal diameter, D_{50}, wide strip moves under the action of 1000 waves, then the number of units passing a given control section in one wave is:

$$S_N = \frac{l_d}{D_{50}} \cdot \frac{N_{od}}{1000} sin\theta_{k,b} = f(N_s^{**}) \qquad (2.36)$$

where:

$$N_s^{**} = \frac{H_k}{C_k \Delta D_{50}} \left(\frac{s_{m,0}}{s_{m,k}}\right)^{-1/5} (cos\theta_0)^{2/5} \qquad (2.37)$$

is the modified stability number (Lamberti and Tomasicchio, 1997) with: H_k = characteristic wave height; $C_k = H_k/H_s$ where H_s =significant wave height; θ_0 = offshore wave obliquity; $s_{m,0}$ = mean wave steepness at offshore conditions and $s_{m,k}$ = characteristic mean wave steepness (assumed equal to 0.03). Lamberti and Tomasicchio (1997) showed that H_k is to be considered equal to $H_{1/50}$, but $H_{2\%}$ can also be adopted. In the first case: C_k = 1.55, in the second case: C_k = 1.40. The second factor in Equation (2.37) is such that $N_s^{**} \cong N_s$ for $\theta_0 = 0$ if $s_{m,0} = s_{m,k}$. For a berm breakwater, strict threshold conditions correspond to $N_s^{**} \cong 2$.

In the case of head-on wave attacks, under the assumption that, offshore the breaking point, the wave energy dissipation is negligible and that waves break as shallow water waves, the following relation holds:

$$F = \frac{1}{8}\rho g H_o^2 c_{go} = \frac{1}{8}\rho g H_b^2 c_{gb} \qquad (2.38)$$

where F is the onshore component of wave energy flux, H_o is the offshore wave height, H_b is the wave height at breaking,

$c_{go} = \frac{1}{2}\sqrt{g/k_0}$ is the offshore group velocity (2.39)

k_0 is the offshore wave number,

$c_{gb} = \sqrt{g\, h_b}$ is the breaking group velocity (2.40)

h_b is the breaking depth, and γ_b is the breaker index, defined through

$H_b = \gamma_b\, h_b$ is the breaking group velocity (2.41)

Considering Equation (2.38) and Equation (2.39), the onshore component of F can be written as:

$$F \propto \rho\, g^{3/2}\, H_0^{5/2} s_0^{-1/2} \qquad (2.42)$$

it can be noticed that the relevant parameter is the onshore energy flux and that the model belongs to the category based on an energy flux approach.
Eqs. (2.38) - (2.41) imply also a simple expression for breaker height:

$$H_b = H_o \left(\frac{\gamma_b}{4k_o H_o}\right)^{1/5} = qH_o s_o^{-1/5} \qquad (2.43)$$

Komar and Gaughan (1972) found the best agreement with field and laboratory data assuming γ_b = 1.42 or the proportionality constant q = 0.56.
It follows that, considering the characteristic wave height at breaking, $H_{k,b}$, and $s_{m,0} = s_{m,k} =$ 0.03, N_s^{**} can be also written as:

$$N_s^{**} \cong \frac{0.89 H_{k,b}}{C_k \Delta D_{50}} \qquad (2.44)$$

According to the refraction theory for plane and monotonically decreasing profiles, $H_{k,b}$ and sin $\theta_{k,b}$, can be evaluated as in the following (Lamberti and Tomasicchio, 1997; Tomasicchio et al., 1994):

$$H_{k,b} = \left(H_k^2 c_g cos\theta \sqrt{\gamma_b / g}\right)^{2/5} \qquad (2.45)$$

$$sin\theta_{k,b} = \frac{c_{k,b}}{c} sin\theta \qquad (2.46)$$

$$c_{k,b} = \sqrt{g H_{k,b} / \gamma_b} \qquad (2.47)$$

where $c_{k,b}$ is the characteristic wave celerity at breaking depth.
The displacement length can be calculated as (Lamberti and Tomasicchio, 1997):

$$l_d = \frac{(1.4 N_s^{**} - 1.3)}{tanh^2(kh)} D_{50} \qquad (2.48)$$

with k = wave number.

N_{od} has been determined following a calibration procedure based on the least-squares method taking into account the full data base. In particular, two different approximating functions have been considered; to accommodate the calibration procedure, N_{od} values calculated from measured data have been partitioned in two subintervals. The first interval refers to $N_s^{**} \leq 23$: from berm breakwaters to gravel beaches. The second one relates to $N_s^{**} > 23$: the interval for sandy beaches. For $N_s^{**} \leq 23$, a third order polynomial approximating function provides a satisfactory agreement as shown by Tomasicchio et al. (2007). For $N_s^{**} > 23$ a good agreement is given by a linear regression in log–log plane.

After the calibration procedure, N_{od} is given as:

$$N_{od} = \begin{cases} 20N_s^{**}(N_s^{**} - 2)^2 & N_s^{**} \leq 23 \\ exp[2.72ln(N_s^{**}) + 1.12] & N_s^{**} > 23 \end{cases} \quad (2.49)$$

The estimated correlation coefficient resulted equal to 0.89 for $N_s^{**} \leq 23$, and 0.92 for $N_s^{**} > 23$, respectively.

LT rate can be also expressed in terms of [m^3/s] as in the following:

$$Q_l = \frac{S_n D_{50}^3}{(1-n)T_m} \quad (2.50)$$

with T_m = mean wave period, and n porosity factor.

Figure 2.20 shows the flowchart of the proposed GLT model to guide the user in a practical application.

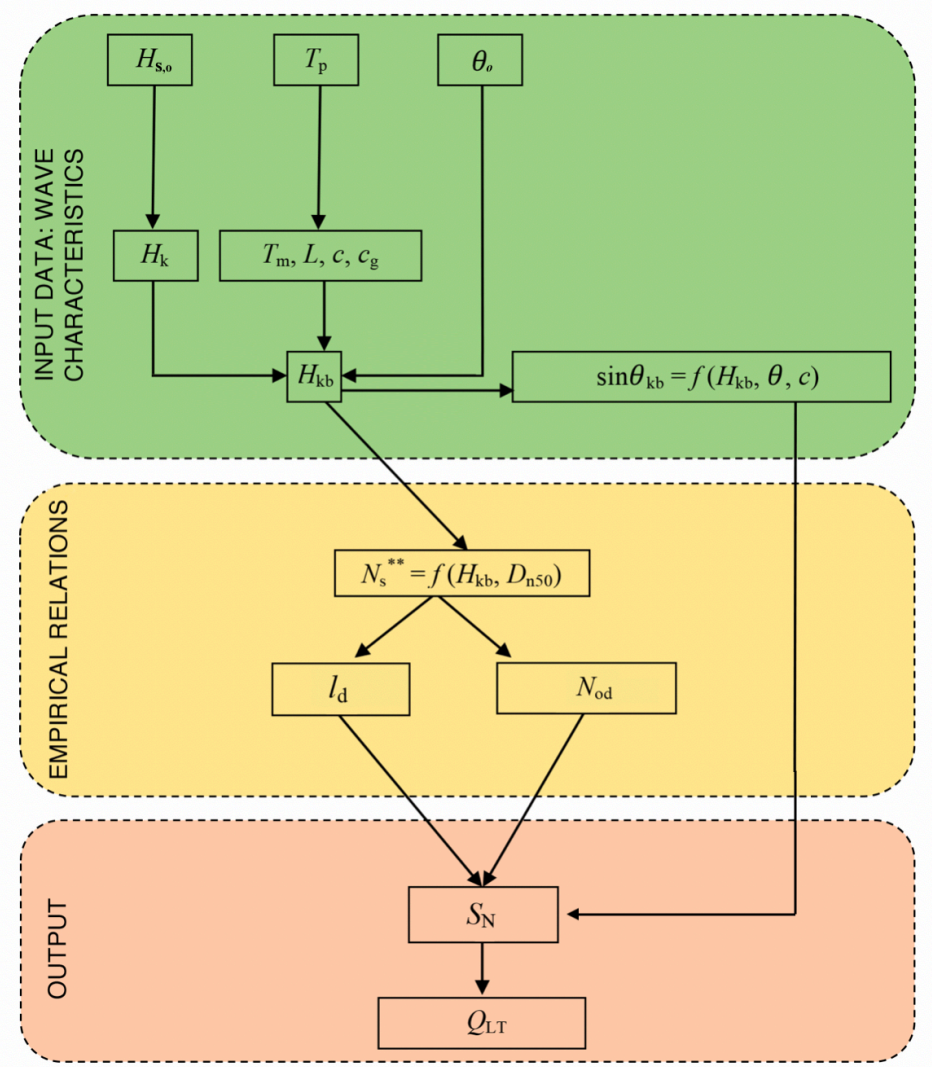

Figure 2.20 - Flowchart of the GLT model (Tomasicchio et al. 2013)

The GLT model has been verified from (Lamberti and Tomasicchio, 1997; Tomasicchio et al., 2013) for an extensive range of conditions: from sandy beaches till reshaping type berm breakwaters. Figure 2.21 shows the relationship between the calculated $S_N/\sin\theta_{k,b}$ versus N_s^{**} (Tomasicchio et al., 2013). With reference to the range of variation of N_s^{**}, the first region refers to the berm breakwaters ($N_s^{**} < 6$), the second region refers to the shingle beaches (cobbles and gravel, $6 < N_s^{**} < 23$), and the third region refers to the sandy beaches ($N_s^{**} > 23$). The results allow to confirm that the GLT model gives reliable estimates of the longshore transport for any type of coastal mound.

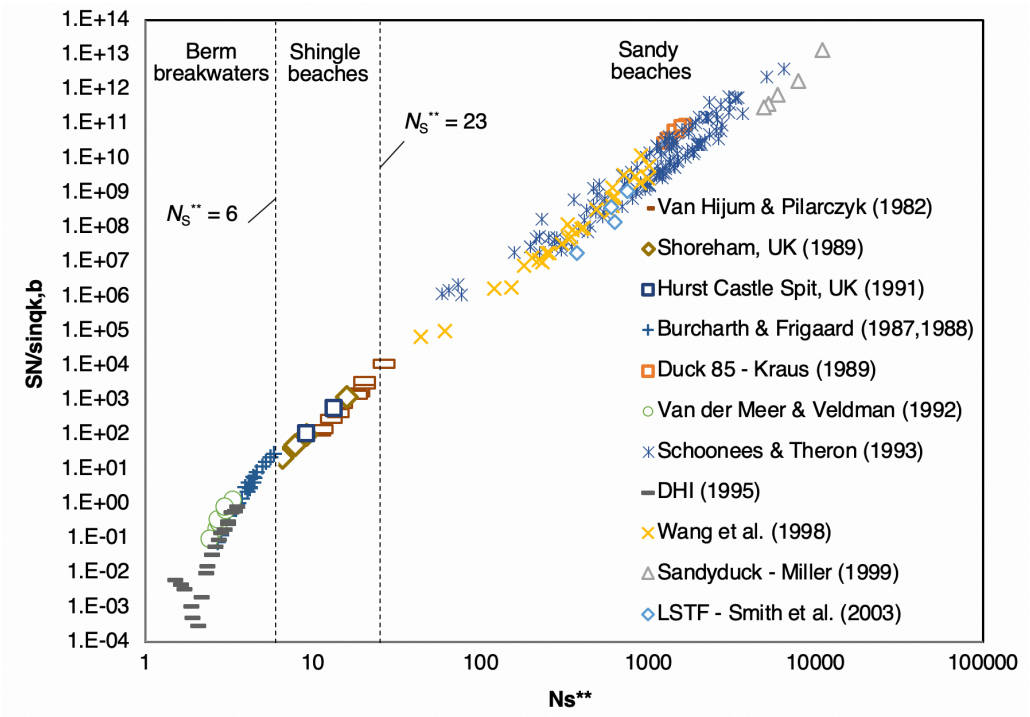

Figure 2.21 - Calculated $S_N/sin\theta_{k,b}$ versus N_s^{**} (Tomasicchio et al., 2013)

2.5.16 Mil-Homens et al. (2013)

Mil-Homens et al. (2013) used a least-squares optimization algorithm to propose new exponents for the Kamphuis (2003) formula as:

$$Q_l = 17.5 H_{sb}^{2.75} T_p^{0.89} m_b^{0.86} D_{50}^{-0.69} \, sin^{0.5}(2\theta_b) \qquad (2.51)$$

where H_{sb} = significant breaking wave height, T_p= peak period, m_b =beach slope at breaking, D_{50}= median grain size, and θ_b = breaking wave angle.

2.5.17 Van Rijn (2014)

Van Rijn (2014) found that the LT is proportional to wave height to the power 3.1 ($\approx H^{3.1}$), to grain size to the power −0.6 ($\approx D_{n50}^{-0.6}$) and to beach slope to the power 0.4 ($\approx \tan\beta^{0.4}$). It is assumed that the longshore transport rate (kg/s) can be represented by the following expression:

$$Q_l = K \, \rho_s \, g^{0.5} (tan\,\beta)^{0.4} (D_{50})^{-0.6} (H_{sb})^{3.1} \, sin(2\,\vartheta_b) \qquad (2.52)$$

with K = calibration coefficient = 0.00018, ρ_s = sediment density, tanβ = slope of beach/surf zone, D_{50} = median grain size, H_{sb} = significant wave height at breaker line, θ_b = wave angle to shore normal at breaker line determined from:

$$sin\theta_b = (c_b/c_o)\, sin\, \theta_o \qquad (2.53)$$

with c_b = wave celerity at breaker line, c_o = wave celerity offshore, θ_o = offshore wave angle. Equation (2.52) does not account for the effect of the wave period on the longshore transport rate.

2.5.18 Discussion

It should be noticed that the most popular LT formulae (e.g. USACE, 1984) were developed predominantly for sandy, dissipative beach environments and have rarely been validated at beaches of coarser grain size or shingle beaches where a steeper slope results in a balance of hydrodynamic processes which is often very different from that at sandy beaches (van Wellen et al., 2000).

The GLT model and the Van Rijn (2014) expression represent the only two available general formulae in literature for the estimation of LT at sand, gravel and shingle beaches.

Tomasicchio et al. (2016) verified the predictive capability of the GLT model compared with the Van Rijn (2014) formula against two field and one laboratory data sets. Figure 2.22 shows the calculated and observed values of Q_{LT} together with the two considered intervals of confidence for GLT and Van Rijn (2014) formulae. It can be observed that the GLT model gives a better agreement with the observed data with respect to the Van Rijn (2014) formula.

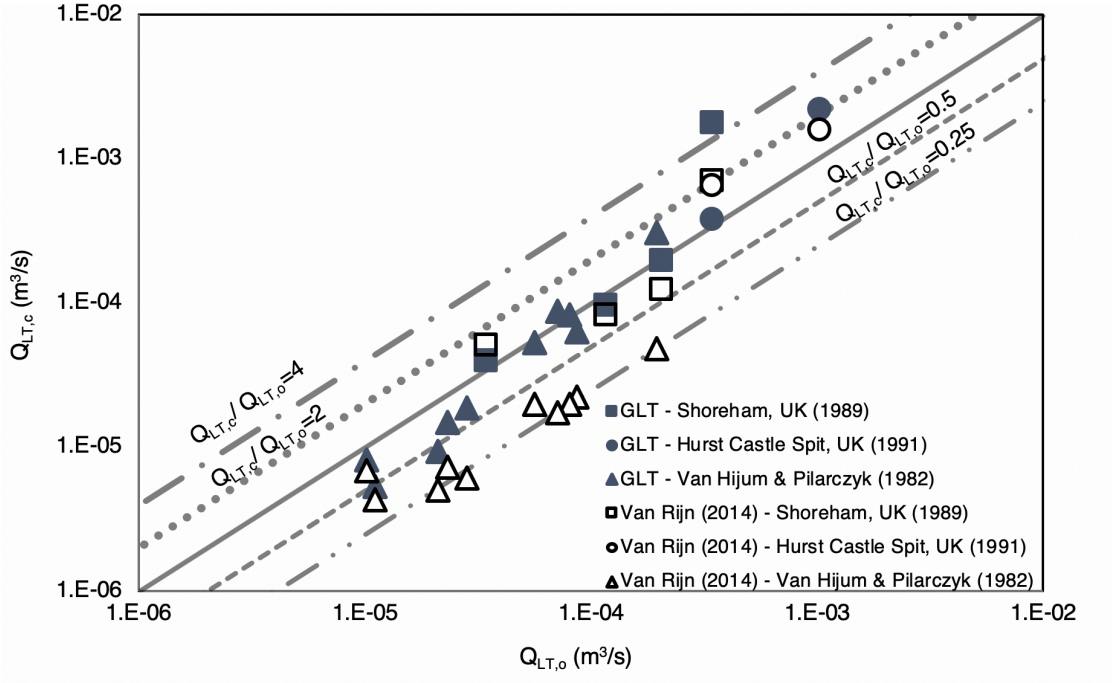

Figure 2.22 - Calculated versus observed LT (m^3/s) (Tomasicchio et al., 2015)

2.6 Cross-shore transport

Cross-shore transport refers to the cumulative movement of beach and nearshore sand perpendicular to the shore by the combined action of tides, wind and waves, and the shore-perpendicular currents produced by them. These forces usually result in an almost continuous movement of sand either in suspension in the water column or in flows at the surface of the seafloor. This occurs in a complex, three-dimensional pattern, varying rapidly with time. At any moment, some sand in the area of interest will have an onshore component while other sand is moving generally offshore (Seymour, 2005).

The accumulated effects of many storms during winter months and long intervals of low waves in summer can produce seasonal effects through cross-shore transport, as illustrated in Figure 2.23.

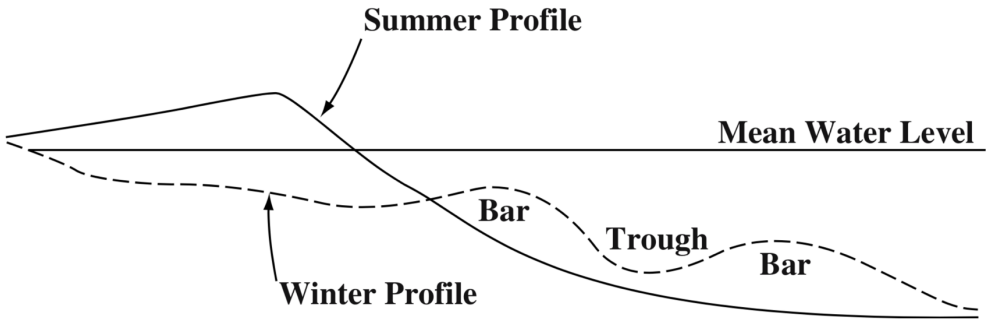

Figure 2.23 – Effects of the cross-shore transport on beach profiles (Seymour, 2005)

Bailard (1981,1982) proposed a method to calculate cross-shore sediment transport based on the energetics approach formulated by Bagnold (1966). Bailard described the component of the cross-shore sediment transport in the surf zone as functions of a combination of velocity moments, the local bottom slope, $\tan\beta$, and sediment parameters (friction coefficient, C_f, angle of internal friction, φ, and fall velocity, ω). The onshore–offshore transport is separated into bed and suspended load, q_b and q_s, expressed as:

$$q_b = \frac{c_f u_m^3}{g(s-1)(1-p)}\left\{\frac{\varepsilon_b}{\tan\varphi}\left(\psi_1 + \frac{2}{3}\delta_u - \frac{\tan\beta}{\tan\varphi}u_3^*\right)\right\} \qquad (2.54)$$

$$q_s = \frac{c_f u_m^3}{g(s-1)(1-p)}\left\{\frac{u_m}{\omega_s}\varepsilon_s\left(\psi_2 + \delta_u u_3^* - \frac{u_m}{\omega_s}\varepsilon_s \tan\beta\, u_5^*\right)\right\} \qquad (2.55)$$

with s = sediment density / water density; p = sediment porosity; ε_b = bed load efficiency coefficient, ε_s = suspended load efficiency coefficient (ε_b= 0.13, ε_s = 0.024, (Péchon and

Teisson, 1996)), u_m is the fluid bottom velocity, δ_u, u_m, ψ_1, ψ_2, u_3^*, u_5^*, are cross-shore velocity moments approximated as function of significant breaking wave height, H_{sb}, based on regression analysis of laboratory experiments as:

$$\delta_u = 0.00458 - 0.157\ H_{sb} C_q \qquad (2.56)$$

$$u_m = 0.319 + 0.403\ H_{sb} C_q \qquad (2.57)$$

$$\psi_1 = 0.303 - 0.144\ H_{sb} C_q \qquad (2.58)$$

$$\psi_2 = 0.603 - 0.510\ H_{sb} C_q \qquad (2.59)$$

$$u_3^* = 0.548 + 0.07333\ H_{sb} C_q \qquad (2.60)$$

$$u_5^* = 1.50 + 0.346\ H_{sb} C_q \qquad (2.61)$$

with C_q= empirical calibration factor for the net transport direction.

The friction coefficient is determined using the expression proposed by Kamphuis (1975) as:

$$c_f = 0.4 \left(\frac{a_b}{k_s}\right)^{-0.75} \qquad (2.62)$$

with a_b = water particle excursion and k_s = roughness coefficient (Péchon and Teisson, 1996) calculated as:

$$a_b = \frac{H_{sb}}{2 \sin h\ k\ d} \qquad (2.63)$$

$$k_s = 3\ D_{50} \qquad (2.64)$$

with k = wave number, d = water depth, and D_{50} the nominal sediment grain size.

The total cross-shore transport rate q_y, can be expressed as:

$$q_y = K_y(q_b + q_s) \qquad (2.65)$$

with K_y= empirical parameter, initially set 0.1 and adjusted during model calibration.

The energetic approach proposed by Bailard (1981,1982) was adopted in mathematical models as UNIBEST (Roelvink and Stive, 1989), SEDITEL (Péchon and Teisson, 1996), LITCROSS (Hedegaard et al., 1991).

2.7 Equilibrium beach profile

The study of cross-shore transport has led to the concept of the equilibrium beach profile (Bruun, 1954 and 1962; Dean, 1991).

Experimental observations in the wave flume show that an initial plane beach will eventually form an equilibrium beach under steady attack of a regular wave conditions. The equilibrium beach will remain unchanged with time. In the field, for a long-time scale of coastal processes, the beach profile also tends to a state of stabilization without any further erosion or accretion (Dang, 2006).

There are two types of equilibrium profile models: static and dynamic. The static profile models are used to average the profile shape (Bruun, 1954; Dean, 1977) and to evolve the profile shape upward and landward under storm surge conditions (Vellinga, 1982). The dynamic models allow the beach profile to vary with time from initial non-equilibrium profiles towards final equilibrium profiles (Bernabeu et al., 2003; Kriebel and Dean, 1985; Larson and Kraus, 1989; Larson and Kraus, 2000; Leontyev, 1996).

The basic properties of the equilibrium beach profile are (Dean 1991):

- They tend to be concave upwards.
- Smaller and larger sand diameters are associated with milder and steeper slopes, respectively.
- The beach face is approximately planar.
- Steep waves result in milder slopes and a tendency for bar formation.

Bruun (1954) suggested two mechanisms that could give an equilibrium profile: a constant net onshore shear stress component and a constant onshore component of the gradient of wave energy flux per unit area. Bruun (1962) first proposed the equilibrium beach profile as:

$$h(y) = Ay^{2/3} \qquad (2.66)$$

where $h(y)$= depth at distance from the shoreline y, and A = profile scale parameter related to the grain size distribution of the sand forming the beach. The scale parameter, A, controls the steepness of the profile, with increasing steepness for coarser sediments. This is an engineering simplification that assumes, under the constant incident wave, a particular beach will evolve toward a certain profile shape.

Dean (1977) provided a physical interpretation of this form in which the wave energy dissipation per unit water volume is uniform across the surf zone based on linear water wave theory.

Moore (1982) in his Master's degree thesis studied the correlation between the scale parameter *A* and the sediment size D_{50} using laboratory and field profiles, in which *A* is related graphically to the median grain size diameters D_{50} ranging from 0.1 mm to 300 mm (Figure 2.24).

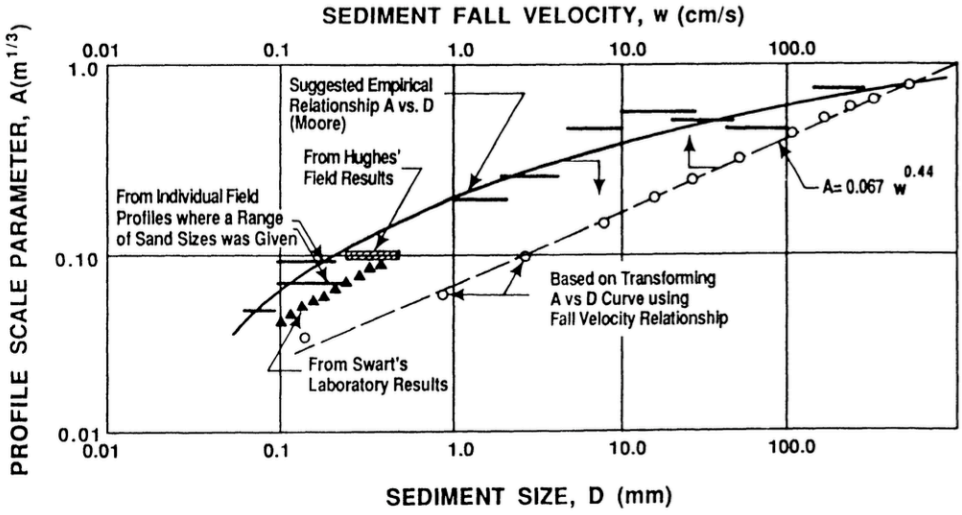

Figure 2.24 – Beach profile factor, A, vs sediment diameter, D_{50}, and Fall velocity, w, in relationship $h = Ax^{2/3}$ (Dean, 1987; modified from Moore, 1982)

As expected, the larger the sediment size D_{50}, the greater the *A* parameter and consequently the steeper the beach slope. Figure 2.25, Figure 2.26 and Figure 2.27 show several profiles used by Moore in establishing the relationship presented in Figure 2.24. Figure 2.27 is of particular interest as the sediment particle size ranges from 150 mm to 300 m.

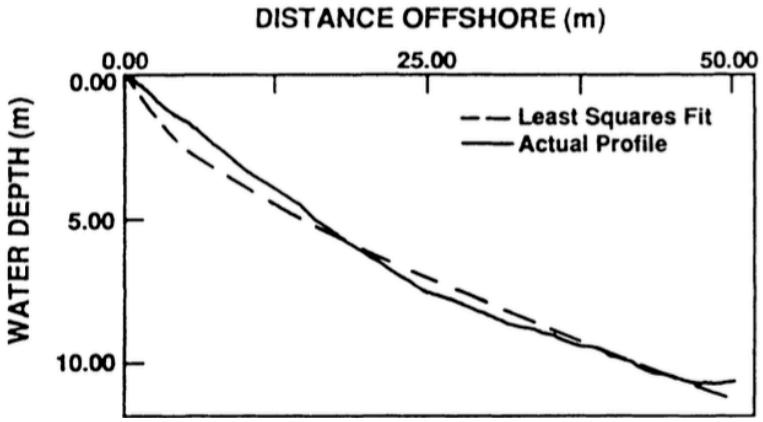

Figure 2.25 – Profile P4 from Zenkovich (1967). A boulder coast in Eastern Kamchatka. Sand diameter D_{50}=150 mm-300 mm. Least squares value of A = 0.82 $m^{1/3}$(Moore, 1982).

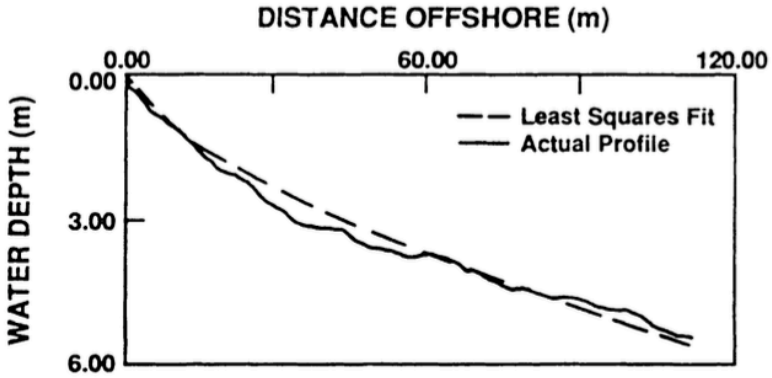

Figure 2.26 - Profile P10 from Zenkovich (1967). Near the end of a spit in western Black Sea. Whole and broken shells. A = 0.25 $m^{1/3}$(Moore, 1982).

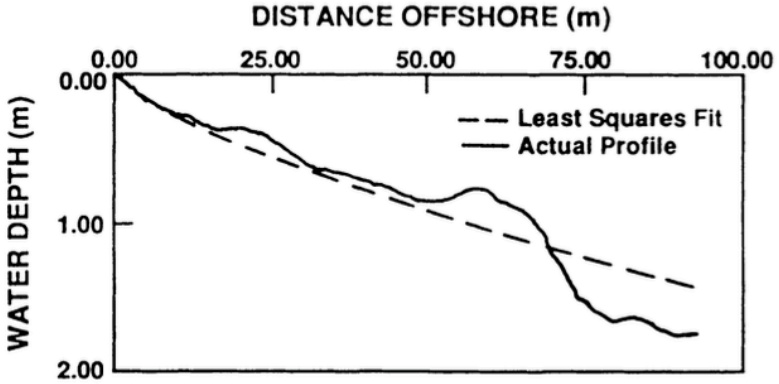

Figure 2.27 - Profile from Zenkovich (1967). Eastern Kamchatka. Mean sand diameter, D_{50}=0.25 mm. Least squares value of A = 0.07 $m^{1/3}$(Moore, 1982).

Dean (1987) proposed a relationship to correlate the scale parameter, *A,* to sediment fall velocity, *w,* as:

$$A = 0.067w^{0.44} \qquad (2.67)$$

Hanson and Kraus (1989) provide an analytical description of Moore's curve based on visual fit, proposing the following equations:

$$\mathrm{A} = 0.41(\mathrm{D}_{50})^{0.94}, \qquad D_{50} < 0.4\ mm \qquad (2.68)$$

$$A = 0.23(D_{50})^{0.32}, \quad 0.4\ mm \leq D_{50} < 10.0\ mm \qquad (2.69)$$

$$A = 0.23(D_{50})^{0.28}, \quad 10.0\ mm \leq D_{50} < 40.0\ mm \qquad (2.70)$$

$$A = 0.46(D_{50})^{0.11}, \qquad D_{50} \geq 40\ mm \qquad (2.71)$$

Bodge (1992) reanalyzed the profile data used by Dean (1987) finding the exponential function:

$$h(y) = B(1 - e^{-ky}) \qquad (2.72)$$

where B and k are empirical coefficients.

Komar and McDougal (1994) modified the formula proposed by Bodge (1992) to include the beach face slope (S_o) and the closure depth (d_c):

$$h(y) = \frac{S_o}{k}(1 - e^{-ky}) \qquad (2.73)$$

with:

$$k = \frac{1}{y_c}\left[\frac{3}{2} - \left(\frac{6d_c}{S_o y_c} - \frac{15}{4}\right)^{1/2}\right] \qquad (2.74)$$

and $y_c =$ cross-shore distance from the shoreline to the closure depth.

The concept of equilibrium profile is widely used in morphodynamics beach modelling.

3 MATHEMATICAL MODELS FOR COASTLINE EVOLUTION

In the last decades, a large number of mathematical models to reproduce the coastal processes have been developed. Larson (2005) presented a schematized description of the main elements for the development of a coastal numerical model (Figure 3.1) considering as a first step the formulation of a mathematical model consisting in the process identification and in the selection of equations to simulate the behaviour of a coast. A suitable numerical technique must be selected to solve the equation governing the problem. The evaluation step consists of verification, calibration, validation, sensitivity analysis and uncertainty estimation of the obtained results. Finally, the developed model can be applied to design, analyse, and predict a coastal intervention.

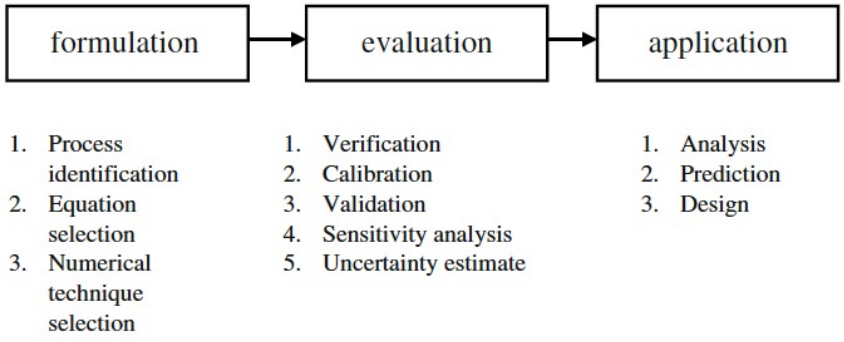

Figure 3.1 - Schematized description of the main elements in numerical model development (Larson, 2005)

Coastal processes cannot be represented by deterministic formulae, and there is high uncertainty in wave and sediment transport data (Kamphuis, 1999); for this reasons, numerous runs are required for sensitivity analysis, calibration and verification of the results (Dabees, 2000).

Classification of numerical models for coastal morphodynamics can be done in relation to the characteristic time and space scales of the process analysed: typical spatial scale and time periods can be in the ranges from meters to kilometres while temporal scales range from hours to decades. Arbitrary numbers and combinations of groynes, detached breakwaters, seawalls, jetties, and beach fills can be represented. Hanson and Kraus (1989) and Larson and Kraus (1995) presented an overview of different coastal evolution models based on characteristic space and time scales (Figure 3.2).

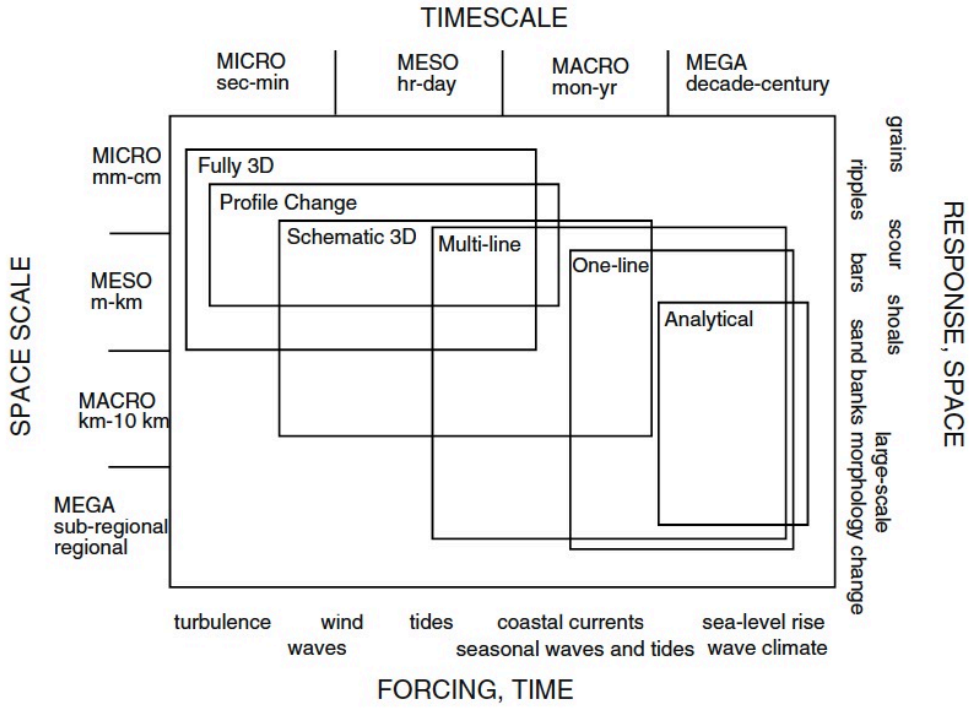

Figure 3.2 - Classification of coastal evolution models in terms of characteristic spatial and temporal scales (Hanson and Kraus, 1989; Larson and Kraus, 1995)

Coastal erosion is influenced by both longshore and cross-shore processes; the prediction of beach changes can be simplified by separating the longshore and cross-shore processes (Miller and Dean, 2004), defining two categories of models:

a. Planform evolution models;
b. Beach profile evolution models.

Shoreline change models only consider longshore sediment transport and appear to be more suitable for the majority of engineering applications in large coastal stretches, modelling long-term morphology evolution in the presence of coastal structures and shore protection methods; they need fewer input data to run (Samaras and Koutitas, 2014).

Beach profile models are mainly used to study short term processes, since they are able to evaluate the profile response produced by severe storms or hurricanes, and initial adjustment of beach fills to wave action and fill loss during a storm (Kriebel and Dean, 1985; Larson and Kraus, 1989). These models only consider cross-shore sediment transport neglecting any differentials in the longshore sediment transport. The cross-shore beach is described by one profile solely, sufficient to evaluate the evolution. The typical timescale of profile response models is hours to days for a storm event. A monthly timescale is used to simulate the profile evolution after a beach recovery or fill adjustment (Larson, 2005).

The most widely used models of the above categories are:

a. GENESIS (Hanson, 1989), ONELINE (Dabees and Kamphuis, 1999), UNIBEST-CL+ (WL | Delft Hydraulics, 1999), Litpack (DHI—Danish Hydraulic Institute, 2003), Beachplan (Blanco, 2003) and SMC (González et al., 2007) for shoreline change modelling;
b. EDUNE (Kriebel, 1982), Dally–Dean model (Dally and Dean, 1984), SBEACH (Larson and Kraus, 1989), UNIBEST (Roelvink and Stive, 1989), LITCROSS (Hedegaard et al., 1991) COSMOS (Southgate and Nairn, 1993), CROSMOR2000 (Van Rijn and Wijnberg, 1996), CIIRC (Rivero et al., 1993), and BEACH1/3D (O'Connor et al., 1998), XBeach (Roelvink et al., 2011), for beach profile change modelling;

Each of the aforementioned models is suitable for different applications and is subject to different limitations regarding its use. Differences in the above-listed shoreline models will be discussed in the following chapter.

3.1 Planform evolution modelling: one-line theory

The one-line theory enables calculation of coastline evolution for a wide range of coasts, waves, coastal structures, and boundaries. The first mathematical theory to calculate the response of a beach to waves was proposed by Pernald-Considere (1956) with the objective to describe long-term variations in shoreline position (Larson et al., 1987).

Price et al. (1973) implemented for the first time the one-line theory numerically and many others followed (Rea and Komar, 1975; Horikawa et al., 1979; Willis, 1977; Perlin, 1979; Mimura et al., 1983; Hanson, 1989; Hanson and Kraus, 1989). Price et al. (1973) attempted to predict the changes in plan shape of a beach following the construction of groynes. They used the equation proposed by the Scripps Institute of Oceanography (1947) and modified by Komar and Inman (1970) to quantify the longshore sediment transport and applied to simulate the shore changes during an experiment conducted in the wave basin reporting good agreement between prediction and measurement.

The one-line theory was used by Grijm (1961) to derive analytic solutions for delta formations from rivers discharging sand.

Bakker and Edelman (1965) investigated the possibilities of closed-form solutions of river delta evolution, assuming different sand transport equations.

Bakker (1969) extended the one-line theory to consider two lines representing the shoreline and the offshore contour. This two-line theory allows for onshore-offshore sediment transport and change in beach slope.

Sasaki (1973) developed two models for nearshore environments: the first model predicts coastal evolution behind a detached breakwater parallel to the coast and the second simulates current in the nearshore zone under the influence of arbitrary bottom topography. These models were tested both in the laboratory and in the field.

Le Mehaute and Soldate (1977) presented some analytic solutions and compared the principles of the one-line and two-line theories with emphasis on long-term evolution. Le Mehaute and Soldate (1980) developed a numerical model for shoreline evolution combining the effects of variation in sea level, wave refraction, wave diffraction, loss of sand by density currents, rip currents and bluff erosion and berm accretion, groynes and beach nourishment. The model was applied to a test case of Holland Harbour, Michigan and model obtaining reasonable results.

Perlin (1979) presented a mathematical model to predict beach the coastal evolution behind of detached breakwaters.

Ozasa and Brampton (1980) attempted to simulate the evolution of a coastal evolution observed during the physical model study of a bay in Japan. They calculated the longshore sediment transport taking into account the sediment transport due to oblique breaking waves and that due to the gradients in longshore wave height.

Kraus and Harikari (1983) used the one-line model to simulate the long-term shoreline changes on sandy beaches adjacent to Oarai Harbour, Japan. They calculated the breaking wave height and angle considering the combined refraction and diffraction effects and comparing the results with field measurements.

Larson et al. (1987) presented analytic solutions for the shoreline evolution on sandy beaches protected by different types of coastal structures.

The one-line concept is based on the hypothesis that the profile shape is assumed to remain constant and the shoreline can be used to represent the coastal change. The bottom contours are parallel during the entire simulation, and the profile translates in the onshore and offshore direction as result of erosion or accretion of the modelled coast. This assumption is satisfied if the cross-shore profile is in equilibrium. This assumption is rarely satisfied in short time simulations where storms produce an extreme change of the coastline. A second assumption is that the longshore sediment transport happens over the active beach profile, defined as the sum of the closure depth, d_c, and the berm height, d_b (Figure 3.3).

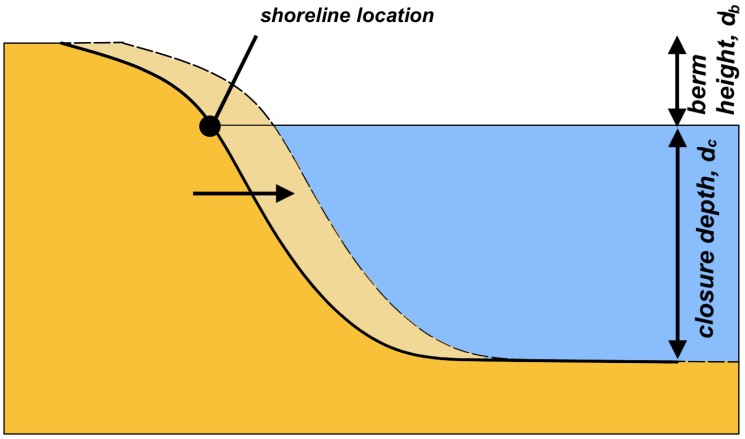

Figure 3.3 - Beach profiles change and shoreline location in one-line models.

The relation between accretion/erosion of the coast and the longshore transport can be formulated considering the continuity equation of sediment in a control volume (Figure 3.4).

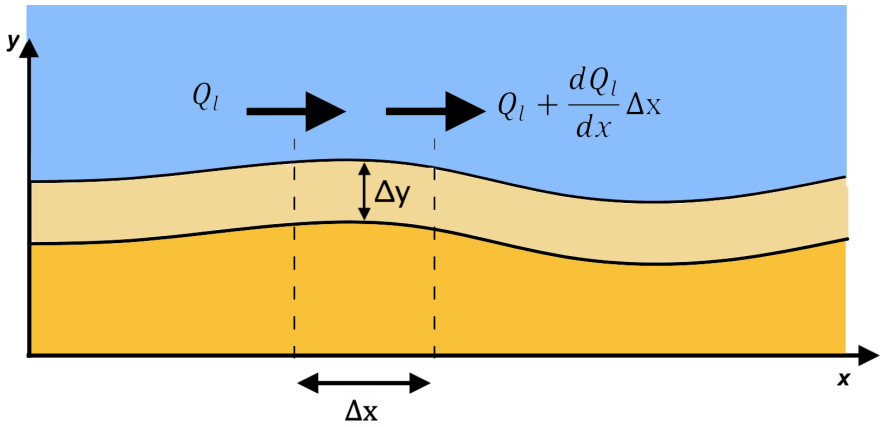

Figure 3.4 – Longshore sediment transport and coastal accretion/erosion (Fredsoe and Deigaard, 1992)

The coastline displacement Δy during a short interval Δt produces a volume of accumulated sediment over the distance Δx equal to:

$$\Delta x \Delta y (d_b + d_c)(1 - n) \qquad (3.1)$$

with n = sediment porosity.

The net sediment inflow during the time Δt is:

$$\left(Q_l - \left(Q_l + \frac{\partial}{\partial x}\frac{dQ_l}{dx}\Delta\mathrm{x}\right)\right)\Delta t = -\frac{dQ_l}{dx}\Delta\mathrm{x}\Delta t \qquad (3.2)$$

If it is assumed that the accretion/erosion in only due to the longshore sediment transport, Q_l, Equation (3.1) and Equation (3.2) give the continuity equations:

$$\frac{\Delta\mathrm{y}}{\Delta\mathrm{t}}(1-n)(d_b + d_c) = -\frac{\Delta Q_l}{\Delta\mathrm{x}} \qquad (3.3)$$

with Q_l = longshore transport rate. Spatial and temporal variations in gradients in longshore transport drive advance or retreat of the shoreline. The model requires predictive expressions for the longshore sediment transport rate.

3.1.1 Numerical methods

Solving the model equations, which generally constitute a set of ordinary or partial differential equations, requires numerical methods. A range of methods have been developed, and each one has its strengths and weaknesses (Abbott, 1979). The most common numerical methods in coastal applications are based on finite elements or finite differences.

Finite element methods use spatial discretization of the solution domain into elements of a selected shape, and the variable of interest is interpolated over the element through a given approximating function (Larson, 2005). This function is obtained based on values of the variable defined at the nodes located in the element corners. Finite element methods are convenient for solving steady-state problems over solution domains of complex geometry where the variable of interest exhibits large spatial variability. An example from coastal applications is diffraction around structures in the nearshore.

Finite difference methods have been utilized more frequently in coastal models because they are fairly simple in the formulation of the equations to be numerically solved and they handle time-dependent problems in a direct way. Finite difference method consists of discretising the problem domain into rectangular elements identified with discrete points or nodes. In these methods, derivatives are written in terms of differences resulting in a set of algebraic equations to be solved. If the approximations of the derivatives are formulated in such a way that the variable of interest can be directly calculated at the next time level (or adjacent space level), the solution scheme is explicit. In cases where the difference scheme involves several time

(space) levels simultaneously, making it necessary to employ iterative techniques in solving for the desired variable, the scheme is implicit (Larson, 2005).

Figure 3.5 shows the finite difference scheme of coastline position and transport rates (Horikowa, 1988).

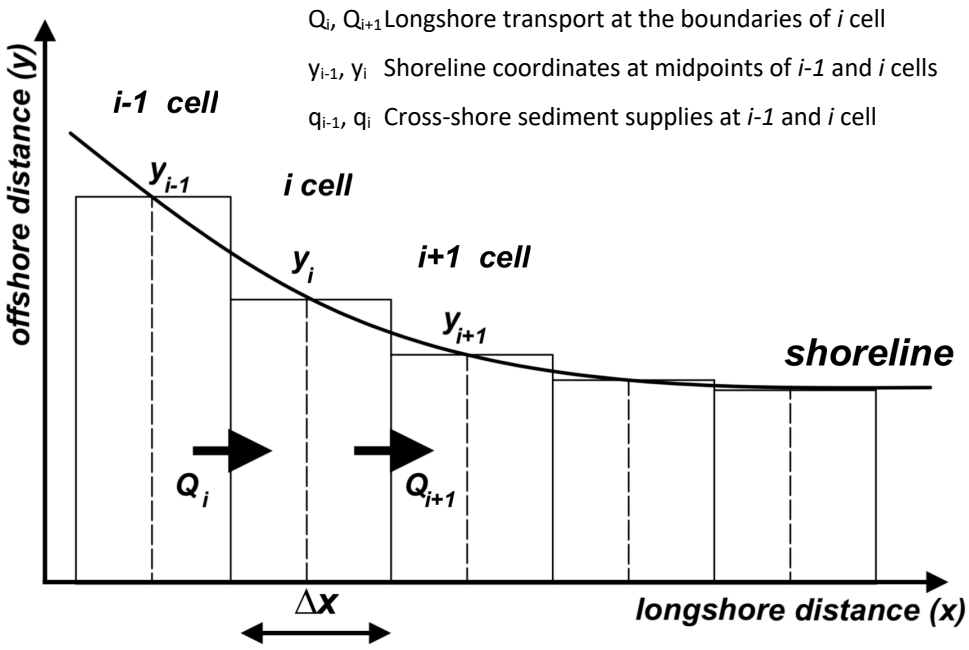

Figure 3.5 – Grid specifications for finite difference scheme (modified from Horikowa, 1988)

In the numerical models of coastline change, the continuity Equation (3.3) is converted to finite difference forms using a typical staggered grid representation as:

$$\frac{y_i' - y_i}{\Delta t} = \lambda \left(\frac{\partial y}{\partial t}\right)_i + (1-\lambda)\left(\frac{\partial y}{\partial t}\right)_i' \qquad (3.4)$$

$$\left(\frac{\partial y}{\partial t}\right)_i = -\frac{1}{d_p}\left(\frac{Q_{i+1} - Q_i}{\partial y}\right) \qquad (3.5)$$

$$\left(\frac{\partial y}{\partial t}\right)_i' = -\frac{1}{d_p}\left(\frac{Q_{i+1}' - Q_i'}{\partial y}\right) \qquad (3.6)$$

where Δt is the time step, i and prime (′) denote the cell number and variables in the next time step, respectively, and λ ($0 \leq \lambda \leq 1$) is a parameter for selected numerical schemes.

For the coastline change models, explicit and implicit scheme can be used depending on the selected λ. For explicit schemes, when $\lambda = 1$, the shoreline can be directly computed as:

$$y_i' = y_i + \frac{1}{d_p}\frac{\Delta t}{\Delta y}(Q_i - Q_{i-1}) \qquad (3.7)$$

The implicit schemes compared to the explicit schemes permit the use of longer time steps of integration. The shoreline change problem being non-linear, the maximum allowable time step to preserve stability can only be determined by trial and error procedure. However, a useful stability criterion can be obtained satisfying the Courant's condition to maintain numerical stability (Courant et al., 1967).

For implicit scheme, when λ = 0.5, the solution is unconditionally stable but is more complicated to program than explicit schemes. Further reading for the implicit and explicit finite difference schemes for shoreline change modelling can be found in Kamphuis (2010).

3.2 Multi-line evolution modelling

In the 1970s, multi-line models got significant attention. Multi-line models schematize a beach profile by an arbitrary number of contour lines. Figure 3.6 (in which the third dimension denotes the time) shows an example of coastal change performed by a 6-line numerical model (Smith, 1988).

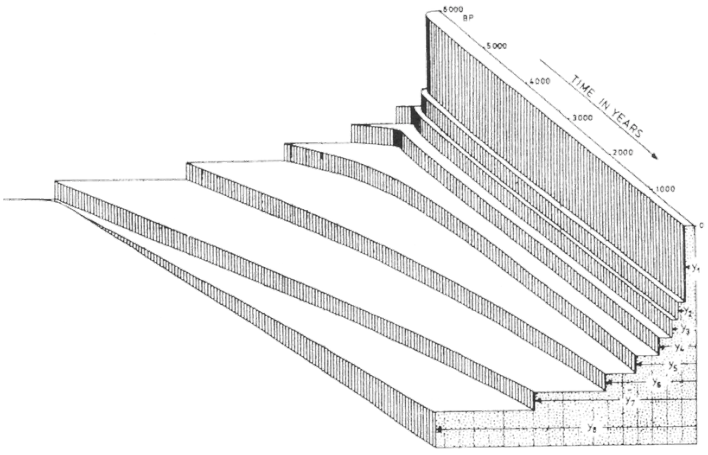

Figure 3.6 - 6-line model (Smith, 1988)

Bakker (1968) developed a two-line model and studied a beach profile change due to longshore and on-offshore sediment transport near a jetty.

Van Overeem (1978) extended concept of two-line model to n-line model for the computation of coastal changes caused by waves and currents.

Perlin and Dean (1983) developed a n-line model to evaluate the beach change response to coastal structures for a monotonic profile using both longshore and cross-shore sediment transport.

The popularity of those kind of models has remained limited (Bakker, 2013). Multi-line models resulted able to predict beach changes. However, this kind of models have not reached the stage of wide application, due to their complexity, requirement for considerable computational resources and need for expertise in operational application (USACE, 1984). The one-line models have proved the most robust and popular for applications due to their stability to small perturbations in beach position (Reeve and Valsamidis, 2014).

3.3 Cross-shore evolution modelling

Coastal profile models simplify the coastal system to a 2D system (elevation and cross-shore distance) and assuming longshore uniformity. These models commonly include wave shoaling, energy loss due to depth-limited wave breaking and bottom friction, cross-shore undertow, tidal currents and sediment transport (Sutherland, 2019).

Swart (1974) studied the beach profiles through laboratory investigations identifying erosive and accretive profiles and relating profile geometry to incident wave conditions and sediment characteristics. A cross-shore sediment transport equation was proposed where the rate was proportional to a geometrically defined deviation from the equilibrium profile shape. A mathematical model was proposed based on the derived empirical relationships and applied to a beach fill case.

Felder (1978) and Felder and Fisher (1980) developed a mathematical model dividing the cross-shore profile into regions using specific transport relationships and simulating the response of the bars to wave action. They found that, in the surf zone, the transport rate depends on the velocity of a solitary wave.

Nilsson (1979) developed a model based on the bars formed by partially reflected Stokes wave groups.

Dally (1980) and Dally and Dean (1984) proposed a model of beach change, assuming that suspended transport is dominant in the surf zone. The cross-shore broken wave height distribution determined by the model supplied the driving mechanism for profile change. An exponentially shaped profile was assumed for the sediment concentration through the water column.

Shibayama and Horikawa (1980) proposed a sediment transport equation for bedload and suspended load based on the Shields parameter. The equations were applied into a mathematical model and verified in the offshore region. The model was unable to describe profile change in the surf zone.

Moore (1982) developed a mathematical model to predict profile change produced by breaking waves. The transport rate is proportional to the dissipation of energy due to breaking waves per unit water volume above an equilibrium value. The calculated profile approximated an equilibrium shape in accordance with the observations of Bruun (1954).

Kriebel (1982) and Kriebel and Dean (1984) developed a model to predict beach erosion using the transport relationship of Moore (1982). The amount of eroded sediment was determined primarily by water level variation, and breaking wave height was entered only to determine the width of the surf zone. The model was verified both against data from large wave tank experiments and from natural beaches taken before and after Hurricane Eloise. The model was also applied to predict erosion rates at Ocean City, caused by storm activity and sea-level rise (Kriebel and Dean, 1984).

Watanabe (1982) developed a two-dimensional model for simulating wave, nearshore current and beach profile changes. Wave transformation was computed from conservation of energy flux. Nearshore currents were computed from depth-averaged momentum and continuity equations. The empirical formula proposed by Komar (1977) was modified to compute local longshore sediment transport. A new formula for computing cross-shore sediment transport was developed on the base of laboratory results of Watanabe et al. (1980).

Sunamura (1983) developed a simple mathematical model of beach morphological change caused by short-term events and described both erosion and accretion phases of a beach in the field. Balsillie (1984) developed a model relating longshore bar formation to breaking waves from field data, to predict profile erosion produced by storm and hurricane activity.

Stive and Battjes (1985) developed a model for cross-shore sediment transport and beach profile deformation under irregular waves assuming the suspended as the dominant factor of sediment transport. The wave model of Battjes and Janssen (1978) was used to compute wave height transformation. They verified the model against the laboratory measurements of profile evolution produced by random waves. Stive (1987) extended the model to include the effects of asymmetry in the velocity field from the waves.

Shibayama and Horikawa (1985) developed a numerical model for computing cross-shore beach transformation. Computation of wave height was based on energy flux conservation by using nonlinear wave theory in the offshore zone and by using the energy dissipation model of

Mizuguchi (1980) inside the surf zone. The model was verified by laboratory experiments in a small-scale wave flume.

Boczar-Karakiewicz and Davidson-Arnott (1987) developed a model to predict the generation of bars comparing the results with field data. In the model, the mass transport velocities associated with the primary wave and the second harmonic were used to calculate net sediment flux across a two-dimensional profile. Model predictions of bar number and spacing, starting with an initially planar slope, correlate well with the field measurements, for the two sets of wave conditions and mean slopes. The model was able to predict seasonal profile changes.

Larson et al. (1988) used two field data sets (18 cases from the US Army Corps of Engineers Water Experiment Station and 24 cases from the CRIEPI, Japan) to develop and verify a mathematical model to simulate beach profile change in the surf zone produced by wave-induced cross-shore sand transport. This model simulated the dynamics of berms and bars at the wave breaking point.

Larson and Kraus (1989) developed the Storm-induced BEAch Change (SBEACH) numerical model based on physical principles to calculate beach and dune erosion under storm water levels and wave action. SBEACH is applicable to the dune, beach face and surf zone and could not predict sediment movement under the nonbreaking waves. Calculations can be performed under both monochromatic and random wave conditions.

Hedegaard et al. (1991) and Skou et al. (1991) developed a deterministic model for predicting the morphological evolution of a coastal profile. The model established the interaction between hydrodynamic conditions and bed-level evolution. The cross-shore profile changes are described by the solution of the bottom sediment continuity equation based on the sediment transport rates.

Rattanapitikon and Shibayama (1996) developed a numerical model for computing beach profiles under regular wave condition. The proposed model separates the computation of suspended load and bedload. The model of Dally et al. (1984) was modified and used to calculate wave height transformation. The beach profile change was computed from the conservation of sediment mass.

Zheng and Dean (1997) developed a model called CROSS based on equilibrium concepts and is calibrated using wave flume tests on profile evolution.

Miller and Dean (2004) developed a model to predict beach profile changes. In this model, several possible forms of rate parameters incorporating local wave and sediment properties were considered and evaluated.

Jayaratne (2004) developed a model based on the energetic approach. The efficiency factors in theoretical models were calibrated using small-scale and field-scale data from regular wave experiments.

Kobayashi et al. (2008) proposed different formulae to predict cross-shore suspended load and bedload transport rates; these formulae were incorporated into a model to predict profile changes for an arbitrary initial beach profile (CSHORE model). The beach profile evolution model was verified with small-scale and large-scale test data.

Roelvink et al. (2011) reported a nearshore process model (XBeach) as a numerical tool to compute the natural coastal response during time-varying storm and hurricane conditions, including dune erosion and overwash. The model consists of formulations for short wave envelope propagation, long wave transformation (generation, propagation and dissipation), nonstationary shallow water equations, sediment transport and bed update. The model has been validated with a series of analytical, laboratory and field test cases.

3.3.1 Numerical methods

The profile change due to cross-shore sediment transport is calculated as a function of the local bottom elevation, the sediment grain size, and the wave characteristics. It is supposed that the changes in the bottom profile have little effect on the hydrodynamics.
The beach profile change is computed using the continuity equation:

$$\frac{\partial z_b}{\partial t} = -\frac{1}{(1-n)}\frac{\partial q_t}{\partial x} \qquad (3.8)$$

with n = sediment porosity, z_b = bed level, q_t = total suspended sediment transport rate from bottom to wave crest calculated as:

$$q_t = \int_{-\delta_s}^{d_t+H} c(z)u_s(z)dz \qquad (3.9)$$

with δ_s = elevation below the bottom surface where there is no effective movement of sand particles, d_t is the depth at wave trough, H = wave height, $c(z)$ = vertical distribution of sediment concentration, $u_s(z)$ = vertical distribution of flow velocity.
Equation (3.8) can be solved using the finite difference method, as:

$$h_i^{k+1} = h_i^k - \frac{\Delta t}{2(1-n)\Delta x}\left(q_{ti+1}^k - q_{ti-1}^k\right) \qquad (3.10)$$

with i = numerical cell number, k = time-step number, h = still water level, Δt = time step, and Δx = grid size. Figure 3.7 illustrates the definition sketch of numerical cell for computing wave height, water depth and sediment transport rate

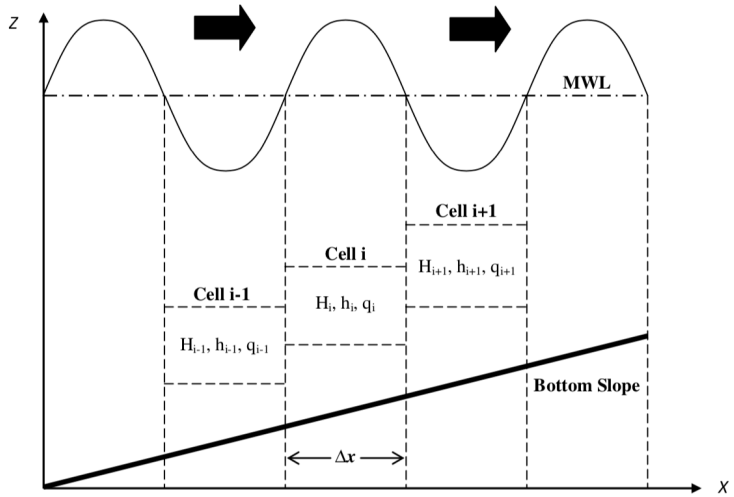

Figure 3.7 - Definition sketch of numerical cell (Jayaratne et al., 2014)

3.4 3D modelling

3D models couple a sediment transport model with a hydrodynamics model, which solves the equations of continuity and momentum over a 3D grid to describe wave action, water levels and currents. The term 3D is exceptionally used in the literature referring to quasi-3D models (Q-3D), coupling two-dimensional horizontal (2DH) and vertical (2DV) models in order to simulate coastal morphology evolution due to both longshore and cross-shore sediment transport.

Watanabe (1985) developed for the first time a complete three-dimensional model for predicting the medium-term beach evolution, involving nearshore waves, currents, sediment transport and beach evolution. Different coastal area models using Q-3D nearshore current model have also been proposed (De Vriend et al., 1989; Briand and Kamphuis, 1993; Ranasinghe et al., 1999). However, the previous models are not sufficiently examined in the field site.

Kuroiwa et al. (2001), have also proposed a morphodynamic model based on Q-3D nearshore current model named the Q3D-ISE (Initial Sedimentation/Erosion) model. The

model has been applied to the prediction of nearshore currents and seabed level changes around a harbour in the field. The accuracy of the model has been inadequate due to the effects that were not taken into account of the wave decay, recovery and secondary breaking process on the arbitrary beaches such as sand bars, the irregularity of waves and the suspension, advection-diffusion and settling processes for sediment particles.

Development of 3D-beach change models is limited by our capability to predict wave climates and sediment transport rates and requires careful consideration of the processes to be simulated and their characteristic scales (Larson, 2005). Simplified assumptions are made in schematic 3D-models, for example, to restrict the shape of the profile or to calculate global rather than point transport rates.

The most common 3D models are:

- The quasi 3D sediment transport model introduced by Rakha (1998);
- The 3D open channel flow hydrodynamic and sediment transport model CH3D, used by the US Army Corps of Engineers and described in Gessler et al. (1999);
- The sediment transport module included in the MIKE models commercialized by DHI (Zyserman and Ronberg, 2001; Lumborg and Windelin, 2003; Lumborg, 2005);
- ECOM-SED, which is a model commercialized by Hydroqual (Hydroqual, 2002);
- The sediment transport module included in DELFT3D (Lesser et al., 2000; van Rijn and Walstra, 2003; Lesser et al., 2004);
- The 3D model for sediment transport in open channels developed at the University of Karlsruhe, Germany (Wu et al., 2000; Fang and Rodi, 2003);
- The coastal sediment transport model developed by Wai et al. (2004);
- The NOPP community sediment transport model, incorporated in ROMS (Warner et al., 2005; Blaas et al., 2007; Warner et al., 2008).
- The sediment transport model (Sisyphe) incorporated in TELEMAC-3D system (Villaret, 2010; Villaret et al., 2013).

The 3D models generally include different flow modules (from 1D to 3D), a wave propagation model and a sand transport model including bedload and suspended load. An extensive review of the above models has been conducted by Amoudry (2008).

4 EXISTING ONE-LINE NUMERICAL MODELS

In the last decades, analytical and numerical models were commonly used to predict the long-term coastline changes (Komar, 1998). Since the 1980s, dozens of different models were developed to simulate coastline change since the first one-line model was proposed by Pernald-Considerè in 1956 (Dean, 2003). The most popular one-line models are:

- GENESIS (Hanson, 1989, Hanson and Kraus, 1989);
- GENCADE (Frey et al., 2012);
- ONELINE (Dabees and Kamphuis, 1999);
- UNIBEST-CL+ (WL | Delft Hydraulics, 1999);
- LITPACK (DHI - Danish Hydraulic Institute, 2003);
- BEACHPLAN (Blanco, 2003);
- SMC (González et al., 2007).

In the present chapter, the above-listed one-line models are described, underlining the main differences and similarities between them.

4.1 **GENESIS** (Hanson, 1989; Hanson and Kraus, 1989)

GENEralized model for SImulating Shoreline change (GENESIS) was developed by Hanson (1987) in cooperative research with the Department of the Army (CERC). GENESIS is a one-line model used to simulate the long-term shoreline change at coastlines 1 to 100 km long over a period of months to years caused primarily by wave action (Hanson, 1987; Hanson and Kraus, 1989; Gravens et al., 1991).

Off-shore wave conditions can be used as input, and the wave module calculates the breaking wave conditions along the modelled coastline. Wave module is based on the linear wave theory with the assumption of a uniformly bottom and parallel contours. Diffraction is included in the calculation of waves characteristics for grid cells located in the lee of diffractive structures. Breaking wave parameters are calculated and used in the transport module.

The coastline change is simulated on the basis of spatial and temporal variability in longshore sediment transport. The computation of the longshore sand transport volume rate is based on an extension of CERC-formula (USACE, 1984) that includes the effects of longshore gradient in wave height (Ozasa and Brampton, 1980), and it is calculated as:

$$Q = \left(H^2 C_g\right)_b \left(a_1 \sin 2\vartheta_b - a_2 \cos\vartheta_b \frac{\partial H_b}{\partial x}\right) \qquad (4.1)$$

where C_g is the wave group velocity (m/s), ϑ_b is the angle of wave crests to the coastline, with the subscript b for the breaking condition, and the non-dimensional parameters a_1 and a_2 are given by:

$$a_1 = \frac{K_1}{16(\rho_s/\rho - 1)(1-p)1.416^{5/2}} \quad (4.2)$$

$$a_2 = \frac{K_2}{8(\rho_s/\rho - 1)(1-p)\tan\beta\, 1.416^{7/2}} \quad (4.3)$$

where K_1 and K_2 are the calibration parameters, ρ_s and ρ are the densities of sediment and water, p is the sediment porosity, and $\tan\beta$ is the average bottom slope from the coastline to the depth of longshore transport.

K_1 and K_2 coefficients have to be adjusted to match measured position of coastline change (Hanson and Kraus, 1989). In the Shore Protection Manual (CERC, 1984) it is recommended K_1 = 0.77 and K_2 in the range of $0.5\ K_1 \leq K_2 \leq 1.0\ K_1$.

Groynes, jetties and detached breakwaters on long-term coastline evolution can be modelled in GENESIS, including two types of sand movement past the structures, bypassing and transmission.

As discussed by Gravens (1991, 1992), preparation of the input data files occupy the majority of the time spent on a detailed coastline change modelling project. GENESIS requires input including the definition of the domain in time and space, wave characteristics at known water depth, coastal structure configurations, values of model calibration coefficient, and calculation time step.

Output information are the intermediate and final calculated coastline position and the net and gross longshore transport rate.

Figure 4.1 shows a simulation performed with GENESIS by Hanson and Kraus, (1989), where the coastline response behind a detached breakwater in function of wave transmission is presented.

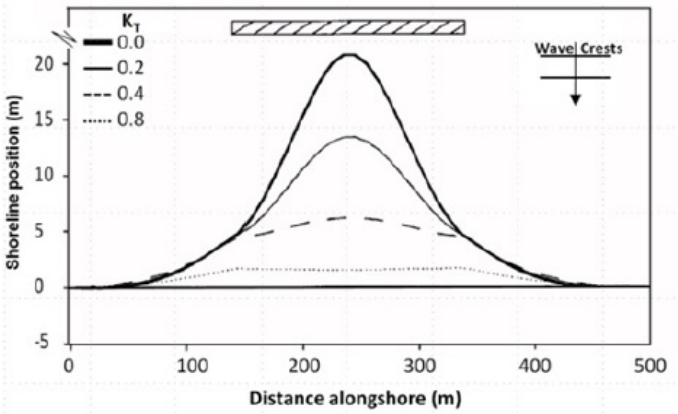

Figure 4.1 - Coastline response inside of a detached breakwater as a function of wave transmission (Hanson and Kraus, 1989)

GENESIS is currently available in two major versions: a code with an implicit numerical solution scheme and a code with an explicit solution scheme, specifically to investigate tombolo formation (GENESIS-T) (Hanson and Kraus, 2004). GENESIS can be operated within the US Army Corps of Engineers (USACE) Surface-Wave Modeling System (SMS) user interface.

4.2 **GENCADE** (Frey et al., 2012)

Frey et al., (2012) combined GENESIS and Cascade (Larson et al., 2002), a regional-scale planning model developed by Larson et al. (2002) giving as a result a new model named GenCade. In Figure 4.2 the capabilities of the combination between GENESIS and Cascade models are presented (Frey et al., 2012).

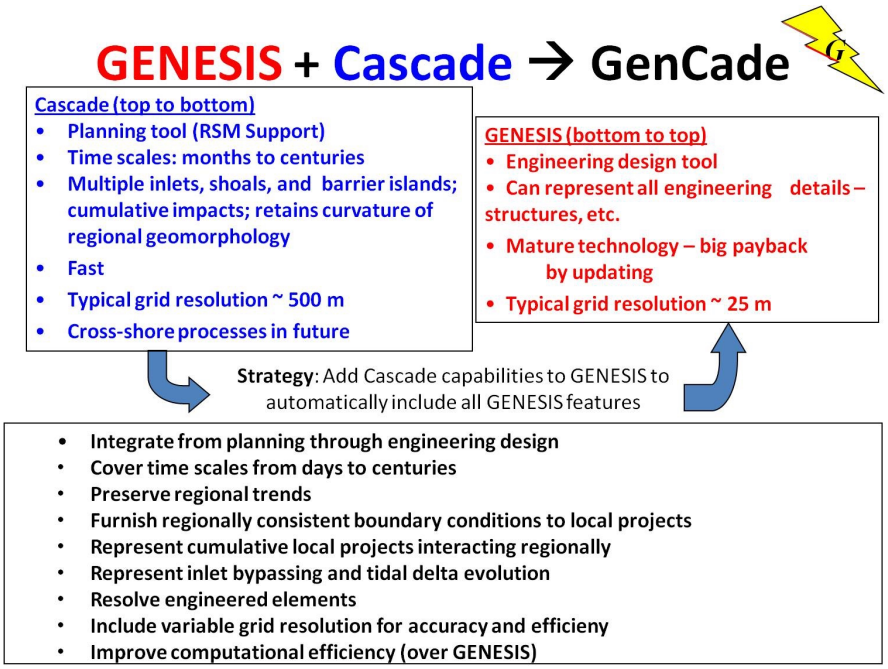

Figure 4.2 – Combination between GENESIS and Cascade (Frey et al., 2012)

Technical documentations about the GENESIS and GenCade features are available in Hanson (1987); Hanson and Kraus (1989); Gravens et al. (1991); Hanson and Kraus (2004); Frey et al. (2012).

4.3 **ONELINE** (Dabees and Kamphuis, 1999)

ONELINE was developed at Queen's University on the base of the one-line theory. The coastline change modelling system provides practical and reliable full, time-dependent simulations of coastline change for coasts controlled by structures and complex boundary conditions (Dabees and Kamphuis, 1999). ONELINE does not make any small angle assumption with respect to the incident wave angle and the coastline direction. (Dabees and Kamphuis, 1999). Figure 4.3 shows the model structure of ONELINE:

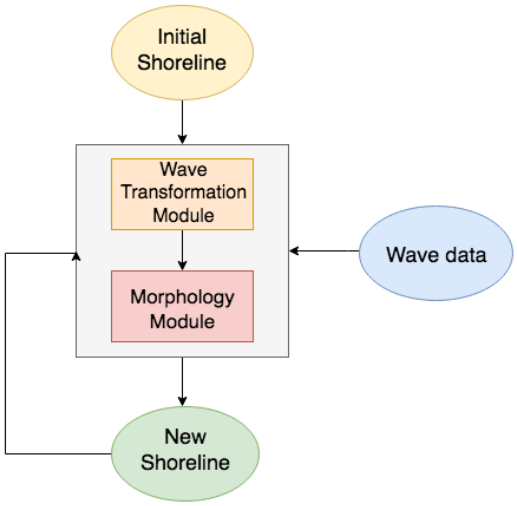

Figure 4.3 - ONELINE model structure

A finite grid is defined longshore to discretize the initial coastline; the simulation time is divided into time steps. For each time step wave shoaling, refraction, diffraction are calculated at each grid point.

Longshore sediment transport rate is computed with the formula proposed by Kamphuis (1991) modified to include transport by alongshore gradient in the wave height (Ozasa and Brampton, 1980) as following:

$$Q_l = C\ K\ H_b^2\ T^{1.5}\ \beta^{0.75}\ {D_{50}}^{-0.25}\left(\sin^{0.6}(2\alpha_b) - \frac{2}{\beta}\cos\alpha_b\frac{\partial H_b}{\partial x}\right) \qquad (4.4)$$

where Q_l is the longshore sediment transport rate, C is a constant that is 7.3 when Q_l is expressed in $m^3/hr.$, K is the ratio of actual over potential sediment transport rate (used an

empirical factor for model calibration), H_b is the breaking wave height, T is the wave period, β is the beach slope in the breaking zone, α_b is the wave angle at breaking, and D_{50} is the nominal grain size.

The cross-shore sediment transport contribution is included in the computation of the coastline change. Cross-shore sediment transport is calculated using a model proposed by Bailard (1982):

$$q = k_s \frac{\rho C_f u_b^3}{(\rho_s - \rho) g p} \left\{ \frac{\varepsilon_B}{\tan\varphi} \left(\Psi_1 + \frac{2}{3}\delta_u - \frac{\tan\beta}{\tan\varphi} u_3^* \right) + \frac{u_m}{\omega_s} \varepsilon_s \left[\Psi_2 + \delta_u u_3^* - \frac{u_o}{\omega_s} \varepsilon_S \tan\beta u_5^* \right] \right\} \quad (4.5)$$

where δ_u, $\Psi_1, \Psi_2, u_3^*, u_5^*$ are cross-shore velocity moments defined by Bailard (1982) as function of wave height; φ is the angle of internal friction; ε_B and ε_S are the coefficients of bed load and suspended load efficiency; C_f is the drag coefficient, u_m is the fluid bottom velocity (treated in Section 2.6) , ρ and ρ_s are the fluid and sediment densities respectively, p is the sediment concentration, ω_s is the fall velocity, and k_s is an empirical factor used for calibration.

The governing equations are solved to determine a new coastline (Dabees and Kamphuis, 1999). Simulations of the coastline response to any combination of detached or shore-connected structures are possible.

Figure 4.4 shows the result of a simulation performed with ONELINE model for the case study of Sea Isle City, New Jersey (Dabees, 2000).

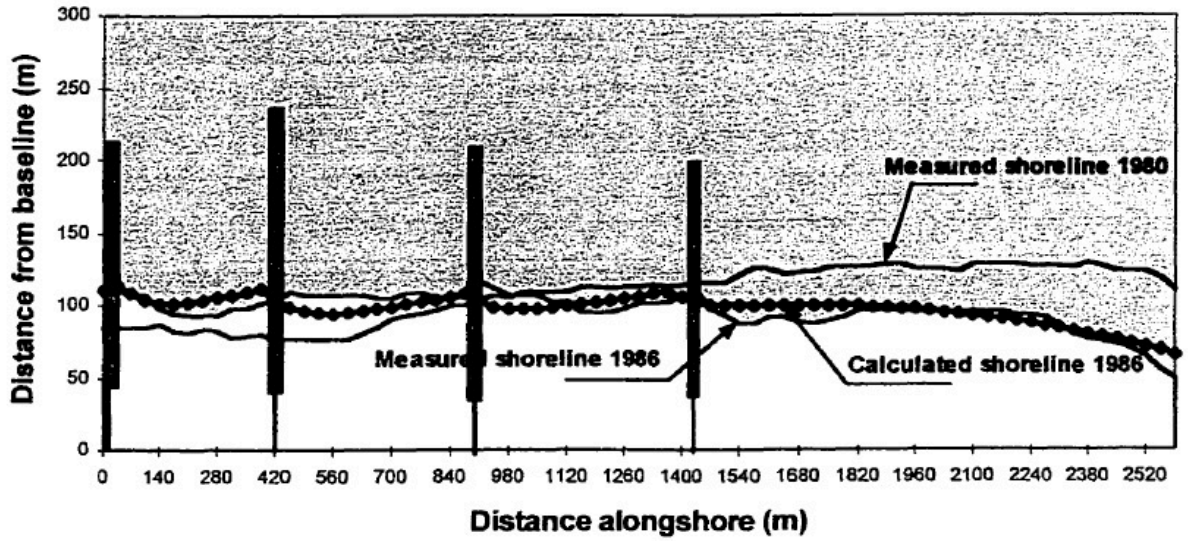

Figure 4.4 -Sea Isle City model calibration results (Dabees, 2000)

ONELINE technical documentations are available in (Dabees and Kamphuis, 1999).

4.4 **UNIBEST-CL+** (WL | Delft Hydraulics, 1999)

UNIform BEach Sediment Transport (UNIBEST-CL+) was developed by Deltares (WL | Delft Hydraulics, 1999) and represents a numerical tool to model longshore sediment transport and coastlines morphodynamics.

The UNIBEST package consists of three separate modules:

- the TC module for the calculation of the cross-shore sediment transport induced by waves, tidal currents and wind;
- the DE module, for the prediction of dune erosion during storm conditions;
- the CL+ module for the calculation of coastline changes due to longshore transport rate.

UNIBEST-CL+ can be used for a wide range of coastal engineering projects and consists of two integrates sub-models: the Longshore Transport module (UNIBEST-LT, 1993) and the CoastLine module (CL-module).

The wave model of Battjes and Janssen (1978) and the roller model of Nairn et al. (1990) modified according to De Vriend et al. (1993) are included in UNIBEST, permitting the propagation of the wave characteristics taking into account the bottom friction, refraction, shoaling, and wave breaking (WL | Delft Hydraulics ,1999).

The distribution of the longshore current along the coastal profile is determined from the depth-averaged momentum equation for the longshore direction including wind-induced, tide-induced and radiation stress terms. Longshore sediment transport is computed by the theoretical models of Bijker (1971), Van Rijn (1993), and Bailard (1981). Bijker (1971) calculates the bedload transport as function of longshore flow velocity, and the suspended load is calculated on the basis of bedload rate. Bailard (1981) is based on an energetic approach: the bedload formulation originates from a force balance between pressure and shear stress gradients in the moving sediment layer and gravitational forces. Van Rijn (1993) takes into account the bed shear stresses in a more detailed way with respect to Bijker (1971). The shape of the active cross-shore profile is constant over time. The cross-shore distribution is computed according to several total-load sediment transport formulae for sand or shingle (Kamphuis, 1991; Van Rijn, 2007; Van der Meer and Pilarczyk, 1987).

Calibration procedure is needed varying the parameters related to sediment transport and wave propagation.

The information needed to perform the numerical analysis are:

- the active profile shape;

- the wave and tide climates;
- the sand grain size.

UNIBEST is able to evaluate the coastline evolution in presence of coastal structures (e.g. groynes, detached breakwaters, etc.). The coastline boundary conditions can be represented with sinks, sources, groynes, or zero transport. Wave and tide climates are needed at a location seaward of the active profile for the hydrodynamics boundary.

Figure 4.5 shows an example of output obtained with UNIBEST-LT (Deltares, 2011), where wave conditions, longshore sediment transport distribution over cross-shore profile and the calculated cross-shore change are presented.

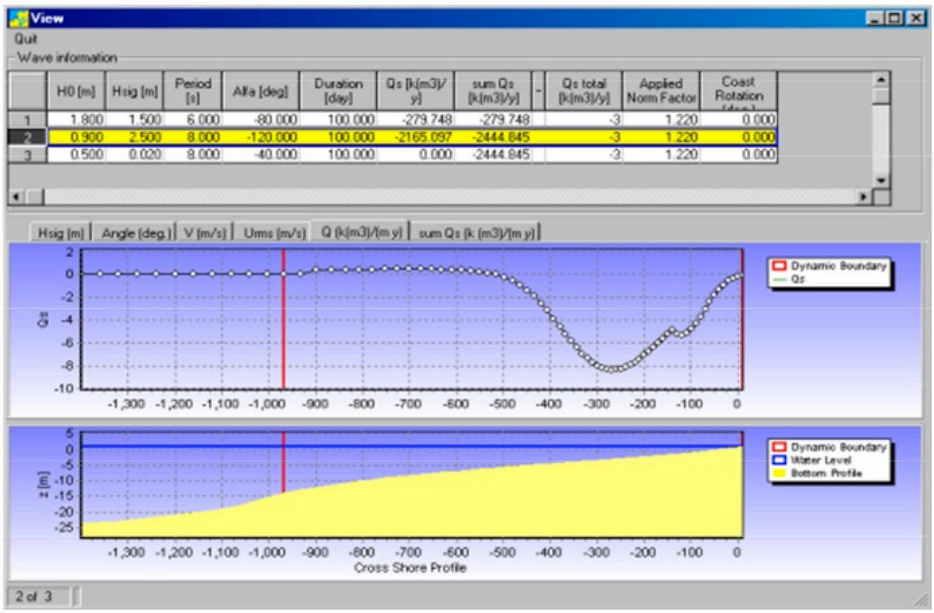

Figure 4.5 - Example of the output of UNIBEST-LT. Top panel: wave conditions. Middle panel: longshore sediment transport distribution over cross-shore profile for the wave condition 2. Bottom panel: Cross-shore profile (Deltares, 2011)

The technical documentation of UNIBEST is available on Deltares (2011).

4.5 **LITPACK - LITLINE** (DHI – Danish Hydraulic Institute, 2003)

LITtoral Processes And Coastline Kinetics (LITPACK) is a software package developed by Danish Hydraulic Institute Water and Environment, for simulating non-cohesive sediment transport under waves and currents action. LITPACK is also able to estimate the littoral drift, the coastline evolution and the cross-shore profile evolution along quasi-uniform beaches (DHI, 2005). It requires a commercial license.

LITPACK is composed by five modules:

- LIST, for the computation of the non-cohesive sediment transport;
- LITDRIFT, to evaluate the erosion by the longshore current and littoral drift calculation;

- LITLINE, for the coastline evolution;
- LITPROF, used to evaluate the cross-shore profile evolution in case of storm and restoring a normal condition;
- LITTREN, for the sedimentation in trenches.

LITLINE is the module for the coastline modelling. It is based on the one-line theory where the shape of the active cross-shore profile is constant over time (Pernald-Considerè, 1956). The coastal morphology is uniquely described by the evolution of the cross-shore position at a given longshore position with respect to a straight baseline.

LITLINE simulates the coastline evolution by the wave climate and five variables:

- beach position;
- sand dunes position;
- height of dunes;
- profile number;
- water depth.

LITLINE solves the continuity equation for sediment volumes $Q(x)$ (DHI, 2003) as:

$$\frac{\partial y_c(x)}{\partial t} = -\frac{1}{h_{act}(x)}\frac{\partial Q_l(x)}{\partial x} + \frac{Q_{sou}}{h_{act}(x)\Delta x} \qquad (4.6)$$

where $y_c(x)$ is the coastline position, t is the time, $Q(x)$ is the longshore sediment transport, x is the longshore position, $h_{act}(x)$ is the height of the active cross-shore profile, Δx is the longshore discretization of the computational domain, Q_{sou} represents a source or sink of sediments including eventual dune erosion.

The longshore transport rate Q_l(x) is determined relating the transport rate to the hydrodynamic conditions at breaking, by the Quasi Three-Dimensional Sediment Transport model (STPQ3D). STPQ3D considers the total sediment transport, q_t, as sum of bed load transport, q_b, and suspended transport , q_s, calculated according Engelund and Fredsoe (1976) and Fredsoe et al. (1985), respectively. More details of the STPQ3D sediment transport model, are available in DHI, (2017).

For given wave properties, the total longshore transport of sediment Q_l is determined as function of the longshore position and the local coastline orientation α. With known values of slope of water surface, *ig*, water level, *wl*, wave period, *T*, height, h_b, and angle ϑ_b of the wave at the breaking line, the longshore transport Q_l, corresponding to the local coastline orientation,

α, can be determined. For each calculation grid cell, x_{cal}, a $Q_l(x_{cal}, \alpha)$ relation is provided, as shown by the solid line in Figure 4.6.

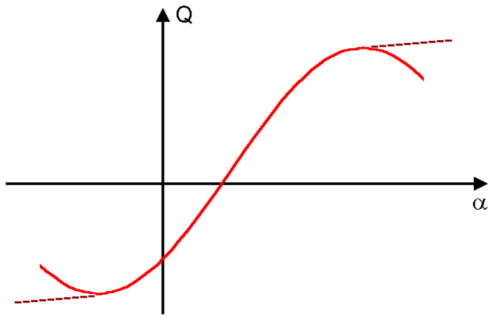

Figure 4.6 - $Q_l(x_{cal}, \alpha)$ for varying α (from DHI, 2017)

To obtain the coastline evolution over time, the continuity equation (4.6) is solved by an implicit Crank-Nicholson scheme (1947) as:

$$a_i y_{i-1,t+1} + b_i y_{i,t+1} + c_i y_{i+1,t+1} = d_i \qquad (4.7)$$

where:

$$a_i = (1-\alpha) dQ_{i-1} \qquad (4.8)$$

$$c_i = (1-\alpha) dQ_i \qquad (4.9)$$

$$b_i = \frac{\Delta x^2 h}{\Delta t} - a_i - c_i \qquad (4.10)$$

$$d_i = a_i y_{i-1,t+1} + b_i y_{i,t+1} + c_i y_{i+1,t+1} - \Delta x (Q_{i,t} - Q_{i-1,t} - QS_i) \qquad (4.11)$$

a_i, b_i, c_i, d_i can be found for the present time step, and with two boundaries (Q and coordinate of each point at $t-1$), the system of equation for all longshore positions can be solved by Gauss-elimination. Q_i represents the transport rate between x_i and x_{i+1} (Figure 4.7). The parameter α is the Crank-Nicholson factor; a value of α = 0 gives a fully implicit solution and a value of α = 1 gives a fully explicit solution.

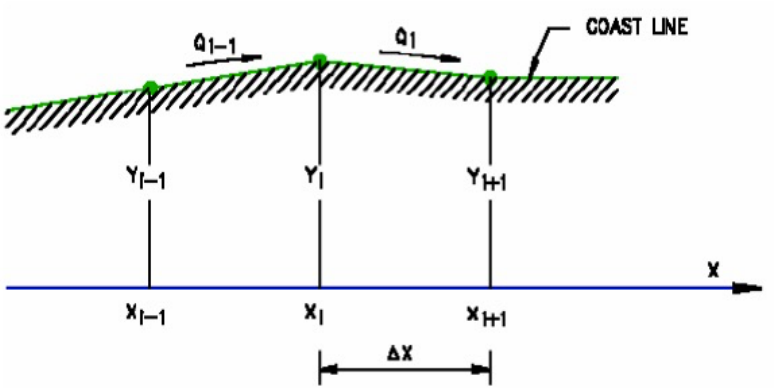

Figure 4.7 - Longshore discretization (Nguyen et al.,2007)

LITLINE uses a fully deterministic approach to estimate longshore transport. Some basic equations applied in other DHI modules, are applied with wave and current forcing on 2D profile at each cross section defined. Detailed discussion of the algorithms used to calculate the sediment transport can be found in DHI (2017) .The changes to the transport conditions caused by the presence of the coastal structures are modelled by introducing internal boundary conditions. When jetties and breakwaters are present, the influence of diffraction are computed.

The calibration procedure of LITLINE (DHI, 2017) consists in tuning the model to reproduce known/measured conditions for a particular situation. To verify the calibrated model, one or more simulations are necessary to compare the numerical results with the measurements available without changing any calibration parameters.

The input for the model are:

- initial coastline position;
- dune position;
- offshore contours;
- cross-shore profile;
- bed roughness coefficient;
- sediment characteristics (d_{50});
- water level: mean water level at deep water relative to the base level of the coastal profile;
- wave conditions (*H, T, dir*);
- coastal structures: number, position and dimension of groynes, jetties, breakwaters and revetments.

The output of the model consisting in:

- coastline position in time (m);
- depth of the topographic bed (m);

- sediment transport rate (m^3/day).

An example of LITLINE simulation is shown in Figure 4.8, where the coastline evolution under the influence of a short groyne after 30 days of simulation is presented.

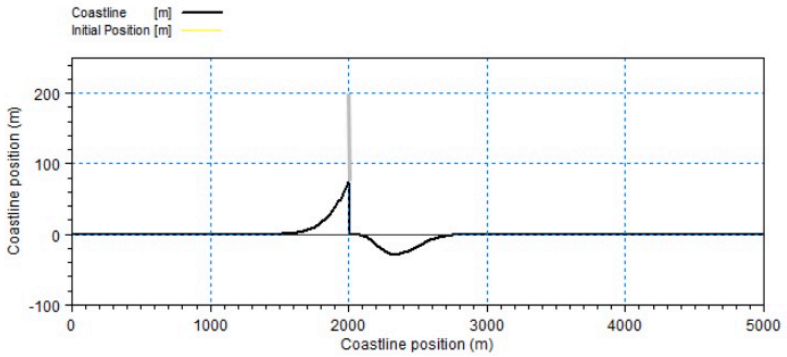

Figure 4.8 - Resulting coastline evolution for short groyne after 30 days. Extension of groyne is indicated. Note distorted scale. (DHI, 2017)

Technical documentation and the user guide are available on DHI (2009a-d) and DHI (2017).

4.6 **BEACHPLAN** (Blanco, 2003)

BEACHPLAN is a one-line model developed by HR Wallingford, and used to simulate changes in the plan shape of a non-cohesive (sand or gravel) beach (Blanco, 2003).

The beach is discretised into a number of cross-shore profiles with a constant shape. The wave conditions can be located in one or several locations at an equal depth contour seawards of the breaker zone. The breaker depth is evaluated at each profile through an iterative procedure until the significant wave height at the depth is 0.55 times the water depth (Sutherland et al., 2013). The breaking wave characteristics are used to calculate the longshore drift rate at each profile, caused by wave breaking.

The coastline change is driven entirely by changes in longshore sediment transport rate considering the constant beach shape and assuming the continuity of sediment. Sediment transport rate is calculated using the CERC equation modified with the term taking into account the effects of longshore variations in breaking wave heights (Ozasa and Brapton, 1980):

$$Q = K_1(\gamma_s)^{-1}E_b(nC)_b\left(\sin 2\alpha_b - 2K_2\frac{\partial H_b}{\partial x}\cot\beta\cos\alpha_b\right) \qquad (4.12)$$

where Q is the bulk longshore drift rate (m^3/s); K_1 and K_2 are calibration coefficients; α is the angle between wave crests and local depth contours; E is the energy density = $\rho g H_b/4$; ρ is the water density (kg/m^3); g is the gravitational acceleration (m/s^2); nC is the wave group

velocity (m/s); γ_s is the submerged weight of the sediment; β is the beach slope; H_b is the breaking significant wave height (m); x is the longshore coordinate (m).

BEACHPLAN calculates the diffraction effect produced in presence of detached breakwaters or groynes.

The computational loop of BEACHPLAN consists of five main steps:

1. Definition or the breaking wave conditions at each beach profile
2. Calculation of the longshore drift at each beach section
3. Calculation of the longshore drift across the sections with groynes and detached breakwaters are present
4. Calculation of the longshore drift for each beach cell, including sources and/or sinks of sediment
5. Update of the resulting coastline

In BEACHPLAN the input data are:

- Initial coastline position
- Initial cross-shore profile
- Wave characteristics (height, period, direction)
- Coastal structures (groynes, detached breakwaters)
- Boundary conditions
- Physical parameters (water density, sediment density and porosity)

Figure 4.9 shows an example of simulation performed with BEACHPLAN, where the coastline change was evaluated in the period from 2009 to 2012 in Poole Bay (UK) (Qiu, 2013).

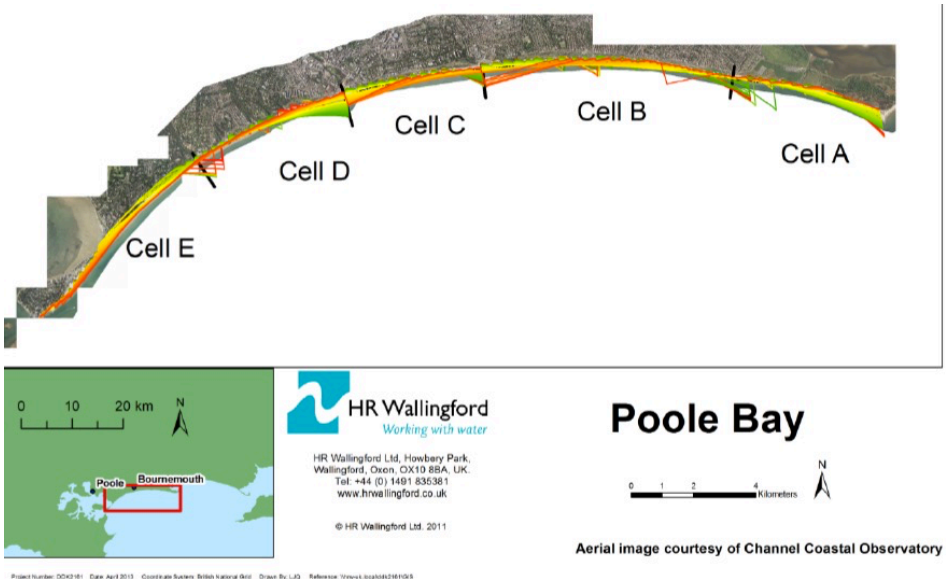

Figure 4.9 - Coastline evolution from 2009 to 2012 in Poole Bay (UK), (Qiu, 2013)

Technical documentations are available on (Sutherland, 2013).

4.7 **SMC** (González et al., 2007)

Sistema de Modelado Costero (SMC) is an user-friendly system developed by the Spanish Ministry of Environment and the Environmental Hydraulics Institute from the University of Cantabria (IHCantabria). SMC is a package composed by five numerical models specifically developed for the application of the methodology proposed in the Spanish Beach Nourishment and Protection Manual (Gonzalez et al., 2007). According to this methodology, the SMC is composed by:

1. Pre-process module, for the bathymetric information, flood level determination and wave characterization
2. Short-term module, for the cross-shore profile evolution
3. Long-term module, for the longshore profile evolution
4. Coastal terrain module, for the terrain modelling
5. Tutorial module, with examples, formulas and procedures in coastal engineering

Long-term module is represented by a one-line model useful to analyse coastal systems on different scales of variability (hours–months–years) evaluating the morphodynamic evolution. The assumptions of the model are (Canovas and Medina, 2012):

- all the profiles must be in equilibrium;
- the difference between wave front angle at breaking and coastline direction is assumed to be small;
- the sediment transport is due to oblique wave incidence and to the wave height gradient.

The wave climate is propagated up to the breaking point considering the diffraction process (González, 2007), by the use of the internal parabolic model to propagate spectral waves. After wave propagation, the breaking wave characteristics are determined at the beach profiles for each sea state: energy flux is due to breaking waves and the gradient in wave height.

The longshore sediment transport is calculated with the CERC equation modified with the term taking into account the effects of longshore variations in breaking wave heights (Ozasa and Brapton, 1980), and considering the parametrization proposed by Kraus and Harikai (1983). The sediment transport rate due to oblique wave incidence (Q_α) and the gradient in wave height (Q_h) can be determined as:

$$Q = Q_\alpha + Q_h \qquad (4.13)$$

where:

$$Q_\alpha = \sum_{i=1}^{i=n} \left({H_{B_i}}^2 \, c_{gB_i}\right)\left(2a_1 \alpha_{Bs_i}\right) \qquad (4.14)$$

$$Q_h = -\sum_{i=1}^{i=n} \left({H_{B_i}}^2 \, c_{gB_i}\right)\left(a_2 \frac{\partial H_{B_i}}{\partial y}\right) \qquad (4.15)$$

where, H_B is the breaking wave height; c_{gB} is the wave group velocity; the non-dimensional parameter a_1 and a_2 are given by Equation (4.2) and Equation (4.3) respectively; α_{s_i} = is the angle of wave crests to the coastline; the subscript *B* indicates the breaking conditions.

The beach reaches a static equilibrium state and every profile is also in equilibrium. The equilibrium beach planform is estimated using parabolic splines which are subject to the following conditions:

1. Initial and end point of every parabolic spline must be on a profile
2. The equilibrium planform must be perpendicular to the normal forcing at every point
3. Continuity condition must be fulfilled at the joints between adjacent splines
4. First point of the equilibrium beach is known

Figure 4.10 shows a long-term analysis performed with SMC at Barceloneta Beach (Gonzalez et al., 2007).

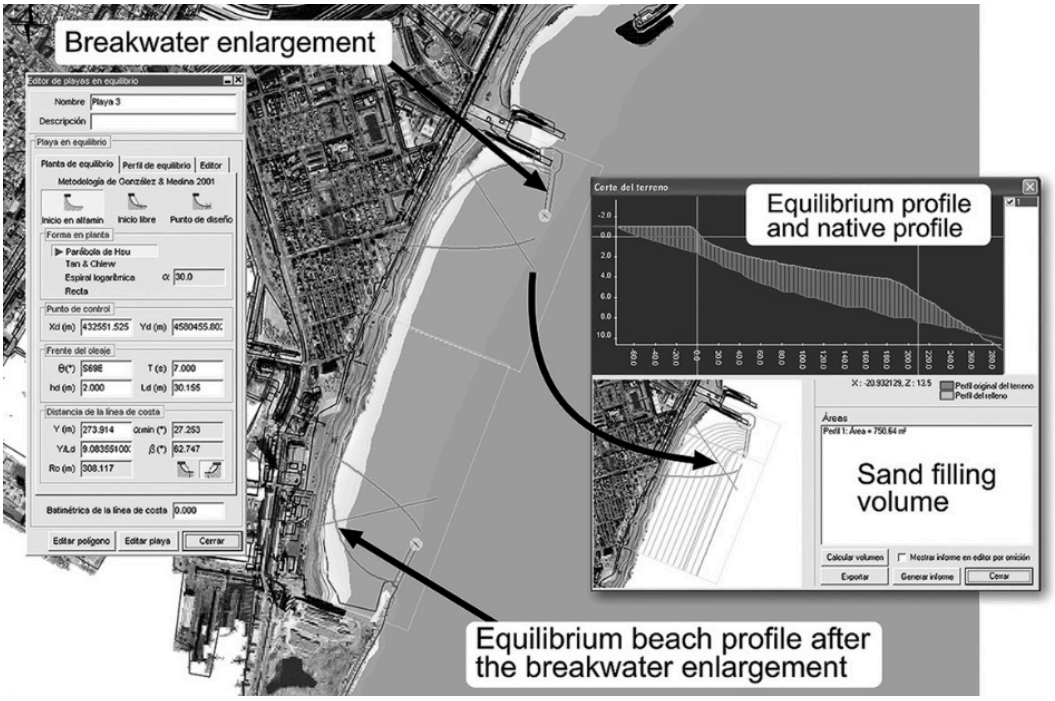

Figure 4.10 - Equilibrium beach (equilibrium profile + equilibrium plan form). Long-term analysis at Barceloneta Beach, Spain (Gonzalez et al., 2007)

Technical documentation and the user guide are available on GIOC (2003).

4.8 Similarities and differences

Numerical one-line models have demonstrated their applicability in design and management of many coastal engineering projects (Hanson and Kraus, 2011). Six numerical models based on the one-line theory was described. A comparation between the main features of these models are given in Table 4.1.

Coastline change in one-line models is driven by gradient in longshore transport. For this reason, the longshore transport represents the most important process calculated. GENESIS, ONELINE, BEACHPLAN and SMC models use the same routine for the computation of the transport rate. The waves characteristic from deep water to nearshore are propagated by an internal model and the breaking wave conditions at the determinates cross-shore profiles are calculated, providing the forcing for the transport equations. GENESIS, BEACHPLAN and SMC use a CERC (1984) formula for the calculation of the sand transport rate including contribution of the longshore gradient in breaking wave height (Ozasa and Brampton, 1980). ONELINE model uses an extension of Kamphuis' formula (1991). UNIBEST calculates longshore transport with a rigorous calculation of the cross-shore transport, from sea to the dune, similar to LITPACK. UNIBEST has the option of applying three formulae for the sediment transport rate: Bijker (1971), Bailard (1981), CERC (1984), and van Rijn (1993). Longshore transport rate calculated with UNIBEST does not consider the term based on the gradient in breaker wave height.

The longshore transport formulae driving the calculated coastline change and used in the existing one-line models are limited on a restricted range of applicability in terms of sediment grain size composing the beach. For this reason, one-line models are commonly used to simulate the dynamic variability of sandy beaches (Hanson,1989). The implementation of a general formula for the calculation of the longshore transport rate, valid for any type of not cohesive material (e.g. sand, gravel, cobbles, mixed, stones) is necessary to extend the range of applicability of the one-line models for coastal change prediction.

Table 4.1 - Main features of the models presented

	2D bathymetry	*Variability of seabed proprieties*	*Wave height*	*Wave transformation*	*Diffraction around the structures*	*Longshore current*	*Longshore sediment transport*	*Beach nourishment*	*Groynes*	*Detached breakwaters*
GENESIS	not required	no	significant	linear wave theory: shoaling, refraction, breaking	yes	no	CERC (1984)	yes	yes	yes
ONELINE	not required	no	significant	linear wave theory: shoaling, refraction, breaking	yes	no	Kamphuis (1991)	yes	yes	yes
UNIBEST	yes, for determination of representative profiles	no	significant	Battjes and Janssen (1978)	no	Longuet and Higgins (1970)	Bijker (1971), van Rijn (1993), Bailard (1981), CERC (1984)	yes	yes	no
LITPACK	yes, for determination of representative profiles	yes	root mean square	Battjes and Janssen (1978)	yes	Longuet and Higgins (1970)	STPQ3D (DHI, 2017)	yes	yes	yes
BEACHPLAN	yes, for determination of representative profiles	yes	significant	linear wave theory: shoaling, refraction, breaking	yes	Longuet and Higgins (1970)	CERC (1984)	yes	yes	yes
SMC	yes, for determination of representative profiles	no	significant	linear wave theory: shoaling, refraction, breaking	yes	no	CERC (1984)	no	no	no

5 GSb NUMERICAL MODEL

5.1 Introduction

The General Shoreline beach (GSb) is a newly morphodynamic model belonging to the one-line model typology, first proposed by Pernald-Considerè (1956) and extensively applied to a computation of shoreline change. It is assumed that the beach cross-shore profile remains unchanged (Bruun, 1954; Dean, 1977), thereby allowing beach change to be described uniquely in terms of the shoreline position.

The peculiarity of the GSb model consists of simulating shoreline evolution based on a longshore transport formula/procedure suitable at any coastal mound: sand, gravel, cobbles, shingle and rock beaches (Tomasicchio et al., 1994; Lamberti and Tomasicchio, 1997; Tomasicchio et al., 2007; Tomasicchio et al., 2013; Tomasicchio et al., 2015). The proposed general formula/procedure considers an energy flux approach combined with an empirical/statistical relationship between the wave-induced forcing and the number of moving units.

The GSb model presents one calibration coefficient solely, K_{GSb}, which does not depend on the grain size diameter and depends on the longshore gradient in breaking wave height (Osaza and Brampton, 1980). The GSb model allows to determine short-term (daily base) or long-term (yearly base) shoreline change for arbitrary combinations and configurations of structures (groynes, detached breakwaters and seawalls) and beach fills that can be represented on a modelled reach of coast.

The GSb assumptions are:

1. The beach cross-shore profile remains constant over time.
2. The longshore sediment transport occurs within the active beach profile, between the berm height, D_B , and the closure depth, D_C , below which the bottom is assumed fixed.
3. The sediment transport is caused by the wave action.

The shoreline change is governed by the longshore sediment movement induced by the waves and by the effect of the nearshore circulation. However, in GSb model, the nearshore circulation is not accounted except for the effect of longshore variations in breaking wave height, which influences the shoreline evolution near structures according to Kraus and Harikai (1983) and Kraus (1983).

In the present chapter, the fundamental equations of the GSb model, the longshore sediment formula used to compute the sediment transport rate, the calculation of the wave characteristics, the equilibrium beach profile, the boundary conditions, and the permeability of the structures are described.

5.1 Longshore sediment transport rate

The GSb model considers the following equation for the longshore transport rate Q_l:

$$Q_l = \frac{S_N D_{\mathrm{n50}}^3}{(1-n)T_m} - \frac{K_{GSb}}{8\left(\frac{\rho_s}{\rho}-1\right)(1-n)\tan\beta\ 1.416^{7/2}} H_{sb}^2 c_{gb}\cos(\theta_{bs})\frac{\partial H_{sb}}{\partial x} \qquad (5.1)$$

where S_N= the number of units passing a given control section in one wave (determined as in Section 2.5.15), D_{n50}= nominal diameter of the unit, n = porosity factor, T_m = mean wave period, K_{GSb}=calibration parameter, ρ_s = density of sediment, ρ = density of water, $\tan\beta$ = average bottom slope from the shoreline to the closure depth, H_{sb} = significant breaking wave height (determined as in the following Section 5.2.4), c_{gb}= group celerity at breaking, θ_{bs}= angle of breaking waves to the local shoreline.

The first term in Equation (5.1) corresponds to the "GLT formula" described in (Tomasicchio et al., 1994; Lamberti and Tomasicchio, 1997; Tomasicchio et al., 2013; Tomasicchio et al., 2015) and accounts for longshore sediment transport at a mound composed of not cohesive grains of any size, from sand to rock units.

The second term in Equation (5.1) similarly to GENESIS (Hanson and Kraus, 1989), ONELINE (Dabees and Kamphuis, 1998), BEACHPLAN (Blanco, 2003), SMC (González et al., 2007) , and GENCADE (Frey et al., 2012), accounts for the longshore sediment transport induced by the longshore gradient in significant wave height (Osaza and Brampton, 1980). The factor 1.416 is used to convert from significant wave height, the statistical wave height required by the model, to root-mean-square (rms) wave height (Hanson and Kraus, 1989).

5.2 Nearshore significant wave height

5.2.1 Shoaling

The shoaling coefficient K_s is a function of the wave period, T, deepwater reference depth, D_1, and breaker line depth, D_2. It is given by

$$K_s = \left(\frac{c_{g1}}{c_{g2}}\right)^{1/2} \qquad (5.2)$$

in which c_{g1} and c_{g2} are the wave group speeds at deepwater, P_1, and breaker line, P_2, respectively (Figure 5.1).

The group speed is defined as:

$$c_g = Cn \qquad (5.3)$$

where $C = L/T$ is the wave phase speed, L = wavelength, T = wave period, D = depth, and $n = 0.5[1 + (2\pi D/L)/\sinh(2\pi D/L)]$.

The wavelength is calculated from the dispersion relation:

$$L = L_o \tanh\left(\frac{2\pi D}{L}\right) \qquad (5.4)$$

with L_o = wavelength in deep water.

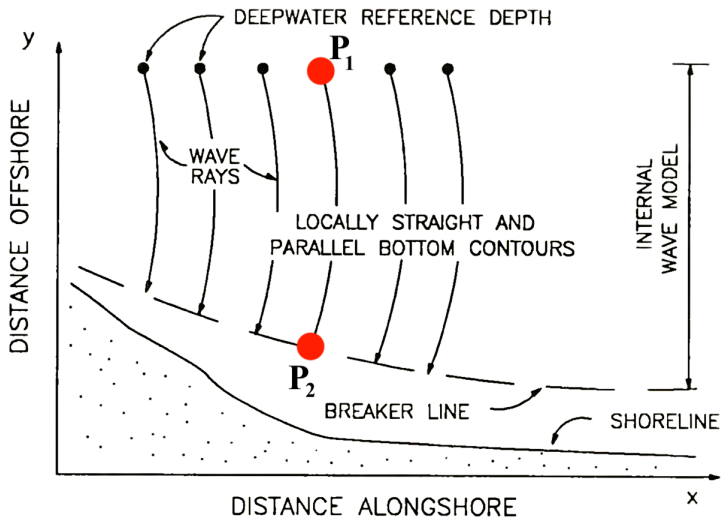

Figure 5.1 – Transformation by internal wave model (Hanson and Kraus, 1989)

5.2.2 Refraction

The refraction coefficient K_R is a function of the starting angle of the ray, ϑ_1, and the angle at the breaker line, ϑ_2. K_R is given by

$$K_R = \left(\frac{\cos\vartheta_1}{\cos\vartheta_2}\right)^{1/2} \qquad (5.5)$$

5.2.3 Diffraction

GSb uses the simplified diffraction calculation procedure from waves with directional spread presented by Goda et al. (1979) to represent diffraction at structures such as detached breakwaters and groynes.

The degree of directional energy concentration is represented by parameter denoted by S_{max} (Goda, 2010). With S_{max} determined at the roundhead of the diffracting structure (details in Goda et al., 1979; Hanson, 1987), the diffraction coefficient, K_D, along a line making the angle ϑ to the incident wave direction at the roundhead can be obtained from Figure 5.2.

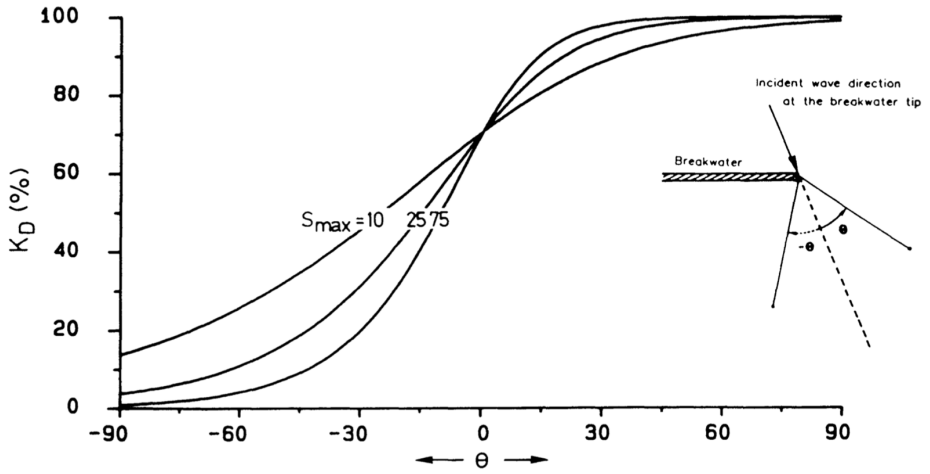

Figure 5.2 – Cumulative distribution of relative wave energy with respect to azimuth from principal wave direction (Hanson and Kraus, 1989; Goda, 2010)

5.2.4 Breaking

The significant breaking wave height, H_{sb}, transformed by shoaling, refraction and diffraction is calculated by:

$$H_{sb} = K_s K_R K_D H_{s\_ref} \qquad (5.6)$$

where, K_s = shoaling coefficient, K_R = refraction coefficient, K_D = diffraction coefficient, H_{s_ref} = significant wave height at the offshore reference depth.

The equation for depth limited wave breaking is given by:

$$H_{sb} = \gamma D_b \qquad (5.7)$$

where D_b is the depth at breaking and γ is the breaker index (γ = 0.78).

The wave angle at breaking is calculated by means of Snell's law:

$$\frac{\sin \vartheta_b}{L_b} = \frac{\sin \vartheta_1}{L_1} \qquad (5.8)$$

in which ϑ_b and L_b are the angle and wavelength at the break point, and ϑ_1 and L_1 are the corresponding quantities at an offshore point.

The three unknowns, H_{sb}, D_b, and ϑ_b, are obtained at intervals alongshore by iterative solution of Equations (5.6), (5.7), and (5.8) as a function of the wave height and angle at the reference depth and wave period.

The calculated value of H_{sb} is adopted for the estimation of the longshore sediment transport (Equation (5.1)) induced by the longshore gradient in wave height (Osaza and Brampton, 1980).

5.3 Explicit solution of sediment continuity equation

Calculated longshore quantities are discretized on a grid where shoreline positions y_i are defined at the centre of the grid cells and transport rates Q_{l_i} at the cell boundary.

The conservation of mass equation, considering only longshore transport is expressed as:

$$\frac{\partial V}{\partial t} + \frac{\partial Q_l}{\partial x} = 0 \qquad (5.9)$$

where V is the control volume of the beach profile, t is the time of coastline evolution, Q is the longshore transport rate, and x is the longshore coordinate.

Figure 5.3 shows a control volume, ∂V, where the sediment continuity equation is equal to:

$$\partial V = \left\{ Q_l - \left(Q_l + \frac{\partial Q_l}{\partial x} \partial x \right) + q \partial x \right\} \partial t \qquad (5.10)$$

with q = inshore / offshore sediment transport.
The control volume ∂V is geometrically equal to:

$$\partial V = \partial x \, \partial y \, (D_C + D_B) \qquad (5.11)$$

with D_B = berm height, D_C = closure depth.

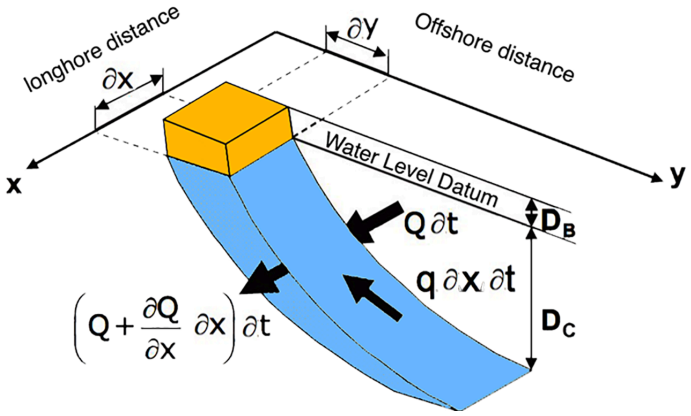

Figure 5.3 - Definition sketch (Hanson, 1989)

Equalizing Equation (5.10) and Equation (5.11) the governing equation for the one-line model is obtained as:

$$\frac{\partial y}{\partial t} = -\frac{1}{D_C + D_B}\left(\frac{\partial Q_l}{\partial x} + q\right) \qquad (5.12)$$

The governing differential Equation (5.12) can be approximated by an explicit scheme. Approximating $\partial y/\partial t$ with $(y_i^{t+1} - y_i^t)/\Delta t$ and $\partial Q_l/\partial x$ with $(Q_{l_{i+1}}^t - Q_{l_i}^t)/\Delta x$ and rewriting the governing differential equation with the approximated derivatives, it comes:

$$\frac{y_i^{t+1} - y_i^t}{\Delta t} = -\frac{1}{D_C + D_B}\left(\frac{Q_{l_{i+1}}^t - Q_{l_i}^t}{\Delta x} + q\right) \qquad (5.13)$$

with Q_{l_i} and $Q_{l_{i+1}}$ the incoming and outgoing sediment transport rate of the i-th control volume at the same time step *t*, respectively. Δx is the width of the calculation cell.

The shoreline position, y, at the next time step, $t+1$, for the i-th control volume can be expressed as:

$$y_i^{t+1} = y_i^t - \left(\frac{1}{D_C + D_B}\right)\left(Q_{l_{i+1}}^t - Q_{l_i}^t + q\Delta x\right)\frac{\Delta t}{\Delta x} \qquad (5.14)$$

with Δx = spatial increment and Δt = temporal increment.

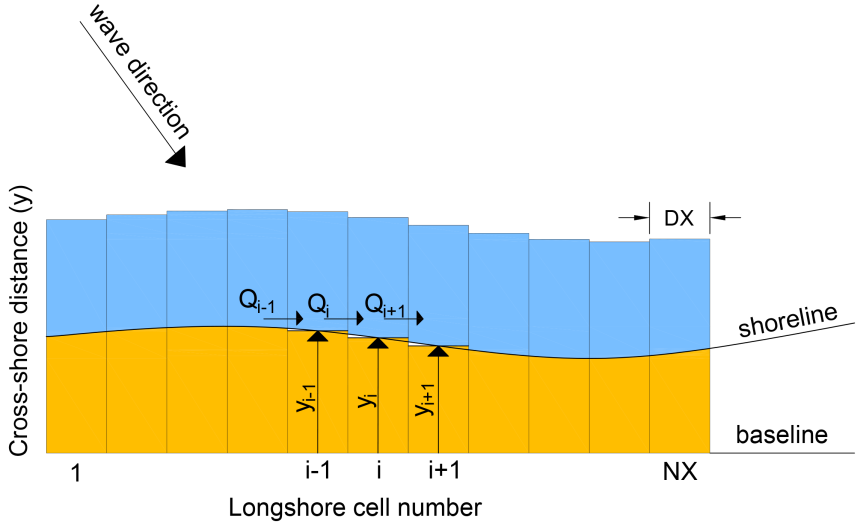

Figure 5.4 - Finite difference grid

Considering the i-th cell in Figure 5.4, with known closure depth, D_C, and berm height, D_B, assuming $q = 0$, if the outgoing sediment $Q_{l_{i+1}}^t$ is greater than the incoming sediment $Q_{l_i}^t$, the shoreline retreats. Otherwise, if $Q_{l_{i+1}}^t$ is less than $Q_{l_i}^t$, the shoreline advances. If $Q_{l_{i+1}}^t$ is equal to $Q_{l_i}^t$, the shoreline at next time step remains unchanged.

5.4 Equilibrium beach profile

In the GSb model, the equilibrium profile shape is calculated as proposed by Bruun (1954) and Dean (1977) and it is used to determine the location of the breaking waves and calculate the average nearshore bottom slope used in longshore transport equation. The average profile shape of the equilibrium beach is described by:

$$h(y) = Ay^{2/3} \qquad (5.15)$$

in which h is water depth (m), A = scale parameter ($m^{1/3}$) and y = offshore distance from the shoreline (m). The scale parameter A is can be calculated as in the following:

$$A = 0.41(D_{50})^{0.94}, \quad D_{50} < 0.4\ mm \qquad (5.16)$$

$$A = 0.23(D_{50})^{0.32}, \quad 0.4\ mm \leq D_{50} < 10.0\ mm \qquad (5.17)$$

$$A = 0.23(D_{50})^{0.28}, \quad 10.0\ mm \leq D_{50} < 40.0\ mm \qquad (5.18)$$

$$A = 0.46(D_{50})^{0.11}, \quad D_{50} \geq 40\ mm \qquad (5.19)$$

5.5 Boundary conditions

The shoreline change at the boundary of the domain must be specified. GSb presents three options for boundary conditions: *pinned*, *moving* and *gated*.

When the *pinned* boundary condition is selected the initial sediment transport rate Q_i is equal to the sediment transport rate at the end of simulation Q_e ($Q_i = Q_e$), then $\partial y/\partial t = 0$ because $\partial Q/\partial x = 0$; it means that y does not change over time.

If the boundaries of the considered beach cannot be represented with the *pinned* conditions, it is possible to force a constant rate of change y_{RC}. This condition is named *moving*, and it can be expressed as: $y_N^{t+1} = y_N^t + y_{RC}$ where the apex denotes the relative time.

When the *gated* boundary conditions are selected, groynes are incorporated as a boundary to interrupt, partially or completely, the movement of sand alongshore at the end of the computational domain.

The extremes of the domain can be selected considering these three options. Large coast in which there are no changes in the longshore transport at the boundaries represent a good choice. In this case the gradient in longshore transport is small and the *pinned* condition can be considered. If the longshore transport is known at some location, a good choice could be to consider that point as boundaries, using the *moving* condition.

5.6 Coastal structures in the GSb model

The coastal protection consists of a reduction or elimination of damage to the shore and backshore caused by flooding or storms (Kraus, 2005). The structures for shore protection can be *soft* or *hard*. Soft protection consists of adding sediment on the beach; this process is called beach nourishment. A hard intervention of coastal defence consists in deployment of one or more coastal structures, composed by natural rocks or artificial concrete blocks.

5.6.1 Groynes

Groynes are *hard* structures built perpendicular to the shoreline to protect the shoreline by blocking the longshore transport, where an accumulation of sand on the updrift side of the groyne is present. However, the block of the sand causes a deficit in the littoral drift budget, producing erosion downdrift (Figure 5.5) (Mangor et al., 2017).

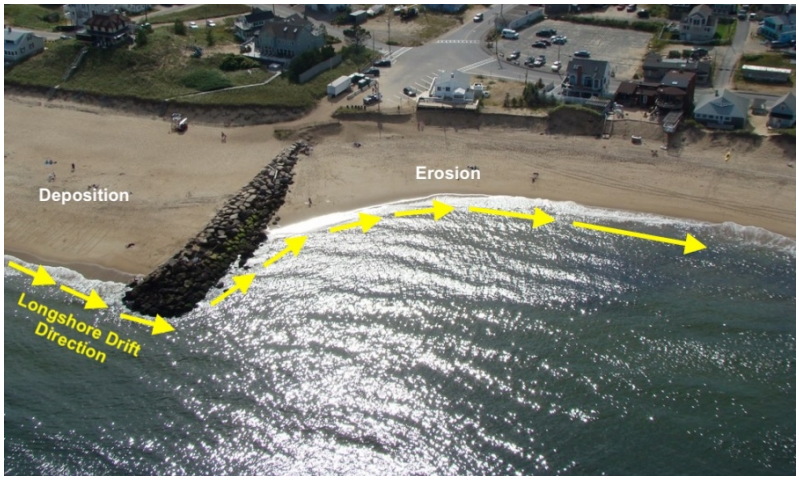

Figure 5.5 – Shoreline response to a single groyne, Plum Island, New York (www.plumislanderosion.com)

In the GSb numerical model, groynes are defined perpendicular to the shoreline. The permeability and offshore length of each groyne can be specified at arbitrary locations along the shoreline. The influence of a groyne on a shore is defined by the ratio of the amount of sand passing that groyne and the amount of sand arriving at the updrift side of that groyne. Sand movement past a groyne is controlled by the combined action of sand moving around the tip of the groyne which is called sand bypassing and sand transmission through or over the groyne.

5.6.2 Detached breakwaters

Detached breakwaters are *hard* structures parallel to the shoreline and located inside or close to the surf-zone. When the cross-shore transport is large, detached breakwaters may be the appropriate shore protection intervention (Kraus, 2005). The sediment transport in the lee of the breakwater decreases due to the attenuated wave and longshore currents in the area protected.

The shoreline response to a detached breakwater is controlled by at least 14 variables (Hanson and Kraus, 1990), making these structures more difficult to design than groynes. The

shoreline response can be of two types: as a *tombolo*, where the shoreline reaches the structure, or as a *salient* where a cuspate morphologic form grows toward, without reaching the structure.

In the GSb numerical model, a detached breakwater can be defined indicating the distance from the boundaries of the structure to the shoreline. This allows to consider various orientation of detached breakwaters with respect to shoreline. The effect of the diffraction due to the presence of a detached breakwater is computed as described in Section 6.4.1. The permeability can be specified, and the permeability corrections are done for the calculation of the diffraction coefficient.

5.6.3 Revetments

A revetment is an armour protection layer, consisting of armour layer, underlying filter layer and toe protection, on a slope to protect the adjacent upland against wave scour by current and wave action (Van Rijn, 1998). The GSb numerical model can deal with revetments.

5.7 Permeability in the GSb model

GSb takes into account the sediment passing through or over the coastal structures modelled. Two types of sediment movement through the structures can be simulated: bypass, when the sediment passes around the seaward end of the groynes, and transmission, where the sediment passes through or over the structures. Transmission occurs due to porosity of the material composing the coastal structure. Bypass occurs when the water depth at the tip of the structure D_G is less than the depth of active longshore transport D_{LT} calculated with Hallermeier (1983). To represent sediment bypassing, a bypass factor BYP is introduced and defined as:

$$BYP = 1 - \frac{D_G}{D_{LT}}, D_G \leq D_{LT} \qquad (5.20)$$

which is calculated at each time step.

Analogously, a permeability factor p is introduced to describe sediment transmission over or through a coastal structure. For a value of $p = 0$, the structure is completely transparent. On the contrary, for a value of $p = 1$ the structure is fully impermeable. Values of p is specified from the user in the input file. With the values of BYP and p, GSb calculates the total fraction F of sand passing over or through a structure as defined by Hanson (1987):

$$F = p\,(1 - BYP) + BYP \qquad (5.21)$$

The F value is calculated at every time step for each structure defined along the model grid.

5.8 Numerical stability

In GSb the governing equation is solved using a finite difference scheme by discretizing the shoreline into a finite grid and the simulation time into time steps. The grid spacing and time step depend on the type of solution scheme. The calculated shoreline position for each grid cell at any time step depends on sediment transport rates and shoreline positions calculated at the previous time step. The explicit finite difference scheme is limited to the appropriate choice of time steps, Δt, and width of calculation cell, Δx, in order to satisfy the stability condition (Dabees, 2000):

$$Rs = \left[\frac{Q}{\alpha_b (D_C + D_B)} \frac{\Delta t}{(\Delta x)^2}\right] < \frac{1}{2} \qquad (5.22)$$

with α_b = wave obliquity at breaking. This relation is known as the Courant condition (Courant et al., 1967) in numerical methods and represents the stability parameters. If stability ratio takes a value greater than 0.5, calculations become unstable showing an unphysical oscillation of the calculated shoreline (Figure 5.6).

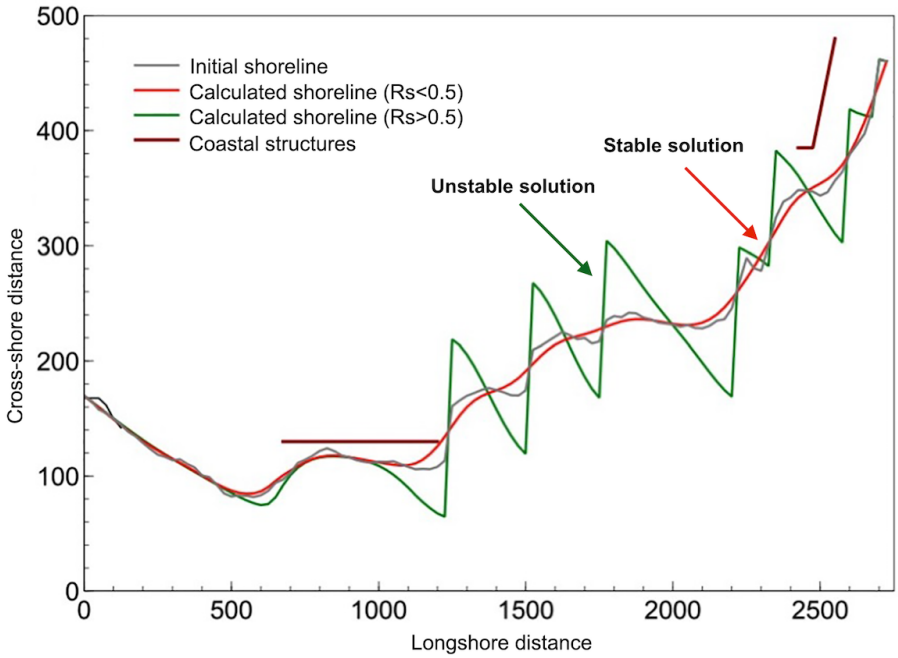

Figure 5.6 – Numerical stability

6 SENSITIVITY ANALYSIS

The robustness of a numerical model may be evaluated performing a sensitivity analysis where the model is used for a selected range of input values and for different model configurations. Evaluating model robustness includes assessing the effects of changes in, for example, model structure, input parameter values, on the calculation result. If small modifications in model formulation or parameter values produce large changes in the result, model robustness is low, and vice versa (Larson, 2005).

Some idealized simulations focused on each of the primary model parameters and coastal structures have been performed to evaluate the GSb capabilities and to exclude potential errors. The cases presented consist of simulating the coastline change for an initially straight shoreline in presence of:

- single groyne;
- single detached breakwater;
- multiple groynes;
- multiple detached breakwaters.

Simulations with single groyne and single detached breakwater have been conducted varying the following key parameters:

- the offshore wave angle ϑ_o, for eleven wave angles between +45-deg and -45-deg;
- the boundary conditions, pinned, moving, and gated;
- the grain size composing the beach D_{50} = 0.3 mm (sand), 30 mm (pebbles), 100 (cobbles);
- the permeability of the structure, p = 0, 25, 50, 75, 100;
- the calibration coefficient K_{GSb}= 0.01, 0.1, 0.25, 0.50.

6.1 Single groyne

The simulation for the case of a single groyne has been performed adopting the parameters assumed in Frey et al. (2012) for the GENCADE verification.

As initial condition, a straight shoreline 3000 m long with a single groyne located at the centre of the domain has been taken into account. A model grid cell resolution, DX, has been selected equal to 10 m with a total number of cells, NX = 300. The adopted median grain size, D_{50} = 0.3 mm. GSb has been run with $K_{GSb} = 0.25$ and the boundary conditions have been set as pinned. The calculation time step has been fixed equal to 0.5 hrs. Wave inputs have been supplied at the 50 m depth contour. The adopted input parameters are given in Table 6.1.

Table 6.1 – GSb input for single groyne simulation (Frey et al., 2012)

Model domain	Number of cells alongshore	NX = 300
	Dimension of cells	DX = 10 m
	Calculation time step	DT = 0.5 hrs
	Median grain size	D_{50} = 0.3 mm
	Berm height	D_B = 1m
	Closure depth	D_C = 8 m
Model forcing (at 50 m contours)	Significant wave height	H_{so} = 0.75 m
	Peak wave period	T_p = 8 sec
	Wave angle	ϑ_o = 15 deg
Model parameters	Calibration parameter	K_{GSb} = 0.25
	Boundary conditions	Pinned
	Duration of simulation	t = 2 years
Structures	Single groyne 75 m long at x = 1500 m	
Initial shoreline	Straight shoreline 3000 m long	

Figure 6.1 shows the results of the GSb simulation in terms of shoreline change and mean net transport rate after 2-years simulation, under a regular wave attack (H_{so} = 0.75 m, T_p = 8 sec, ϑ_o = 15 deg).

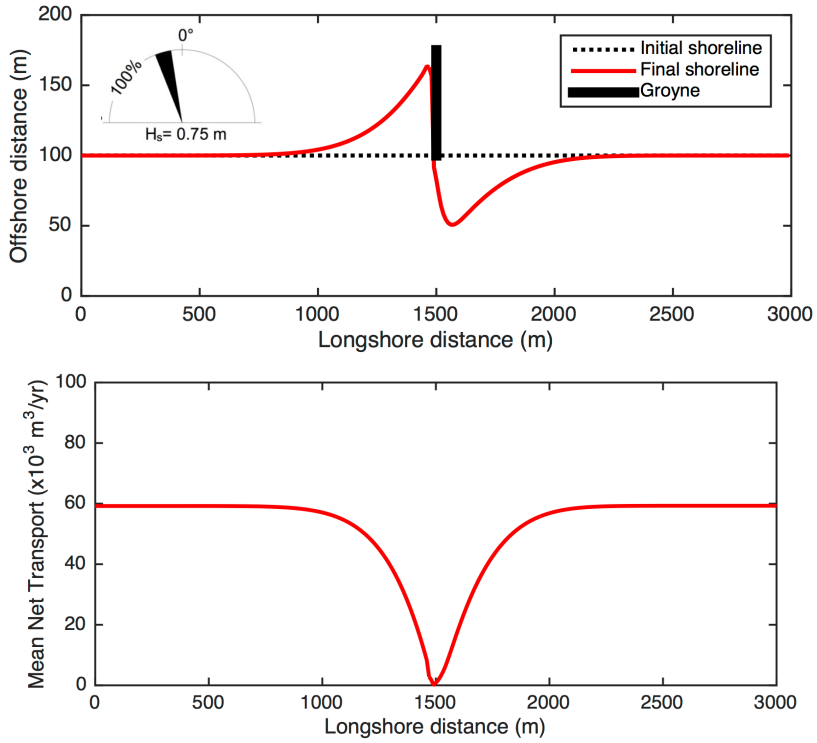

Figure 6.1 - Calculated shoreline change and mean net transport rate for straight shoreline with single groyne with H_{so} = 0.75m, T_p = 8 sec, ϑ_o = +15 deg

The groin presents a total obstruction to longshore transport, which results in a shoreline advance seaward on the left (updrift) side of the groin, as the transport rates decrease from 60,000 m^3/yr to 0 m^3/yr at the groin. Conversely, as transport rates increase from 0 m^3/yr in the vicinity of the groin, back to 60,000 m^3/yr outside of the region of groin influence, the expected downdrift shoreline retreat has been observed.

6.1.1 Wave angle

Simulations varying the offshore wave angle, from - 45 to + 45 deg have been conducted. The adopted input parameters are given in Table 6.2.

Table 6.2 - GSb input for single groyne simulation, varying the offshore wave angles

Model domain	Number of cells alongshore	NX = 300
	Dimension of cells	DX = 10 m
	Calculation time step	DT = 0.5 hrs
	Median grain size	D_{50} = 0.3 mm
	Berm height	D_B = 1m
	Closure depth	D_C = 8 m
Model forcing (at 50 m contours)	Significant offshore wave height	H_{so} = 0.75 m
	Peak wave period	T_p = 8 sec
	Wave angle	ϑ_o = – 45, – 35, – 25, –15 , – 5, 0, +5, +15, +25, +35, +45 deg
Model parameters	Calibration parameter	K_{GSb} = 0.25
	Boundary conditions	Pinned
	Duration of simulation	t = 2 years
Structures	Single groyne 75 m long at x = 1500 m	
Initial shoreline	Straight shoreline 3000 m long	

For considered values of ϑ_o = -45, -35, -25, -15, -5, 0 deg, Figure 6.2 shows the calculated shoreline change induced by sediment transport, acting from right to left, which results in a sediment accumulation and retreat on the right and left sides of the groyne, respectively. Maximum accumulation/retreat rates for ϑ_o = -35 and ϑ_o = -25 deg have been obtained. It is noticed that, for the case of ϑ_o = 0, in correspondence of the groyne, a small shoreline advance has been observed, probably due to diffraction effect.

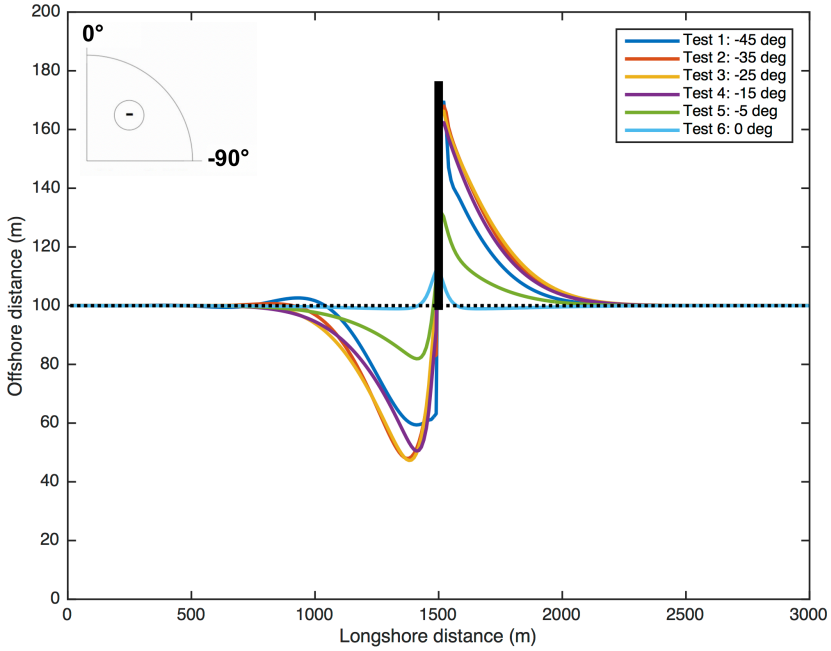

Figure 6.2 – Calculated shoreline change for straight initial shoreline and single groyne at the center of the domain with H_{so} = 0.75m, T_p = 8 sec, and ϑ_o = - 45 deg (Test 1), - 35 deg (Test 2), - 25 deg (Test 3), -15 deg (Test 4), - 5 deg (Test 5), 0 deg (Test 6)

For considered values of ϑ_o = -45, -35, -25, -15, -5, 0 deg, Figure 6.3 shows the calculated mean net transport rate. With reference to values ϑ_o = -15, -5 deg, the groyne presents a total obstruction to longshore transport, which results in a shoreline advance seaward on the right (updrift) side of the groin, as the transport rates decrease from approximately 60,000 and 20,000 m^3/yr, respectively, to 0 m^3/yr at the groin. On the contrary, as transport rates increase from 0 m^3/yr in the vicinity of the groin, back to 60,000 and 20,000 m^3/yr, respectively, outside of the region of groin influence, the expected downdrift shoreline retreat has been observed on the left (downdrift) side. For considered values of ϑ_o = -45, -35, -25 deg, the groin presents a partial obstruction to longshore transport, which results in a shoreline advance seaward on the right (updrift) side of the groin, as the transport rates decrease from approximately 96,000, 100,000 and 87,000 m^3/yr to approximately 55,000, 40,000 and 20,000 m^3/yr, respectively, at the groin.

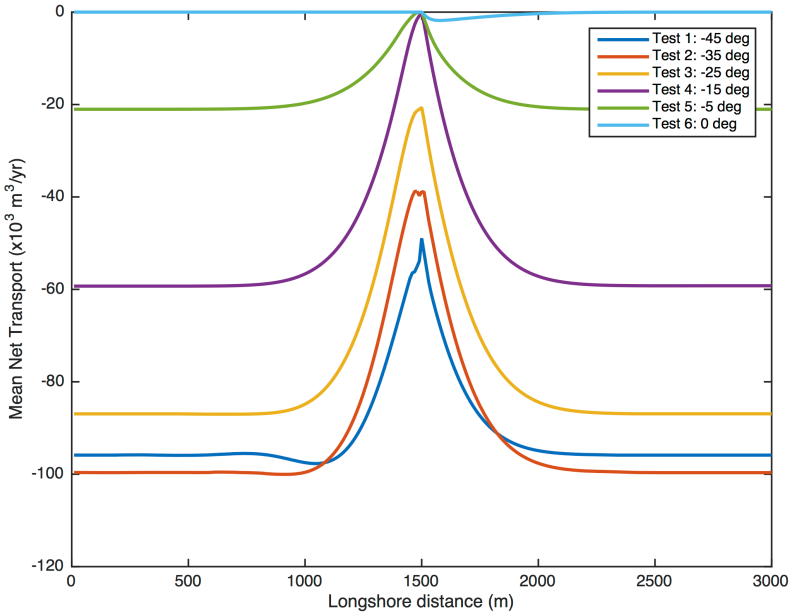

Figure 6.3 – Calculated mean net transport rate for straight initial shoreline and single groyne at the center of the domain with H_{so} = 0.75m, T_p = 8 sec, and ϑ_o = - 45 deg (Test 1), - 35 deg (Test 2), - 25 deg (Test 3), -15 deg (Test 4), - 5 deg (Test 5), 0 deg (Test 6)

For considered values of ϑ_o = 5, 15, 25, 35, 45 deg, Figure 6.4 shows the calculated shoreline change induced by sediment transport, acting from left to right, which results in a sediment accumulation and retreat on the left and right sides of the groyne, respectively. Maximum accumulation/retreat rates for ϑ_o = 35 and ϑ_o = 25 deg have been obtained.

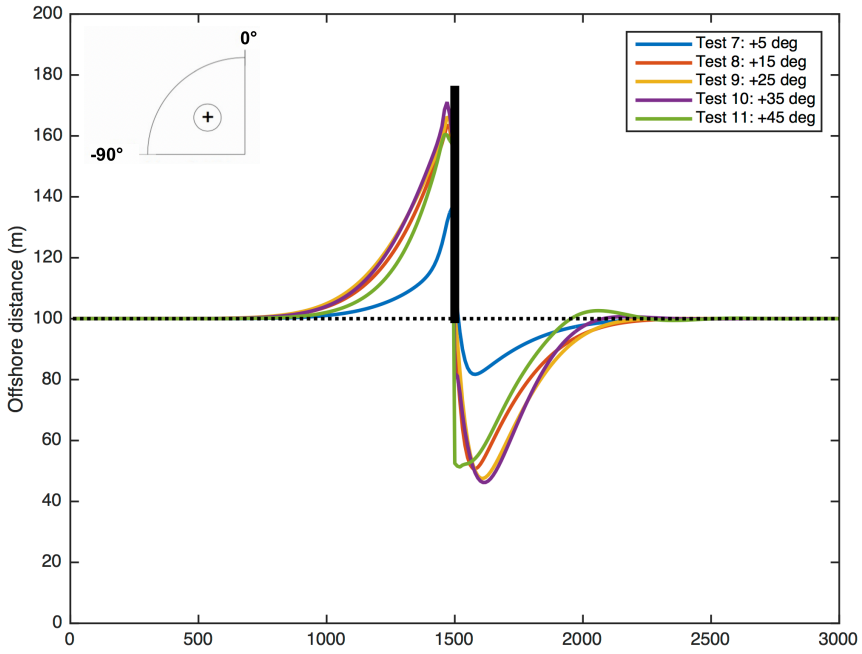

Figure 6.4 - Calculated shoreline change for straight initial shoreline and single groyne at the center of the domain with H_{so} = 0.75m, T_p = 8 sec, and ϑ_o = +5 deg (Test 7), + 15 deg (Test 8), + 25 deg (Test 9), + 35 deg (Test 10), + 45 deg (Test 11)

For considered values of ϑ_o = 5, 15, 25, 35, 45 deg, Figure 6.5 shows the calculated mean net transport rate. With reference to values ϑ_o = 5, 15 deg, the groyne presents a total obstruction to longshore transport, which results in a shoreline advance seaward on the left (updrift) side of the groin, as the transport rates decrease from approximately 20,000 and 60,000 m^3/yr, respectively, to 0 m^3/yr at the groin. On the contrary, as transport rates increase from 0 m^3/yr in the vicinity of the groin, back to approximately 60,000 and 20,000 m^3/yr, respectively, outside of the region of groin influence, the expected downdrift shoreline retreat has been observed on the right (downdrift) side. For considered values of ϑ_o = 25, 35, 45 deg, the groin presents a partial obstruction to longshore transport, which results in a shoreline advance seaward on the right (updrift) side of the groyne, as the transport rates decrease from approximately 87,000, 100,000 and 96,000 m^3/yr to approximately 20,000, 40,000 and 55,000 m^3/yr, respectively, at the groyne.

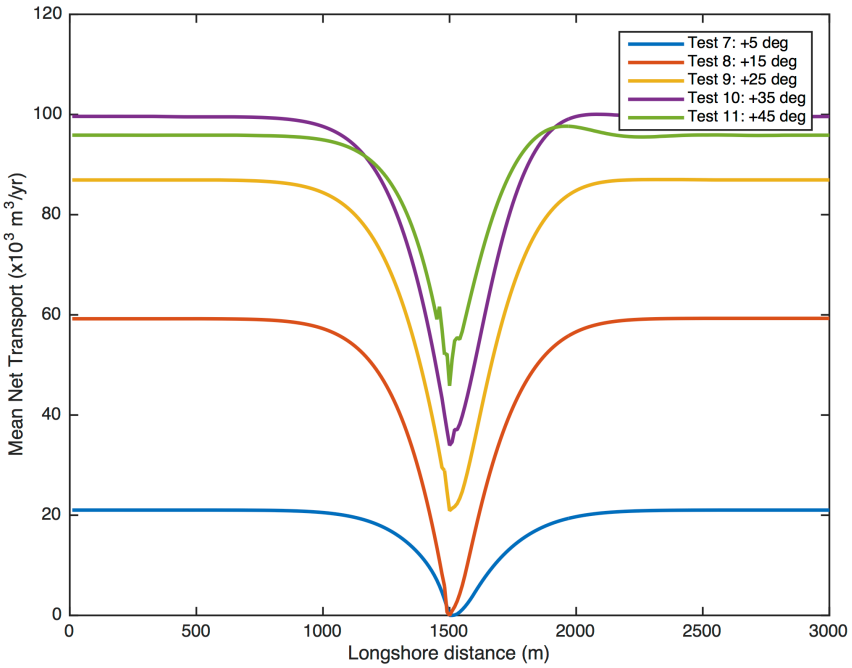

Figure 6.5 – Calculated mean net transport rate for straight initial shoreline and single groyne at the center of the domain with H_{so} = 0.75m, T_p = 8 sec, and ϑ_o = +5 deg (Test 7), + 15 deg (Test 8), + 25 deg (Test 9), + 35 deg (Test 10), + 45 deg (Test 11)

6.1.2 Boundary conditions

The sensitivity analysis of the boundary conditions has been evaluated considering pinned, gated and moving boundaries with the adopted input parameters summarised in Table 6.3.

Table 6.3 - GSb input for single groyne simulation, varying the boundary conditions

Model domain	Number of cells alongshore	NX = 300
	Dimension of cells	DX = 10 m
	Calculation time step	DT = 0.5 hrs
	Median grain size	D_{50} = 0.3 mm
	Berm height	D_B = 1m
	Closure depth	D_C = 8 m
Model forcing (at 50 m contours)	Offshore wave height	H_{so} = 0.75 m
	Peak wave period	T_p = 8 sec
	Wave angle	ϑ_o = +15 deg
Model parameters	Calibration parameter	K_{GSb} = 0.25
	Boundary conditions	Pinned, Gated, Moving (+ 10 m left, - 10 m right)
	Duration of simulation	t = 2 years
Structures	Single groyne 75 m long at x = 1500 m	
Initial shoreline	Straight shoreline 3000 m long	

For considered boundary conditions, pinned, gated and moving, Figure 6.6 shows the calculated shoreline change induced by sediment transport, acting from left to right.

Approximatively from x = 750 m to x = 2250 m, the calculated shoreline change appears independent of the selected boundary. This result highlights that in proximity of the groyne the behaviour (advance/retreat) of the shoreline is not influenced by the selection of the boundary.

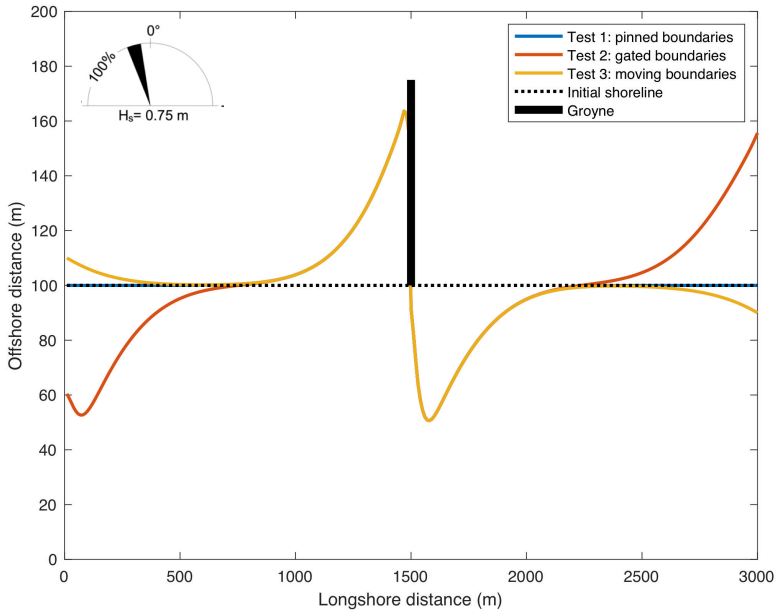

Figure 6.6 - Calculated shoreline change for straight initial shoreline and single groyne at the center of the domain with H_{so} = 0.75m, T_p = 8 sec, ϑ_o = 15 deg, and boundaries: a) pinned (Test 1), b) gated (Test 2), c) moving (+ 10 m left, - 10 m right) (test 3)

Figure 6.7 shows the calculated mean net transport rate for the considered three boundary conditions. In particular, at x = 0 m and x = 3000 m, values of Q_l = 60,000, 0, and 67,000 m^3/yr have been obtained. In the interval between x = 750 to x = 2250 m, for the three different boundaries, very similar values of Q_l have been determined, with $Q_l = 0$ at the groyne.

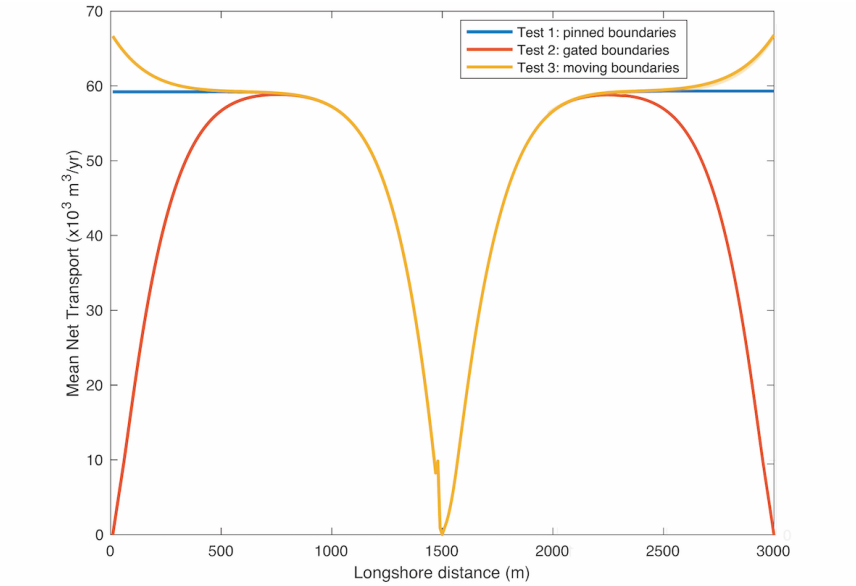

Figure 6.7 – Calculated mean net transport rate for straight initial shoreline and single groyne at the center of the domain with H_{so} = 0.75m, T_p = 8 sec, ϑ_o = 15 deg, and boundaries: pinned (Test 1), gated (Test 2), moving (+ 10 m left, - 10 m right) (test 3)

6.1.3 Median grain size

One important aspect of the GSb model regards the possibility to simulate the shoreline evolution for a mound composed of not cohesive grains of any size, from sand to rock units. In order to evaluate the correct shoreline response for different type of sediment when a groyne is present, some simulations varying the median grain size, D_{50}, have been performed. The adopted input parameters are described in Table 6.4.

Table 6.4 - GSb input for single groyne simulation, varying the boundary conditions

Model domain	Number of cells alongshore	NX = 300
	Dimension of cells	DX = 10 m
	Calculation time step	DT = 0.5 hrs
	Median grain size	D_{50} = 0.3 mm (sand), 30 mm (pebbles), 100 mm (cobbles)
	Berm height	D_B = 1m
	Closure depth	D_C = 8 m
Model forcing (at 50 m contours)	Offshore wave height	H_{so} = 0.75 m
	Peak wave period	T_p = 8 sec
	Wave angle	ϑ_o = +15 deg
Model parameters	Calibration parameter	K_{GSb} = 0.25
	Boundary conditions	Pinned
	Duration of simulation	t = 2 years
Structures	Single groyne 75 m long at x = 1500 m	
Initial shoreline	Straight shoreline 3000 m long	

Figure 6.8 shows the shoreline change after 2 years, under a regular wave attack (H_o = 0.75 m, T = 8 sec, ϑ_o = 15 deg) for different sediment diameters: 0.3, 30, and 100 mm corresponding to sand, pebbles, and cobbles, respectively. As expected, a lower shoreline advance/retreat has been observed when considering bigger sediment diameters. In the left (updrift) side of the groyne, maximum values of shoreline advance, equal to 60, 40, and 20 m, have been obtained for D_{50} = 0.3, 30, and 100 mm, respectively.

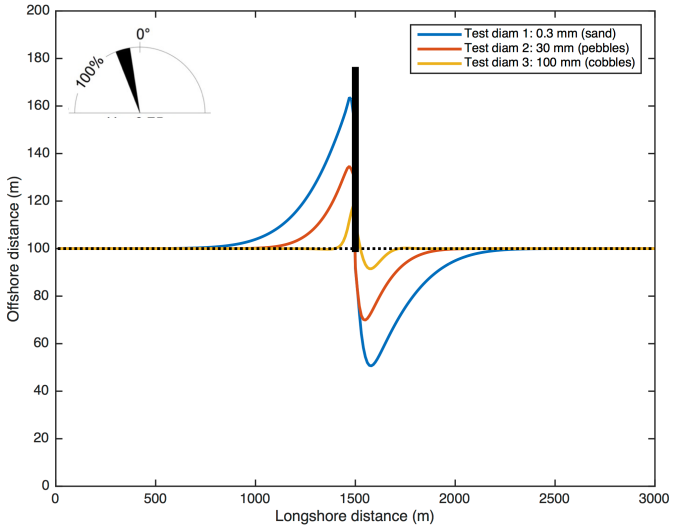

Figure 6.8 - Calculated shoreline change for straight initial shoreline and single groyne at the center of the domain with H_{so} = 0.75m, T_p = 8 sec, ϑ_o = 15 deg, and median grain size: D_{50} = 0.3 mm (Test diam 1), D_{50} = 30 mm (Test diam 2), D_{50} = 100 mm (Test diam 3)

For considered values of D_{50} = 0.3, 30, and 100 mm, shows the mean net transport rate which results at the boundaries and, due to the groin obstruction to longshore transport, zero around the groin.

As shown in Figure 6.9, the mean net transport rate attains positive values (60,000, 23,000, and 3,000 m^3/yr, respectively) at the boundaries, whereas, due to the total groyne obstruction to longshore transport, $Q_l = 0$ at x = 1500 m.

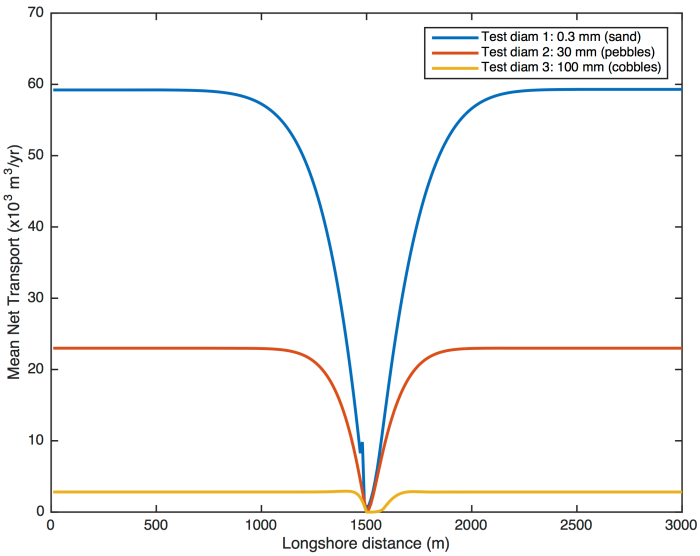

Figure 6.9 – Calculated mean net transport rate for straight initial shoreline and single groyne at the center of the domain with H_{so} = 0.75m, T_p = 8 sec, ϑ_o = 15 deg, and median grain size: D_{50} = 0.3 mm (Test diam 1), D_{50} = 30 mm (Test diam 2), D_{50} = 100 mm (Test diam 3)

6.1.4 Permeability

In order to check if a groyne acts correctly when it is permeable, simulations have been performed with different permeability percentage. The adopted input parameters are given in Table 6.5.

Table 6.5 - GSb input for single groyne simulation, varying the permeability factor

Model domain	Number of cells alongshore	NX = 300
	Dimension of cells	DX = 10 m
	Calculation time step	DT = 0.5 hrs
	Median grain size	D_{50} = 0.3 mm
	Berm height	D_B = 1m
	Closure depth	D_C = 8 m
Model forcing (at 50 m contours)	Significant offshore wave height	H_{so} = 0.75 m
	Peak wave period	T_p = 8 sec
	Wave angle	$\vartheta_o = +15$ deg
Model parameters	Calibration parameter	K_{GSb} = 0.25
	Boundary conditions	Pinned
	Duration of simulation	t = 2 years
Structures	Single groyne 75 m long at x = 1500 m with permeability p = 0 % (imperm), 25 %, 50 %, 75 %,100 % (fully perm.)	
Initial shoreline	Straight shoreline 3000 m long	

Figure 6.10 shows the shoreline evolution after 2 years, for different values of permeability factor: p = 0%, 25%, 50%, 75%, 100% where p= 0% and 100% corresponds to impermeable and fully permeable groyne, respectively.

As expected, a lower shoreline advance/retreat has been observed when considering higher value of p. In the left (updrift) side of the groyne, maximum values of shoreline advance, equal to 62, 44, 22, and 15 m, have been obtained for p = 0%, 25%, 50% 75%, respectively. In case of p = 100% (groyne fully permeable), the calculated shoreline coincides to the initial shoreline.

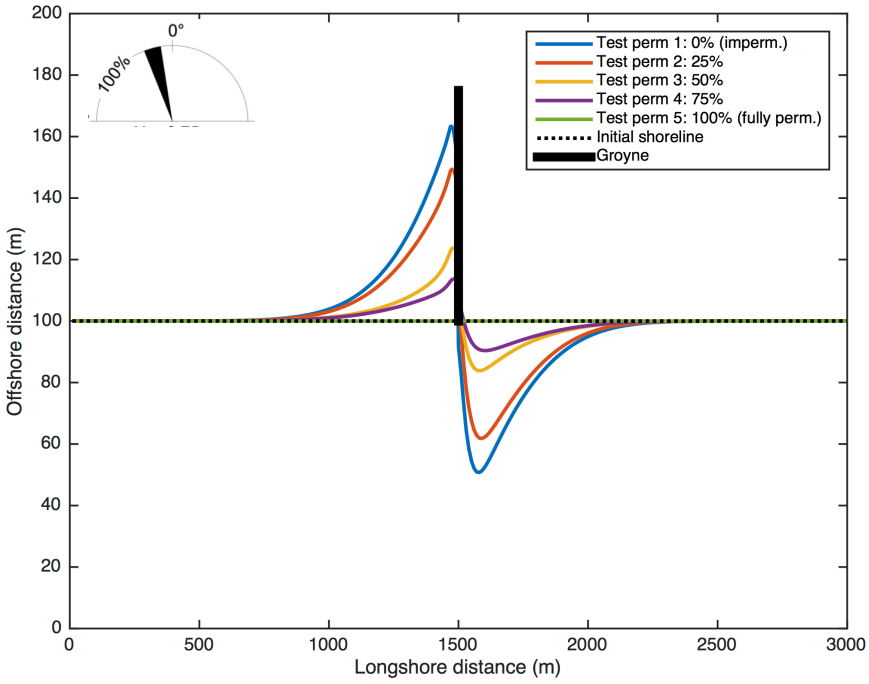

Figure 6.10 - Calculated shoreline change for straight initial shoreline and single groyne at the center of the domain with H_{so} = 0.75m, T_p = 8 sec, ϑ_o = 15 deg, and permeability p = 0% (Test perm 1), 25% (Test perm 2), 50% (Test perm 3), 75% (Test perm 4), 100% (Test perm 5)

Figure 6.11 shows the behaviour of the mean net transport rate for the considered permeability factor, p = 0%, 25%, 50%, 75%. For p = 0 %, the groyne presents a total obstruction (impermeable groyne) to longshore transport, which results in a shoreline advance seaward on the left (updrift) side of the groin, as the transport rates decrease from approximately 60,000 m^3/yr to 0 m^3/yr at the groin. For p = 25%, 50%, 75%, the groin presents a partial obstruction (permeable groyne) to longshore transport, which results in a shoreline advance seaward on the left (updrift) side of the groyne, as the transport rates decrease from approximately 16,000 m^3/yr to approximately 45,000, and 50,000 m^3/yr, respectively, at the groyne. For a value of p =100% (fully permeable groyne), the mean net transport rate is constant and approximatively equal to 60,000 m^3/yr.

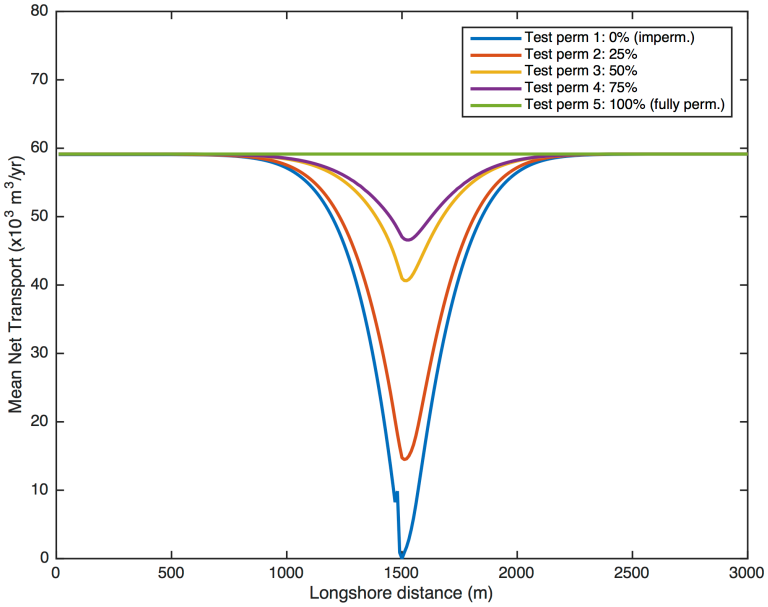

Figure 6.11 - Calculated mean net transport rate for straight initial shoreline and single groyne at the center of the domain with H_{so} = 0.75m, T_p = 8 sec, ϑ_o = 15 deg, and permeability p = 0% (Test perm 1), 25% (Test perm 2), 50% (Test perm 3), 75% (Test perm 4), 100% (Test perm 5)

6.1.5 K_{GSb} parameter

The sensitivity analysis of the GSb calibration parameter has been performed for different value of K_{GSb}. The adopted input parameters are given in Table 6.6.

Table 6.6 - GSb input for single groyne simulation, varying the calibration parameter K_{GSb}

Model domain	Number of cells alongshore	NX = 300
	Dimension of cells	DX = 10 m
	Calculation time step	DT = 0.5 hrs
	Median grain size	D_{50} = 0.3 mm
	Berm height	D_B = 1m
	Closure depth	D_C = 8 m
Model forcing (at 50 m contours)	Offshore significant wave height	H_{so} = 0.75 m
	Peak wave period	T_p = 8 sec
	Wave angle	ϑo = +15 deg
Model parameters	Calibration parameter	K_{GSb} = 0.01, 0.10, 0.25, 0.50
	Boundary conditions	Pinned
	Duration of simulation	t = 2 years
Structures	Single groyne 75 m long at x = 1500 m	
Initial shoreline	Straight shoreline 3000 m long	

Figure 6.12 shows the shoreline evolution after 2 years, for the considered values of calibration parameters: K_{GSb} = 0.01, 0.1, 0.25, 0.5. For values of K_{GSb} = 0.50, and 0.01, a shoreline advance/retreat of 68 and 54 m/ 48 and 53, respectively, has been observed.

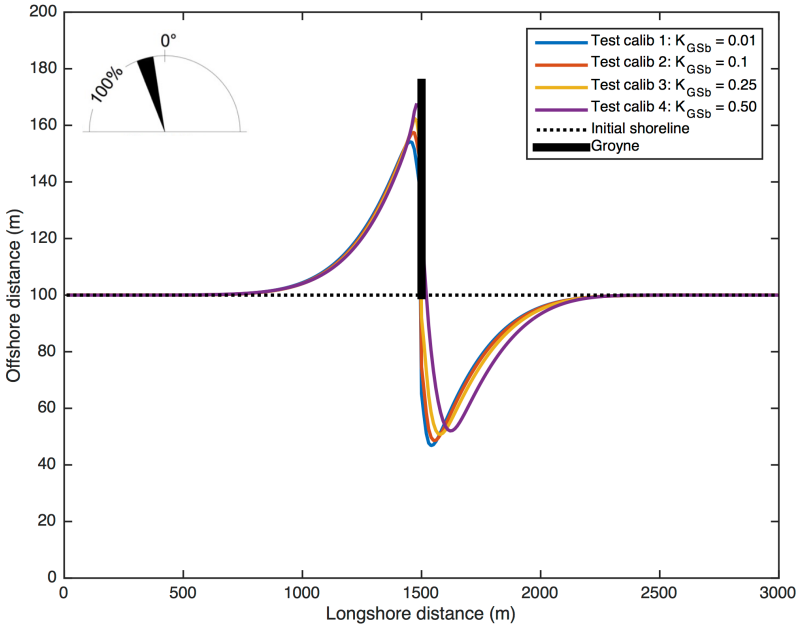

Figure 6.12 - Calculated shoreline change for straight initial shoreline and single groyne at the center of the domain with H_{so} = 0.75m, T_p = 8 sec, ϑ_o = 15 deg, and calibration parameter K_{GSb} = 0.01 (Test calib 1), 0.10 (Test calib 2), 0.25 (Test calib 3), 0.50 (Test calib 4)

Figure 6.13 shows the mean net transport rate for the considered calibration parameters, K_{GSb}= 0.01, 0.1, 0.25, 0.5, in which the net transport rate results approximatively 60,000 m^3/yr at the boundaries, decreasing up to 0 m^3/yr at the groin.

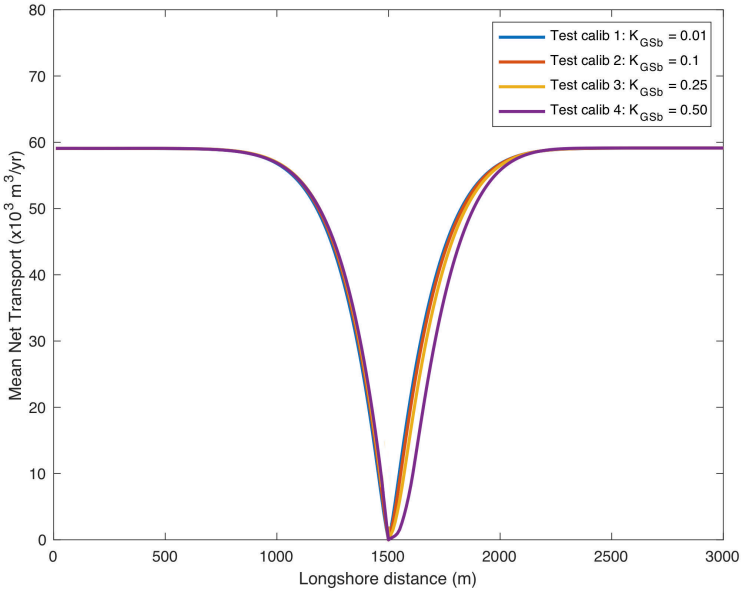

Figure 6.13 - Calculated mean net transport rate for straight initial shoreline and single groyne at the center of the domain with H_{so} = 0.75m, T_p = 8 sec, ϑ_o = 15 deg, and calibration parameter K_{GSb} = 0.01 (Test calib 1), 0.10 (Test calib 2), 0.25 (Test calib 3), 0.50 (Test calib 4)

6.2 Single detached breakwater

The benchmark simulations for the case of single detached breakwater have been performed. The shoreline change for a straight shoreline 3000 m long with a single detached breakwater 100 m long located 175 m offshore (y = 175 m) at the centre of the domain (from x = 1450 to x = 1550 m) has been calculated. A model grid cell resolution, DX, has been selected equal to 10 m with a total number of cells, NX = 300. The adopted median grain size, D_{50}=0.3 mm. GSb has been run with $K_{GSb} = 0.25$, and the boundary conditions have been set as pinned. The calculation time step has been fixed equal to 0.5 hrs. Wave inputs have been supplied at the 50 m depth contour. The adopted input parameters are given in Table 6.7.

Table 6.7 – GSb input for single detached breakwater simulation (Frey et al., 2012)

Model domain	Number of cells alongshore	NX = 300
	Dimension of cells	DX = 10 m
	Calculation time step	DT = 0.5 hrs
	Median grain size	D_{50} = 0.3 mm
	Berm height	D_B = 1m
	Closure depth	D_C = 8 m
Model forcing (at 50 m contours)	Significant offshore wave height	H_{so} = 0.75 m
	Peak wave period	T_p = 8 sec
	Wave angle	ϑo = 15 deg
Model parameters	Calibration parameter	K_{GSb} = 0.25
	Boundary conditions	Pinned
	Duration of simulation	t = 2 years
Structures	Single detached breakwater, 100 m long, from x = 1450 to x = 1550 m, at y = 175 m	
Initial shoreline	Straight shoreline 3000 m long	

Figure 6.14 shows the results of the GSb model in terms of shoreline change and mean net transport rate after 2-years simulation. Formation of a salient behind the breakwater that extends approximately 50 m from the initial shoreline has been observed. The transport rate, firstly 60,000 m^3/yr, increases on the left side of the structure to approximately 73,000 m^3/yr and then decreases on the right side of the structure to approximately 53,000 m^3/yr.

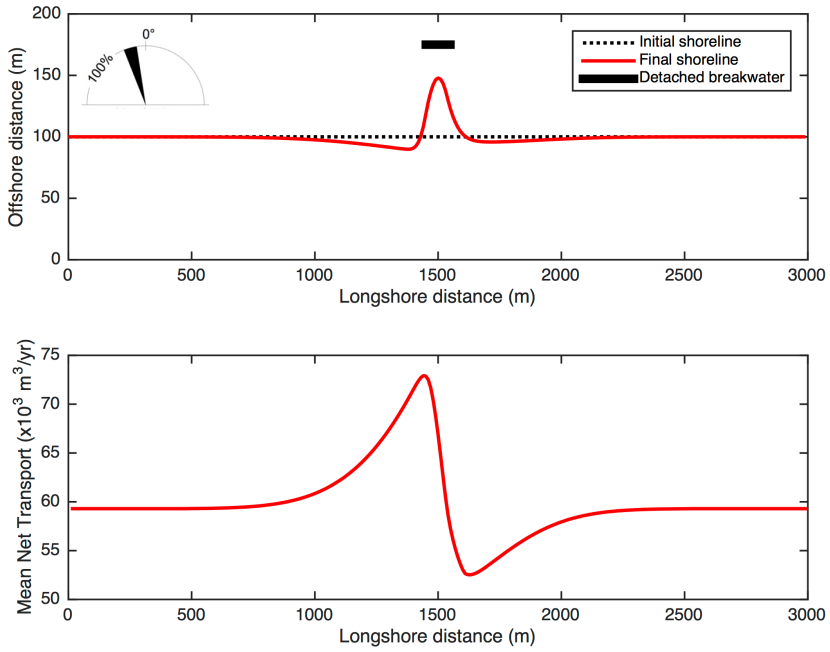

Figure 6.14 - Calculated shoreline change (top) and mean net transport rate (bottom) for straight shoreline with single detached breakwater, and H_o = 0.75m, T = 8 sec, ϑ_o = +15 deg

6.2.1 Wave angle

Simulations varying the offshore wave angle, from - 45 to + 45 deg have been conducted. The adopted input parameters are given in Table 6.8.

Table 6.8 - GSb input for single detached breakwater, varying the offshore wave angles

Model domain	Number of cells alongshore	NX = 300
	Dimension of cells	DX = 10 m
	Calculation time step	DT = 0.5 hrs
	Median grain size	D_{50} = 0.3 mm
	Berm height	D_B = 1m
	Closure depth	D_C = 8 m
Model forcing (at 50 m contours)	Significant offshore wave height	H_{so} = 0.75 m
	Peak Wave period	T_p = 8 sec
	Wave angle	$\vartheta o = -45, -35, -25, -15, -5, 0, +5, +15, +25, +35, +45$ deg
Model parameters	Calibration parameter	K_{GSb} = 0.25
	Boundary conditions	Pinned
	Duration of simulation	t = 2 years
Structures	Single detached breakwater, 100 m long, from x = 1450 to x = 1550 m, at y = 175 m	
Initial shoreline	Straight shoreline 3000 m long	

For considered values of ϑ_o = -45, -35, -25, -15, -5, 0 deg, Figure 6.15 shows the calculated shoreline change induced by sediment transport. Tombolo development for values of ϑ_o = - 45 and ϑ_o = -35 deg has been obtained. It is noticed that, for the cases of ϑ_o = -25, -15, -5, and 0 deg, a salient formation approximately 68, 55, 49, and 48 m, respectively, has been observed.

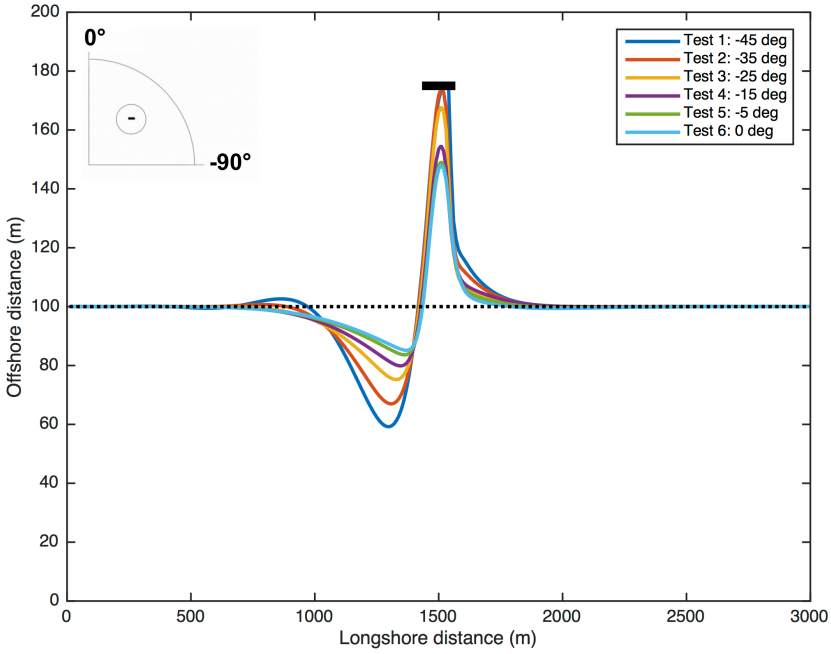

Figure 6.15 - Calculated shoreline change for straight initial shoreline and single detached breakwater at the center of the domain with H_{so} = 0.75m, T_p = 8 sec, and ϑ_o = - 45 deg (Test 1), - 35 deg (Test 2), - 25 deg (Test 3), -15 deg (Test 4), - 5 deg (Test 5), 0 deg (Test 6)

For considered values of ϑ_o = -45, -35, -25, -15, -5, 0 deg, Figure 6.16 shows the calculated mean net transport rate highlighting a decrease from 95,000, 100,000, 85,000, 60,000, 20,000, 0 m^3/yr, to 57,000, 65,000, 60,000, 35,000, 5,000, 0 m^3/yr, respectively, at the left side of the breakwater. It is noticed that, for the case of ϑ_o = 0, in correspondence of the right side of the breakwater, a small mean net transport increase has been observed.

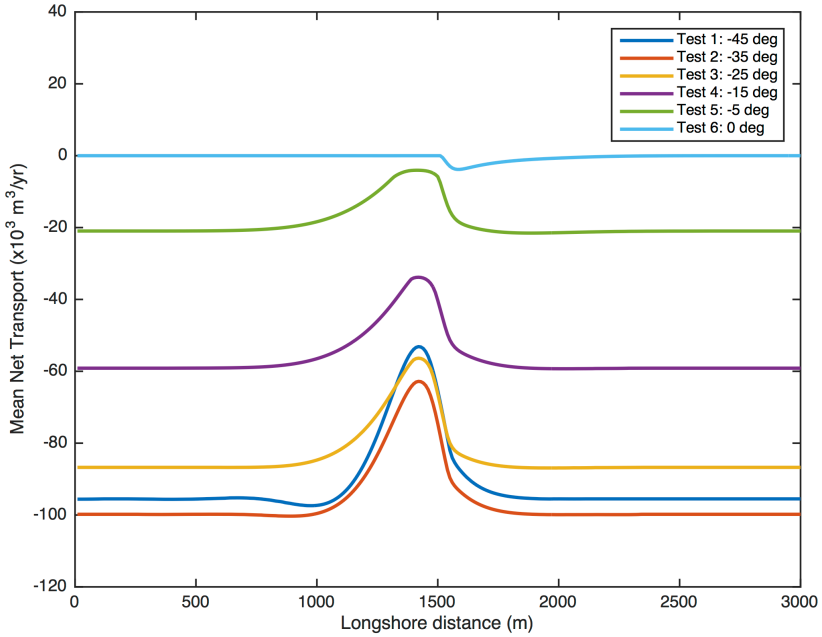

Figure 6.16 - Calculated mean net transport rate for straight initial shoreline and single detached breakwater at the center of the domain with H_{so} = 0.75m, T_p = 8 sec, and ϑ_o = - 45 deg (Test 1), - 35 deg (Test 2), - 25 deg (Test 3), -15 deg (Test 4), - 5 deg (Test 5), 0 deg (Test 6)

Figure 6.17 shows, for the considered wave angles, the calculated shoreline change. A sediment accumulation directly behind the breakwater structure, with a salient formation of 47, 48, 55, 58 and 61 m, for ϑ_o = -45, -35, -25, -15, -5, and 0 deg, respectively, has been observed.

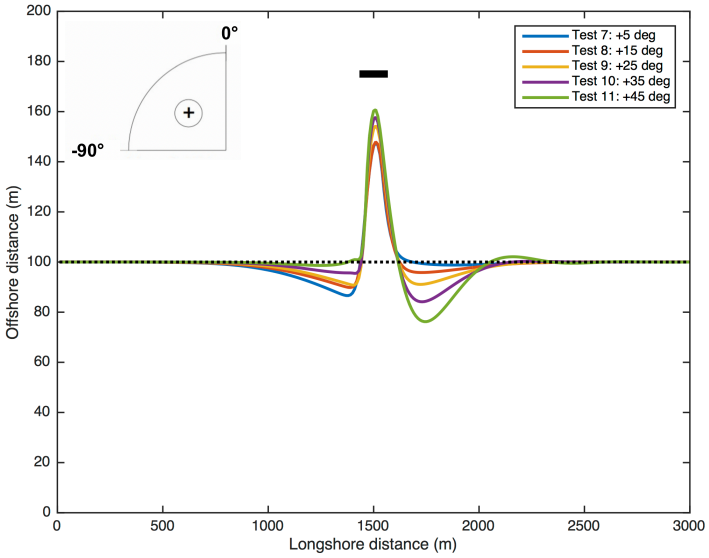

Figure 6.17 - Calculated shoreline change for straight initial shoreline and single detached breakwater at the center of the domain with H_{so} = 0.75m, T_p = 8 sec, and ϑ_o = +5 deg (Test 7), + 15 deg (Test 8), + 25 deg (Test 9), + 35 deg (Test 10), + 45 deg (Test 11)

For ϑ_o = -45, -35, -25, -15, -5, and 0 deg, Figure 6.18 shows the calculated mean net transport rate showing an increase from 20,000, 60,000, 85,000, 100,000, and 97,000 m^3/yr, to 40,000, 75,000, 97,000, 97,500, and 105,000 m^3/yr, respectively, at the left side of the breakwater, and a following decrease up to 19,000, 50,000, 75,000, 80,000, and 71,000 m^3/yr, respectively, at the right side of the breakwater.

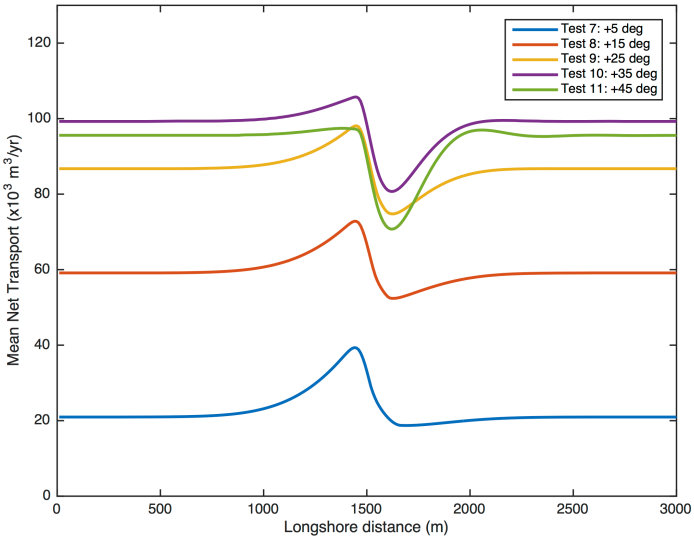

Figure 6.18 - Calculated mean net transport rate for straight initial shoreline and single detached breakwater at the center of the domain with H_{so} = 0.75m, T_p = 8 sec, and ϑ_o = +5 deg (Test 7), + 15 deg (Test 8), + 25 deg (Test 9), + 35 deg (Test 10), + 45 deg (Test 11)

6.2.2 *Boundary conditions*

The sensitivity analysis of the boundary conditions has been evaluated considering pinned, gated and moving boundaries. The adopted input parameters are given in Table 6.9.

Table 6.9 – GSb input for single detached breakwater simulation, varying the boundary conditions

Model domain	Number of cells alongshore	NX = 300
	Dimension of cells	DX = 10 m
	Calculation time step	DT = 0.5 hrs
	Median grain size	D_{50} = 0.3 mm
	Berm height	D_B = 1m
	Closure depth	D_C = 8 m
Model forcing (at 50 m contours)	Significant offshore wave height	H_{so} = 0.75 m
	Peak wave period	T_p = 8 sec
	Wave angle	ϑ_o = 15 deg
Model parameters	Calibration parameter	K_{GSb} = 0.25
	Boundary conditions	Pinned, Gated, Moving (+ 10 m left, - 10 m right)
	Duration of simulation	t = 2 years
Structures	Single detached breakwater, 100 m long, from x = 1450 to x = 1550 m, at y = 175 m	
Initial shoreline	Straight shoreline 3000 m long	

Figure 6.19 shows the shoreline change after 2 years for the considered three boundary conditions: pinned, gated and moving. Approximatively from x = 750 m to x = 2250 m, the calculated shoreline change appears independent of the selected boundary. This result highlights that in proximity of the breakwater the behaviour (advance/retreat) of the shoreline is not influenced by the selection of the boundary.

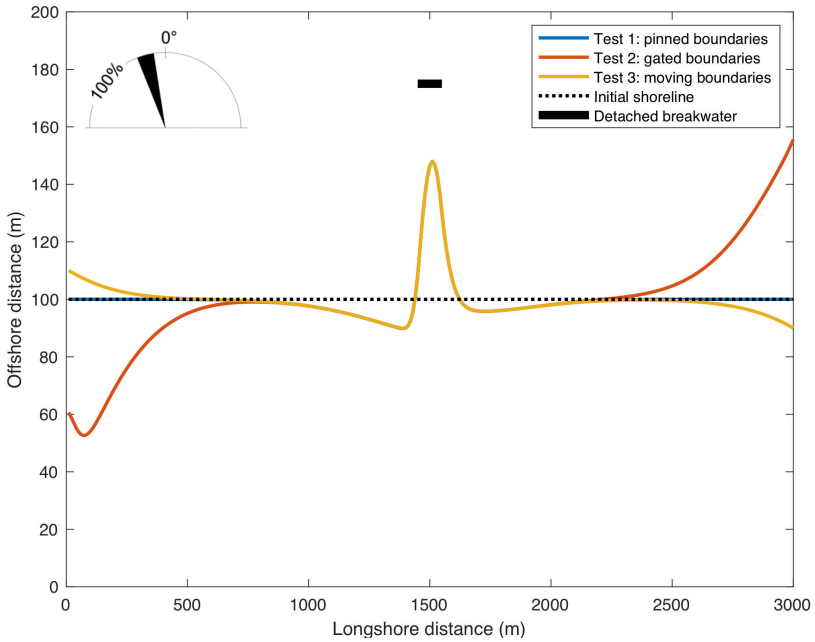

Figure 6.19 - Calculated shoreline change for straight initial shoreline and single detached breakwater at the center of the domain with H_{so} = 0.75m, T_p = 8 sec, ϑ_o = 15 deg, and boundaries: pinned (Test 1), gated (Test 2), moving (+ 10 m left, - 10 m right) (test 3)

Figure 6.20 shows the calculated mean net transport rate for the considered three boundary conditions. In particular, at x = 0 m and x = 3000 m, values of Q_l = 60,000, 0, and 67,000 m^3/yr have been obtained. In the interval between x = 750 to x = 2250 m, for the three different boundaries, very similar values of Q_l have been determined.

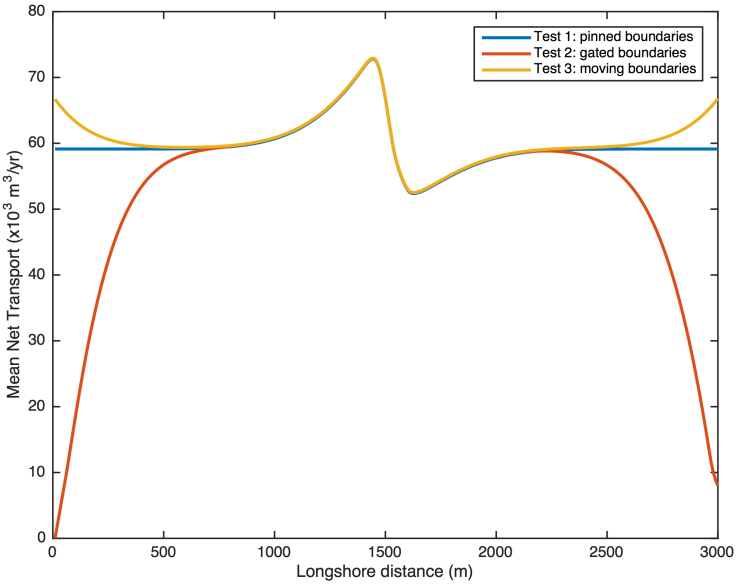

Figure 6.20 - Calculated mean net transport rate for straight initial shoreline and single detached breakwater at the center of the domain with H_{so} = 0.75m, T_p = 8 sec, ϑ_o = 15 deg, and boundaries: pinned (Test 1), gated (Test 2), moving (+ 10 m left, - 10 m right) (test 3)

6.2.3 Median grain size

In order to evaluate the correct shoreline response for different type of sediment when a detached breakwater is present, some simulations varying the median grain size, D_{50}, have been performed. The adopted input parameters are given in Table 6.10.

Table 6.10 - GSb input for single detached breakwater simulation, varying the boundary conditions

Model domain	Number of cells alongshore	NX = 300
	Dimension of cells	DX = 10 m
	Calculation time step	DT = 0.5 hrs
	Median grain size	D_{50} = 0.3 mm (sand), 30 mm (pebbles), 100 mm (cobbles)
	Berm height	D_B = 1m
	Closure depth	D_C = 8 m
Model forcing (at 50 m contours)	Significant offshore wave height	H_{so} = 0.75 m
	Peak wave period	T_p = 8 sec
	Wave angle	ϑ_o = +15 deg
Model parameters	Calibration parameter	K_{GSb} = 0.25
	Boundary conditions	Pinned
	Duration of simulation	t = 2 years
Structures	Single detached breakwater, 100 m long, from x = 1450 to x = 1550 m, at y = 175 m	
Initial shoreline	Straight shoreline 3000 m long	

Figure 6.21 shows the shoreline change after 2 years for different sediment diameters: D_{50} = 0.3, 30, and 100 mm corresponding to sand, pebbles, and cobbles, respectively. As expected, a lower salient evolution has been observed when considering bigger sediment diameters. Behind the breakwater, maximum values of shoreline advance, equal to 48, 31, and 13 m, have been obtained for D_{50} = 0.3, 30, and 100 mm, respectively.

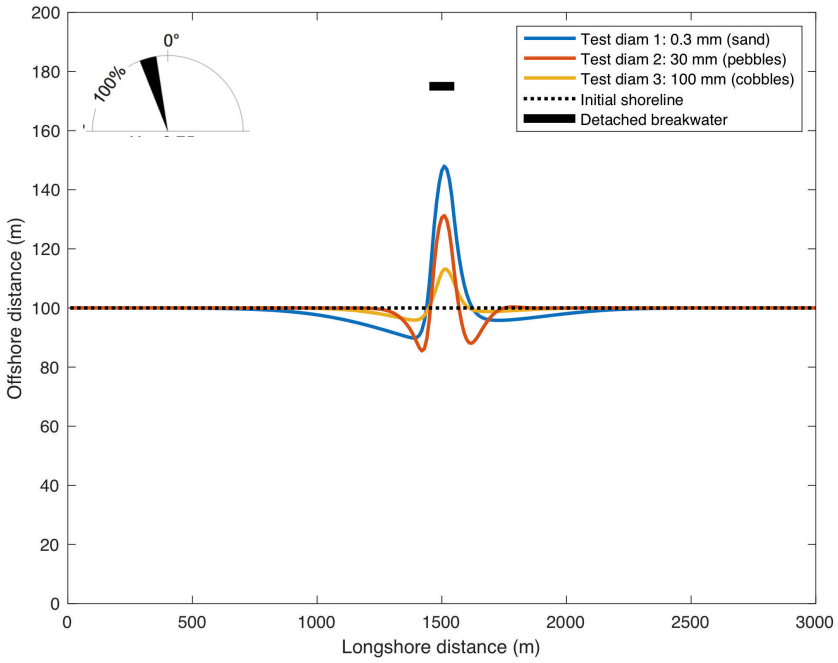

Figure 6.21 - Calculated shoreline change for straight initial shoreline and single detached breakwater at the center of the domain with H_{so} = 0.75m, T_p = 8 sec, ϑ_o = 15 deg, and median grain size: D_{50} = 0.3 mm (Test diam 1), D_{50} = 30 mm (Test diam 2), D_{50} = 100 mm (Test diam 3)

Figure 6.22 shows an increase of the mean net transport rate, from 60,000, 22,000, and 3,000 m^3/yr, at x = 0 to approximately 73,000, 25,000, and 9,000 m^3/yr, on the left side of the breakwater for D_{50} = 0.3, 30, and 100 mm, respectively, has been observed. It is noticed that, for the three cases, in correspondence of the right side of the structure, a value of Q_l = 53,000, 20,000, and 0,0 m^3/yr, has been observed.

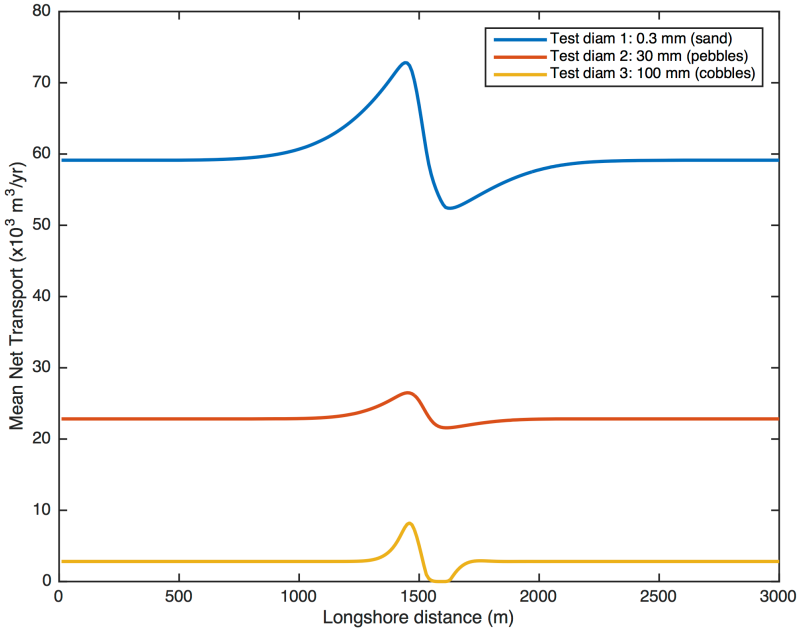

Figure 6.22 - Calculated mean net transport rate for straight initial shoreline and single detached breakwater at the center of the domain with H_{so} = 0.75m, T_p = 8 sec, ϑ_o = 15 deg, and median grain size: D_{50} = 0.3 mm (Test diam 1), D_{50} = 30 mm (Test diam 2), D_{50} = 100 mm (Test diam 3)

6.2.4 Permeability

In order to check if a detached breakwater acts correctly when it is permeable, simulations have been performed with different values of permeability percentage. The adopted input parameters are given in Table 6.11.

Table 6.11 - GSb input for single detached breakwater simulation, varying the permeability factor

Model domain	Number of cells alongshore	NX = 300
	Dimension of cells	DX = 10 m
	Calculation time step	DT = 0.5 hrs
	Median grain size	D_{50} = 0.3 mm
	Berm height	D_B = 1m
	Closure depth	D_C = 8 m
Model forcing (at 50 m contours)	Significant offshore wave height	H_{so} = 0.75 m
	Peak wave period	T_p = 8 sec
	Wave angle	$\vartheta_o = +15$ deg
Model parameters	Calibration parameter	K_{GSb} = 0.25
	Boundary conditions	Pinned
	Duration of simulation	t = 2 years
Structures	Single detached breakwater, 100 m long, from x = 1450 to x = 1550 m, at y = 175 m with permeability p = 0% (imperm), 25%, 50%, 75%,100% (fully perm.)	
Initial shoreline	Straight shoreline 3000 m long	

Figure 6.23 shows the shoreline evolution after 2 years for different values of permeability factor: p = 0%, 25%, 50%, 75%, 100% where p= 0% and 100% corresponds to impermeable and fully permeable detached breakwater, respectively.

As expected, a lower salient formation has been observed when considering higher value of p. Behind the breakwater, maximum values of shoreline advance, equal to 48, 46, 38, and 23 m, have been obtained for p = 0%, 25%, 50% 75%, respectively. In case of p = 100% (breakwater fully permeable), the calculated shoreline coincides to the initial shoreline.

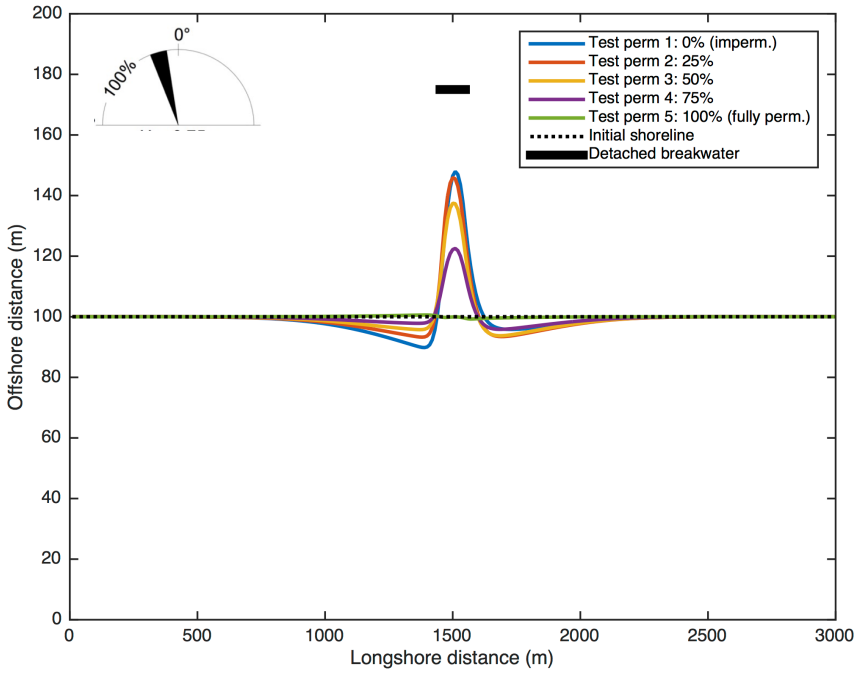

Figure 6.23 - Calculated shoreline change for straight initial shoreline and single detached breakwater at the center of the domain with H_{so} = 0.75m, T_p = 8 sec, ϑ_o = 15 deg, and permeability p = 0% (Test perm 1), 25% (Test perm 2), 50% (Test perm 3), 75% (Test perm 4), 100% (Test perm 5)

Figure 6.24 shows the behaviour of the mean net transport rate for the different values of permeability factor. For p = 0%, 25%, 50%, 75%, the transport rates increase from 60,000 m^3/yr at x = 0 m, to 72,000, 68,000, 65,000 and 62,000 m^3/yr, respectively, behind the left side of detached breakwater. Mean net transport rate decreases in correspondence of the right side of the structure, assuming values of Q_l = 52,000, 49,000, 50,000, and 53,000 m^3/yr for p = 0%, 25%, 50%, 75%, respectively. For a value of p =100% (fully permeable detached breakwater), the mean net transport rate appears constant and approximatively equal to 60,000 m^3/yr.

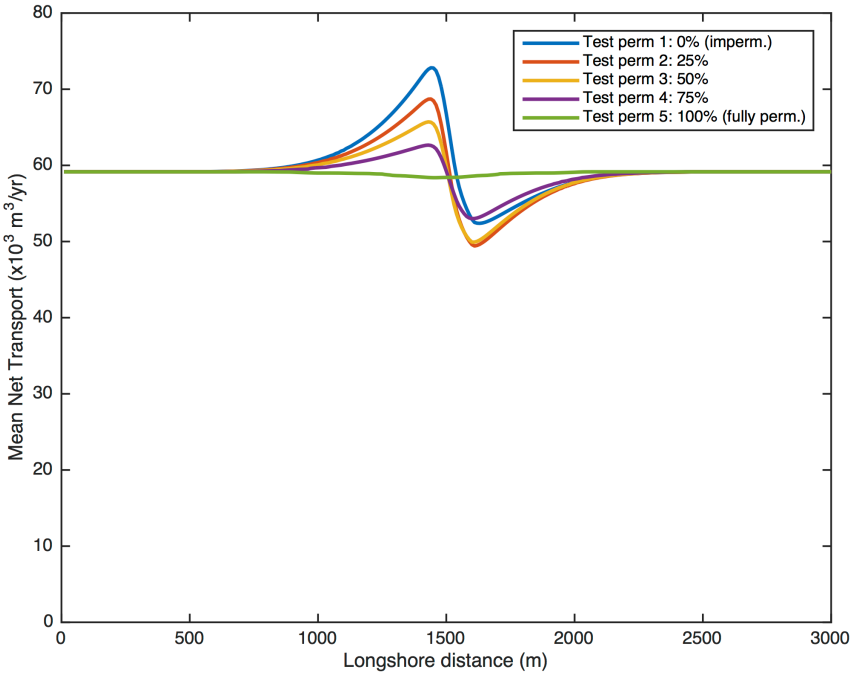

Figure 6.24 - Calculated mean net transport rate for straight initial shoreline and single detached breakwater at the center of the domain with H_{so} = 0.75m, T_p = 8 sec, ϑ_o = 15 deg, and permeability p = 0% (Test perm 1), 25% (Test perm 2), 50% (Test perm 3), 75% (Test perm 4), 100% (Test perm 5)

6.2.5 K_{GSb} parameter

The sensitivity analysis of the GSb calibration parameter has been performed for different value of K_{GSb}. The adopted input parameters are given in Table 6.12.

Table 6.12 - GSb input for single detached breakwater simulation, varying the calibration parameter K_{GSb}

Model domain	Number of cells alongshore	NX = 300
	Dimension of cells	DX = 10 m
	Calculation time step	DT = 0.5 hrs
	Median grain size	D_{50} = 0.3 mm
	Berm height	D_B = 1m
	Closure depth	D_C = 8 m
Model forcing (at 50 m contours)	Significant offshore wave height	H_{so} = 0.75 m
	Peak wave period	T_p = 8 sec
	Wave angle	ϑ_o = +15 deg
Model parameters	Calibration parameter	K_{GSb} = 0.01, 0.10, 0.25, 0.50
	Boundary conditions	Pinned
	Duration of simulation	t = 2 years
Structures	Single detached breakwater, 100 m long, from x = 1450 to x = 1550 m, at y = 175 m	
Initial shoreline	Straight shoreline 3000 m long	

Figure 6.25 shows the shoreline evolution after 2 years for different values of K_{GSb}: 0.01, 0.1, 0.25, 0.5. For values of K_{GSb} = 0.01, 0.1, 0.25, a salient formation of 7, 19 and 48 m,

respectively, has been observed. It is noticed that for K_{GSb} = 0.40 the salient reaches the breakwater.

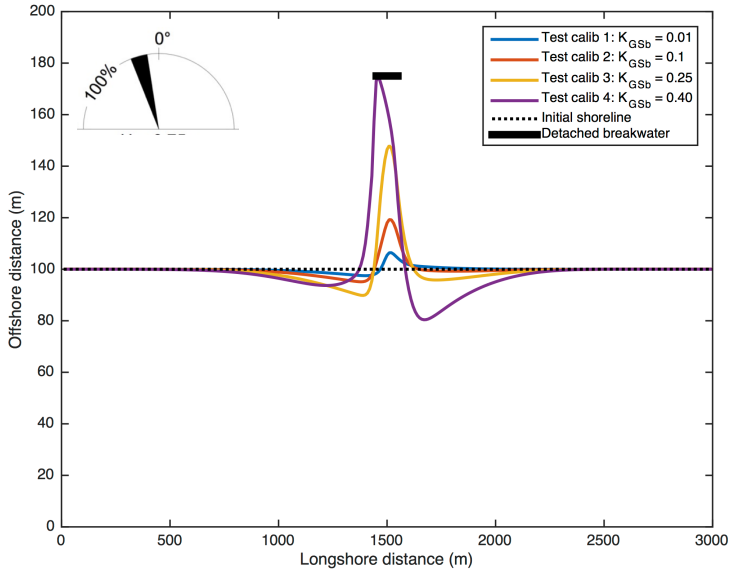

Figure 6.25 - Calculated shoreline change for straight initial shoreline and single detached breakwater at the center of the domain with H_{so} = 0.75m, T_p = 8 sec, ϑ_o = 15 deg, and calibration parameter K_{GSb} = 0.01 (Test calib 1), 0.10 (Test calib 2), 0.25 (Test calib 3), 0.50 (Test calib 4)

Figure 6.26 shows the behaviour of the mean net transport rate for the different values of calibration coefficient. For K_{GSb} = 0.01, 0.1, 0.25, and 0.40 the transport rates increase from 60,000 m^3/yr at x = 0 m, to 62,000, 66,000, 73,000 and 70,000 m^3/yr, respectively, behind the left side of detached breakwater. Mean net transport rate decreases, with values of Q_l = 58,000, 52,000, and 35,000 m^3/yr for K_{GSb} = 0.1, 0.25, and 0.40, respectively, in correspondence of the right side of the structure, have been observed.

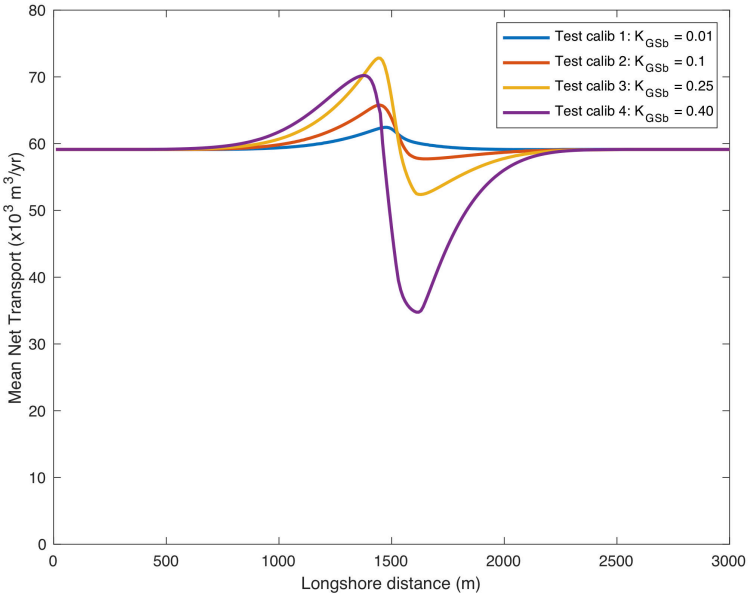

Figure 6.26 - Calculated mean net transport rate for straight initial shoreline and single detached breakwater at the center of the domain with H_{so} = 0.75m, T_p = 8 sec, ϑ_o = 15 deg, and calibration parameter K_{GSb} = 0.01 (Test calib 1), 0.10 (Test calib 2), 0.25 (Test calib 3), 0.40 (Test calib 4)

6.3 Multiple groynes

In order to extend the numerical investigations aimed to verify the model capabilities with predicting the shoreline evolution under wave attacks in presence of coastal structures, the case of multiple groynes has been considered. As initial condition, a straight shoreline 3000 m long with three groynes, 75 m long, located at x = 750, x = 1500, x = 2250, respectively, has been taken into account. A model grid cell resolution, DX, has been selected equal to 10 m with a total number of cells, NX = 300. The adopted median grain size, D_{50}=0.3 mm. GSb has been run with $K_{GSb} = 0.25$, and the boundary conditions have been set as pinned. The calculation time step has been fixed equal to 0.5 hrs. Wave inputs have been supplied at the 50 m depth contour. The adopted input parameters are given in Table 6.13.

Table 6.13 – GSb input for multiple groynes simulation

Model domain	Number of cells alongshore	NX = 300
	Dimension of cells	DX = 10 m
	Calculation time step	DT = 0.5 hrs
	Median grain size	D_{50} = 0.3 mm
	Berm height	D_B = 1m
	Closure depth	D_C = 8 m
Model forcing (at 50 m contours)	Significant offshore wave height	H_{so} = 0.75 m
	Peak wave period	T_p = 8 sec
	Wave angle	ϑ_o = 15 deg
Model parameters	Calibration parameter	K_{GSb} = 0.25
	Boundary conditions	Pinned
	Duration of simulation	t = 2 years
Structures	Three groynes 75 m long at x = 750, 1500, 2250 m	
Initial shoreline	Straight shoreline 3000 m long	

Figure 6.27 shows the shoreline change after 2-years simulation. The groynes determine a total obstruction to longshore transport, which results in a shoreline advance seaward on the left (updrift) side of the structures. As expected, this use of multiple, correctly spaced groins forces the erosion to be displaced to the last groin in the groin field (Dean and Darlymple, 2004).

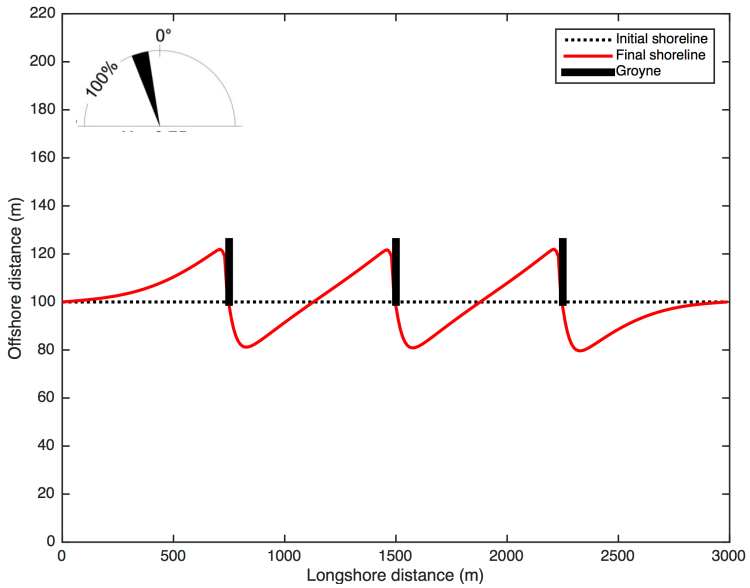

Figure 6.27 - Calculated shoreline change for straight shoreline with multiple groynes

6.4 Multiple detached breakwaters

A further verification of the model capabilities with predicting the shoreline evolution under wave attacks has been performed by considering the presence of multiple detached breakwaters.

As initial condition, a straight shoreline 3000 m long with multiple detached breakwater 100 m long and 175 m offshore (y = 175 m), located from x = 700 to x = 800, from x = 1450 to x = 1550 m, and from x = 2200 to x = 2300, has been taken into account. A model grid cell resolution, DX, has been selected equal to 10 m with a total number of cells, NX = 300. The adopted median grain size, D_{50}=0.3 mm. GSb has been run with $K_{GSb} = 0.25$, and the boundary conditions have been set as pinned. The calculation time step has been fixed equal to 0.5 hrs. Wave inputs have been supplied at the 50 m depth contour. The adopted input parameters are given in Table 6.7.

Table 6.14 – GSb input for multiple detached breakwaters simulation

Model domain	Number of cells alongshore	NX = 300
	Dimension of cells	DX = 10 m
	Calculation time step	DT = 0.5 hrs
	Median grain size	D_{50} = 0.3 mm
	Berm height	D_B = 1m
	Closure depth	D_C = 8 m
Model forcing (at 50 m contours)	Significant offshore wave height	H_{so} = 0.75 m
	Peak wave period	T_p = 8 sec
	Wave angle	ϑ_o = 15 deg
Model parameters	Calibration parameter	K_{GSb} = 0.25
	Boundary conditions	Pinned
	Duration of simulation	t = 2 years
Structures	Three detached breakwaters, 100 m long, from x = 700 to x = 800, from x = 1450 to x = 1550 m, and from x = 2200 to x = 2300, at y = 175 m	
Initial shoreline	Straight shoreline 3000 m long	

Figure 6.28 shows the shoreline change after 2-years simulation. For the selected conditions, the detached breakwaters determine the development of a tombolo, which results in a shoreline advance behind the structures.

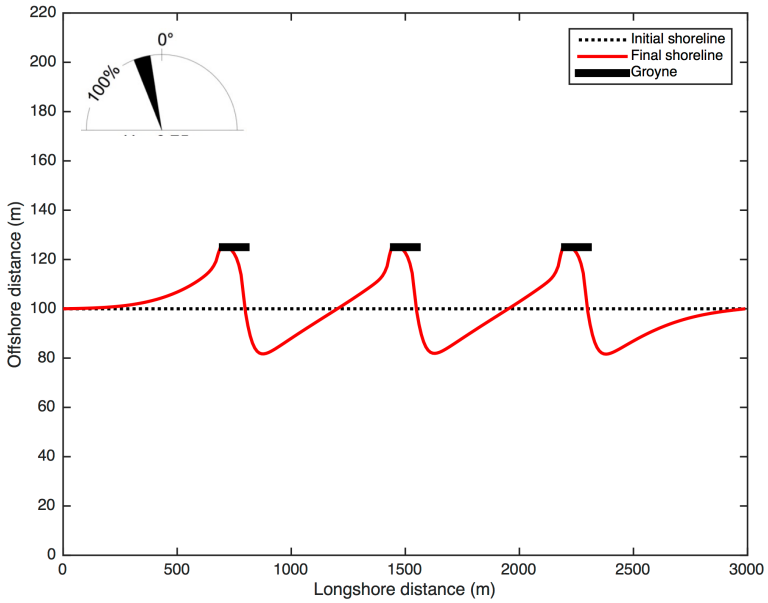

Figure 6.28 - Calculated shoreline change for straight shoreline with multiple detached breakwaters

7 GSb CALIBRATION AND VERIFICATION

In the present chapter the calibration and verification of GSb model against field and laboratory experiments are presented. Numerical simulations were performed for different cases (i.e. groynes, detached breakwaters), comparing the numerical results with:

- the field data collected at Sisal (Mexico) during a daily permanence of an impermeable groyne on a sandy beach and after one week from its removal (Medellin et al., 2018; Tomasicchio et al., 2018; Francone et al., 2018, Francone et al., 2019) (Section 7.1);
- the field data collected at Milford on Sea (UK), where a temporary groyne was deployed on a mixed beach (sand and gravel) during a period of two months (Martin-Grandes et al. 2009) (Section 7.2);
- the experimental data collected in the Large-Scale Sediment Transport Facility (LSTF) of U.S. Army Corps of Engineers (USACE), where the shoreline evolution behind a detached breakwater was reported by Gravens and Wang (2007) (Section 7.3);
- the experimental data collected from Ming and Chiew (2000), where the shoreline evolution was measured for 18 different configurations of a single detached breakwater (Section 7.4).

7.1 Field case 1 - Sandy beach at Sisal, Mexico

The observations collected in a field campaign conducted in Spring 2015 at Sisal beach (Mexico) were used to calibrate and verify the GSb model on a sandy beach (Medellin et al., 2018; Tomasicchio et al., 2018; Francone et al., 2018, Francone et al., 2019). A temporary groyne was deployed in the morning (08:00) of 27/05/2015 to investigate the beach resistance. Moreover, the groyne was removed 24-hours later on the morning of 28/05/2015, and beach surveys continued for the following days until beach recovery, to investigate the beach resilience.

The study area is located on a barrier island in the northern Yucatan Peninsula (Figure 7.1a), at the fishing village of Sisal, 40 km west of the commercial port of Progreso. The area is characterized by a micro-tidal range, intense sea breeze conditions, and low energy waves. The field experiment site is located between the Sisal Port and the Sisal Pier (Figure 7.1b). Moreover, winds, offshore waves, and mean sea level were observed by UNAM (Universidad Nacional Autónoma de México) over the past years in order to characterize the main forcing mechanisms affecting the coastal region.

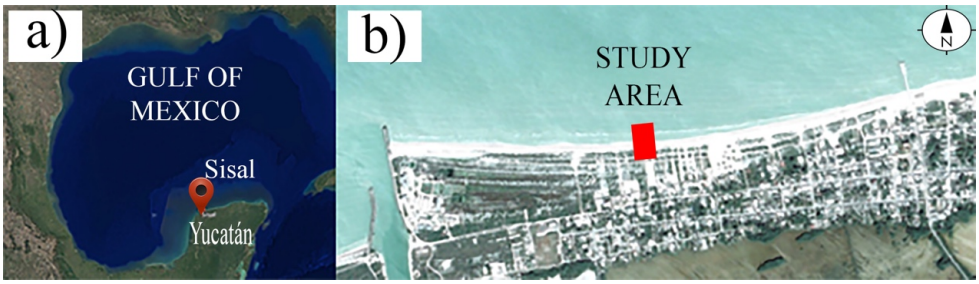

Figure 7.1 - Location map showing (a) the Yucatan peninsula at the SE of the Gulf of Mexico, (b) a section of the Yucatan north coast showing the barrier island and wetlands, and (c) study area location and existing monitoring systems (Medellin et al., 2018)

A bathymetric survey of the study area showed the presence of a sand bar system (Figure 7.2). The outer bar is relatively uniform alongshore, whereas inner bars present a high seasonal variability at some location. However, the beach orientation between the Sisal port and Sisal pier is relatively uniform for a 1 km stretch of coast located in the middle section. Beach evolution during the intense sea breeze season (May-September), at the two transects bounding the study area and represented in Figure 7.2, presented low variability (±3 m) in the shoreline position. Therefore, in order to assess beach resistance, a temporary groyne was deployed between these two transects, owing to the low natural beach variability observed at this location.

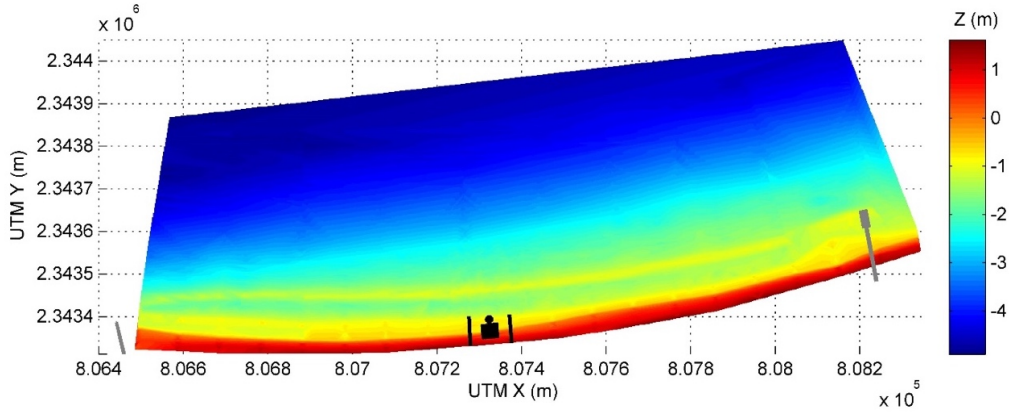

Figure 7.2 - Bathymetry observed two days before the experiment (05/25/2015), showing the study area (■), the ADV (●), and the updrift/downdrift control lines (black solid lines) locations. The study site is located between the jetty of the Sisal port entrance channel (left-hand side, grey line) and the Sisal pier (right-hand side grey feature) (Medellin et al., 2018)

Offshore wave conditions, observed at 10 m water depth using an RDI Acoustic Doppler Current Profiler (ADCP) located 11 km offshore, were characterized by NE waves highly correlated with local winds (Figure 7.3).

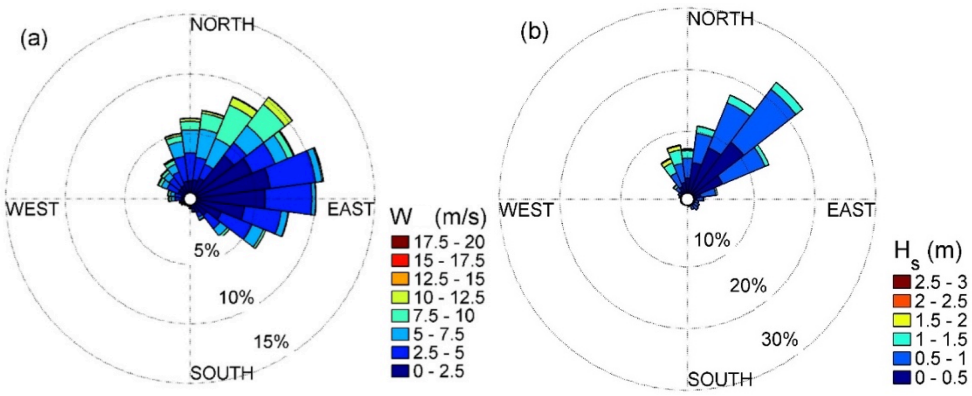

Figure 7.3 - (a) Wind and (b) wave roses in the study area. Wind data are taken from the Sisal weather station MeteoSisal (www.weather underground.com 01/01/2009-06/17/2016) and the wave data were collected from an ADCP located at 10 m water depth in front of Sisal (10/12/2013-20/04/2016) (Medellin et al., 2018)

The temporary groyne was based on the design proposed by Wang and Kraus (1999) for similar field conditions. Wood-sections 0.19 m thick of 2.40 m by 1.20 m were installed using a frame made of iron pipes and clamps. The groyne consisted of six and a half sections, with a 20 cm overlap between sections, with a total length of 14.4 m. Furthermore, sandbags were deployed along the base of the structure to avoid bed scouring that led to the sediment bypass (Figure 7.4).

Figure 7.4 - Temporary groyne made of wood sections (Medellin et al., 2018)

Beach morphology was evaluated by analysing the Real-Time Kinematic and Differential GPS (RTK DGPS) survey data (Figure 7.5). The bathymetrical survey, W0730, before the structure deployment, shows the alongshore uniformity of the beach (Figure 7.5a). The deployment of a temporary impermeable structure at x = 0 m induces sediment impoundment at the updrift side of the structure and erosion at the downdrift side associated with the direction

of the alongshore sediment transport. The morphology change is significant for water depth, h>-0.6 m after 24 hours with significant beach accretion/erosion at the down-/up- drift side (Figure 7.5b). On the other hand, the beach morphology 24 hours after the structure removal presents alongshore uniformity for the submerged area (h < 0 m) but a clear disturbance in subaerial beach profiles corresponding to the swash zone (Figure 7.5c). The disturbance smoothed out during the following days and became negligible 144 hrs after removal (Figure 7.5d).

The bulk effect of the impermeable groyne on the littoral transport was evaluated by analysing the relative sand volumetric changes, where the pre-structure deployment survey was used as the baseline. The sediment impoundment reached 70 m^3 in 24 hours at the updrift side, whereas the volume loss at the downdrift for the same period was less than 40 m^3.

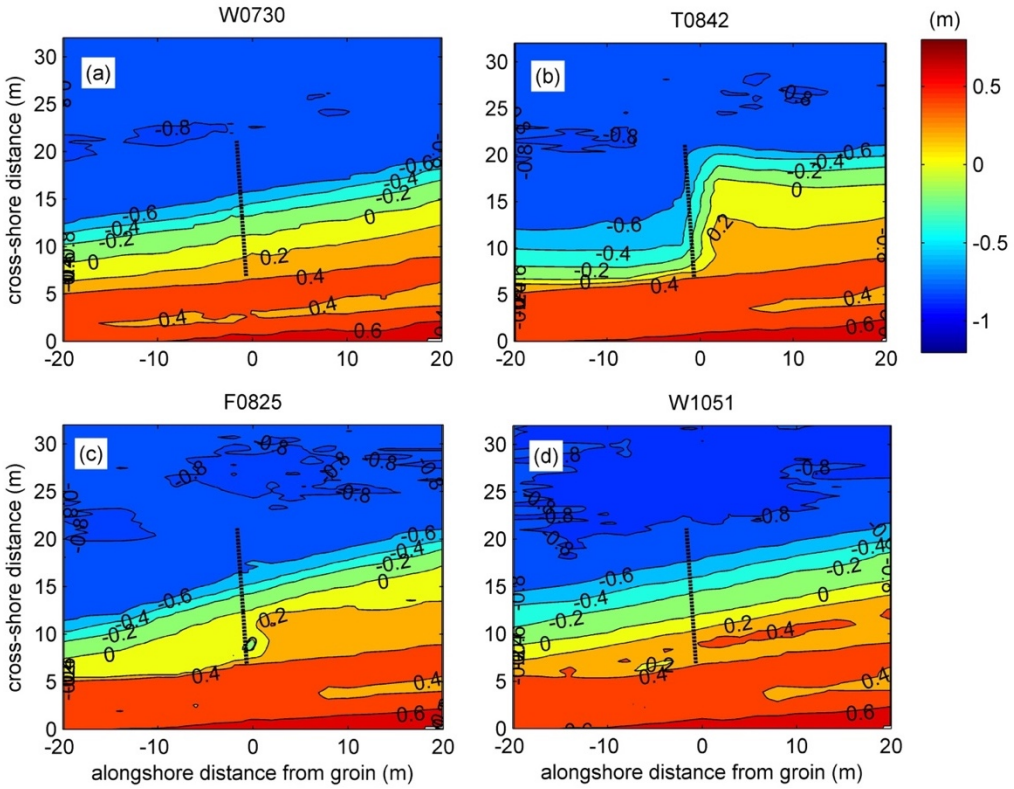

Figure 7.5 - Beach survey (**a**) right before groyne deployment, (**b**) right before groyne removal (24 h later), (**c**) 24 h after groyne removal, (**d**) 144 h after groyne removal (Medellin et al., 2018)

Field conditions were employed to calibrate and verify the GSb model to investigate beach resistance and resilience in the study area. Thus, a 14.4 m long groyne (10 m wet plus 4.4 m dry) was positioned at the centre of the domain. The GSb model computational domain was assumed 41 m. Model grid cell resolution, DX, was set equal to 1 m with a total number of cells, NX, equal to 41, whereas the model experiment was simulated adopting a calculation time

step, DT, equal to 0.005 hours. For a direct comparison with field measurements, the recording time step of the output files was set to 1 hour. The median grain size, D_{50}, was set to 0.3 mm and the closure depth, h_c , 0.8 m. The hourly wave conditions recorded ADCP located 11 km offshore the beach was adopted as input to the GSb model and are listed in Table 7.1.

Table 7.1 - Offshore wave conditions, observed at 10 m water depth using an RDI Acoustic Doppler Current Profiler (ADCP) located 11 km offshore, from 27/05/2015 to 03/06/2015; M = month, D = day, H = hour, Hs = significant wave height, Tp = peak wave period, ϑ = wave direction

M	D	H	H_s (m)	T_p (s)	ϑ (°)	M	D	H	H_s (m)	T_p (s)	ϑ (°)	M	D	H	H_s (m)	T_p(s)	ϑ (°)
5	27	7	0.54	3.7	41	5	29	17	0.47	2.5	71	6	1	3	0.57	3.3	36
5	27	8	0.51	3.6	51	5	29	18	0.49	2.9	67	6	1	4	0.53	3.4	37
5	27	9	0.5	3.8	26	5	29	19	0.55	3	30	6	1	5	0.5	3.1	56
5	27	10	0.48	3.6	38	5	29	20	0.61	3.3	45	6	1	6	0.4	4.5	29
5	27	11	0.5	3.4	36	5	29	21	0.66	3.7	16	6	1	7	0.4	4.1	34
5	27	12	0.47	3.2	26	5	29	22	0.71	3.4	41	6	1	8	0.33	4.3	36
5	27	13	0.47	2.7	77	5	29	23	0.7	3.6	65	6	1	9	0.32	4.3	13
5	27	14	0.42	3	51	5	30	0	0.6	3.3	62	6	1	10	0.28	4.3	12
5	27	15	0.38	3.8	19	5	30	1	0.56	3.5	36	6	1	11	0.27	3.7	358
5	27	16	0.39	4.1	43	5	30	2	0.59	3.9	43	6	1	12	0.28	3.8	62
5	27	17	0.46	2.7	24	5	30	3	0.71	3.3	52	6	1	13	0.31	3.5	41
5	27	18	0.62	1.4	32	5	30	4	0.75	3.4	45	6	1	14	0.31	3.3	48
5	27	19	0.68	3.5	28	5	30	5	0.76	3.5	83	6	1	15	0.24	3.8	14
5	27	20	0.74	3.6	22	5	30	6	0.72	3.4	8	6	1	16	0.24	4.1	22
5	27	21	0.8	3.7	26	5	30	7	0.69	3.3	63	6	1	17	0.22	4.2	358
5	27	22	0.85	3.8	24	5	30	8	0.64	1.4	13	6	1	18	0.19	4.2	6
5	27	23	1.05	4.2	32	5	30	9	0.6	3.6	71	6	1	19	0.3	2.5	260
5	28	0	0.84	4.5	19	5	30	10	0.53	4.2	27	6	1	20	0.2	4.1	11
5	28	1	0.83	3.8	55	5	30	11	0.49	4.2	14	6	1	21	0.18	4.2	10
5	28	2	0.9	3.4	70	5	30	12	0.52	2.9	45	6	1	22	0.26	2.3	64
5	28	3	0.85	3.3	30	5	30	13	0.45	3.7	33	6	1	23	0.42	2.7	22
5	28	4	0.78	3.8	32	5	30	14	0.46	3.8	15	6	2	0	0.46	3.2	9
5	28	5	0.74	3.9	47	5	30	15	0.45	1.6	53	6	2	1	0.41	3.2	23
5	28	6	0.66	4.3	28	5	30	16	0.41	3.2	9	6	2	2	0.47	5.2	357
5	28	7	0.57	1.4	32	5	30	17	0.44	4.3	19	6	2	3	0.41	3.3	352
5	28	8	0.48	4.6	20	5	30	18	0.46	2.7	17	6	2	4	0.35	3	37
5	28	9	0.47	3.4	46	5	30	19	0.52	3.2	56	6	2	5	0.31	3.8	2
5	28	10	0.43	4.5	25	5	30	20	0.58	3	14	6	2	6	0.27	3.4	32
5	28	11	0.39	4.2	31	5	30	21	0.61	3.5	44	6	2	7	0.39	1.4	11
5	28	12	0.36	3.8	25	5	30	22	0.67	3.7	39	6	2	8	0.23	2.7	22
5	28	13	0.38	3.6	12	5	30	23	0.75	3.8	32	6	2	9	0.21	3.2	46
5	28	14	0.37	3.9	25	5	31	0	0.76	3.9	16	6	2	10	0.16	3.3	28
5	28	15	0.38	4.1	18	5	31	1	0.71	3.7	21	6	2	11	0.12	3	66
5	28	16	0.45	2.9	43	5	31	2	0.78	3.8	39	6	2	12	0.13	2.6	146
5	28	17	0.53	3.1	55	5	31	3	0.72	3.5	32	6	2	13	0.2	2	47
5	28	18	0.63	3.2	84	5	31	4	0.67	3.7	28	6	2	14	0.21	2.1	58
5	28	19	0.63	3.5	51	5	31	5	0.6	3.7	48	6	2	15	0.19	2.5	239
5	28	20	0.63	3.4	20	5	31	6	0.54	3.4	45	6	2	16	0.15	2.1	76
5	28	21	0.83	3.7	37	5	31	7	0.53	3.9	360	6	2	17	0.27	2.1	80
5	28	22	0.77	4.1	55	5	31	8	0.56	2.8	70	6	2	18	0.29	1.9	41
5	28	23	0.83	3.4	54	5	31	9	0.51	4.2	32	6	2	19	0.29	2.3	52
5	29	0	0.69	3.4	53	5	31	10	0.49	3.6	32	6	2	20	0.29	2.4	64

M	D	H	H_s (m)	T_p (s)	ϑ (°)	M	D	H	H_s (m)	T_p (s)	ϑ (°)	M	D	H	H_s (m)	T_p(s)	ϑ (°)
5	29	1	0.78	3.6	34	5	31	11	0.52	1.5	61	6	2	21	0.34	2.4	62
5	29	2	0.7	3.9	19	5	31	12	0.43	4.5	28	6	2	22	0.36	2.3	54
5	29	3	0.81	3.8	56	5	31	13	0.41	4.1	31	6	2	23	0.36	2.6	40
5	29	4	0.82	3.9	38	5	31	14	0.39	3.1	51	6	3	0	0.32	2.7	69
5	29	5	0.77	4.1	30	5	31	15	0.35	4.8	37	6	3	1	0.38	2.6	55
5	29	6	0.77	4.1	54	5	31	16	0.31	3.9	41	6	3	2	0.32	2.7	82
5	29	7	0.76	4.1	29	5	31	17	0.33	1.9	352	6	3	3	0.27	2.7	353
5	29	8	0.6	3.9	43	5	31	18	0.43	2.7	55	6	3	4	0.29	2.6	51
5	29	9	0.61	3.7	38	5	31	19	0.54	3	17	6	3	5	0.26	2.7	62
5	29	10	0.57	3.6	45	5	31	20	0.58	3.4	49	6	3	6	0.27	2	52
5	29	11	0.54	3.7	17	5	31	21	0.57	3.4	53	6	3	7	0.26	9.4	282
5	29	12	0.52	3.2	28	5	31	22	0.66	3.4	26	6	3	8	0.24	2.9	53
5	29	13	0.53	3.5	57	5	31	23	0.65	3.5	25	6	3	9	0.27	1.8	21
5	29	14	0.45	3.6	30	6	1	0	0.7	3.8	25	6	3	10	0.24	3.4	222
5	29	15	0.39	3.3	49	6	1	1	0.69	3.7	53						
5	29	16	0.44	1.5	25	6	1	2	0.67	3.7	49						

A sensitivity analysis of K_{GSb} parameter was conducted in order to calibrate the model with the observed field data collected after 23 hrs from the groyne deployment (Figure 7.6).

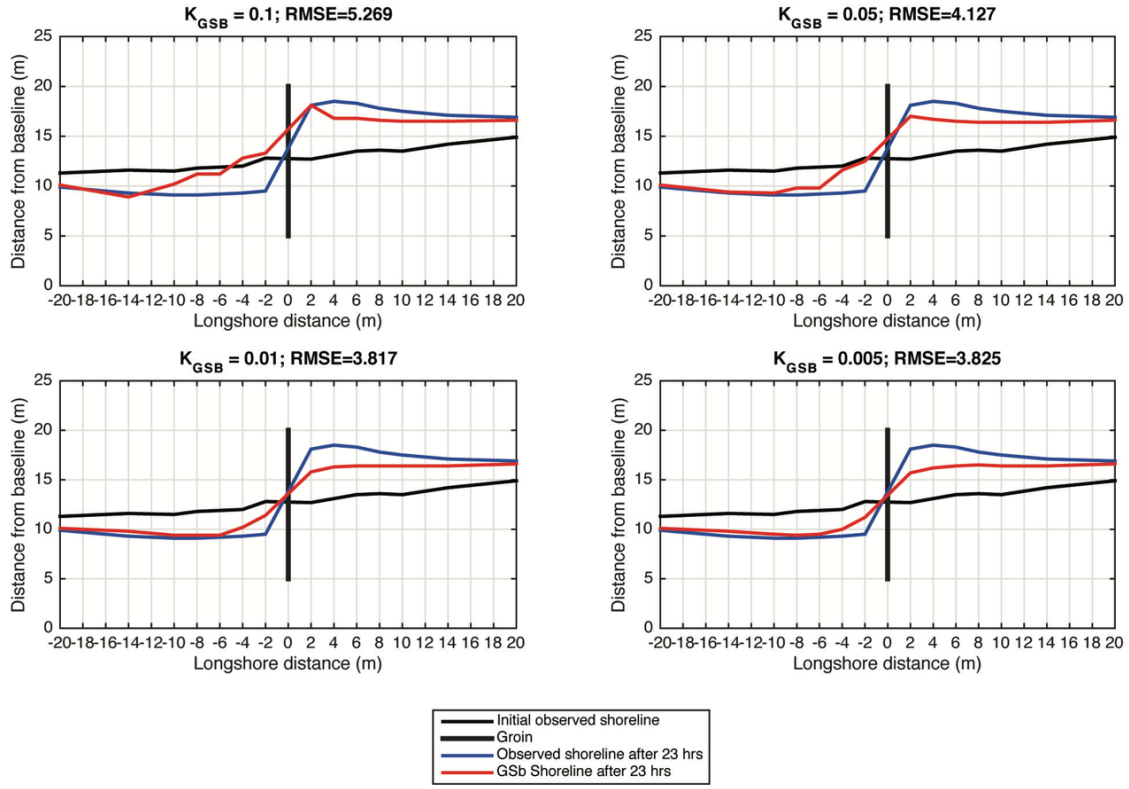

Figure 7.6 - Sensitivity analysis of K_{GSb} parameter

Table 7.2 shows the values of the Root Mean Square Error ($RMSE$) from the comparison of the observed and calculated (for different K_{GSb} values) shoreline positions, at 23 hours after the groyne deployment; the RMSE is defined as:

$$RMSE = \sqrt{\frac{\sum_{i=1}^{N}\left(y_{i,GSb} - y_{i,obs}\right)^2}{N}} \qquad (7.1)$$

where $y_{i,GSb}$ is the cross-shore distance from the baseline to the calculated shoreline, $y_{i,obs}$ is the cross-shore distance from the baseline to the observed shoreline, N is the number of transects along the considered shoreline.

Table 7.2 - Calculated and observed shoreline positions at 14 transects along the shoreline and relative values of Root Mean Square Error (RMSE)

	Longshore distance from groyne [m]	-20	-14	-10	-8	-6	-4	-2	2	4	6	8	10	14	20	*RMSE*
Cross-shore distance from baseline [m]	Initial Shoreline	11.3	11.6	11.5	11.8	11.9	12	12.8	12.7	13.1	13.5	13.6	13.5	14.2	14.9	
	Field data at 23 hours	9.9	9.3	9.1	9.1	9.2	9.3	9.5	18.1	18.5	18.3	17.8	17.5	17.1	16.9	
	GSb, K_{GSb} = 0.005	10.1	9.8	9.5	9.4	9.5	10	11.2	15.7	16.2	16.4	16.5	16.4	16.4	16.6	3.825
	GSb, K_{GSb} = 0.01	10.1	9.8	9.4	9.4	9.4	10.2	11.4	15.8	16.3	16.4	16.4	16.4	16.4	16.6	**3.817**
	GSb, K_{GSb} = 0.05	10.1	9.4	9.3	9.8	9.8	11.6	12.5	17	16.7	16.5	16.4	16.4	16.4	16.6	4.127
	GSb, K_{GSb} = 0.1	10.1	8.9	10.2	11.2	11.2	12.8	13.3	18.1	16.8	16.8	16.6	16.5	16.5	16.6	5.269

A K_{GSb} = 0.01 value determined the lowest RMSE, showing a better agreement between the calculated and the observed shoreline positions. As expected, a small value of K_{GSb} has been obtained, since a beach characterized by a gently slope with approximately straight and parallel depth contours, also in the presence of a groyne, determined negligible values of $\partial H_{sb}/\partial x$, the gradient in longshore breaking wave height (Equation 5.1)

Numerical simulations were conducted for two different lateral boundary conditions: pinned or moving lateral boundary. Figure 7.7 shows the comparison of the simulated shoreline positions obtained after 23 hours for the two different lateral boundaries; as expected, the shoreline shapes differ in vicinity of the lateral boundaries, but overlap in vicinity of the groyne. If a moving lateral boundary condition is selected, the boundary will move a specified distance over a certain time period. GSb lateral boundaries were selected as moving boundaries.

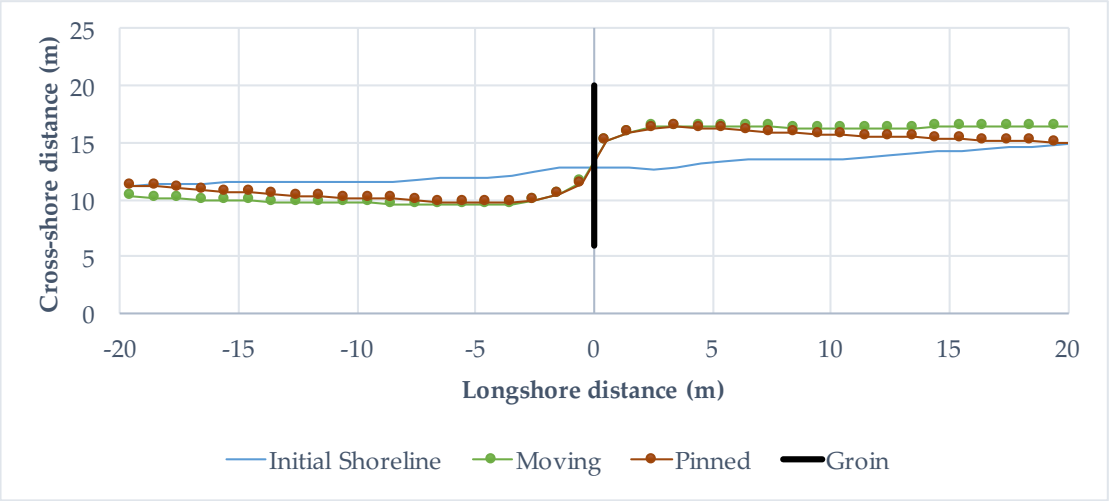

Figure 7.7 - Comparison of the simulated shoreline positions obtained after 23 hours for the two different lateral boundaries

The first beach survey was assumed as the initial shoreline position in the numerical model. In particular, at the down-drift (x = 0 m) and up-drift (x = 41 m) boundaries of the computational domain, the observed specific distances from the first beach survey, equal to -1.4 m and 1.8 m, respectively, over a period of 24 hours, were assumed. On the other hand, for the post structure removal condition the computation duration was extended to 168 hours taking as initial condition the survey at t = 24 hours.

Figure 7.8c-g show that the calibrated numerical model satisfactorily predicts the downdrift shoreline evolution, whereas the maximum shoreline advance, at t = 21 hours, in the updrift side is under-predicted (Figure 7.8h).

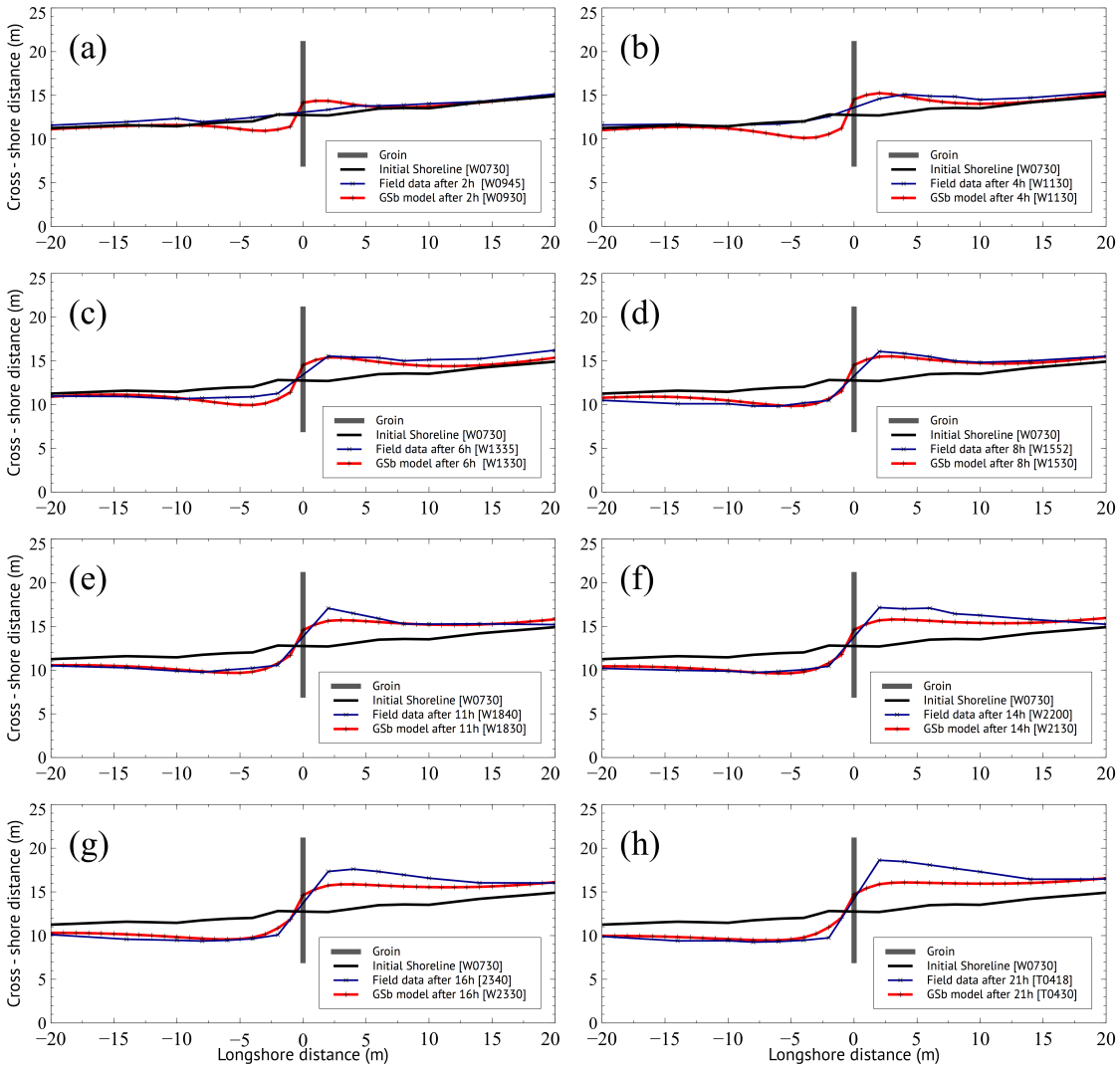

Figure 7.8 - Measured and calculated shoreline position (a) 2 h, (b) 4 h, (c) 6 h, (d) 8 h, (e) 11 h, (f) 14 h, (g) 16 h and (h) 21 h after the structure deployment

The model capability to predict the shoreline resilience after the structure removal was investigated (verification). The assumed initial shoreline position corresponds to the beach survey performed immediately before the structure removal, and the numerical model was run without the structure using the daily mean conditions as measured for the following seven days. The numerical model calculated the drastic change occurring during the first 24 hours after the groyne removal (Figure 7.9a-e). Furthermore, it calculated the beach recovery occurring after approximately 7 days (Figure 7.9f).

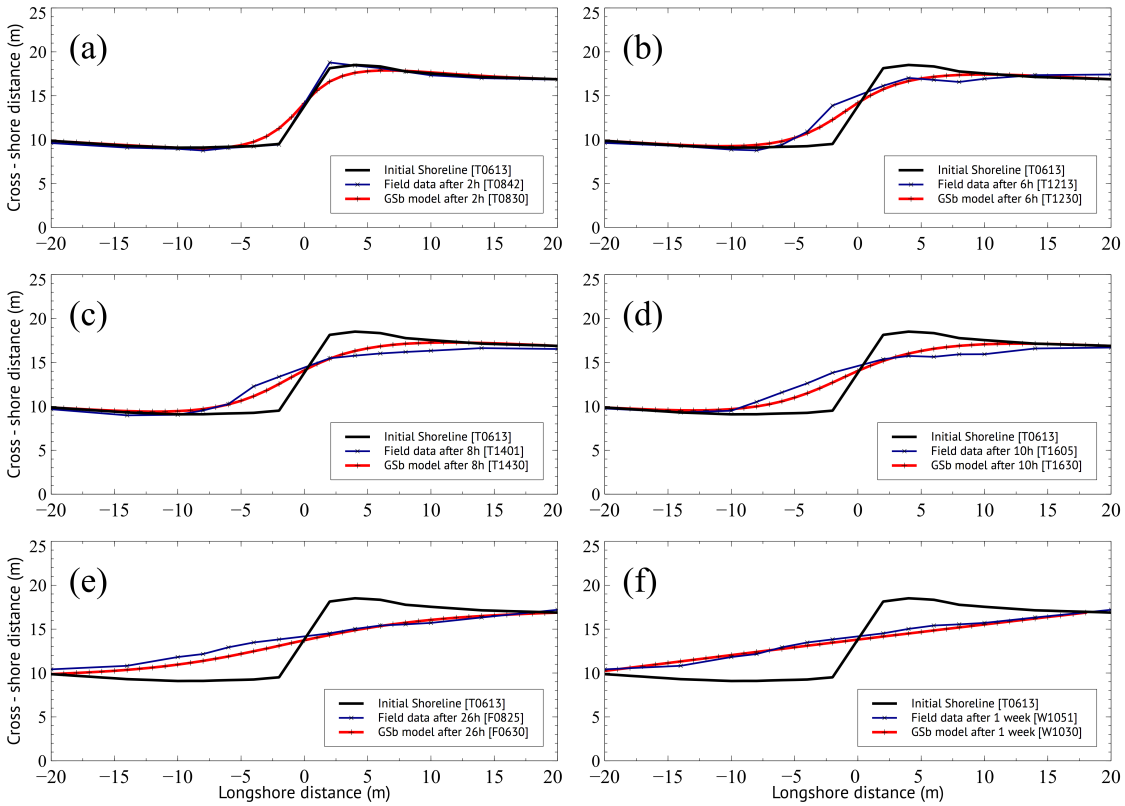

Figure 7.9 - Measured and calculated shoreline position (a) 2 h, (b) 6 h, (c) 8 h, (d) 10 h, (e) 26 h, and (f) 1 week after the structure removal

Within the framework of the field data adopted for the investigation (sea-breeze conditions and sandy beach), the model can be considered as a reliable tool to conduct a numerical study on beach resistance and resilience for the considered study area.

7.2 Field case 2 - Mixed beach at Milford on Sea, UK

The performance of the GSb model for a mixed beach (D_{50} = 10 mm; D_{85}/D_{15} = 27.66) and in presence of a groyne was evaluated. The observations collected in a field campaign conducted in 2007 at Milford-on-Sea, Hampshire, UK (Martin-Grandes et al., 2009) were compared with the numerical results gained with GSb.

Milford-on-Sea is located in the county of Hampshire on the Southern coast of the UK. It is a managed mixed, shingle and sand, beach sited at the eastern side of Christchurch Bay (Figure 7.10).

Figure 7.10 - Study area location (from Google Earth Pro and Google Panoramio, 2019)

In the field campaign, an impoundment technique was applied, in which a temporary impermeable groyne 46 m long was deployed along the beach for two months, acting a barrier for the sediments moving along the coast.

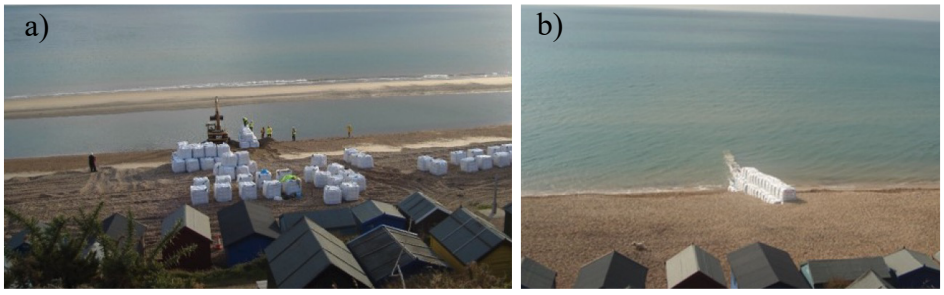

Figure 7.11 – a) Groyne construction, filling the geobags during low tide the 27/09/2007. b) View of the temporary structure from the top of Hordle Cliff the 6/10/2007 (from courtesy of prof. David Simmonds, University of Plymouth)

In Section 7.2.1, the field experiment dataset is described. In Section 7.2.2, the calibration of GSb model is performed; the numerical results are compared with the field data in order to evaluate the shoreline evolution during the groyne experiment using nearshore Acoustic Wave and Current (AWAC) data, located approximately 600 m offshore at 7 m depth. In Section 7.2.3, calculated mean transport rate and the data available in SCOPAC (2003) are compared. In Section 7.2.4, GSb verification is performed, considering (i) Wave-Rider buoy data provided by Channel Coast Observatory (CCO) located 1500 m offshore at 10 m depth (Section 7.2.4.1), (ii) Argus Beach Monitoring System (ABMS) shorelines (Section 7.2.4.2), (iii) propagated Wave-Rider buoy data by SWAN wave model for shallow water (Booij et al., 1997) and ARGUS shorelines (Section 7.2.4.3).

7.2.1 Field experiment dataset

A Differential Global Positioning System (DGPS) was used to conduct the surveys at low tide (Martín-Grandes et al., 2009). The shoreline positions were obtained processing the data of the beach profiles by the use of MATLAB software (MathWorks, 2019). Daily beach profiles surveys are available over a 300 m survey grid from 01/10/2007 to 25/11/2007. That grid was defined with 15 transects on either side of the groyne location (Figure 7.12.a). The contour plot of the beach profiles data was plotted (Figure 7.12.b). The shoreline was extracted (Figure 7.12.c). The extracted line was rotated: the grid was aligned to the general direction of the shoreline. The rotation was 199.75 degrees (180° + 19.75°) in an anti-clockwise direction from the Northing/Easting grid (Figure 7.12.d).

Moreover, the Argus Beach Monitoring System (ABMS) was available; it was formed by five cameras facing the beach and mounted along a most 16 m high, at the top of the cliff. Images were collected from January 2007 until October 2011.

With regard to the wave data, two datasets are available:

- Acoustic Wave and Current (AWAC) data, nearshore;
- Directional Wave-Rider Buoy Data of Channel Coast Observatory (CCO), offshore.

The onshore Acoustic Wave and Current (AWAC) profiler observed significant wave height, peak period and directional spectrum from 01/10/2007 to 25/11/2007 (Figure 7.13). Waves were recorded in intervals of one hour, approximately 600 m offshore at 7 m depth. The wave angles were rotated to the general direction of the selected shoreline. The rotation used was 199.75 degrees (180° + 19.75°) in an anti-clockwise direction from the Northing/Easting grid as for the shorelines.

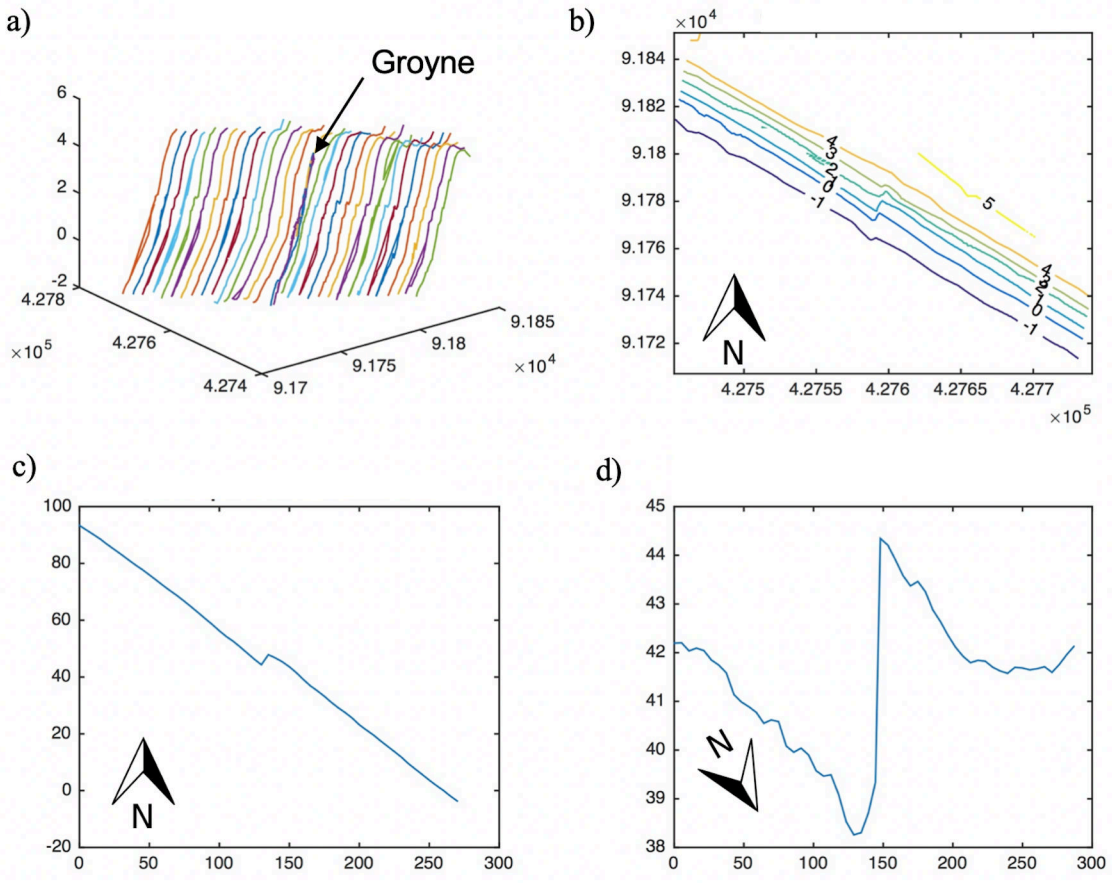

Figure 7.12 –Milford-on-Sea, 14 November 2007 a) Profiles collected with DGPS; b) Contour plot; c) Shoreline; d) Shoreline rotated

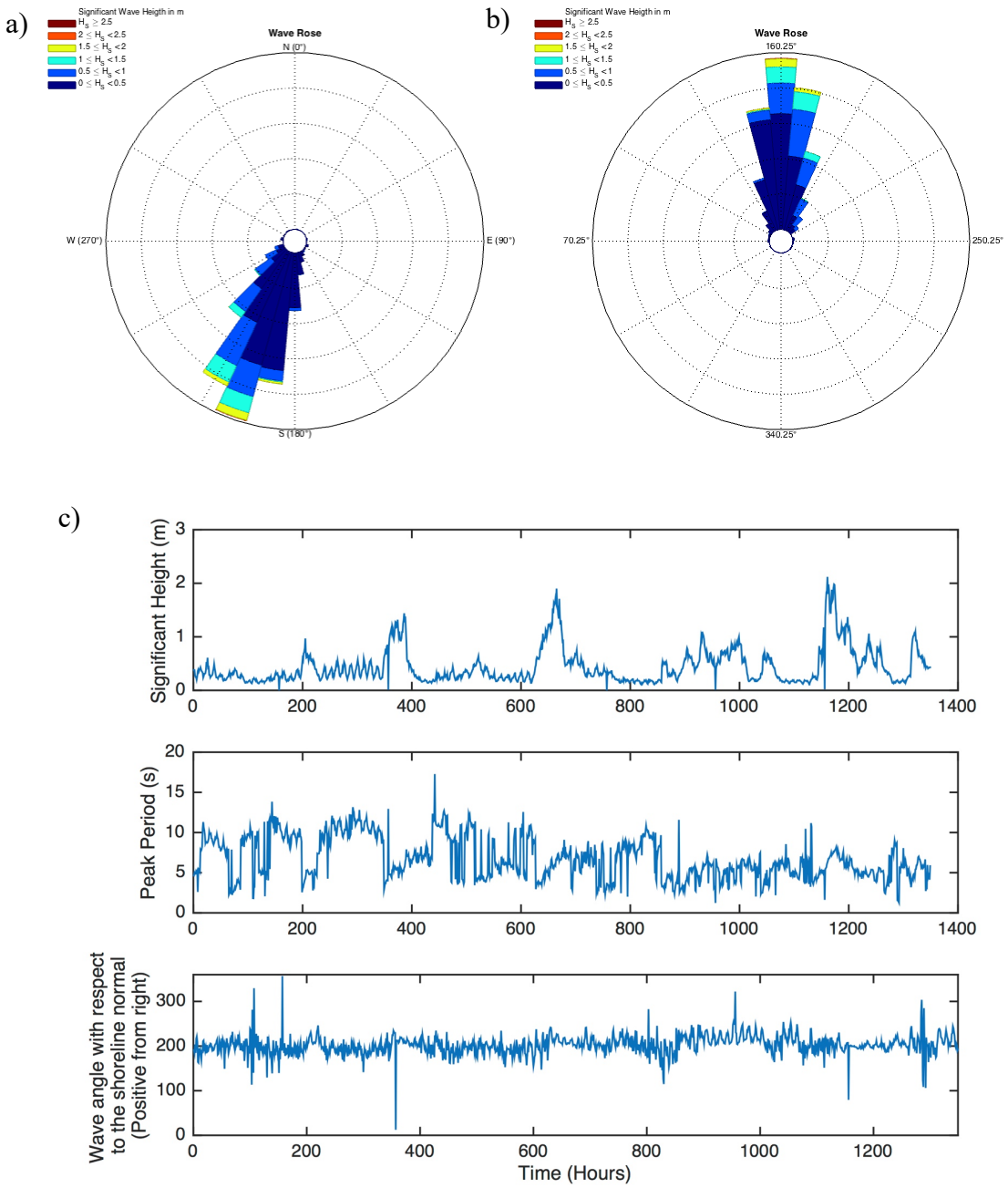

Figure 7.13 –AWAC wave data: a) Wave rose b) Wave rose rotated for the GSb model wave input file c)time series of Significant Height, Peak period and Wave angle

The offshore Directional Wave-Rider Buoy Mk III from Channel Coast Observatory (CCO) is located at 50° 42.75' N 1° 36.91' W (50.71137, -1.61306), approximately 1500 m offshore at 10 m depth. Significant wave height, peak period and wave direction are considered in the period of the simulation, from 01/10/2007 to 25/11/2007 (Figure 7.14). As done for the AWAC wave data, the wave angles were rotated to the general direction of the selected shoreline.

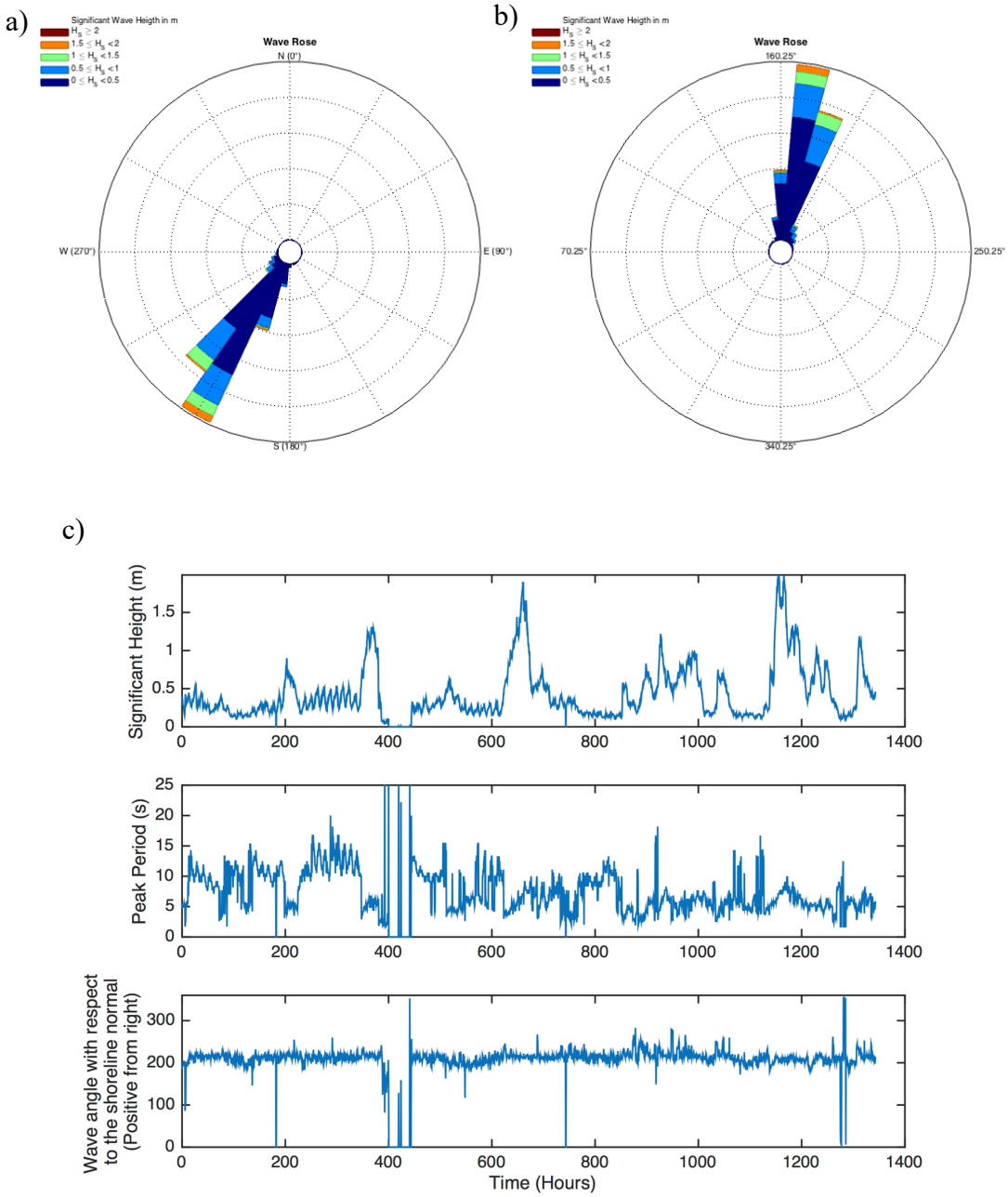

Figure 7.14 – CCO Wave-Rider buoy wave data: a) Wave rose b) Wave rose rotated for the GSb model wave input file c)time series of Significant Height, Peak period and Wave angle

7.2.2 DGPS shorelines and nearshore wave data (AWAC)

The shoreline evolution in presence of a groyne 46 m long (19 m wet and 27 dry) was evaluated by the GSb model for the period 01/10/2007 - 15/11/2007.

The computational domain was assumed 280 m. Model grid cell resolution, DX, was set equal to 5 m with a total number of cells, NX, equal to 57. A calculation time step, DT, was set to 0.005 hours (18 s). The recording time step of the output files was 24 hours. The median grain size, D_{50}, was 10 mm (Martin Grandes et al., 2009), representing the median diameter of the total sample composing the beach. (Figure 7.15)

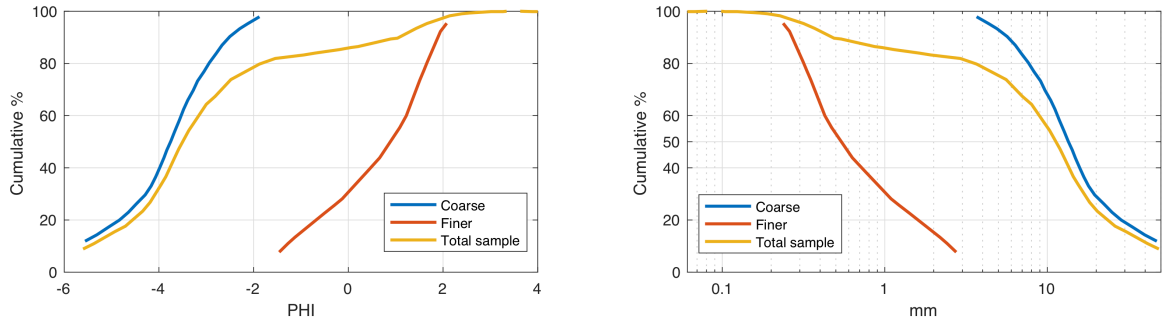

Figure 7.15 – Curve of the percentage of the cumulative weight of sample (Martin Grandes et al., 2009)

GSb simulations were carried out for pinned, gated and moving boundaries, and the results were compared. Due to reduced number of historical wave data, the value of the closure depth D_C and the berm height D_B, based an accurate evaluation of the profile evolution over time, were selected equal to 1 m and 3 m, respectively (Figure 7.16).

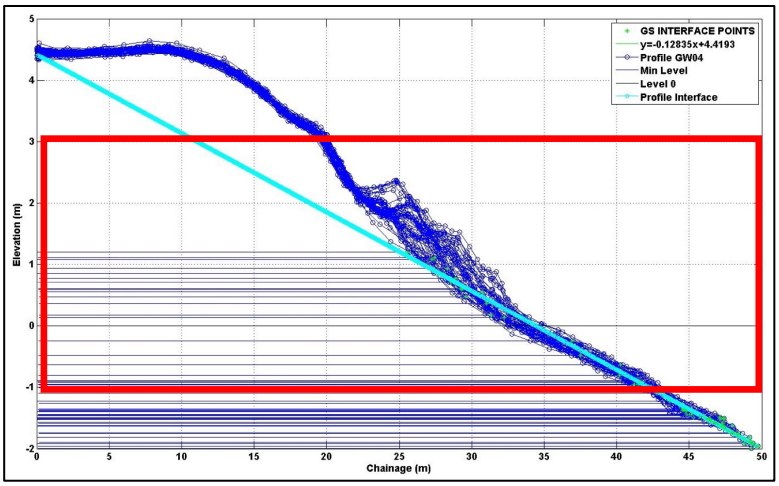

Figure 7.16 - Active beach profile evaluated at Milford On Sea (Martin Grandes et al., 2009)

Table 7.3 presents the GSb values adopted as input for the calibration procedure.

Table 7.3 - GSb input

Model domain	Number of cells alongshore	NX = 57
	Dimension of cells	DX = 5 m
	Calculation time step	DT = 0.005 hrs
	Median grain size	D_{50} = 10 mm
	Active beach profile	D_C+D_B = 4 m
Model forcing	Hourly waves parameters (H_s, T_p, Dir) from AWAC measurements at the 7 m depth contour, located 600 m offshore	
Model parameters	Calibration parameter	K_{GSb} = 0.005, 0.01, 0.05, 0.1, 0.2
	Boundary conditions	Pinned, Gated, moving (0.678 m -Left; 0.655 -Right)
	Recording time step	DTS = 24 hour
Structures	Groyne 46 m long (19 m wet / 27 dry) at x = 150 m	
Initial shoreline	Shoreline of 01/10/2007 extracted from DGPS profile	

The model was run with the hourly wave conditions depth (H_s, T_p, Dir) collected by AWAC approximately 600 m offshore at 7 m depth (Figure 7.13).

The first beach survey collected in presence of the groyne (01/10/2007) was assumed as the initial shoreline position in the numerical model (dotted black line). The groyne, 46 m long, was positioned at the 31st cell of the domain, corresponding to x = 150/155 m.

Figure 7.17 shows the calibration procedure consisting in a sensitivity analysis of the K_{GSb} parameter; GSb was run with 5 different K_{GSb} values (K_{GSb} = 0.005, 0.01, 0.05, 0.1, 0.2) and the corresponding Root Mean Square Error (RMSE) was calculated, comparing the observed shoreline after 45 days from the groyne deployment and the calculated shoreline. K_{GSb} = 0.1 produced a better agreement between observed and calculated shoreline with a lowest RMSE value. The difference between the RMSE calculated by comparing the results obtained with the five calibration parameters K_{GSb} considered, is lower than 0.3; this makes evident that the numerical solution, for this case, is not strictly dependent on the calibration parameter K_{GSb}.

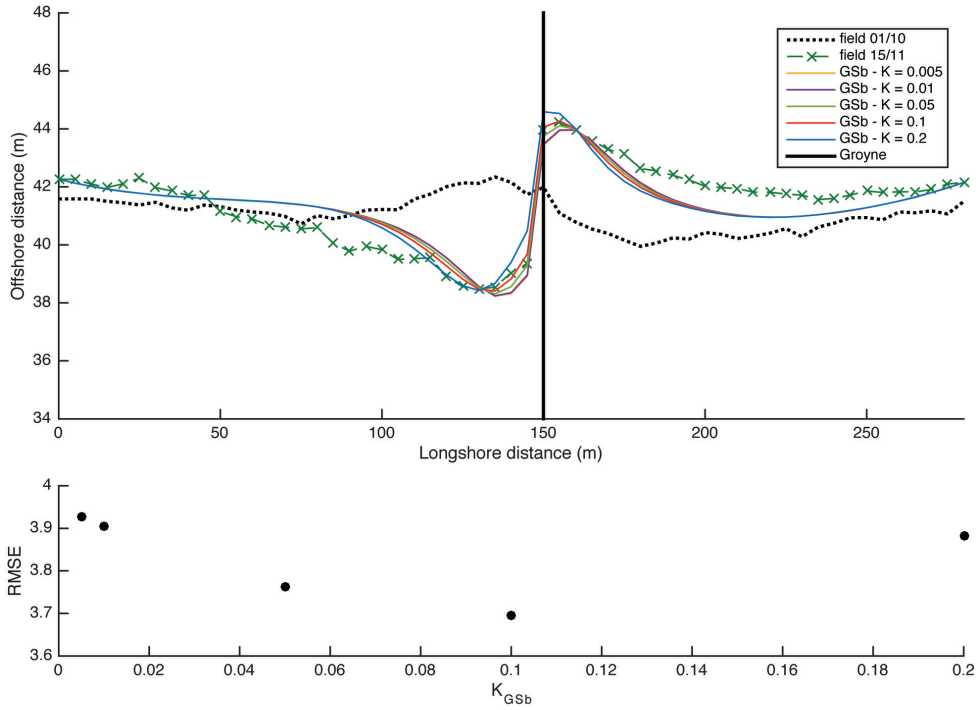

Figure 7.17 - Sensitivity analysis of K_{GSb}

After assessing the calibrated value for K_{GSb} (0.1), a sensitivity analysis of the boundary conditions was performed. Results are shown in Figure 7.19a. When pinned boundary conditions are specified (yellow line), the shoreline at the boundary does not move from the initial shoreline position over the calculation interval. If a moving boundary condition is selected (red line), the shoreline at the boundary moves at a defined distance, set in the input file. For a gated condition, the boundary is bounded with a groyne (blue line). It is known that, in One-Line numerical models, the equation governing shoreline change is formulated by conservation of sediment volume. Thus, the gated boundaries guarantee the conservation of sediment into the domain. On the contrary, for pinned and moving boundary conditions, a sediment gain/loss in/out of the computational domain is admitted. This value may be provided at the end of GSb simulation.

The simulations were performed and the RMSE was calculated comparing the numerical results obtained using the three different boundary conditions with the field observation for each day of the simulation (Figure 7.19*b*). From first to 14th day, the RMSE appears independent of the boundary selected. The RMSE increases in case of the gated boundary conditions, from 28th day after the groyne deployment until the end of the simulation. At the end of the simulation, 45 days after the groyne deployment, RMSE is lower when using moving boundary conditions. The difference between the RMSE using pinned and moving boundary conditions is small. Therefore, the overall result is not driven from the boundaries. The

maximum RMSE values when moving and pinned boundary conditions are selected (black and red dots) coincide with the 2 storms (Figure 7.19) occurred on 16th and 27th days after the groyne deployment. This happens because the principal assumption of the one-line model (constant cross-shore profile over time) is not satisfied.

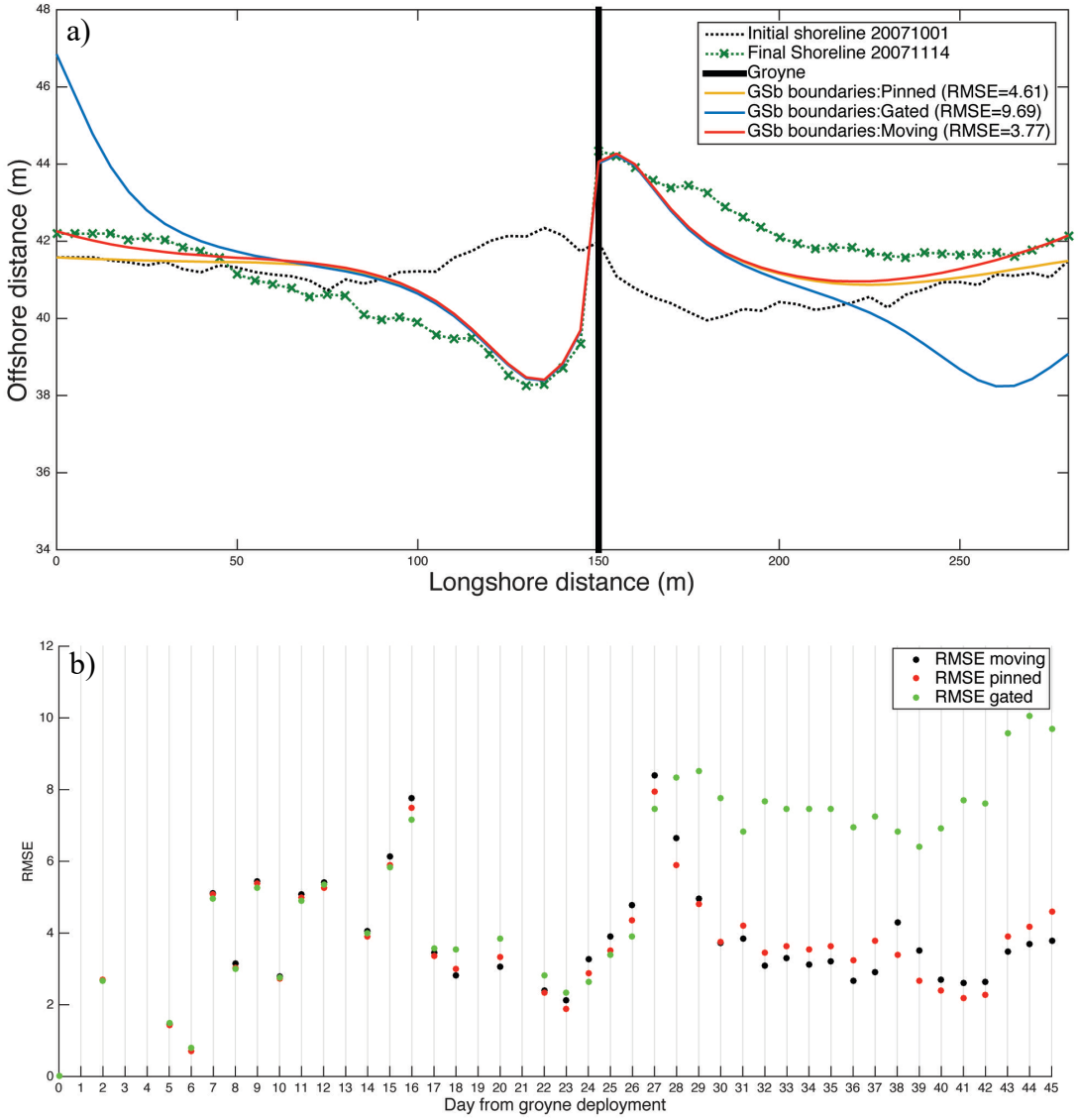

Figure 7.18 -- a) Differences in shoreline evolution at the end of the simulation (45 days) varying the boundary conditions b)Time-series of the daily root mean square error (RMSE) between the calculated and the observed and calculated shoreline positions

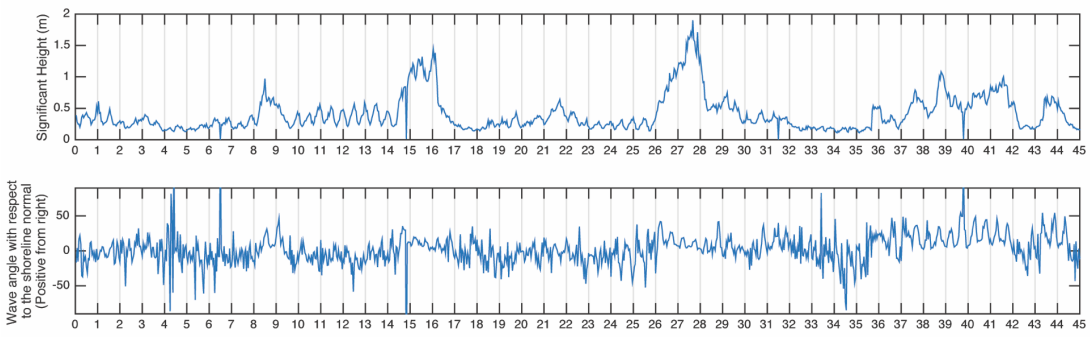

Figure 7.19 - Wave time-series from nearshore AWAC data

As a final step, the influence of the computational domain on the calculated shoreline was evaluated considering five domains having a different length (*NX*) and same cell size (*DX*). The original domain, extracted from DGPS profiles, was 280 m long. The RMSE obtained comparing observed and calculated shorelines was calculated for *NX* = 36, 46, 56, 66, 76 corresponding to computational domains of 180 m, 230 m, 280 m, 330 m, 380 m, respectively (Figure 7.20). The boundaries conditions for these cases were pinned.

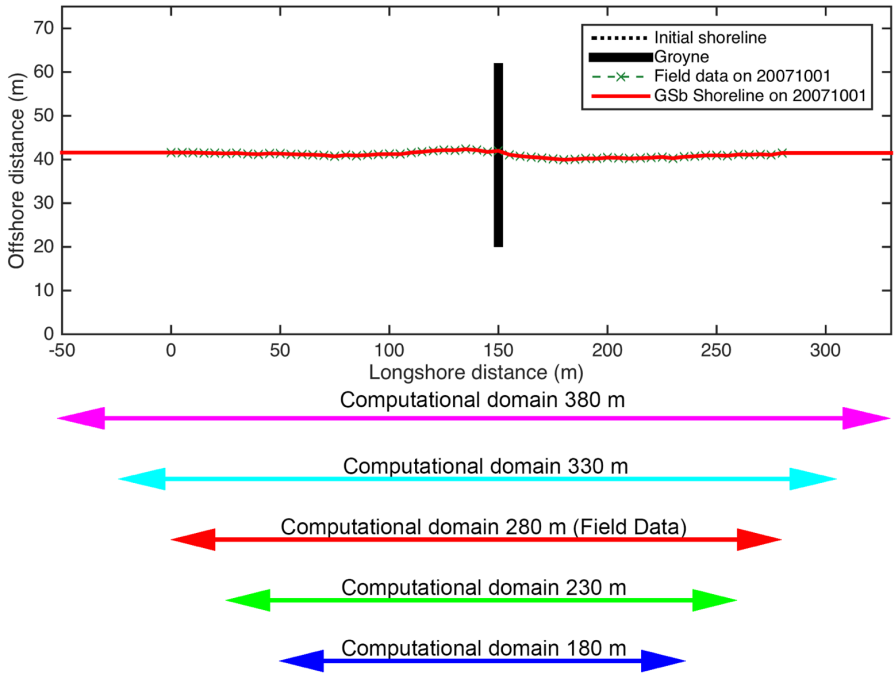

Figure 7.20 – Setup of five computational domains: 180 m, 230 m, 280 m, 330 m, 380 m

Results in Figure 7.21 show that varying the computational domain, initially 280 m long, and using for all the cases pinned boundary conditions, the result improves at 16 and 27 days after the groyne installation, in correspondence of the two storm events. The better overall solution is if a domain 180 m long (blue dots) is considered.

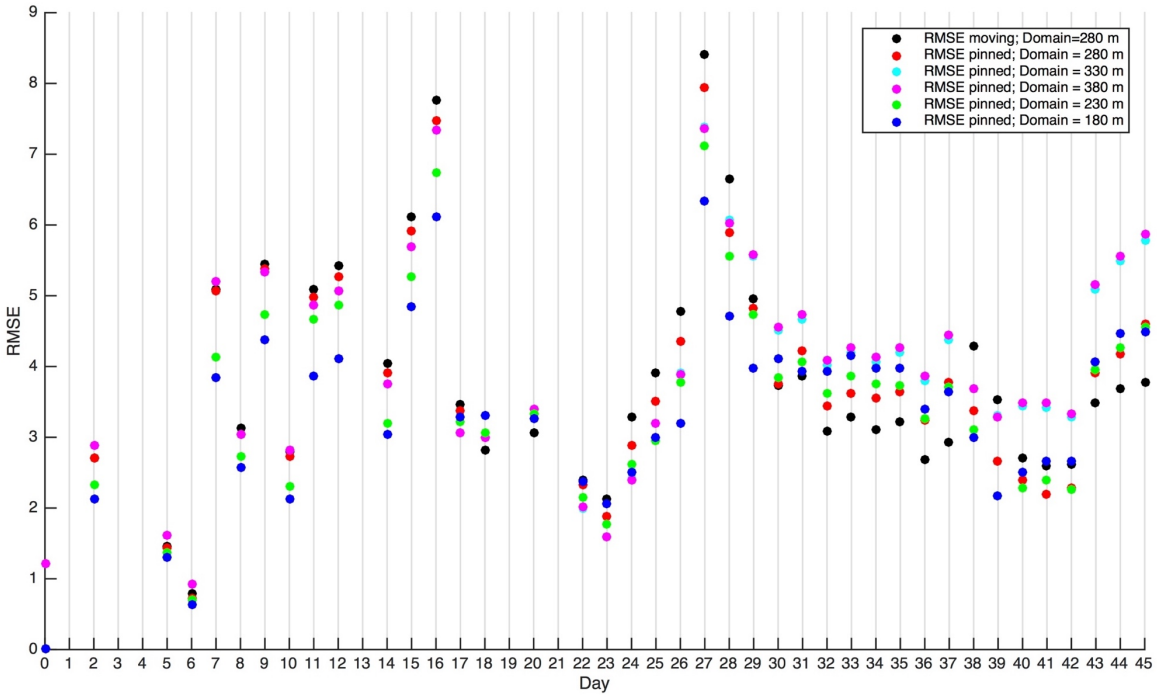

Figure 7.21 –RMSE over time calculated for 5 different domains. Simulations were performed using nearshore AWAC wave data

As an example, Figure 7.22 shows the calculated shoreline and the difference between calculated and observed shoreline, 45 days from the groyne installation, in case of a computational domain x = 180 m (NX=36), and pinned boundary conditions.

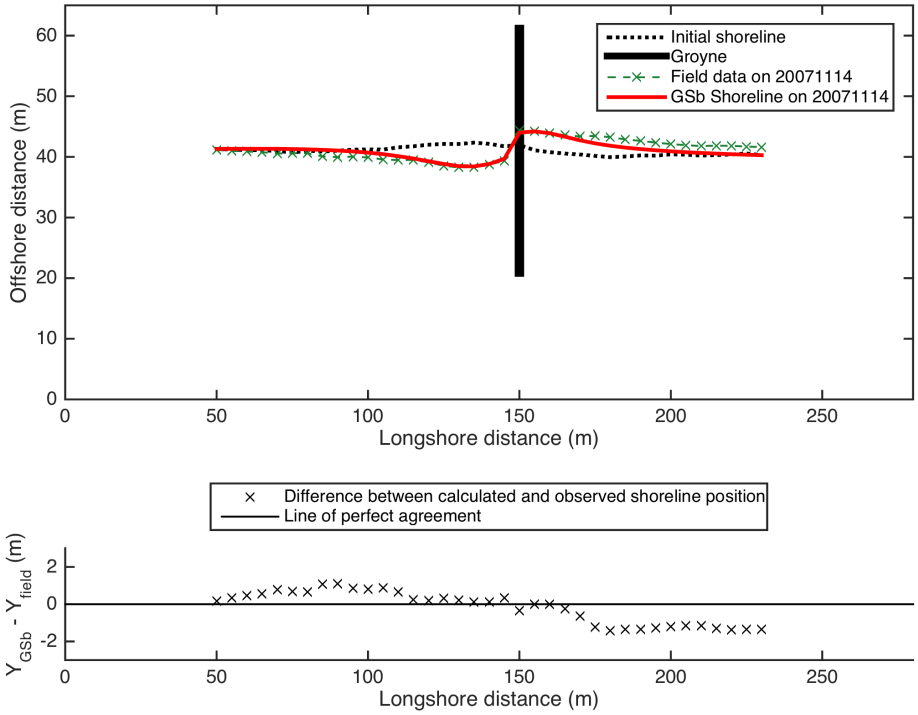

Figure 7.23 - Calculated and observed shoreline and difference between them, for a 45 days long simulation, from 01/10/2007 to 14/11/2007, for the 180 m computational domain and pinned beach boundaries conditions. Simulation performed using nearshore AWAC wave data

After the sensitivity analysis of the calibration parameter (K_{GSb}= 0.1), simulations were performed considering the input described in Table 7.4 , using the AWAC nearshore wave data, collected at 7 m depth.

Table 7.4 - GSb model input of the simulation with offshore wave data (CCO)

Model domain	Number of cells alongshore	NX = 57
	Dimension of cells	DX = 5 m
	Calculation time step	DT = 0.005 hrs
	Median grain size	D_{50} = 10 mm
	Active beach profile	D_C+D_B = 4 m
Model forcing	Hourly waves parameters (H_s, T_p, Dir) from AWAC measurements at the 7 m depth contour, located 600 m offshore	
Model parameters	Calibration parameter	K_{GSb} = 0.1
	Boundary conditions	Moving (0.678 m -Left; 0.655 -Right)
	Recording time step	DTS = 24 hour
Structures	Groyne 46 m long (19 m wet / 27 dry) at x = 150 m	
Initial shoreline	Shoreline of 01/10/2007 extracted from DGPS profile	

Figure 7.24 shows the comparison between the calculated (red line) and observed (green dotted line) shorelines on 14/11/2007 (45 days after the groyne deployment). The positive distance extends in the westerly direction. The y-axis extends in the positive direction offshore.

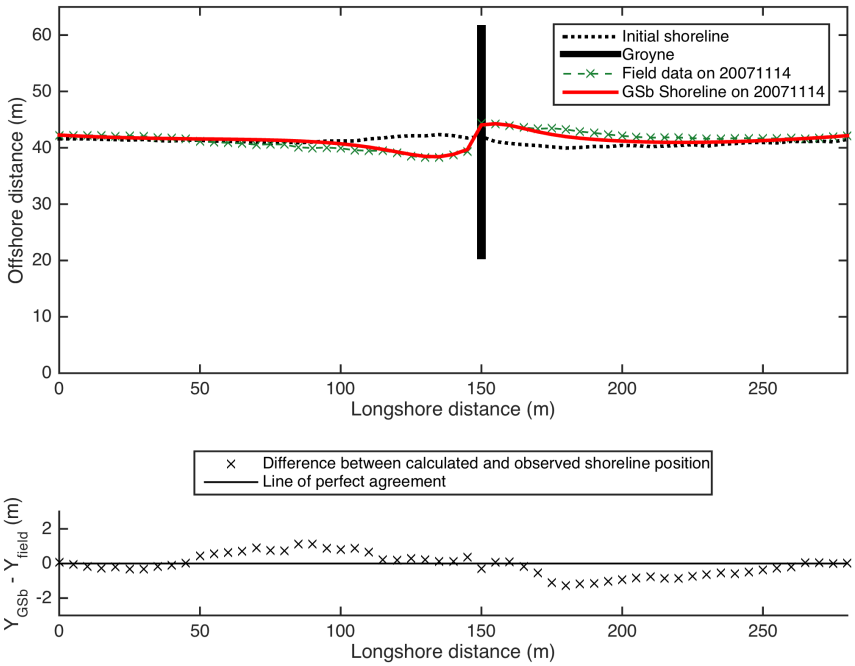

Figure 7.24 – Calculated and observed shoreline and difference between them, for a 45 days long simulation, from 01/10/2007 to 14/11/2007, using nearshore AWAC wave data

GSb model satisfactorily predicts the shoreline evolution at both groyne sides at the end of the simulation. The difference between calculated and observed shoreline positions is small in the area close to the groyne, from x = 120 m to x = 180 m.

In the following, are shown some representative comparison between observed data and calculated shoreline, after 7, 18, 25 and 36 days after the groyne deployment (Figure 7.25, Figure 7.26, Figure 7.27, Figure 7.28).

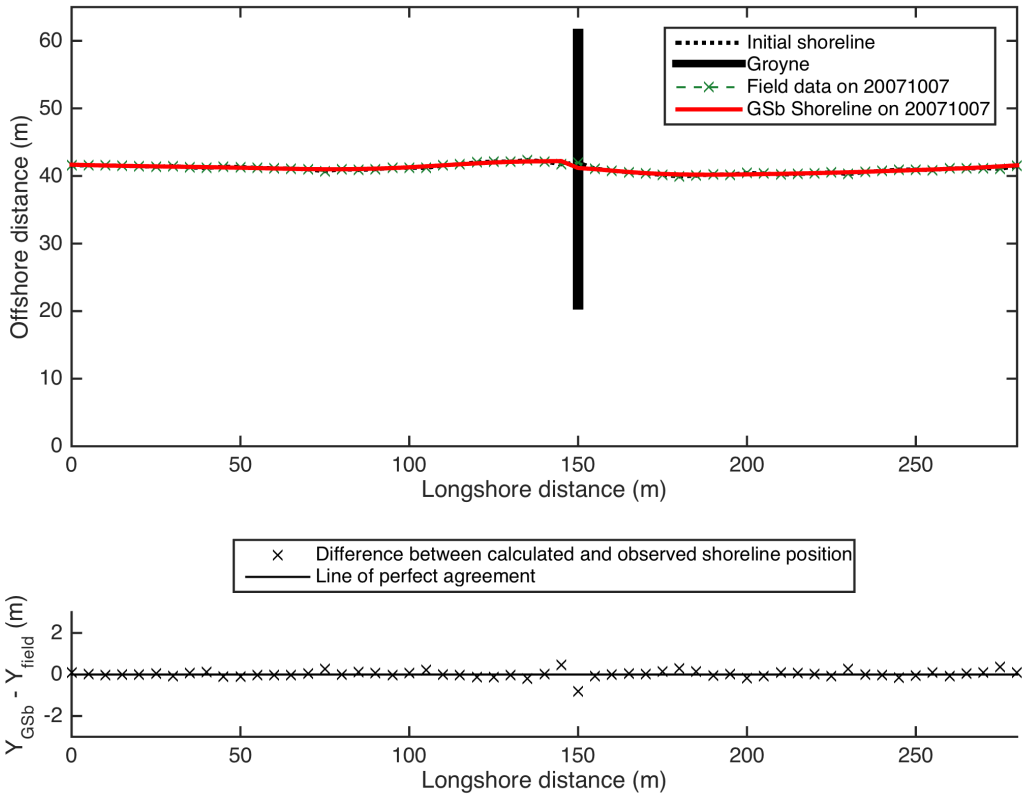

Figure 7.25 - Calculated and observed shoreline and difference between them, for a 7 days long simulation, from 01/10/2007 to 07/10/2007, using nearshore AWAC wave data

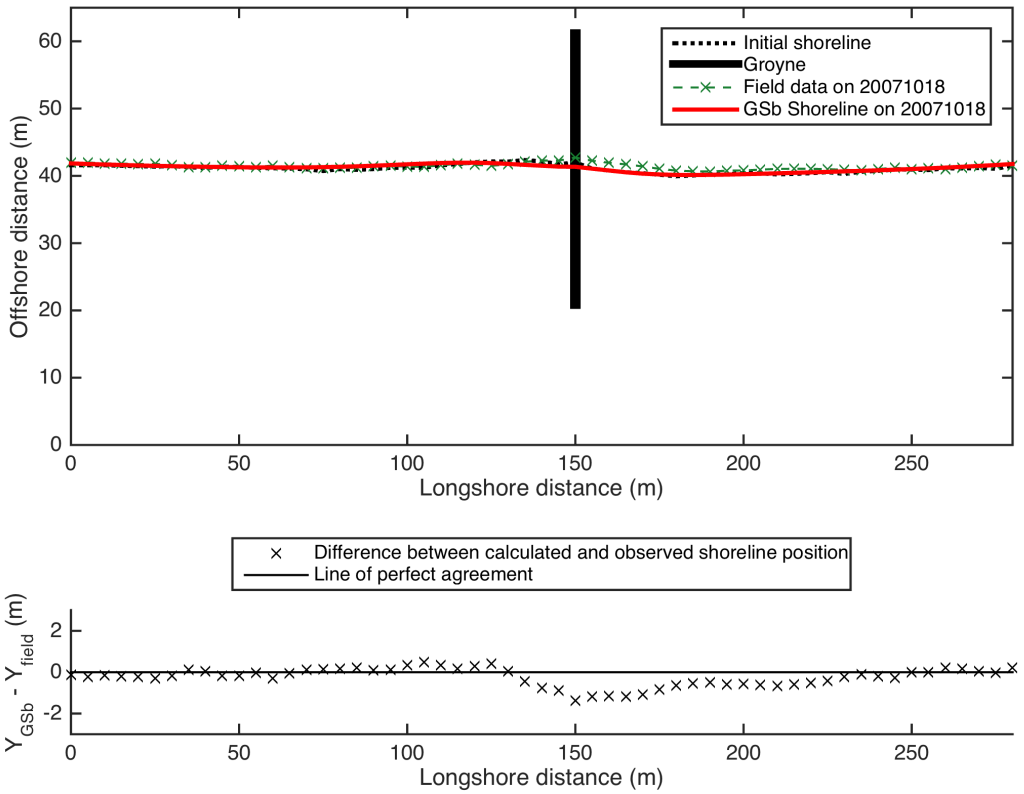

Figure 7.26 - Calculated and observed shoreline and difference between them, for a 18 days long simulation, from 01/10/2007 to 18/10/2007, using nearshore AWAC wave data

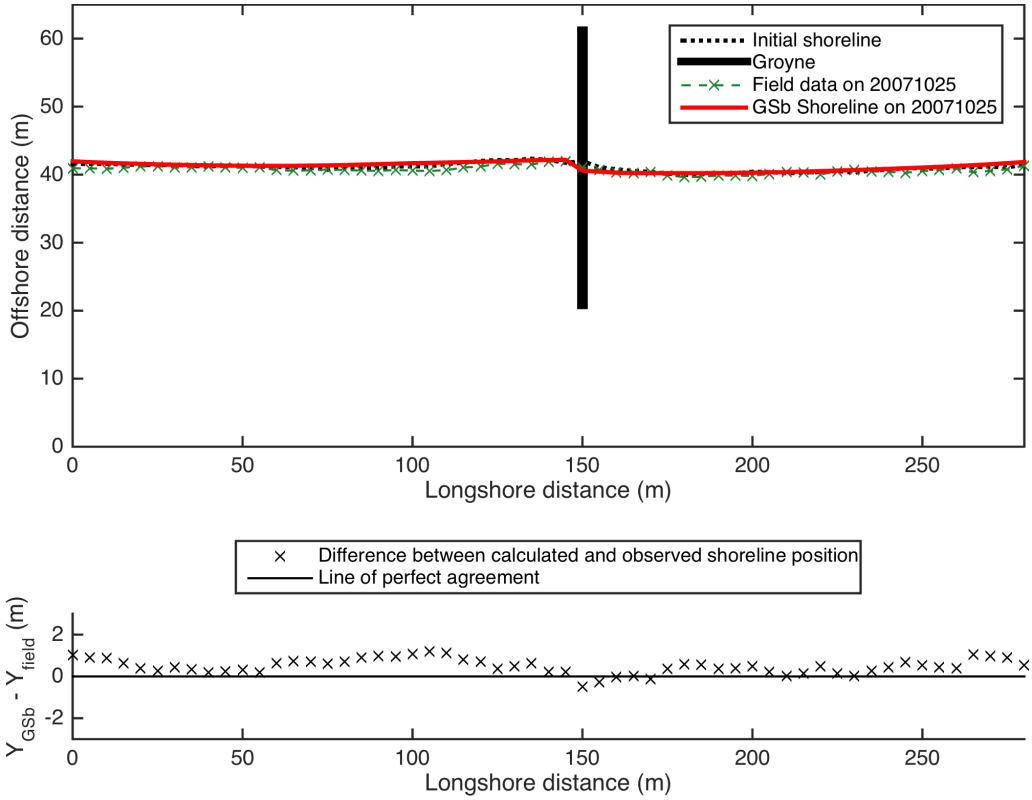

Figure 7.27 - Calculated and observed shoreline and difference between them, for a 25 days long simulation, from 01/10/2007 to 25/11/2007, using nearshore AWAC wave data

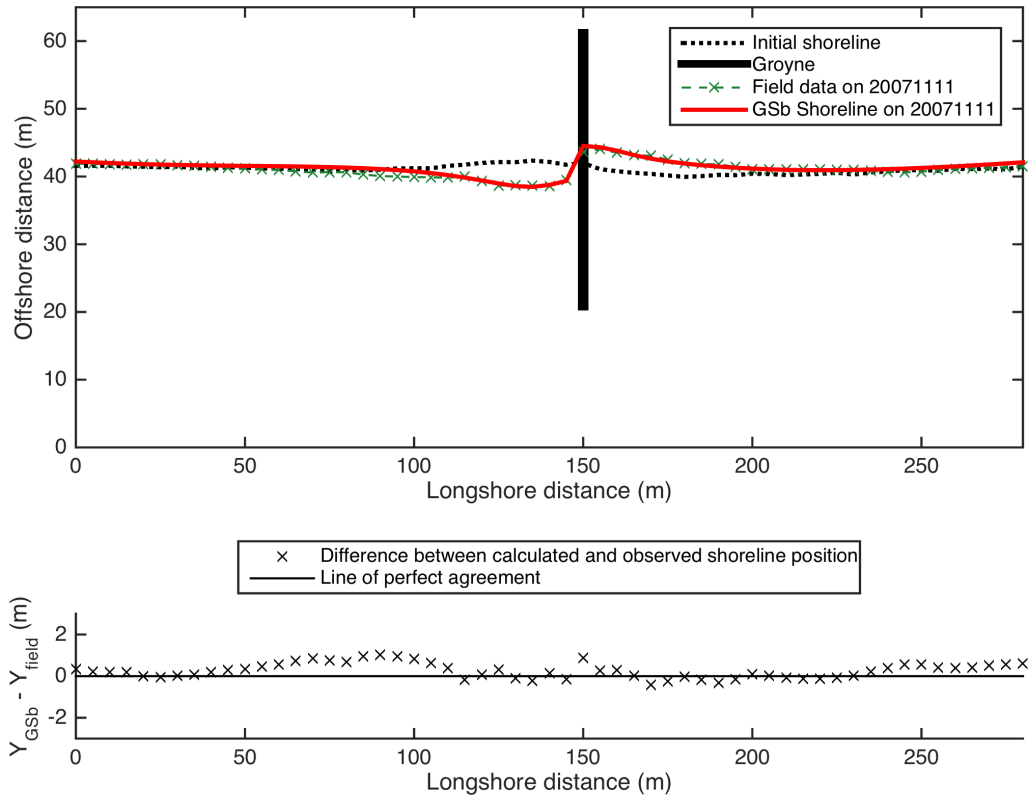

Figure 7.28 - Calculated and observed shoreline and difference between them, for a 36 days long simulation, from 01/10/2007 to 11/11/2007, using nearshore AWAC wave data

Figure 7.27 and Figure 7.28 show the model capability to predict the shoreline evolution 25 and 36 days after the groyne installation. The difference between calculated and observed shoreline near the groyne position (x = 150 m) remains negligible over time.

A calculation of the RMSE for two different domain, one restricted to the groyne area and one of the entire domain, was performed to evaluate the quality of the result near to the structure. Figure 7.29 shows the RMSE calculated comparing the observed and calculated shorelines of the entire domain (black dots) and the reduced domain near the groyne, from x = 120 m to x = 180 m (red dots). The comparison shows that the RMSE is the smallest when calculated in the reduced domain.

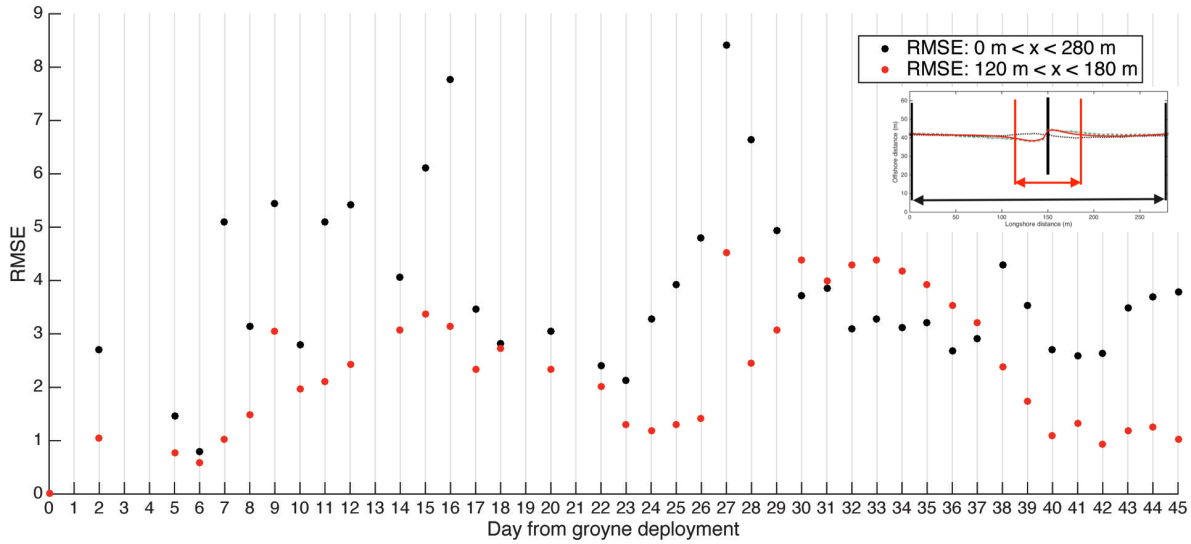

Figure 7.29 - Comparison of the RMSE over time calculates in the entire domain (black dots) and close the groyne (red dots). Simulations performed using nearshore AWAC wave data

7.2.3 Mean net annual transport

The mean net annual transport for Milford on Sea was calculated with GSb model: this value depends on the cell considered, and it is between 3000 and 5000 m^3y^{-1} eastward. In SCOPAC (2003) the littoral drift for Christchurch Bay was observed. In particular, the direction of the gravel and sand transport was observed from West to East. In particular, at the study site (Milford On Sea beach), the littoral drift evaluated was comprised between 3000 and 10000 m^3y^{-1} (*Figure 7.30*) with medium reliability of information (SCOPAC, 2003).

The mean net annual transport calculated with GSb resulted in agreement with the data furnished by SCOPAC (2003).

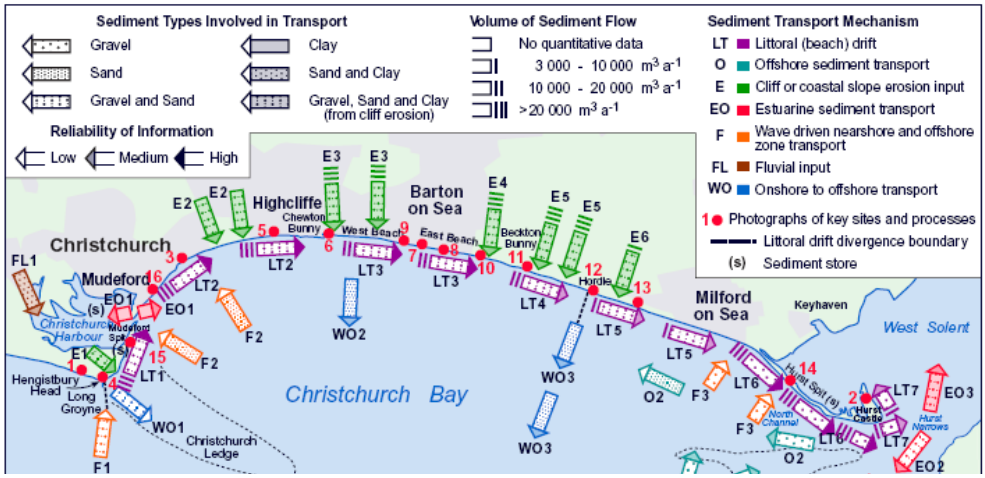

Figure 7.30 - Sediment transport patterns at Christchurch Bay, from Hengistbury Head to Hurst Spit (from SCOPAC, 2003)

7.2.4 Verification for the mixed beach

After the calibration of K_{GSb} (Section 7.2.2), in order to get a verification, the model was used for the following cases:

1. DGPS shorelines and offshore wave rider buoy data (CCO), (Section 7.2.4.1)
2. Argus shorelines and nearshore wave data (AWAC), (Section 7.2.4.2)
3. Argus shorelines and nearshore SWAN wave data, (Section 7.2.4.3)

7.2.4.1 DGPS shorelines and offshore wave rider buoy data (CCO)

After the calibration of K_{GSb} (Section 7.2.2), the model was used using the Wave-Rider Buoy Data (CCO), described in (Figure 7.14). The buoy was located 1500 m offshore, approximately at 10 m water depth.

In Table 7.5 the input parameters are shown:

Table 7.5 - GSb model input of the simulation with offshore wave data (CCO)

Model domain	Number of cells alongshore	NX = 57
	Dimension of cells	DX = 5 m
	Calculation time step	DT = 0.005 hrs
	Median grain size	D_{50} = 10 mm
	Active beach profile	$D_C + D_B$ = 4 m
Model forcing	Hourly waves parameters (H_s, T_p, Dir) from Wave-Rider Buoy Data provided by Channel Coast Observatory, located 1500 m offshore, approximately at 10 m water depth	
Model parameters	Calibration parameter	K_{GSb} = 0.1
	Boundary conditions	Moving (0.678 m -Left; 0.655 -Right)
	Recording time step	DTS = 24 hour
Structures	Groyne 46 m long (19 m wet / 27 dry) at x = 150 m	
Initial shoreline	Shoreline of 01/10/2007 extracted from DGPS profile	

Figure 7.31 shows the results of the numerical simulation compared with the observed shoreline and the relative difference between them, after 45 days from the groyne deployment, from 01/10/2007 to 14/11/2007.

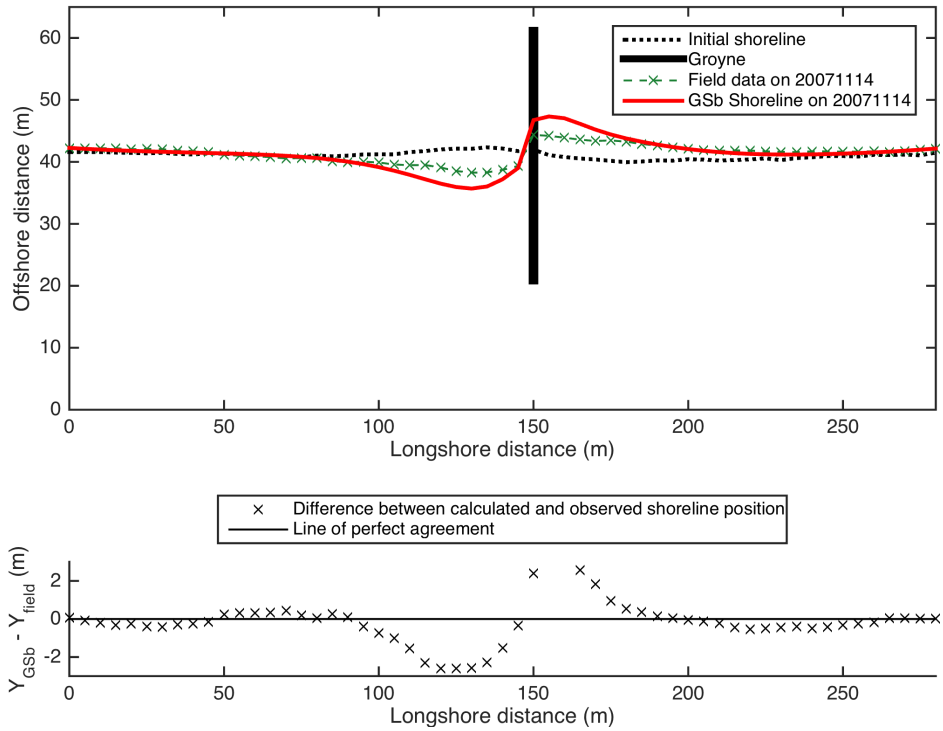

Figure 7.31 - Calculated and observed shoreline and difference between them, for a 45 days long simulation, from 01/10/2007 to 14/11/2007. Simulation performed using offshore CCO wave data

It is noticed that, when the offshore wave data are used, the GSb model overestimated the evolution near to the groyne. This suggests that, in order to have a more reliable result in term of shoreline evolution, nearshore wave data need to be used in GSb model.

As done for the case with nearshore wave data (Section 7.2.2), calculation of the RMSE in two different domains, one restricted to the groyne area and one for the entire domain, was performed to evaluate the quality of the result near to the structure.

Figure 7.32 shows the RMSE calculated comparing the observed and calculated shorelines for the entire domain (black dots) and the reduced area near the groyne, from x = 120 m to x = 180 m (red dots). In the present case, the comparison shows that the RMSE is lowest if calculated in the entire domain.

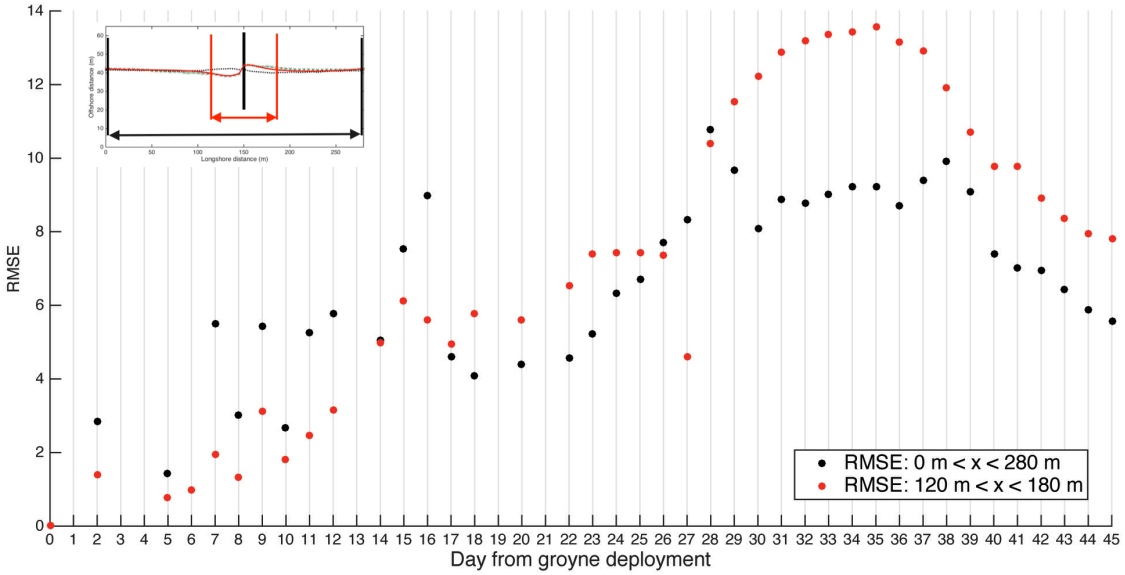

Figure 7.32 - Comparison of the RMSE over time calculates in the entire domain (black dots) and close the groyne (red dots). Simulations performed using offshore CCO wave data

7.2.4.2 Argus shorelines and nearshore wave data (AWAC)

After the calibration of K_{GSb} (Section 7.2.2), Argus data were used to verify the GSb model to predict the accretion and the erosion up-drift and down-drift of the groyne when a longer computational domain is considered. In this case, the Argus domain is 740 m long. Argus data are available from 20/03/2007 to 10/05/2008. Table 7.6, shoes the Argus data available in the period of the groyne deployment, from 01/10/2007 to 14/11/2007; selected data refer to similar tidal conditions measured by a tide gauge deployed at Becton Bunny (Martin-Grandes, 2014).

Table 7.6 - Tidal level at Becton Bunny (Barton on Sea) at the moment of the Argus image acquisition

Filename	*Date*	*Time*	*Tidal level at Becton Bunny*
wl.milford.20071001.gmt1650.cx.mat	20071001	16:50	0.1344
wl.milford.20071002.gmt0930.cx.mat	20071002	09:30	0.2032
wl.milford.20071003.gmt0630.cx.mat	20071003	06:30	0.13
wl.milford.20071004.gmt1350.cx.mat	20071004	13:50	0.1505
wl.milford.20071005.gmt1550.cx.mat	20071005	15:50	0.1455
wl.milford.20071006.gmt1500.cx.mat	20071006	15:00	0.1379
wl.milford.20071007.gmt1530.cx.mat	20071007	15:30	0.1232
wl.milford.20071008.gmt1619.cx.mat	20071008	16:19	0.1702
wl.milford.20071009.gmt1700.cx.mat	20071009	17:00	0.1924
wl.milford.20071010.gmt1730.cx.mat	20071010	17:30	0.1522
wl.milford.20071011.gmt0600.cx.mat	20071011	06:00	0.1415

Filename	*Date*	*Time*	*Tidal level at Becton Bunny*
wl.milford.20071013.gmt0650.cx.mat	20071013	06:50	0.1798
wl.milford.20071014.gmt1520.cx.mat	20071014	15:20	0.1927
wl.milford.20071015.gmt0730.cx.mat	20071015	07:30	0.1839
wl.milford.20071016.gmt1650.cx.mat	20071016	16:50	0.1249
wl.milford.20071017.gmt0820.cx.mat	20071017	08:20	0.1184
wl.milford.20071018.gmt0900.cx.mat	20071018	09:00	0.1369
wl.milford.20071019.gmt1300.cx.mat	20071019	13:00	0.134
wl.milford.20071020.gmt1500.cx.mat	20071020	15:00	0.1257
wl.milford.20071021.gmt1430.cx.mat	20071021	14:30	0.139
wl.milford.20071022.gmt1449.cx.mat	20071022	14:49	0.1364
wl.milford.20071023.gmt1530.cx.mat	20071023	15:30	0.1489
wl.milford.20071024.gmt1619.cx.mat	20071024	16:19	0.1533
wl.milford.20071025.gmt1230.cx.mat	20071025	12:30	0.1799
wl.milford.20071026.gmt1319.cx.mat	20071026	13:19	0.1927
wl.milford.20071029.gmt0719.cx.mat	20071029	07:19	0.2107
wl.milford.20071101.gmt1050.cx.mat	20071101	10:50	0.151
wl.milford.20071102.gmt1500.cx.mat	20071102	15:00	0.1244
wl.milford.20071103.gmt1400.cx.mat	20071103	14:00	0.1302
wl.milford.20071104.gmt1650.cx.mat	20071104	16:50	0.1364
wl.milford.20071105.gmt1650.cx.mat	20071105	16:50	0.1352
wl.milford.20071107.gmt1600.cx.mat	20071107	16:00	0.1278
wl.milford.20071108.gmt1250.cx.mat	20071108	12:50	0.1593
wl.milford.20071109.gmt1350.cx.mat	20071109	13:50	0.1901
wl.milford.20071110.gmt1350.cx.mat	20071110	13:50	0.2249
wl.milford.20071111.gmt0650.cx.mat	20071111	06:50	0.2557
wl.milford.20071112.gmt0640.cx.mat	20071112	06:40	0.2402
wl.milford.20071113.gmt0710.cx.mat	20071113	07:10	0.1852
wl.milford.20071114.gmt1530.cx.mat	20071114	15:30	0.2042

The picture of 05/10/2007 15:50 (Figure 7.33e) represent the first Argus image where the shoreline is clearly detectable; the shoreline was assumed as the initial line in the numerical model.

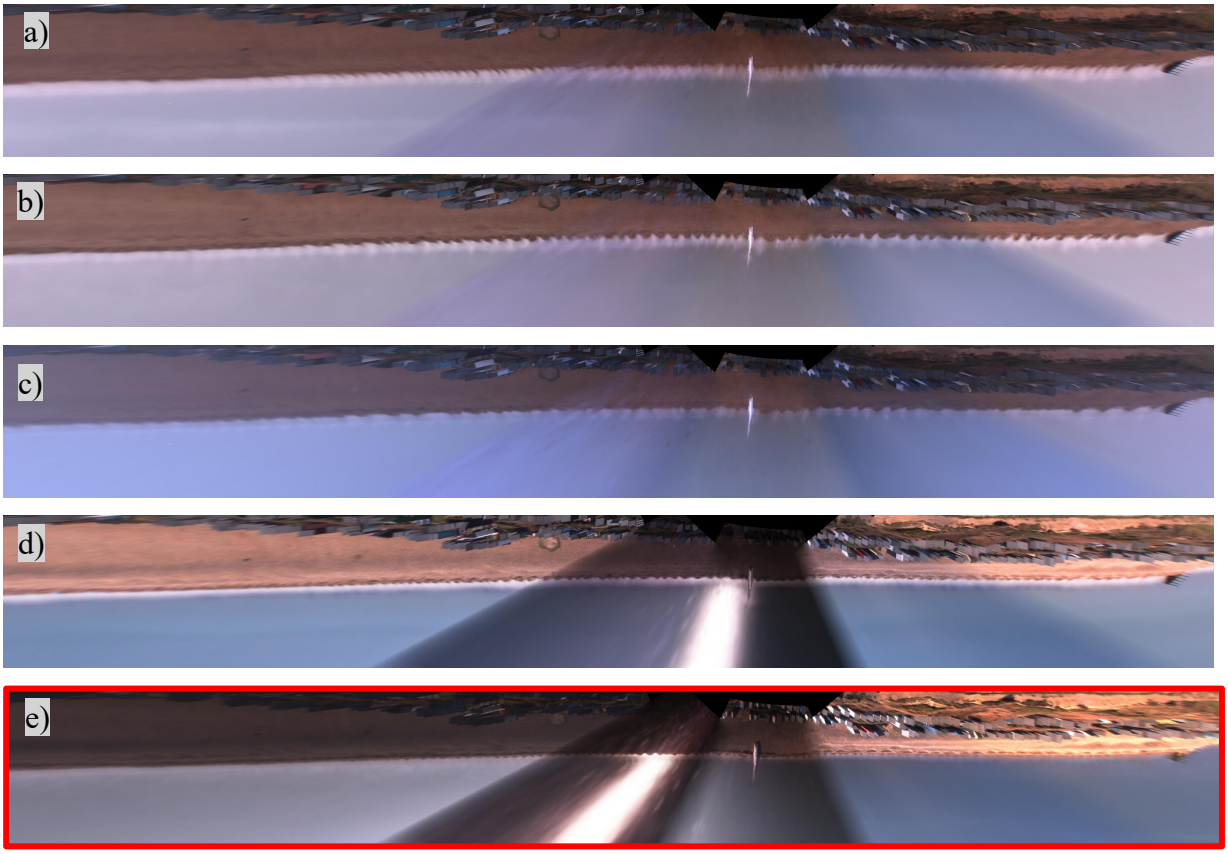

Figure 7.33 – Argus images a) 01/10/2007 16:50 b) 02/10/2007 09:30 c) 03/10/2007 06:30 d) 04/10/2007 13:50 e) 05/10/2007 15:50

The simulations were performed using the input mentioned in Table 7.7, and considering the nearshore AWAC Wave data.

Table 7.7 - GSb model input for simulation with Argus shoreline and nearshore AWAC wave data

Model domain	Number of cells alongshore	NX = 148
	Dimension of cells	DX = 5 m
	Calculation time step	DT = 0.005 hrs
	Median grain size	$D50$ = 10 mm
	Active beach profile	$D_C + D_B$ = 4 m
Model forcing	Hourly waves parameters (H_s, T_p, Dir) from AWAC measurements at the 7 m depth contour, located 600 m offshore	
Model parameters	Calibration parameter	K_{GSb} = 0.1
	Boundary conditions	Pinned
	Recording time step	DTS = 24 hour
Structures	Groyne 46 m long (19 m wet / 27 dry) at x = 250 m	
Initial shoreline	Shoreline of 05/10/2007 extracted from ARGUS picture	

The calculated shoreline position (red line) was compared with the observed Argus data (Green dotted line) after 39 days after the groyne deployment (13/11/2017). The result shows that the model is able to predict the accretion/erosion occurred up-drift/down-drift of the groyne using the same calibration coefficient (K_{GSb}= 0.1) gained after the calibration procedure (Section 7.2.2). The calculated accretion in the up-drift side results slightly overestimated.

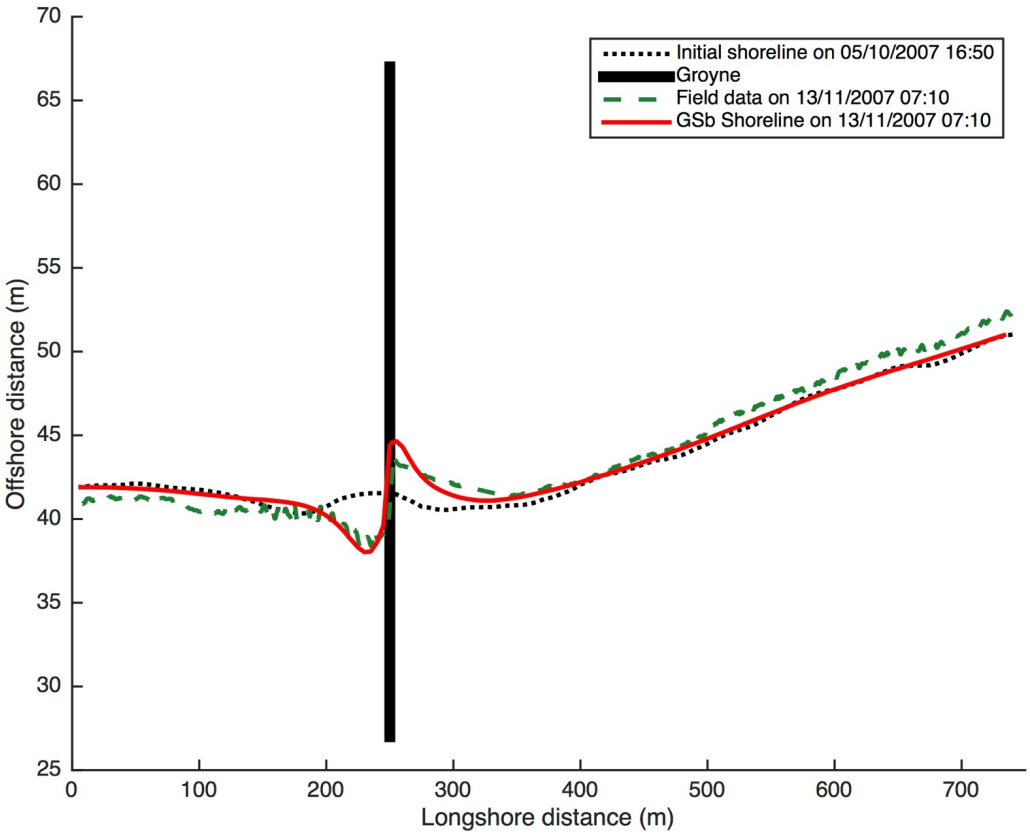

Figure 7.34 - Calculated and observed shoreline, for a 39 days long simulation, from 05/10/2007 to 13/11/2007, with the computational domain 740 m long and pinned beach boundaries conditions. Simulation conducted with nearshore AWAC wave data

Figures 7.35 a-e show the comparisons between the calculated shoreline (red line) and the Argus images on the *a)* 05/10/2007 (Initial shoreline), *b)* 13/10/2007, *c)* 21/10/2007 *d)* 11/11/2007 and *e)* 13/11/2007 (Final shoreline), where a more detailed view of the shorelines is shown in Figures 7.36 a-e.

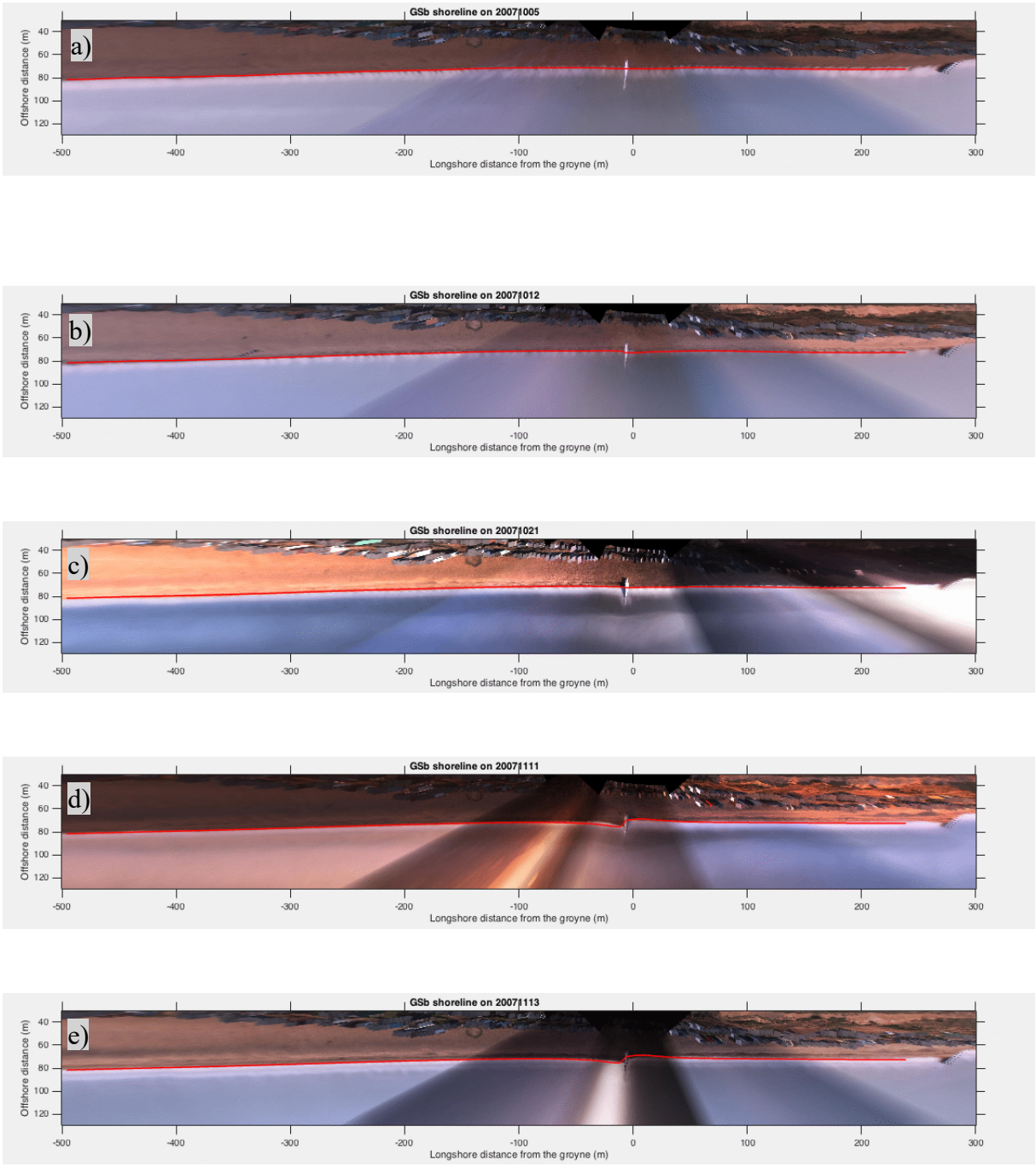

Figure 7.35 – Comparison between calculated shoreline and ARGUS images a) 05/10/2007, b) 13/10/2007, c) 21/10/2007, d) 11/11/2007 and e) 13/11/2007

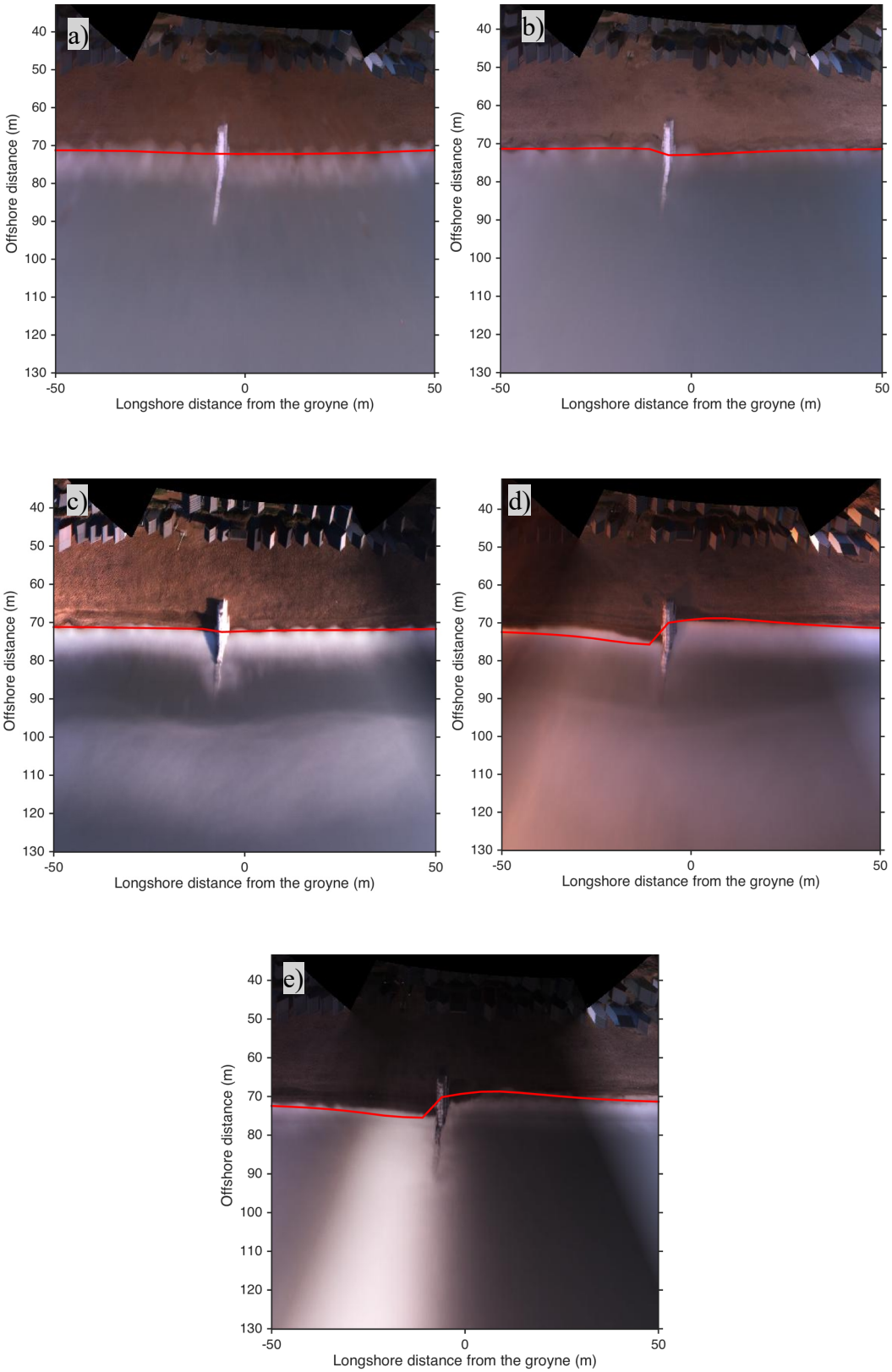

Figure 7.36 – Comparison between calculated shoreline and ARGUS images in the groyne area for a) 05/10/2007, b) 13/10/2007, c) 21/10/2007, d) 11/11/2007 and e) 13/11/2007

7.2.4.3 Argus shorelines and nearshore SWAN wave data

After the calibration of K_{GSb} (Section 7.2.2), a third-generation wave model, SWAN, developed by Delft University of Technology (Booij et al., 1997), was used to compute the wave propagation from the Directional Wave Rider Buoy Data, collected approximately 600 m offshore with 10 m water depth (Figure 7.14), to nearshore. The obtained nearshore wave characteristics were used to perform the GSb simulations and to verify the model results, from 05/10/2007 to 13/11/2007, in the period of the groyne presence, by comparing the numerical shorelines with the Argus shorelines.

Acoustic Wave and Current (AWAC) data collected during the groyne experiment (Martín Grandes et al., 2015) from 1/10/2007 to 25/11/2007 were used to evaluate the SWAN numerical simulation accuracy of the results obtained in terms of wave characteristics.

The Wave-Rider buoy (CCO) was located at 50,71229 N latitude and -1,61568 E longitude. The AWAC instrument location is at 50.72015 N Latitude and -1.61450 E Longitude (Figure 7.37). The AWAC wave data were collected with respect to the geographic North.

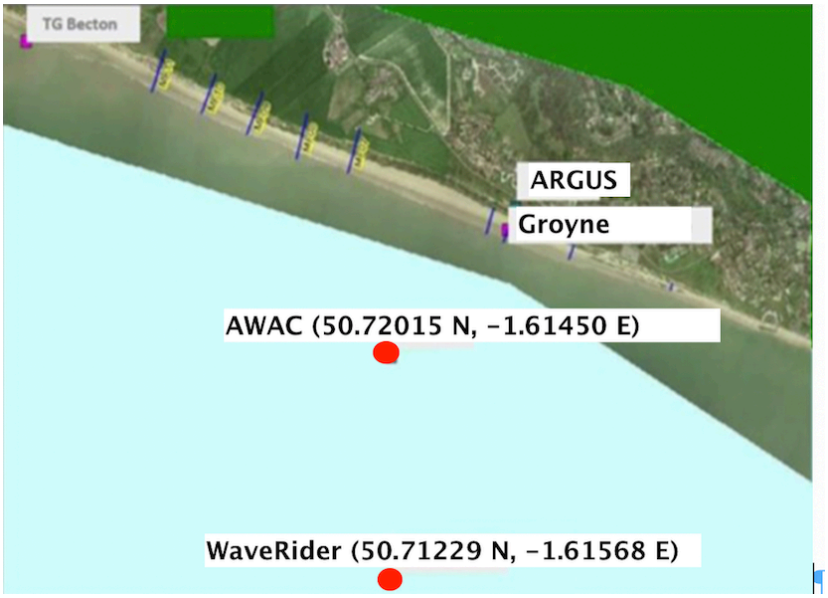

Figure 7.37 - Aerial view from Becton Bunny to Milford on Sea

The bathymetry data of Milford-on-Sea were downloaded from the EMODNET portal (http://portal.emodnet-bathymetry.eu/#), in ESRI ASCII format. The "Area of interest" was selected as shown in Figure 7.38:

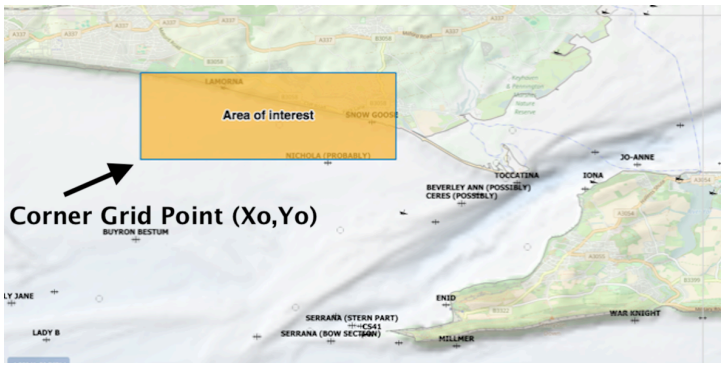

Figure 7.38 - Screenshot of the EMODnet bathymetry portal and selection of the "area of interest" with a corner grid point (Xo,Yo)

The bathymetry file is composed by:

```
NCOLS 68
NROWS 23
XLLCORNER -1.6553306579589844
YLLCORNER 50.71031570434571
CELLSIZE 0.0010416666699999998
NODATA_VALUE -32767.0
```

The corner-grid point has coordinates X_0,Y_0 (-1.6553306579589844 E, 50.71031570434571 N), the Wave-Rider buoy coordinates X_p,Y_p (-1.61568 E, 50.71229 N) and the AWAC instrument has coordinates X_A,Y_A (-1.61450 E, 50.72015 N). These points were plotted by https://www.geoplaner.com/ (Figure 7.39).

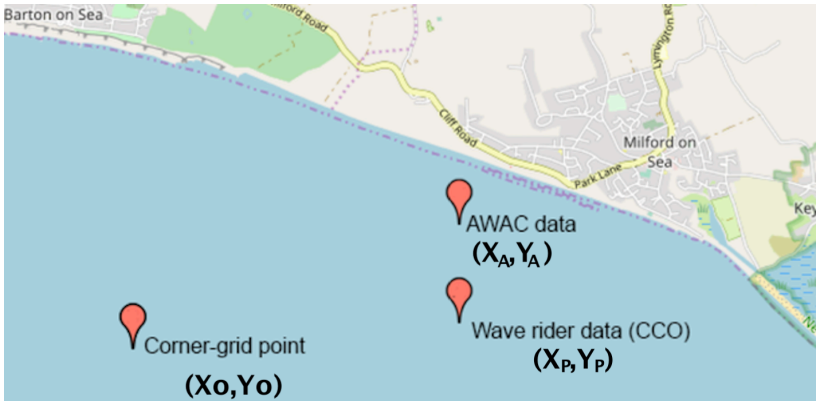

Figure 7.39 – Screenshot of GeoPlaner service (https://www.geoplaner.com/): plot of the Corner Gridpoint and Wave-Rider Buoy Coordinates

The cell size of the EMODnet data grid is expressed in degree (`CELLSIZE 0.0010416666699999998`) and conversion in meters is needed for the SWAN Input Data. The conversion of the length of one degree in meter, for a known value of latitude and longitude, was done by the calculator of the *National Geospatial Agency* where the latitude of the study site was indicated (50.71 degrees). The conversion showed that a degree of Latitude is equal to

111243 meters and a degree of Longitude is equal to 70634 meters at Milford-on-sea (Figure 7.40).

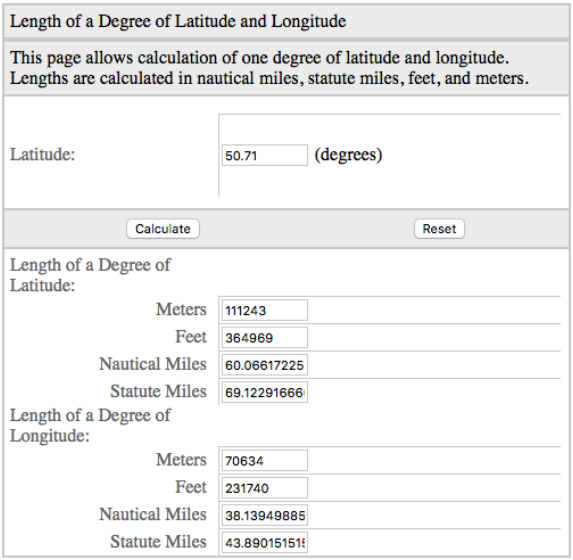

Figure 7.40 – Screenshot of the National Geospatial Agency calculator (https://msi.nga.mil/msisitecontent/staticfiles/calculators/degree.html)

The bathymetry domain is composed by 23 rows and 68 columns with grid spacing 73.5770836 m in the x-direction and 115.878125 m in the y-direction; the total grid length in the x-direction is 4929.6646 m and 2598.31876 m in the y-direction. Table 7.8 summarizes the grid information:

Table 7.8 - Data Grid Information of the EMODNET bathymetry

n. row	23
n. columns	68
Cell size (°)	0.001041667
Cell size x (m)	73.57708357
Cell size y (m)	115.8781254
total grid length x-direction (m)	4929.664599
total grid length y-direction (m)	2549.318758
origin axis (latitude N, longitude E)	50.7103157 -1.655330658

The contour map and 3D-mesh of the study site are shown in Figure 7.41.

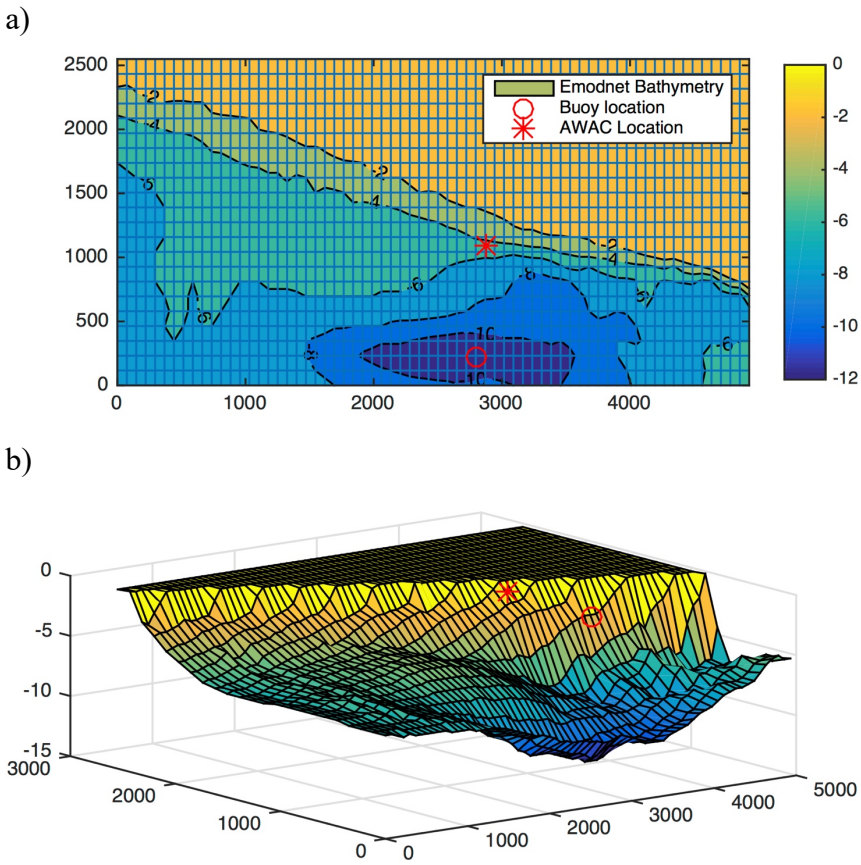

Figure 7.41 - Emodnet bathymetry: a) Contour plot; b) 3D-mesh plot

The spatial grid of the bathymetry was defined as indicated in the SWAN user manual.

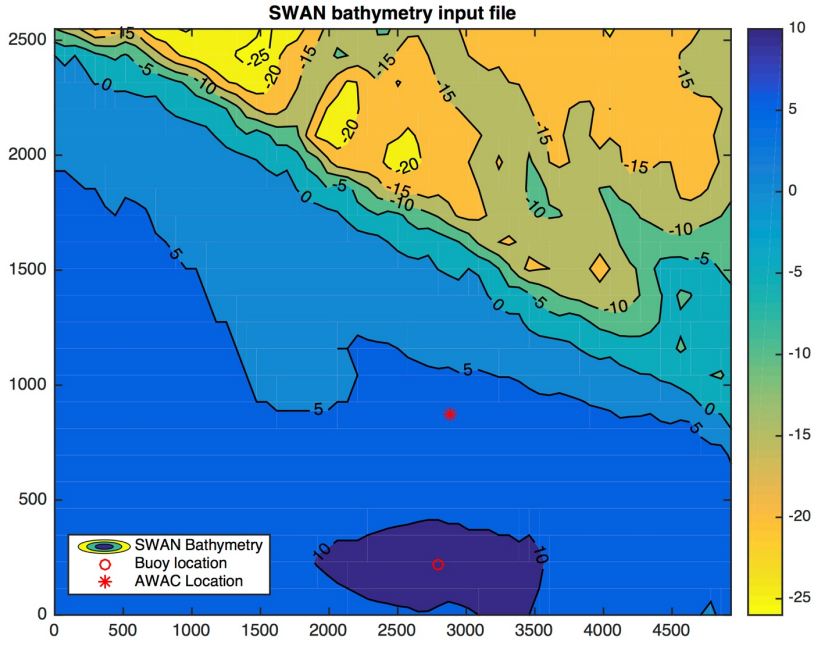

Figure 7.42 – Contour plot of SWAN bathymetry file

A uniform rectangular computational grid was defined, with the origin in *xpc* = 0.0 and *ypc* = 0.0. The computational grid is 4929 m length in the x-direction and 2549 m in the y-direction. The mesh consists of 67 cells 73.48 m long in the x-direction and 22 cells 115.88 m long in the y-direction. The wave input data were considered at the South, West and East Boundaries using the clockwise convention for the wave direction. The wave characteristics in P1 (Wave-Rider buoy location) and P2 (AWAC location) were required as model output. The SWAN input file was named *input.swn* and it contains 22 lines:

```
PROJECT  'Milford'   '1'
MODE STATIONARY
SET 0 90 0.01 200 2 NAUTical
CGRID  REGULAR 0. 0. 0. 4929. 2549. 67 22 SECTOR 135 315 21 0.01 0.5 30
INPGRID BOTTOM 0. 0. 0. 67 22 73.58 115.88 EXC 0.
READINP BOTTOM 1. 'milford.prn' 1 0
BOUND SHAPESPEC JONSWAP
BOUNDPAR2 SIDE SOUTH CLOCKW CON PAR 2.00 7.00 180 18
BOUNDPAR2 SIDE WEST CLOCKW CON PAR 2.00 7.00 180 18
BOUNDPAR2 SIDE EAST CLOCKW CON PAR 2.00 7.00 180 18
BREAKING CONSTANT 1.0 0.73
BREAKING
OFF QUADRUPL
OFF WCAPPING
POINTS 'P1' 2800. 219.
POINTS 'P2' 2884. 874.
FRAME 'GRIGLIA' 0. 0. 0. 4929. 2549. 67 22
TABLE 'P1' HEADER 'P1_1.dat' XP YP HSIGN DIR RTP DEPTH
TABLE 'P2' HEADER 'P2_1.dat' XP YP HSIGN DIR RTP DEPTH
TABLE 'GRIGLIA' HEADER 'Output_1.dat' HSIGN TMM10 TM02 DIR RTP DEPTH
COMPUTE
STOP
```

The offshore wave data collected by the Wave-Rider Buoy (CCO) from 01/10/2007 to 25/11/2007 were used as wave input for SWAN model; the directional rose is shown in Figure 7.43.

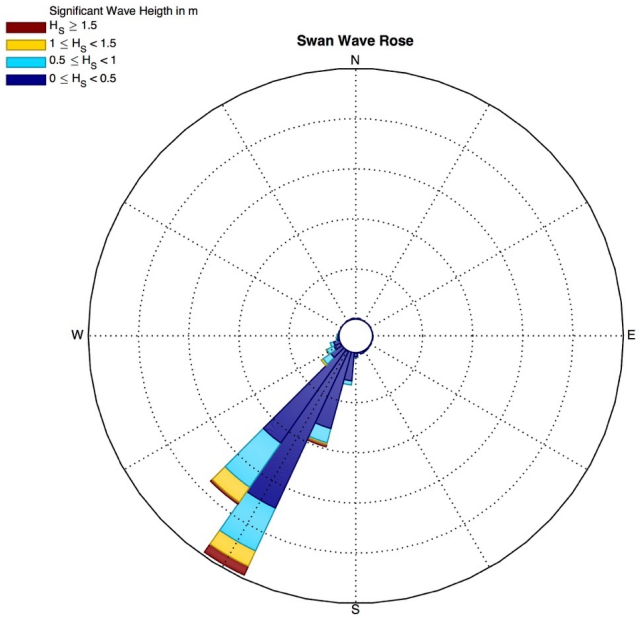

Figure 7.43 – Wave rose of Wave-Rider buoy (CCO) data used as wave input for SWAN model

The directional rose of the data collected by AWAC instrument is shown in Figure 7.44a. The wave characteristics at the point where the AWAC instrument was installed were calculated with SWAN model and are shown in Figure 7.44b.

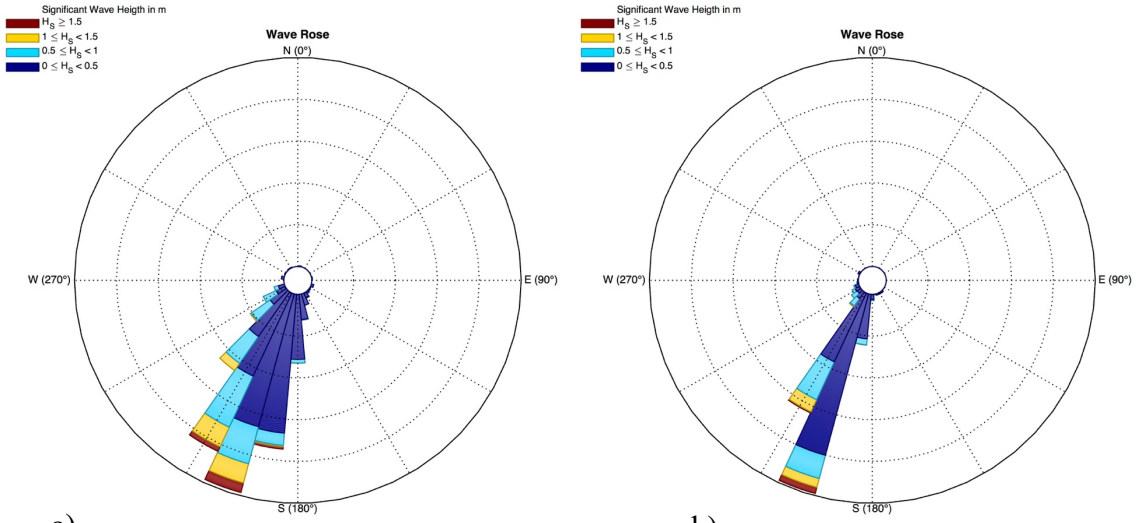

Figure 7.44 – Wave rose of a) AWAC data b) SWAN output

AWAC and SWAN time series of the significant wave height are shown in Figure 7.45:

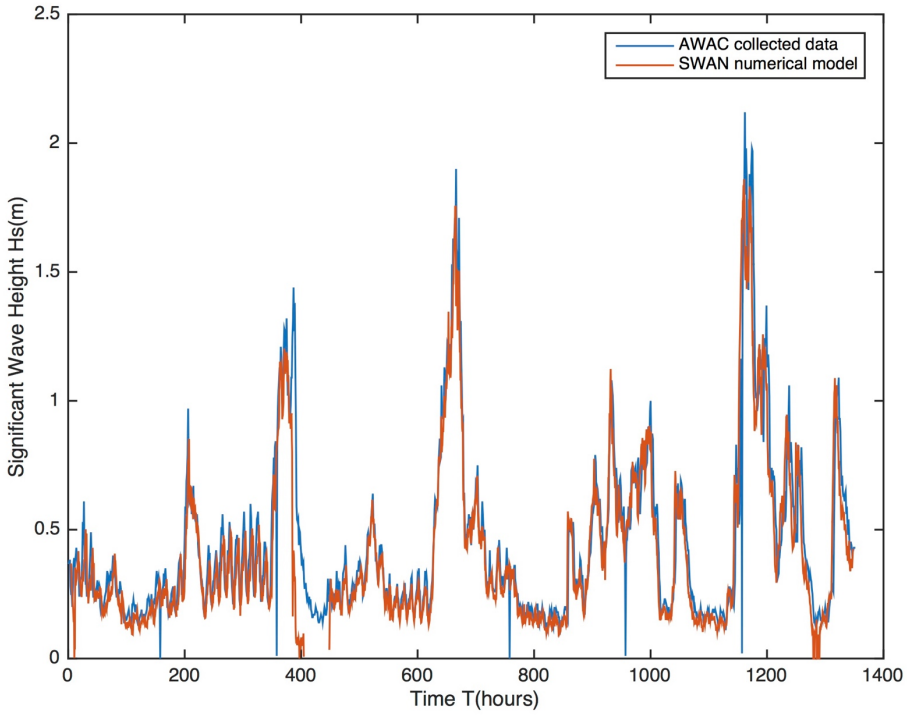

Figure 7.45 - Time series of the significant wave height, H_S, measured (red line) and calculated (blue line)

The nearshore wave characteristics obtained with SWAN were used to perform the GSb simulations, from 05/10/2007 to 13/11/2007, in the period of the groyne presence. The calculated shoreline was compared with the observed Argus shoreline.

The GSb simulation was performed with the initial ARGUS shoreline of the 05/10/2007. The boundaries conditions were set moving (Figure 7.46a) and pinned (Figure 7.46b).

The obtained result (Figure 7.46) shows that the GSb model is able to predict the shoreline evolution considering the propagated SWAN waves, and using the calibration parameter K_{GSb} gained in Section 7.2.2 (K_{GSb} =0.1). Moreover, the comparison of the results with pinned and moving boundaries shows that the result is not driven from the boundary conditions.

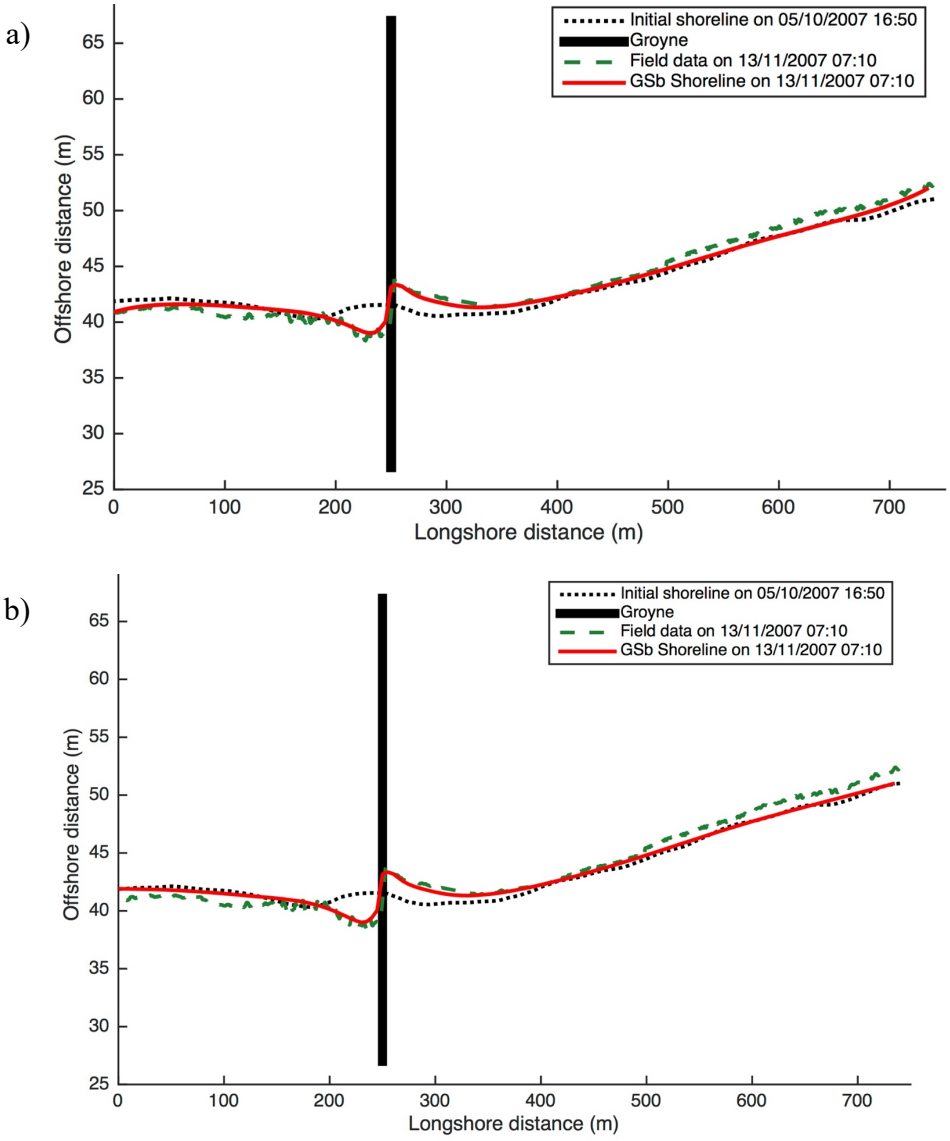

Figure 7.46 – Shoreline evolution obtained using the wave data calculated with SWAN model and considering the initial ARGUS shoreline of the 05/10/2007 with: a)moving boundary conditions; b) pinned boundary conditions

7.3 Lab tests 1 - LSTF experiments (Gravens and Wang, 2007)

The GSb model calibration was performed comparing calculated shoreline with laboratory results of an experiment conducted in the USACE-ERDC-CHL Large-Scale Sediment Transport Facility (LSTF); the methodology and results of laboratory tests are described in Gravens and Wang (2007). GSb model verification of shoreline evolution was performed following the procedure exposed for GENESIS model (Hanson et al., 2006) and for Gencade model (Frey et al.,2012). The verification experiment analyses the capability of the GSb model to calculate the salient evolution and tombolo formation behind a detached breakwater. The GSb model domain was set to reproduce the LSTF Test 1 (Figure 7.47).

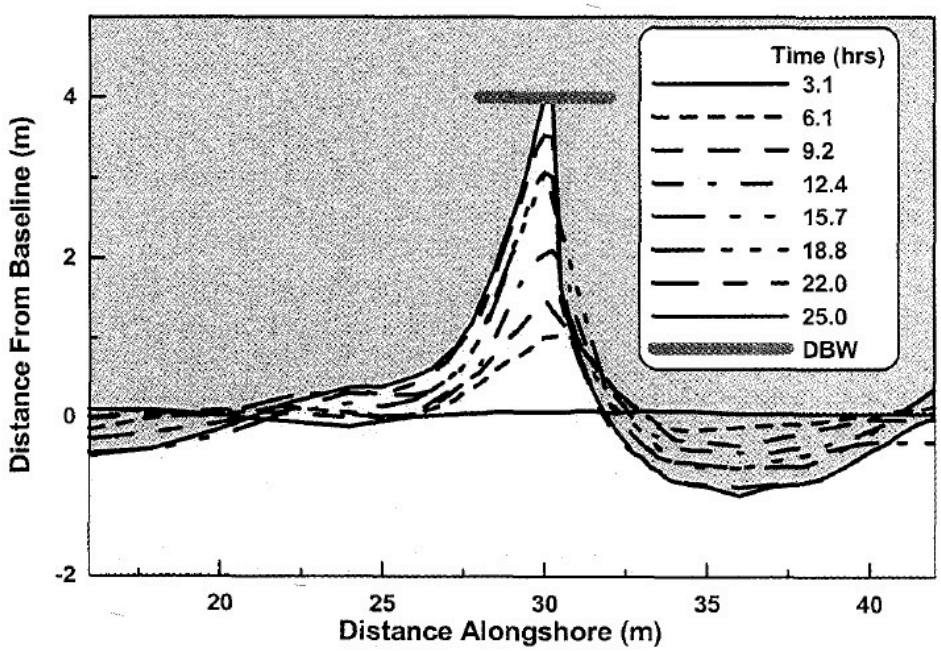

Figure 7.47 - Measured shoreline evolution in LSTF Test 1 (Hanson et al., 2006)

The model grid was 60 m long, as the simulation performed in Frey et al., (2012), with 120 cells total (model grid cell resolution DX = 0.5 m). A 4 m long detached breakwater positioned in the centre of the domain 4 m offshore of the initial shoreline position at a depth of 0.17 m. The duration of the numerical simulation was 24 hours as for the case of the laboratory test. GSb lateral boundaries were selected as pinned. The median grain size (D_{50}) was set 0.15 mm. The berm height, D_B, was set to 0.35 m, and the closure depth, D_C, was 0.5 m.

Wave forcing applied to the GSb model was held constant during the simulation such that breaking wave heights were H = 0.26 m, T = 1.5 sec, and Dir = 6.5 -deg as measured in the LSTF experiment. Wave inputs were supplied at the h = 0.9 m depth contour.

GSb model was calibrated choosing the calibration parameter K_{GSb} in order to have the maximum salient reaching the breakwater and no-tombolo condition.

Figure 7.48 shows the differences in the calculated shoreline using three different calibration coefficient K_{GSb}: 0.27, 0.24, and 0.20. Figure 7.49 shows a comparison between the observed and the relative calculated salient evolution for the three cases. The result changes both for shoreline and salient evolution depending on the chosen calibration value. The shoreline reaches the breakwater after 15 hours, and then the tombolo is formed when using a calibration coefficient $K_{GSb} = 0.27$. The calculated shoreline with $K_{GSb} = 0.20$ does not reach the breakwater in 24 hours of simulation, and the accretion behind the breakwater is equal to 3.05 m. The calculated shoreline reaches the breakwater in 24 hours, as in the laboratory case, when K_{GSb} is equal to 0.24. The solution shows two different zones where the recession of shoreline occurred, to the left and right sides of the salient. The first calculated eroded zone begins at the start of the domain (x = 0 m) and ends at x = 27.5 m presenting a maximum retreat equal to y = -1.25 m. The second eroded zone begins at x = 33.77 m and ends at the end of the domain (x = 60 m).

The calculated shoreline on the left side of the salient differs from the experimental solution where the eroded zone ended for x = 21.09 m with a maximum retreat equal to y = - 0.49 m compared to y = -1.25 m of the GSb model. This indicates that an improvement in the diffraction computation is necessary. The second calculated eroded zone is in a reasonable agreement with the laboratory data, where the maximum retreat was equal to y = - 0.64 m with a difference with the calculated shoreline of 0.32 m.

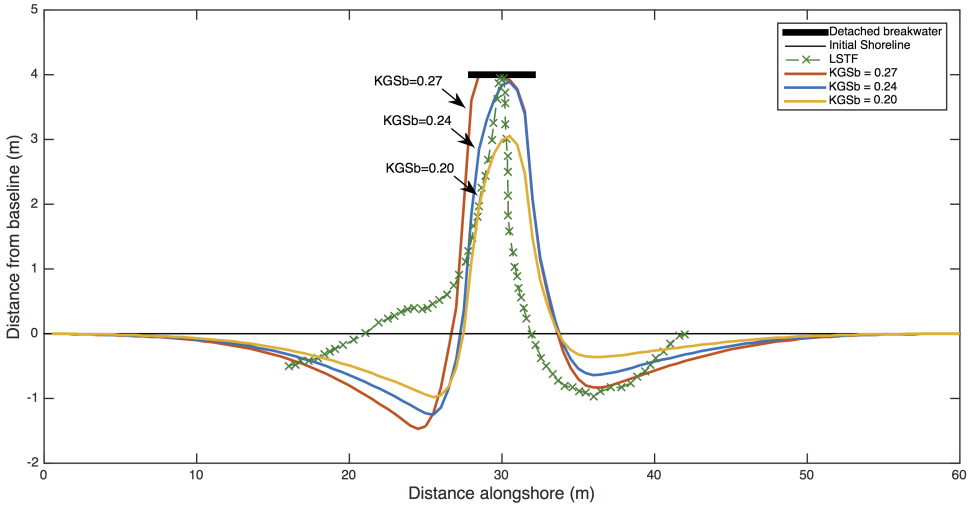

Figure 7.48 – Observed and calculated shoreline evolution for K_{GSb} = 0.27, 0.24, and 0.20

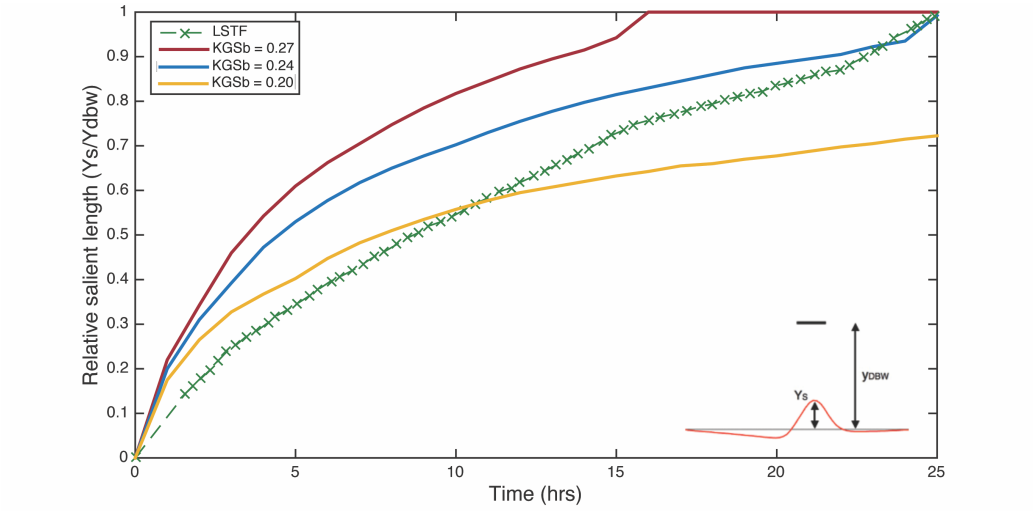

Figure 7.49 – Observed and calculated salient evolution for K_{GSb} = 0.27, 0.24, and 0.20

7.3.1 Influence of the grid size in the computational domain

GSb model simulations with three different domains parameters (*NX, DX*) were performed to evaluate the influence of the grid size on the calculated shoreline. GSb computational grid is characterized by two parameters: the number of the cells, *NX*, and the model grid cell resolution, *DX*. Figure 7.50 shows the results obtained for three cases, named *Test domain 1, 2, 3* where *NX* = 200, 120, 80 and *DX* = 0.3, 0.5, 0.7, respectively. In the *Test domain 1*, shoreline reaches the detached breakwater forming a tombolo, with a slight difference in the rest of the calculated shoreline if compared with the *Test domain 2*. In *Test domain 3,* the length of the salient behind the breakwater is equal to y = 3.48 m, with a difference of -13 % of the salient evolution with respect to the experimental data.

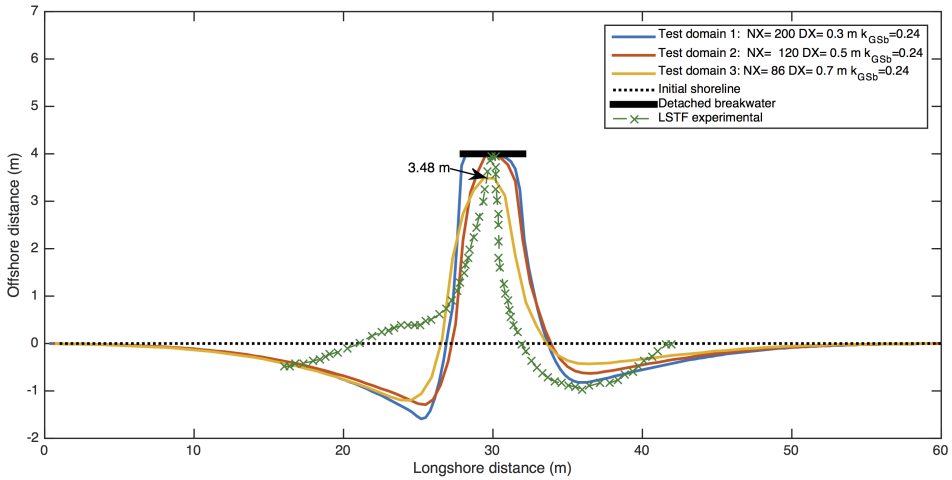

Figure 7.50 – Shoreline evolution for different grid size: Test domain 1: NX = 200, DX = 0.3 m (blue line); Test domain 2: NX = 120 (red line), DX = 0.5 m; Test domain 3: NX = 86, DX = 0.7 (yellow line)

Simulation of the *Test domain 1* was performed by reducing the K_{GSb} calibration coefficient, from 0.24 (*Test domain 1a*) to 0.21 (*Test domain 1b*). The result is presented in Figure 7.51 and shows that reducing the GSb calibration coefficient the tombolo condition disappears; the result behind the detached breakwater resulted improved for $NX = 200$ and $DX = 0.3$.

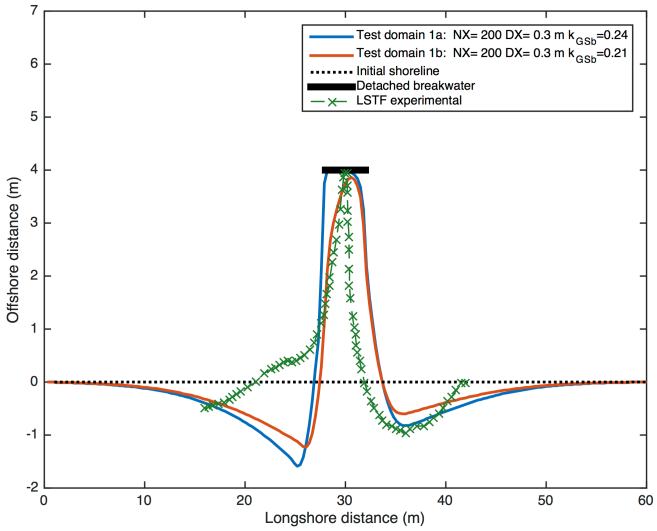

Figure 7.51 – Shoreline evolution for Test domain 1 with different calibration coefficient: K_{GSb} = 0.24 (blue line) and K_{GSb} = 0.20 (red line)

Simulation of the *Test domain 3* was performed by increasing the K_{GSb} calibration coefficient, from 0.24 (*Test domain 3a*) to 0.27 (*Test domain 3b*). The result presented in Figure 7.52 shows that increasing the GSb calibration coefficient, from 0.24 to 0.27, the salient reaches the detached breakwater, improving the result.

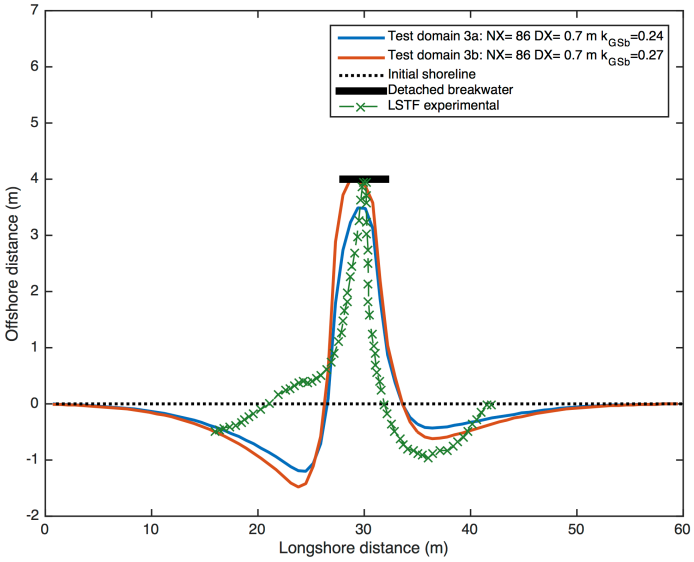

Figure 7.52 - Shoreline evolution for Test domain 3 with different calibration coefficient: K_{GSb} = 0.24 (blue line) and K_{GSb} = 0.27 (red line)

Table 7.9 shows the GSb model salient calculated for three values of calibration coefficient K_{GSb} = 0.21, 0.24. 0.27 varying the grid size parameters *NX* and *DX*.

Table 7.9 – Maximum salient y for K_{GSb} = 0.21, 0.24, 0.27 and NX = 86, 120, 200, 300 cells

NX	*DX (m)*	*K_{GSb}*	*DT (hrs.)*	*GSb Salient y (m)*	*Difference from the observed salient*
86	0.7	0.21		2.78	-30.50%
120	0.5	0.21		3.32	-17%
200	0.3	0.21		3.75	-6.25%
300	0.2	0.21		3.95	-1.25%
86	0.7	0.24		3.41	-14.75%
120	0.5	0.24	0.0005	3.95	-1.25%
200	0.3	0.24		4	0%
300	0.2	0.24		4	0%
86	0.7	0.27		4	0%
120	0.5	0.27		4	0%
200	0.3	0.27		4	0%
300	0.2	0.27		Nan	-

Figure 7.53 shows the shoreline evolution for the domains parameters *NX* = 86, 120, 200, 300 cells and *DX* = 0.7, 0.5, 0.3, 0.2 m respectively in case of: K_{GSb} = 0.21 (Figure 7.53a); K_{GSb} = 0.24 (Figure 7.53b); K_{GSb} = 0.27 (Figure 7.53c).

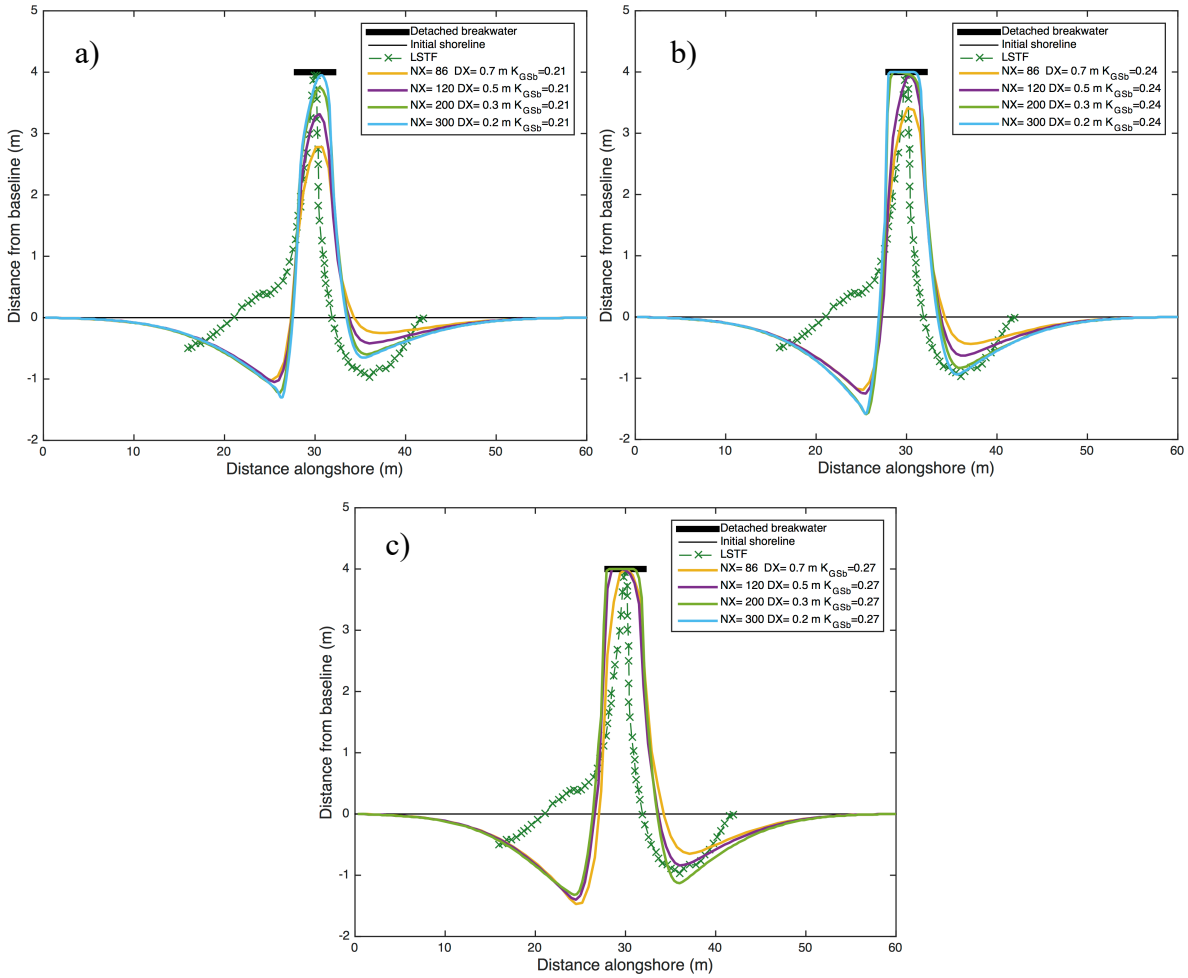

Figure 7.53 - Shoreline evolution with NX = 86, 120, 200, 300 cells and DX = 0.7, 0.5, 0.3, 0.2 m respectively in case of: a) K_{GSb} = 0.21 b) K_{GSb} = 0.24 ; c) K_{GSb} = 0.27

In order to have a domain with smaller cells than 0.2 m, it is necessary to decrease the calculation time step, *DT*, respecting the Courant relation (Courant et al., 1967). In GSb model the minimum value of *DT* is 0.000125 hrs.

The results obtained by the GSb simulations in case of a single detached breakwater, suggested a value of K_{GSb} between 0.21 and 0.24 when *DX* is in the range of 0.20 m and 0.30 m. The suggested value of K_{GSb} ranges between 0.24 and 0.27 when the model grid cell resolution *DX* is in the range of 0.30 m and 0.70 m. A summary of the suggested values of K_{GSb} is shown in Table 7.10.

Table 7.10 - Values of K_{GSb} suggested for detached breakwater

Case	*DX*	K_{GSb}
Detached breakwater	0.20 - 0.30	0.21 - 0.24
	0.30 - 0.70	0.24 - 0.27

7.4 Lab tests 2 - Ming and Chiew (2000) experiments

The model calibrated with the LSTF experiments was verified on laboratory tests performed by Ming and Chiew, (2000), that conducted 18 experiments to observe shoreline changes caused by the presence of a detached breakwater under the influence of pure wave action. The breakwater length, *B*, and its distance from the initial shoreline, *X*, were the two main investigated parameters. The study analysed the effect of these two factors on shoreline changes.

The observed results were compared with the calculated shoreline obtained setting the GSb calibration coefficient K_{GSb} as suggested in Section 7.3.1.1 and Table 7.10.

The GSb model inputs were set to reproduce all the experiments conducted by Ming and Chiew (2000) listed in Table 7.11.

Table 7.11 – Laboratory test conditions (Ming and Chiew, 2000)

Test	Model Setup				Waves			
	B (m)	X (m)	h_b (cm)	h_c (m)	H_o (cm)	T_o (s)	D (m)	T_d (h)
1	0.90	0.60	6.00	0.118	5.00	0.85	0.335	18
2	1.20	0.60	6.00	0.118	5.00	0.85	0.335	18
3	1.50	0.60	6.00	0.118	5.00	0.85	0.335	18
4	0.60	0.90	8.00	0.118	5.00	0.85	0.335	18
5	0.90	0.90	8.00	0.118	5.00	0.85	0.335	17
6	1.20	0.90	8.00	0.118	5.00	0.85	0.335	19
7	1.50	0.90	8.00	0.118	5.00	0.85	0.335	19
8	0.60	1.20	10.00	0.118	5.00	0.85	0.335	18
9	0.90	1.20	10.00	0.118	5.00	0.85	0.335	18
10	1.20	1.20	10.00	0.118	5.00	0.85	0.335	18
11	1.50	1.20	10.00	0.118	5.00	0.85	0.335	20
12	0.60	1.50	12.00	0.118	5.00	0.85	0.335	17
13	0.90	1.50	12.00	0.118	5.00	0.85	0.335	16
14	1.20	1.50	12.00	0.118	5.00	0.85	0.335	18
15	1.50	1.50	12.00	0.118	5.00	0.85	0.335	43
16	1.00	0.50	5.00	0.1596	5.00	1.15	0.37	21
17	1.00	1.40	11.00	0.1596	5.00	1.15	0.37	21
18	1.00	1.40	11.00	0.1915	6.00	1.15	0.37	21

Symbols in Table 7.11 are defined as follows: B = length of the breakwater; X = distance of the breakwater to the initial shoreline; h_b = water depth at the breakwater; h_c = closure depth (Hallermeier, 1978); H_o = deep water wave height; T_o = wave period; D = water depth in the wave basin, and T_d = test duration.

According to the physical model tests characteristics, the model grid was 6 m long with 30 cells total (model grid cell resolution DX = 0.2 m). A detached breakwater was positioned in the centre of the domain with the characteristics of the physical model (length of the breakwater, distance of the breakwater to the initial shoreline, water depth at the breakwater) proposed by Ming and Chiew (2000). GSb lateral boundaries were selected as pinned. The median grain size (D_{50}) was set equal to 0.25 mm.

As for the physical model tests, wave forcing applied to the GSb model was held constant during the simulation such that breaking wave heights measured during the experiment are listed in Table 7.11. The calibration parameter K_{GSb} was selected equal to 0.24, as suggested in Section 7.3.1.1 for the case with DX = 0.2 m.

Figure 7.54 shows the comparison between the observed and the calculated shoreline when the detached breakwater is a distance of 0.60 m form the initial shoreline. The duration of the simulations was 18 hours. The offshore wave conditions were held constant throughout the simulations (H_o = 0.05 m, T_o = 0.85 sec, ϑ = 0 deg).

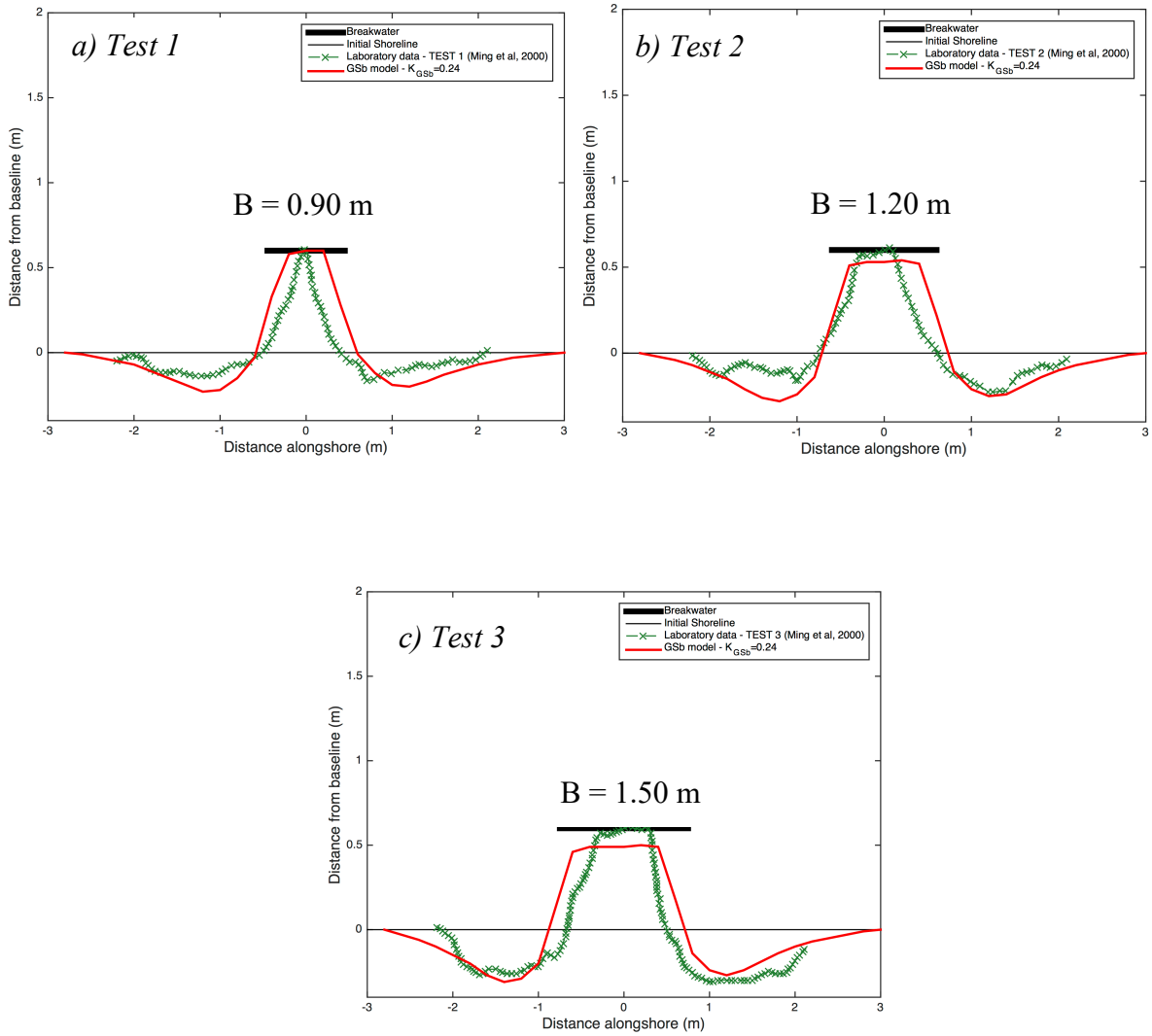

Figure 7.54 - Observed (green crosses) and calculated (red line) shoreline with detached breakwater at distance of X = 0.60 m from the initial shoreline and length of breakwater: a) B = 0.90 m (Test 1) ; b) B = 1.20 m (Test 2); c) B = 1.50 m (Test 3)

Figure 7.55 shows the comparison between the observed and the calculated shoreline when the detached breakwater is at a distance of 0.90 m from the initial shoreline. The duration of the simulations was 18 hours for *Test 4*; 17 hours for *Test 5*; 19 hours for *Test 6* and *Test 7*. The offshore wave conditions were held constant throughout the simulations ($H_o = 0.05$ m, $T_o = 0.85$ sec, $\vartheta = 0$ deg).

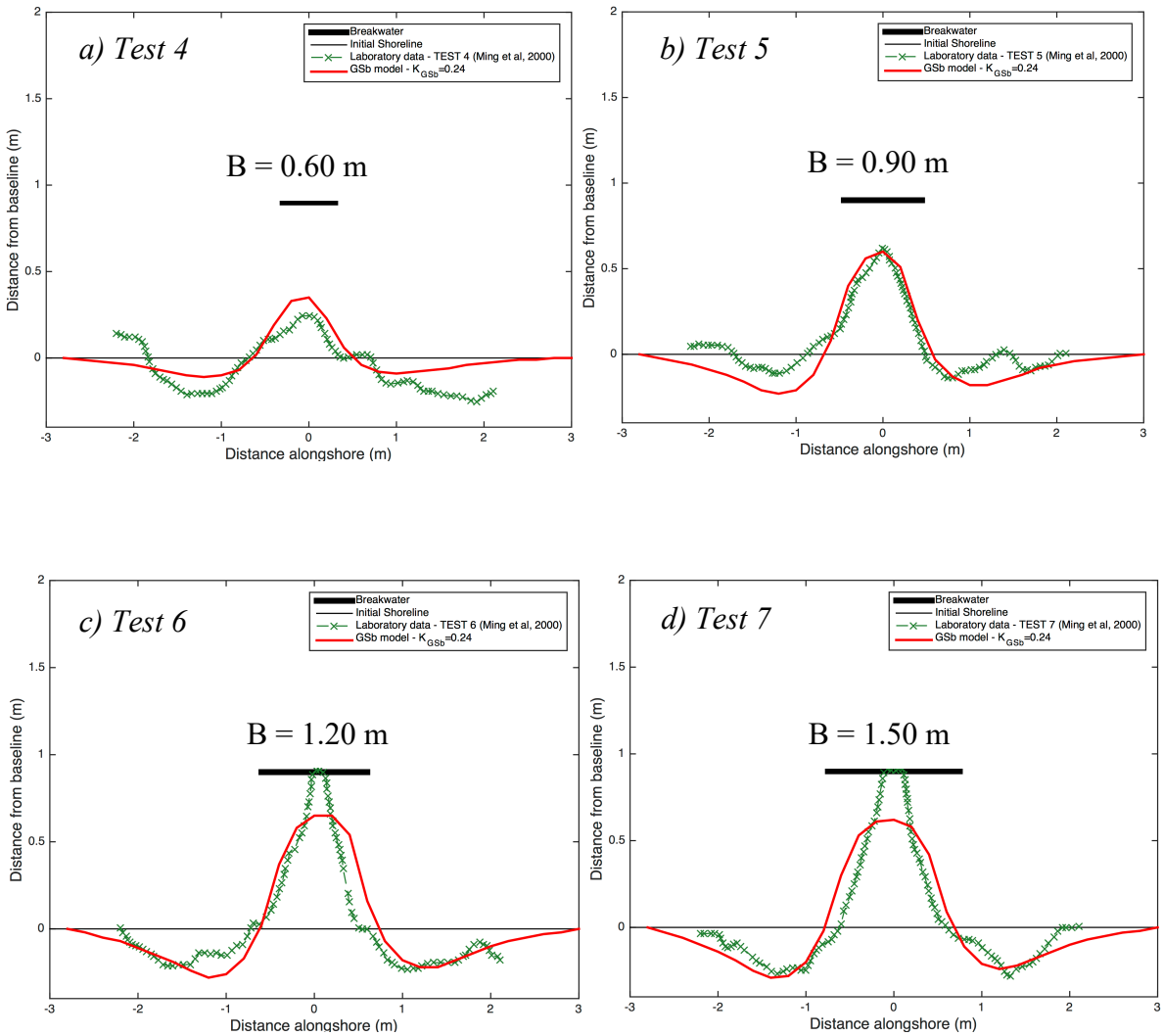

Figure 7.55 - Observed (green crosses) and calculated (red line) shoreline with detached breakwater at distance of X = 0.90 m from the initial shoreline and length of breakwater: a) B = 0.60 m (Test 4); b) B = 0.90 m (Test 5) ; c) B = 1.20 m (Test 6); d) B = 1.50 m (Test 7)

Figure 7.56 shows the comparison between the observed and the calculated shoreline when the detached breakwater is at a distance of 1.20 m from the initial shoreline. The duration of the simulations was 18 hours for *Test 8*, *Test 9*, *Test 10*; 20 hours for *Test 11*. The offshore wave conditions were held constant throughout the simulations (H_o = 0.05 m, T_o = 0.85 sec, ϑ = 0 deg).

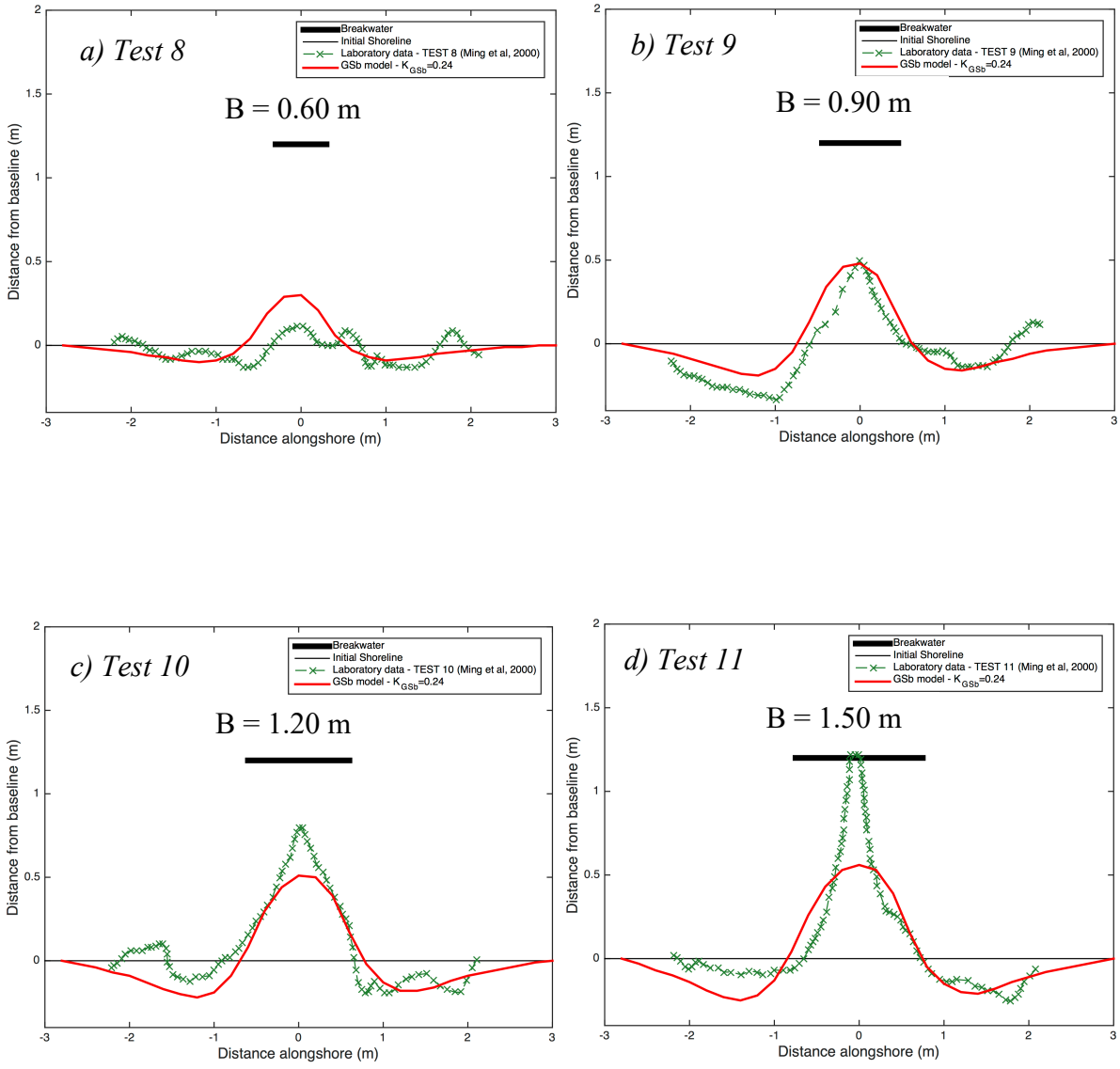

Figure 7.56 - Observed (green crosses) and calculated (red line) shoreline with detached breakwater at distance of X = 1.20 m from the initial shoreline and length of breakwater: a) B = 0.60 m (Test 8); b) B = 0.90 m (Test 9) ; c) B = 1.20 m (Test 10); d) B = 1.50 m (Test 11).

Figure 7.57 shows the comparison between the observed and the calculated shoreline when the detached breakwater is at a distance of 1.50 m from the initial shoreline. The duration of the simulations was 17 hours for *Test 12*; 16 hours for *Test 13*; 18 hours for *Test 14*; 43 hours for *Test 15*. The offshore wave conditions were held constant throughout the simulations (H_o = 0.05 m, T_o = 0.85 sec, ϑ = 0 deg).

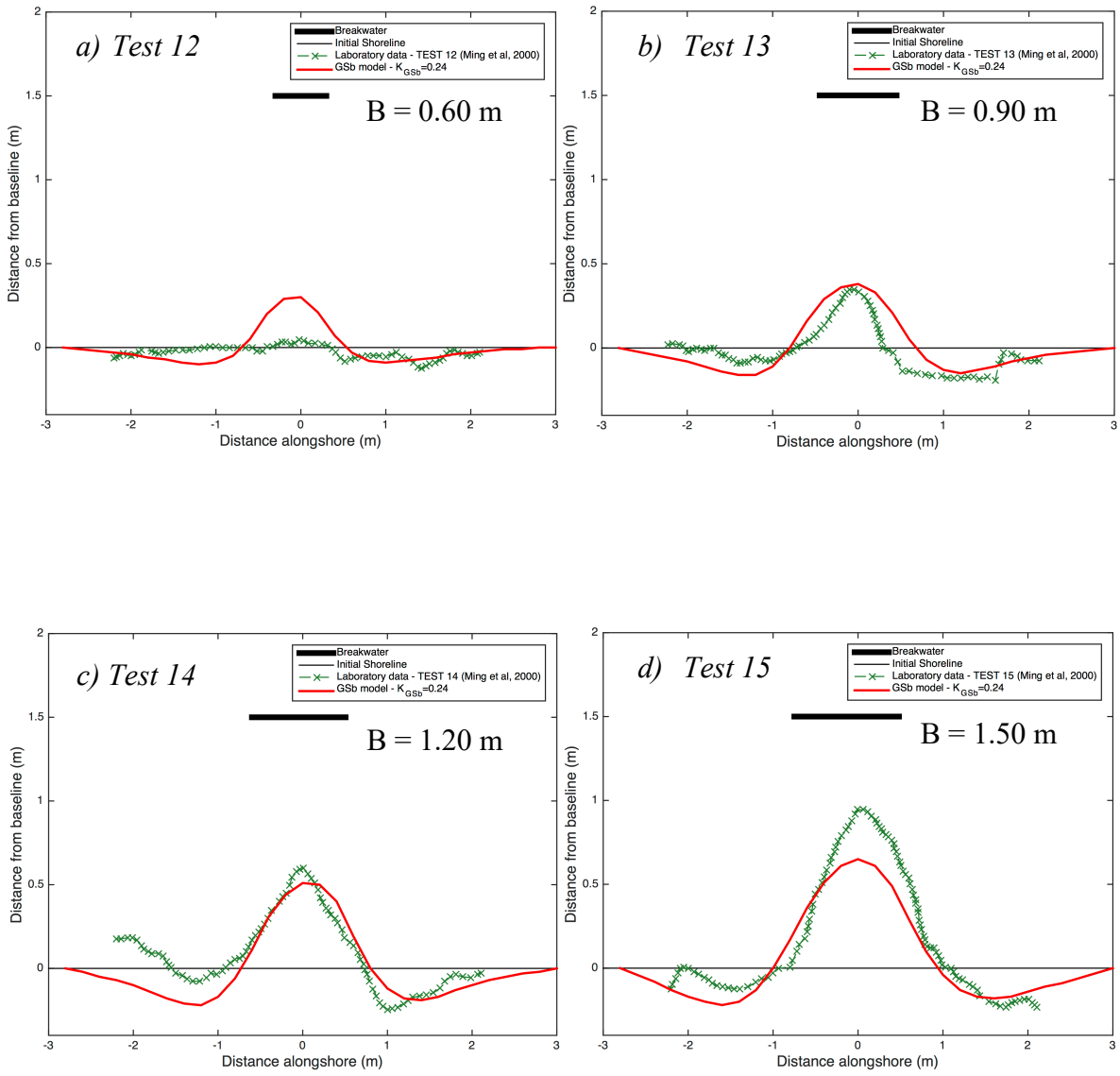

Figure 7.57 - Observed (green crosses) and calculated (red line) shoreline with detached breakwater at distance of X = 1.50 m from the initial shoreline and length of breakwater: a) B = 0.60 m (Test 12); b) B = 0.90 m (Test 13) ; c) B = 1.20 m (Test 14); d) B = 1.50 m (Test 15)

Figure 7.58 shows the comparison between the observed salient projection (green point) and the calculated shoreline (red line) when the detached breakwater is at a distance of 0.50 m from the initial shoreline (*Test 16*). The duration of the simulations was 21 hours. The offshore wave conditions were held constant throughout the simulations (H_o = 0.05 m, T_o = 1.15 sec, ϑ = 0 deg).

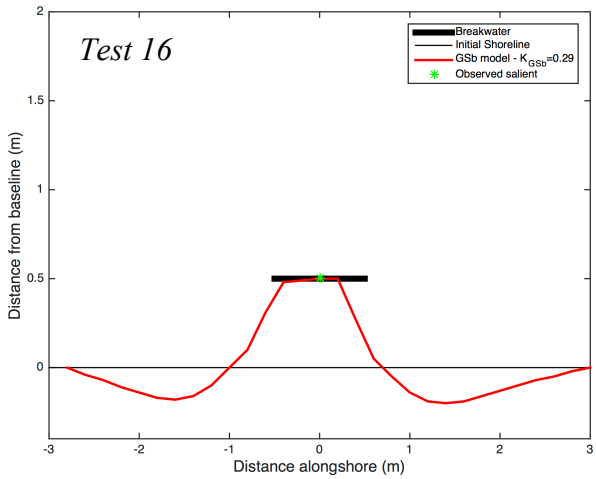

Figure 7.58 – Observed salient projection (green point) and calculated shoreline (red line) with detached breakwater at distance of X = 0.50 m from the initial shoreline and length of breakwater B = 1.00 m with Ho = 0.05 m and To = 1.15 s

Figure 7.59 shows the comparison between the observed salient projection (green point) and the calculated shoreline (red line) when the detached breakwater is at a distance of 1.40 m from the initial shoreline (*Test 17*, *Test 18*). The duration of the simulations was 21 hours. The offshore wave conditions were held constant throughout the simulations, H_o = 0.05 m and T_o = 1.15 sec for the *Test 17* and H_o = 0.06 m, T_o = 1.15 sec for the *Test 18*.

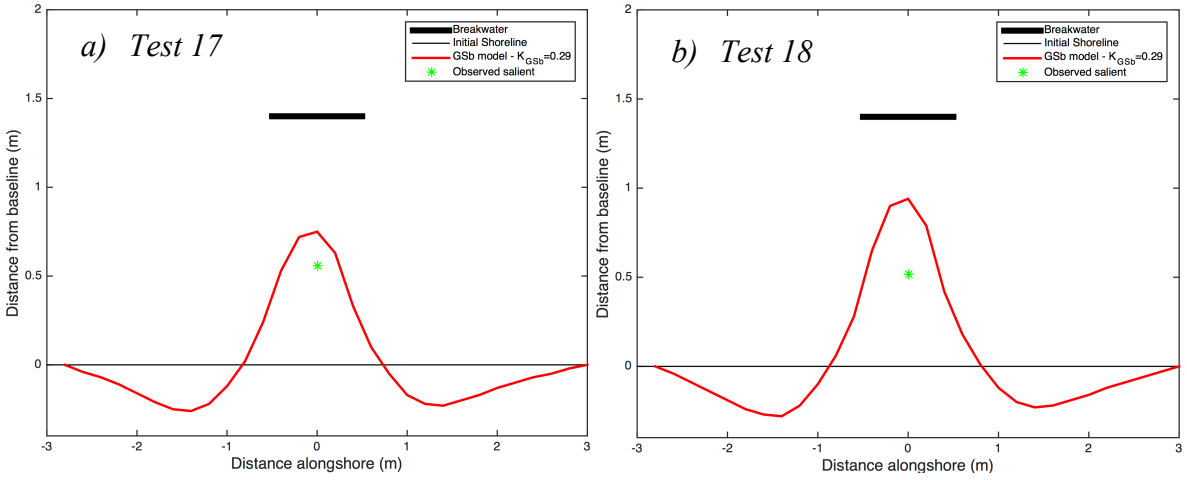

Figure 7.59 - Observed salient projection (green point) and calculated shoreline (red line) with detached breakwater at distance of X = 1.40 m from the initial shoreline and length of breakwater B = 1.00 m, To = 1.15 s and: a) Ho = 0.05 m (Test 17); b) Ho = 0.06 m (Test 18)

Figure 7.60 shows the results of the GSb simulations in terms of salient projection compared with the experimental observations and the laboratory conditions of the tests.

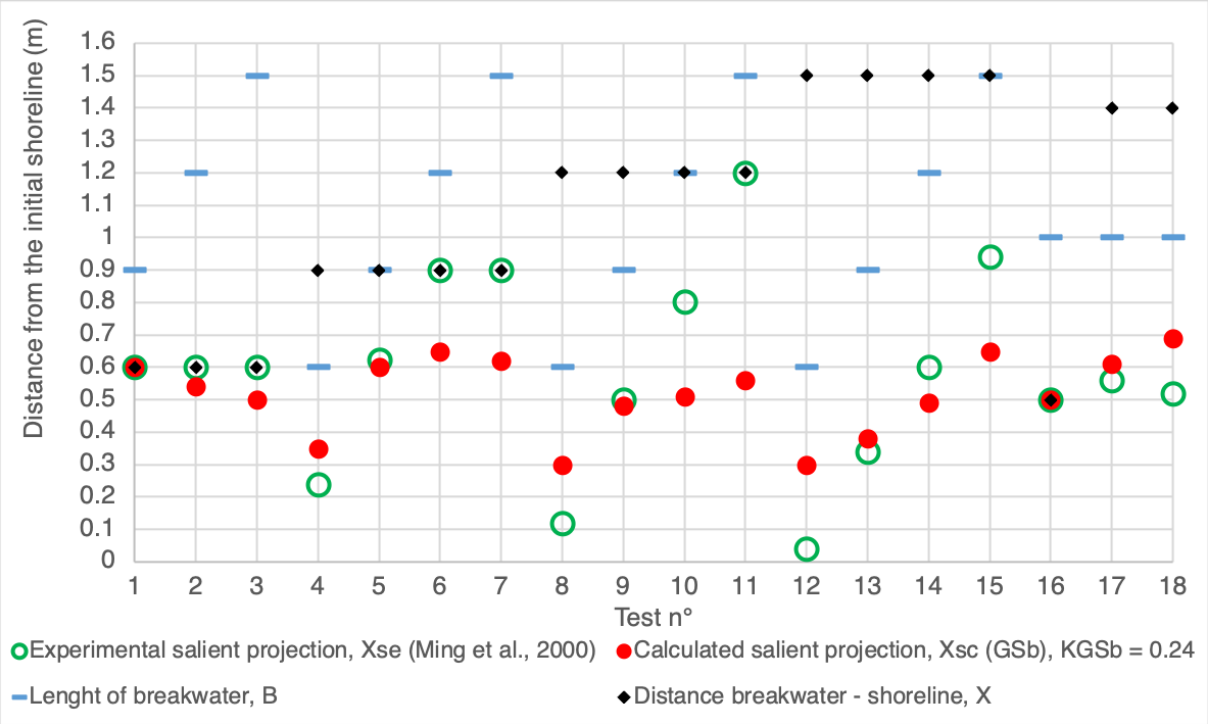

Figure 7.60 – Summary of the test conditions and results for salient projections calculated with K_{GSb} = 0.24

GSb model showed a good agreement between observed and calculated salient projections; it was able to reproduce the accretion tendency of the shoreline except for Test 11 where the numerical model strongly underestimated the observed salient projection and for Test 12 where the numerical model has overestimated the shoreline advance.

Verification of the calculated shoreline obtained with the GSb model for a calibration parameter K_{GSb} = 0.24 was performed; GSb was used to simulate the 18 experimental tests using 2 different calibration coefficients, K_{GSb} = 0.27, 0.29, and comparing the results in terms of salient evolution and Root Mean Square Error (RMSE).

Table 7.12 describes the salient observed, *Xse*, and calculated, *Xsc*, for K_{GSb} = 0.24, 0.27, 0.29 and the percentage variation of the calculated salient projection with respect the observed one.

Table 7.12 – Salient observed and calculated for K_{GSb} = 0.24, 0.27, 0.29 and percentage variation of the calculated salient projection with respect the observed salient one

Test	Xse(Exp) (m)	Xsc (GSb) (K_{GSb}= 0.24) (m)	Xsc (GSb) (K_{GSb}= 0.27) (m)	Xsc (GSb) (K_{GSb}= 0.29) (m)	Salient Per. Var. (K_{GSb}= 0.24) (%)	Salient Per. Var. (K_{GSb}= 0.27) (%)	Salient Per. Var. (K_{GSb}= 0.29) (%)
1	0.600	0.600	0.600	0.600	0%	0%	0%
2	0.600	0.540	0.600	0.600	-10%	0%	0%
3	0.600	0.500	0.550	0.580	-17%	-8%	-3%
4	0.240	0.350	0.400	0.430	46%	67%	79%
5	0.624	0.600	0.700	0.770	-4%	12%	23%
6	0.900	0.650	0.720	0.780	-28%	-20%	-13%
7	0.900	0.620	0.670	0.700	-31%	-26%	-22%
8	0.120	0.300	0.340	0.360	150%	183%	200%
9	0.500	0.480	0.550	0.600	-4%	10%	20%
10	0.804	0.510	0.580	0.630	-37%	-28%	-22%
11	1.200	0.560	0.640	0.690	-53%	-47%	-43%
12	0.040	0.300	0.330	0.350	650%	725%	775%
13	0.340	0.380	0.420	0.450	12%	24%	32%
14	0.600	0.490	0.560	0.610	-18%	-7%	2%
15	0.940	0.650	0.750	0.820	-31%	-20%	-13%
16	0.500	0.500	0.500	0.500	0%	0%	0%
17	0.560	0.610	0.690	0.750	9%	23%	34%
18	0.520	0.690	0.870	0.940	33%	67%	81%

Figure 7.61 shows the observed salient projection and the calculated salient projection for K_{GSb} = 0.24 (red dots), K_{GSb} = 0.27 (yellow dots), K_{GSb} = 0.29 (blue dots).

Figure 7.61 – Observed and calculated salient projections for K_{GSb} = 0.24 (red dots), K_{GSb} = 0.27 (yellow dots), K_{GSb} = 0.29 (blue dots)

The discussion of the results, in terms of salient projection, shows that the numerical model calibrated with K_{GSb} = 0.24 is able to simulate the shoreline evolution when the length of the breakwater B is 0.60 m and 0.90 m. However, when B = 1.20 m and 1.50 m, the calculated projection position improves if K_{GSb} = 0.29

In order to evaluate the overall quality of the solution, the RMSE was calculated comparing the observed and calculated shorelines with K_{GSb} = 0.24 (red dots), K_{GSb} = 0.27 (yellow dots), K_{GSb} = 0.29 (blue dots) (Figure 7.62). The RMSE for K_{GSb} = 0.24 presented the lowest RMSE, showing a better agreement between the calculated and the observed shoreline positions, except for the *Test 15* where the best calculated solution corresponds to a value of K_{GSb} = 0.29 (Table 7.13).

Table 7.13 - RMSE calculated on the base of observed and calculated results obtained using K_{GSb} = 0.24, 0.27, 0.29

Test	*RMSE (K_{GSb}= 0.24)*	*RMSE (K_{GSb}= 0.27)*	*RMSE (K_{GSb}= 0.29)*
1	0.4646	0.5151	0.5325
2	0.4503	0.5651	0.6165
3	0.4931	0.5094	0.5441
4	0.4332	0.4444	0.4578
5	0.4565	0.6627	0.8169
6	0.3652	0.4799	0.5802
7	0.4225	0.5281	0.6491
8	0.3874	0.4241	0.4503
9	0.4829	0.5448	0.5918
10	0.4795	0.4777	0.5130
11	0.5459	0.6003	0.6536
12	0.379	0.4303	0.4593
13	0.4406	0.4923	0.5481
14	0.4695	0.5314	0.5964
15	0.8044	0.7888	0.7709
16	-	-	-
17	-	-	-
18	-	-	-

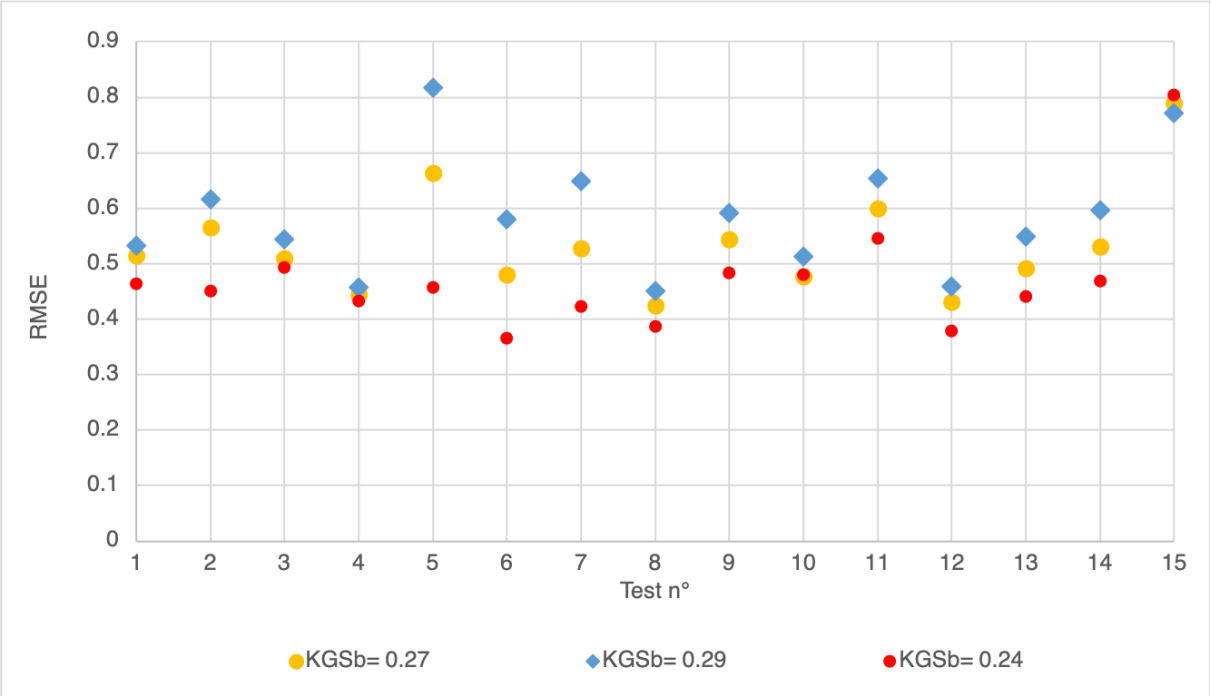

Figure 7.62 – RMSE calculated comparing the observed and calculated results obtained using K_{GSb} = 0.24, 0.27, 0.29

8 SUMMARY WITH CONCLUSIONS

Sediment transport is one of the most central topics in the field of coastal engineering because it is the primary process that drives the beach morphodynamics. Urbanisation in the coastal area brings to an alteration of the natural equilibrium of the coast. The understanding of the sediment processes and the evaluation of the structure's impact on the beach morphodynamics are complicated due to the difficulties and uncertainties of the interaction between wind, waves, currents, tides and coastal structures. Over recent decades, many efforts have been made to find robust methods for predicting coastline evolution and its interaction with the coastal structures. This requires a rigorous understanding of the key coastal processes that drive sediment transport. Once this understanding is achieved a method for predicting morphological evolution is required. In this context, numerical modelling plays an important role. To date, the development and use of numerical models on sandy beaches (e.g. GENESIS) have received the majority of the attention. The number of numerical simulations performed for the case of sandy beaches is significant, in contrast with the numerical works regarding gravel cobbles and mixed beaches with some notable exceptions (McCall et al., 2015; Polidoro et al., 2018).

Based on the assumption of the one-line theory, a novel morphodynamic model, named General Shoreline beach (GSb), is proposed. GSb can be used to simulate shoreline change in the presence of coastal structures such as groynes, jetties, detached breakwaters, seawalls, beach fills. The longshore sediment transport rate is estimates by means of a general formula/procedure proposed in literature (Tomasicchio et al., 1994; Lamberti and Tomasicchio, 1997; Tomasicchio et al., 2013; Tomasicchio et al. 2015), combining an energy flux approach with an empirical/statistical relationship between the wave-induced forcing and the number of moving sediment particles. Without any calibration, the general formula/procedure has been proved to be an engineering tool suitable for a large range of conditions, from sandy beaches till reshaping breakwaters.

A sensitivity analysis, where GSb was used for different configurations and varying the input parameters, has been performed, allowing to highlight the robustness of the proposed model. The coastline change has been evaluated numerically for a straight shoreline in presence of single groyne, single detached-breakwater, multiple groynes, and multiple detached-breakwaters. Simulations have been performed varying the wave angle, the boundary

conditions, the grain size composing the beach, the permeability of the structure, and the calibration coefficient.

The GSb model presents one calibration coefficient solely, K_{GSb}, which does not depend on the grain size diameter, but depends on the alongshore gradient in breaking wave height.

The GSb has been calibrated and verified against two different observed field data.

The first case regarded a sandy beach, performed with observations from a field experiment conducted in 2015 during intense sea breeze conditions on a micro-tidal dominated beach located in Sisal, Yucatán, México (Medellin et al., 2018). The mean wave conditions in the study area are characterised by high-angle and low-energy sea waves that drive a significant westward sediment transport. A temporary impermeable groin 14.4 m long has been deployed for 24-hours. Beach morphology evolution, winds, offshore waves, and surf zone hydrodynamics have been measured concurrently during the structure deployment and after its removal. The observed data showed that a temporary impermeable groyne induces significant beach morphology changes in the 24-hours period. It has been observed a shoreline position advance/retreat of 6 m/-3 m, associated with a volume change of +70 m^3/-35 m^3 in the up-drfit/down-drift side of the structure location. Furthermore, beach monitoring conducted after structure removal, under similar wave conditions, showed that the beach requires 140 hours to recover (i.e., beach resilience). The observed data have been adopted to calibrate and verify the predictive accuracy of the GSb model before (calibration) and after (verification) the groin removal. The GSb was able to predict both the groin effect on the shoreline position and the subsequent shoreline recovery after the structure removal.

The second case study regarded a mixed beach subjected to a field experiment conducted in 2007 at Milford-on-Sea, Hampshire, UK (Martin-Grandes et al., 2009). A temporary impermeable groyne, 46 m long has been deployed on the mixed beach as a barrier to the longshore sediment transport. Beach cross-shore profiles have been measured daily at 30 transects over two months using a Differential Global Positioning System (DGPS). The nearshore hydrodynamic conditions were measured by collecting wave and tidal data concurrently over the deployment of the temporary groyne. Wave breaking on the inner of three bars drove the alongshore current over the mixed beach face. Consequently, the beach morphology reflected perturbation of this current by the impermeable groyne, with a shoreline accretion that reaches 3.13 m at the up-drift side of the groyne after 45 days from its deployment. The observed data have been adopted to verify the accuracy of the GSb model to

predict the shoreline evolution for a mixed beach at different time steps after the groyne deployment. GSb model has been able to predict the beach evolution, except during extreme storm events. Numerical simulations using 5 different grid sizes have been done in order to evaluate the influence of the computational domain on the numerical solution. The results obtained adopting a domain 180 m long have shown a better overall solution. The ARGUS shorelines have been used to perform a verification. GSb model has been able to evaluate a 740 m long coastline evolution adopting the same calibration coefficient of the case of DGPS shorelines. A further verification was performed using the propagated wave data obtained by SWAN numerical model. The comparison between numerical and observed data resulted favourably.

Both field cases (Sisal and Milford-on-Sea) present short-term observations of the shoreline (each hour at Sisal and each day at Milford-on-Sea). Comparisons between observed and calculated shorelines has shown that the GSb is capable to simulate beach morphodynamics for a short-term event. This is a major capability of GSb respect the other available one-line models.

The GSb calibration and verification for detached breakwaters with various wave conditions has been performed comparing the calculated shoreline with results of two laboratory experiments. A calibration was performed reproducing numerically an experiment reported by Gravens and Wang (2007). The capability of the GSb model to calculate the salient evolution and tombolo formation behind a detached breakwater was evaluated. A verification for a detached breakwater has been performed by the comparison with 18 laboratory experiments performed by Ming and Chiew, (2000). The results showed a good agreement between the measured shoreline and the calculated shoreline.

As said, a calibration and verification procedure has been conducted for different field and laboratory data sets referring to simple groyne and detached breakwater, with beaches composed of sand and mixed material (sand and gravel), respectively. The calibration procedure gained the optimal values of K_{GSb} valid for (i) different types of not cohesive grains (i.e. sandy, gravel and mixed beaches); (ii) a wide range of irregular (field site) and regular (laboratory) wave conditions; (iii) different types of coastal structures (i.e. groynes, detached breakwaters). Results for K_{GSb} values are reported in Table 8.1.

Table 8.1 -Suggested K_{GSb} values

Beach	Structure	K_{GSb}
Sandy	Single groyne	0.01
Mixed (Sand and Gravel)	Single groyne	0.10
Sandy	Single detached breakwater	0.24

The result is that the modeller, for the considered cases in the present thesis, can select the more appropriate value of K_{GSb} to be considered for a specific case to be modelled.

Finally, within a project for the Environmental Agency of Abu Dhabi, the GSb model has been used as an engineering tool to forecast the performance of a nourishment intervention at Saadiyat beach located in Abu Dhabi (UAE); results are reported in Appendix A.

A demo version of the GSb model, for Mac and Windows systems, has been released for the scientific community and is available at www.scacr.eu.

APPENDIX A: GSb model as a design tool

The GSb model was used to predict the shoreline evolution of a sandy beach located at Saadiyat island, of the Abu Dhabi city in the United Arab Emirates. The main objective of the present study was to evaluate the nourishment performance for different scenarios of coastal defence by the use of GSb model. The results were published in Hamza et al. (2019).

Saadiyat beach is situated in Saadiyat island, a large low-lying 27 km^2 island of the Arabian Gulf (also named Persian Gulf) within the Municipality of Abu Dhabi of the United Arab Emirates (Figure A.1). Saadiyat island comprises a SW–NE oriented, 9 km long natural sandy beach, Saadiyat beach, of moderate to flat slope (Figure A.2). The shape and orientation of the beach were modified several times for the development of the Cultural District of Saadiyat island.

Where the urban plan requires the realization of sustainable coastal protection structures, different design scenarios are proposed by the Tourism Development Investment Company (TDIC), described in the relative TDIC master plan. According to the last development plan as approved by TDIC, the intervention for Saadiyat beach involved a large sand nourishment intervention and the construction of four (4) groynes located in a position decided by TDIC.

Figure A.1 - Left: view of the Arabic Gulf area showing the position of Abu Dhabi; Right: aerial view Saadiyat island, in the Abu Dhabi Municipality; the red rectangle indicates the position of the beach study area. (Hamza et al., 2019)

Figure A.2 - Saadiyat beach (Google Images, 2019)

In order to quantify the efficacy for each of the design scenarios proposed by TDIC, the morphodynamics response of the shoreline to the various coastal defence scenarios of the TDIC development plan was required (Goda, 2010; Tomasicchio et al., 2013; USACE, 1984; Van der Meer, 1988).

The observed data collected by in-situ monitoring instruments, survey campaigns, satellite imagery served as a basis for the numerical model simulations of the wave conditions and of the morphological changes in the natural shape of the coastline under the influence of the planned interventions. The outcomes of the performed numerical simulations allowed the identification of the more environmentally sustainable scenario for Saadiyat beach.

The present study focused on the western area of Saadiyat beach, a 2 km long beach. The study area is characterised by medium sand with the median grain size D_{50} = 0.26 mm and the sorting parameter D_{15}/D_{85}= 2.44 where: D_{15} (transition layer) is the 15th percentile particle size in the transition layer material, meaning that 15% of the sand is smaller than D_{15} mm, and D_{85} (filter media) is the 85th percentile particle size in the filter media.

In vicinity of the study area, the Abu Dhabi Municipality (ADM) installed two Argonaut-XR ADCP (Acoustic Doppler Current Profiler) to observe the atmospheric and oceanographic conditions (water level, significant wave height, peak wave period, water temperature, and wind speed and direction). The coordinates of the positions of the two instruments and the relative water depth are reported in Table A.1. The data from instrument "04" presented a very high percentage of data gaps, and they were not analysed. The recorded data from instrument "03", indicated as *ADMins* in the following, span the period from June 2015 to January 2018 (included), with a time resolution of 10 min and 30 min for the atmospheric and oceanographic variables, respectively (Hamza et al., 2018). Figure A.3 shows the location of the *ADMins*. In addition, Figure A.3 shows also the grid node of the NOAA offshore wave data (coordinates 25°N and 54°E, 16 m water depth) used to calculate the closure depth.

The NOAA National Centers for Environmental Prediction (NCEP) developed the Climate Forecast System (CFS), a fully coupled model representing the interaction between the Earth's atmosphere, oceans, land, and sea ice. A reanalysis of the sea and atmosphere state for the period of 1979–2009 was conducted, resulting in the CFS Reanalysis (CFSR) dataset (Saha et al., 2010). The vertical discretization of the atmosphere consists of 64 layers. The temporal resolution for the atmospheric variables is 3 h. Using the CFSR dataset, the NOAA Marine Modeling and Analysis Branch (MMAB) has produced a wave hindcast for the same period. The wave hindcast dataset was generated using the WAVEWATCH III (WW3) model (v3.14) (Tolman 1997, 2009), and it is suitable for use in climate studies. The wave model suite consists of global and regional nested grids. The rectilinear grids were developed using ETOPO-1 bathymetry (Amante and Eakins, 2009) together with v1.10 of the Global Self-consistent Hierarchical High-resolution Shoreline (GSHHS) database. The spatial resolution of the considered data is 1/6°, which corresponds to roughly 20 km. The North West Indian Ocean computational grid, adopted in the considered data, extends in longitude from 30°E to 70°E (with 241 grid nodes) and in latitude from 20°S to 31°N (307 grid nodes). The NOAA datasets (both wind and waves) are freely available.

Figure A.3 - Location of ADMins, and NOAA nearshore and offshore grid points for the wind/wave model data

Table A.1 - Coordinates of the positions of the two instruments installed by ADM and the relative water depth

Instrument	Longitude (E)	Latitude (N)	Water depth (m)
03 (*ADMins*)	54°24'29.52"	24°34'17.04"	6
04	54°16'39.72"	24°44'31.56"	18

To model the longshore sediment transport with the GSb numerical model, the 2 km long analysed shoreline was divided in three cells and 6 sectors. The cells are indicated as the West cell, the VVIP cell, in the centre, and St. Regis cell at the eastern boundary of the beach. The sectors divide the West cell, the St.Regis cell and the area between groynes 3 and 4 each one in half and they were used as a reference for the computation of the maximum accretion/erosion areas along the beach. Figure A.4 shows the adopted initial design scenario, the cells and the reference sectors.

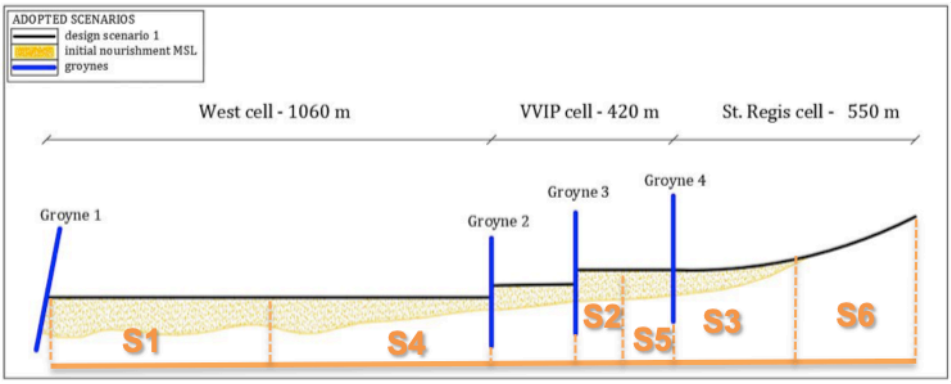

Figure A.4 - Schematic initial design scenario and reference sectors for the computation of the maximum accretion/erosion along the beach (Hamza et al. 2019)

The actual adopted solution by the contracting company, involves the construction of 4 groynes: groyne 1 is 287 m long and reaches water depth 2.5 m; and groynes 2, 3 and 4 are respectively 230 m, 263 m and 287 m long and reach water depth 2.6 m, 3.3 m and 3.1 m, respectively. The intervention comprises a large initial nourishment to create an area suitable for human beach recreational facilities and to increase the longevity of the beach. The sand will be taken from stockpiles in the south of Saadiyat island.

The GSb model computational domain was assumed equal to 2000 m. The model grid cell resolution, DX, was set equal to 40 m with a total number of cells, NX, equal to 50, whereas the model experiment was carried out adopting a calculation time step, DT, equal to 1 hour. GSb boundaries were selected as pinned beach, meaning that the shoreline does not change over time in the extremes of the domain (Frey et al., 2012).

The closure depth, h_c (Hallermeier, 1981) was calculated by the following equation:

$$h_c = 2.28\, H_s - 68.5\left(H_{s,0-12}^2 / g T_{s,0-12}^2\right) \quad \text{(A.1)}$$

where H_s is the significant wave height; $H_{s,0-12}$ is the significant wave height exceeded for 12 hours in one year and $T_{s,0-12}$ is the associated wave period; g is the gravitational acceleration. The closure depth was calculated by means of the NOAA offshore wave data (at the grid node with coordinates 25°N and 54°E, indicated in Figure A.3) at 16 m water depth. The calculated closure depth resulted equal to 3.6 m.

The estimation of the longshore sediment transport calibration coefficient, K_{GSb}, was obtained based on the available historical data. Two available Google Earth satellite images, relative to the years 2008 and 2009, were considered to set the initial/final shoreline position and to determine the optimal value for the calibration coefficient. Different values of K_{GSb}, ranging between 0.005 and 0.5 were adopted; for each of them, a measure of the error between the resulting calculated 2009 shoreline and the actual one was determined, with a similar procedure as in Sections 7.1 and 7.2 (Medellin et al., 2018). The minimum value of the error is related to the optimal value for the calibration coefficient K_{GSb}, which was assumed equal to 0.3. Figure A.5 shows the 2008 and 2009 satellite shorelines and the shoreline resulting from the GSb calibration procedure. The resulting Root Mean Square Difference (RMSD) value is also shown in Figure A.5, together with the distribution of the difference between the 2009 shoreline and the GSb model output (with K_{GSb} = 0.3) and the difference of the two 2008 and 2009 shorelines.

A period of one year was simulated, from 01/01/2008 to 31/12/2008, considering the wave time series resulting from (Hamza et al., 2018) with NOAA climate forecast system reanalyses dataset input winds (years 1979-2009) as input data (indicated as NOAA nearshore in Figure A.3).

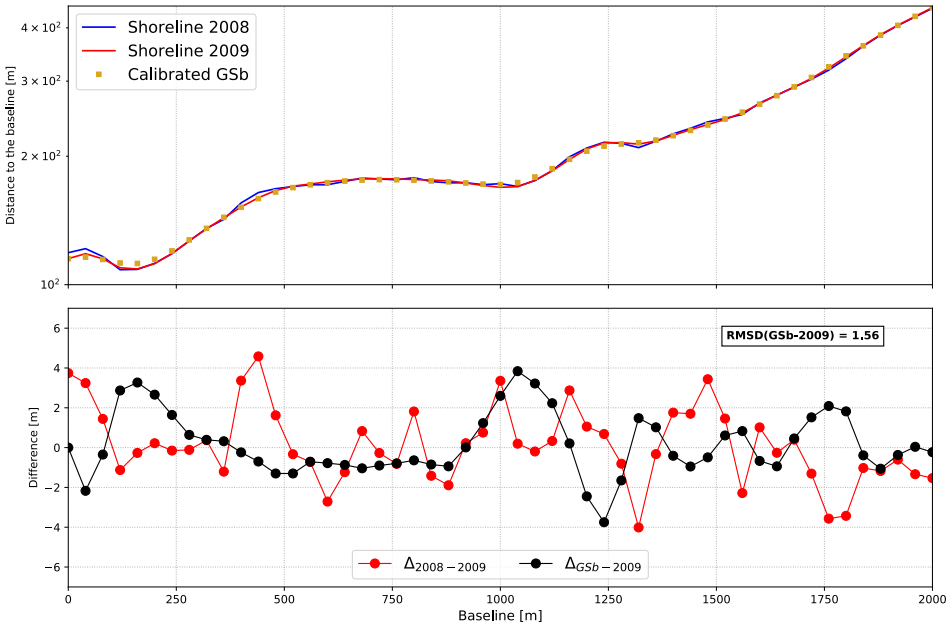

Figure A.5 - Top: historical shorelines adopted for the calibration of the GSb model; bottom: distribution of the difference between the 2009 shoreline and the GSb model output (with K_{GSb} = 0.3) and the difference of the two 2008 and 2009 Google Earth shorelines (Hamza et al. 2019)

GSb model was used to simulate some possible alternatives to verify the longevity of the beach and to propose a sustainable solution over the years. In particular, a different orientation of the as built shoreline and different volume of sand for the nourishment were tested. Figure A.6 shows the scenarios with different orientations of the initial design shoreline.

In the scenario 1, the initial alignment of the design shoreline was obtained from the nourishment of the entire stretch of coast. In particular, 600'000 m^3 are necessary for the West cell, 240'000 m^3 for the VVIP cell and 180'000 m^3 for the St. Regis cell.

In the scenario 2, a rotation of the shoreline alignment for the west cell and the VVIP cell, respectively 5° and 10° counter clockwise, was proposed, with a consequent increase in the sand volume, which was necessary for the initial nourishment (respectively 830'000 m^3 for the West cell and 270'000 m^3 for the VVIP cell).

The difference of scenario 3 with respect to scenario 2 consists in the fact that the shoreline alignment in the West cell is around the centreline.

In the scenario 4, the initial shoreline alignment is the same as in scenario 1 but a counter clockwise rotation of 5° is expected for the West cell, from the centre of the cell to the groyne 2, with a relative increase in the nourishment sand requirement, from 600'000 m^3 to 650'000 m^3.

In the scenario 5, the shoreline alignment is similar to scenario 1, but a clockwise rotation of 5° was imposed for the West cell, from the centre of the cell to the groyne 1. The volume of sand required is 50'000 m^3 more than the volume foreseen in the scenario 1.

A summary of the volumes of sand needed for the initial nourishment in the different scenarios is reported in Table A.2.

Table A.2 - Summary of the five design scenarios

Scenarios	Sand volume (x 10^3 m^3)		
	W cell	VVIP cell	St. Regis cell
1	600	240	180
2	830	270	180
3	600	270	180
4	650	240	180
5	650	270	180

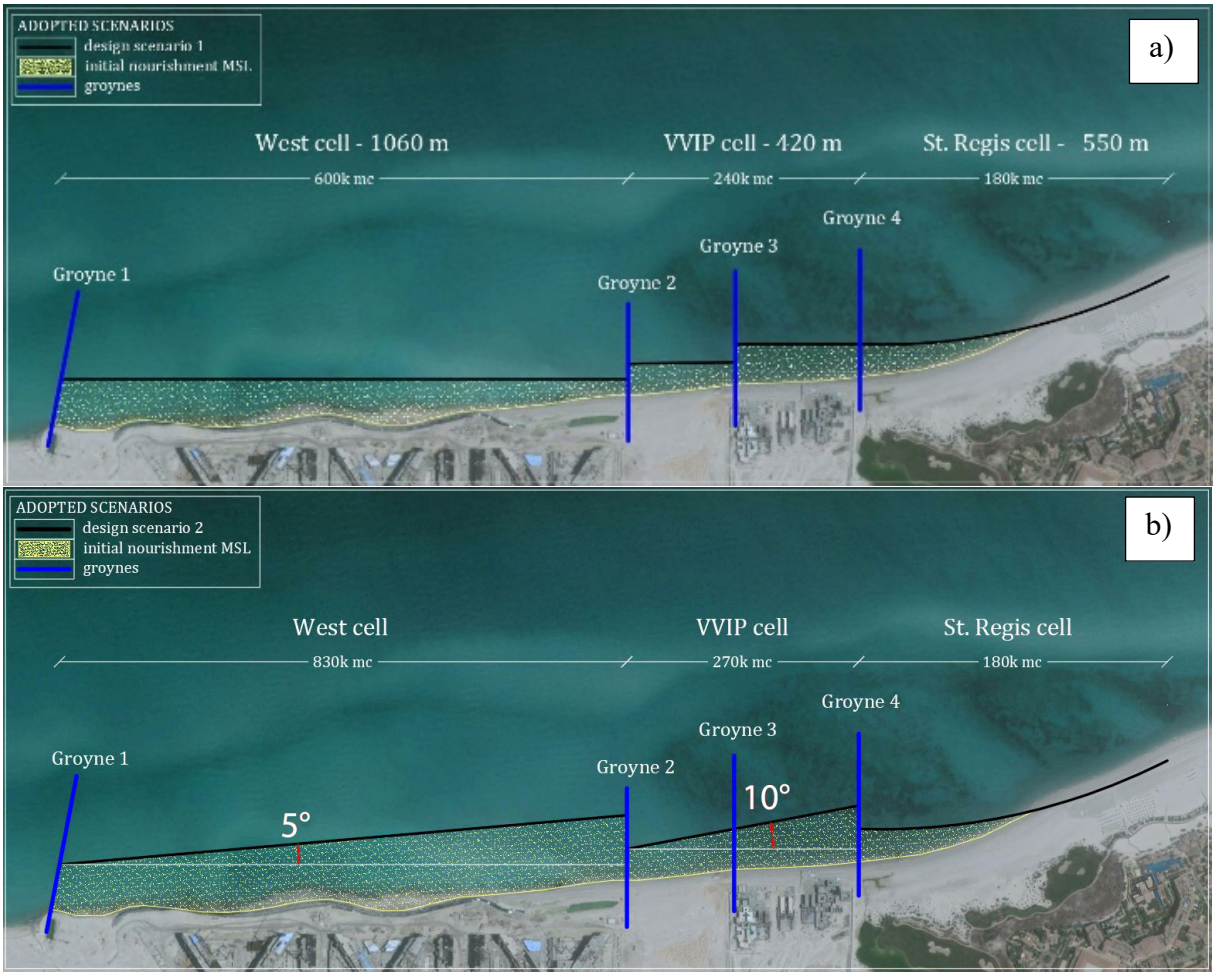

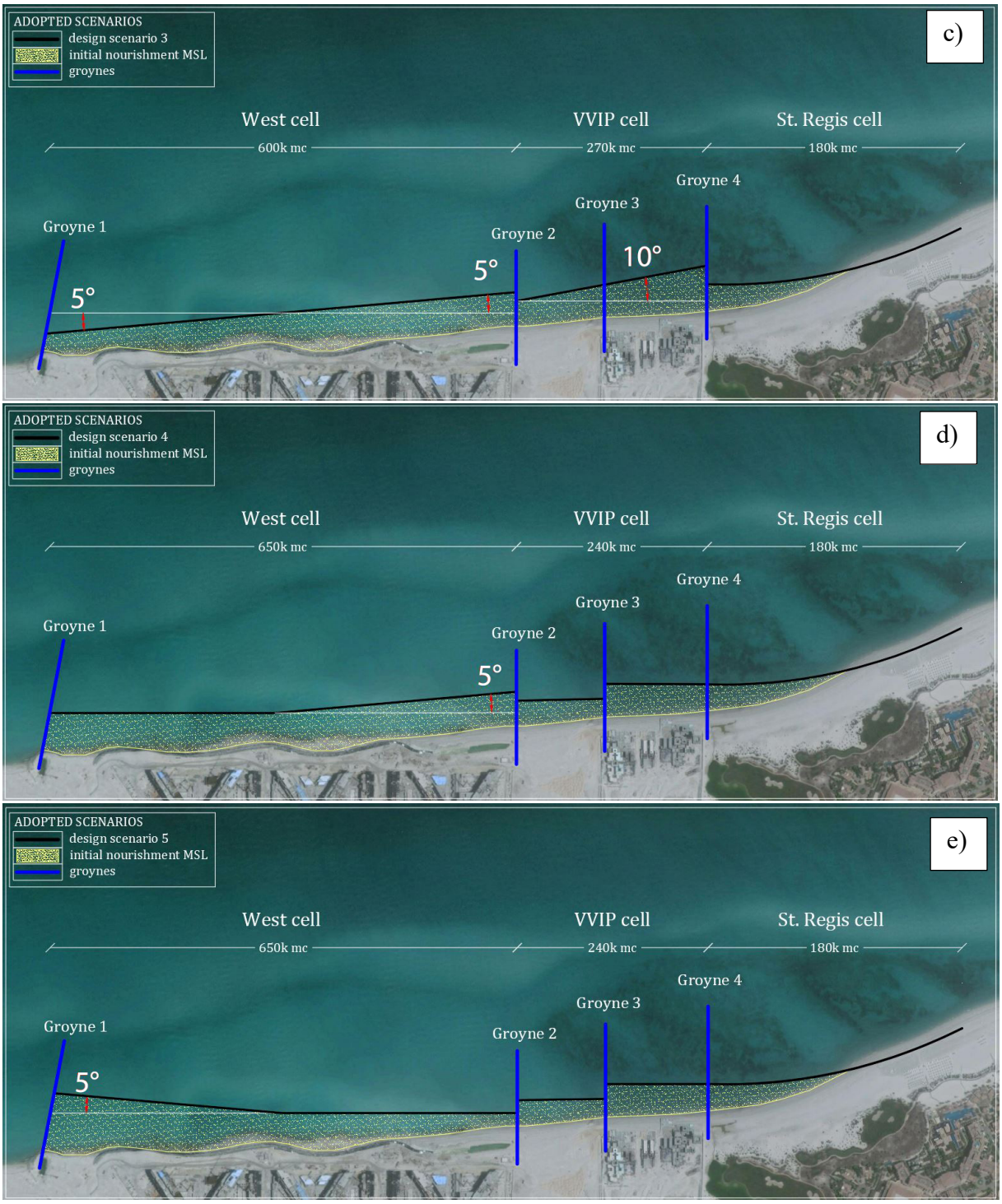

Figure A.6 - Schematic scenarios: a) Design scenario 1; b) Design scenario 2; c) Design scenario 3; d) Design scenario 4; e) Design scenario 5 (Hamza et al., 2019)

The shoreline evolution for each of the 5 considered scenarios was modelled with the GSb model. The numerical simulations were performed considering the evolution of the initial shoreline after 1 year, 2 and 5 years from the end of the intervention. The input of GSb model are described in Table A.3:

Table A.3 – GSb input for the simulation of Saadiyat coastline change

Model domain	Number of cells alongshore	NX = 50
	Dimension of cells	DX = 40 m
	Calculation time step	DT = 1.0 hrs
	Median grain size	D_{50} = 0.3 mm
	Closure depth	D_C = 3.6 m
Model forcing (at 50 m contours)	Wave height Wave period Wave angle	NOOA climate forecast system. Time series in Hamza et al. (2018)
Model parameters	Calibration parameter	K_{GSb} = 0.30
	Boundary conditions	Pinned
	Duration of simulation	t = 1 year, 2 and 5 years
Structures	4 groynes (Figure A.4)	
Initial shoreline	5 different scenarios (Figure 6a, 6b, 6c, 6d, 6e)	

Figure A.7 and Figure A.8 show a comparison between the results for, respectively, the evolution in 1 year and in 5 years, in terms of maximum accretion/recession.

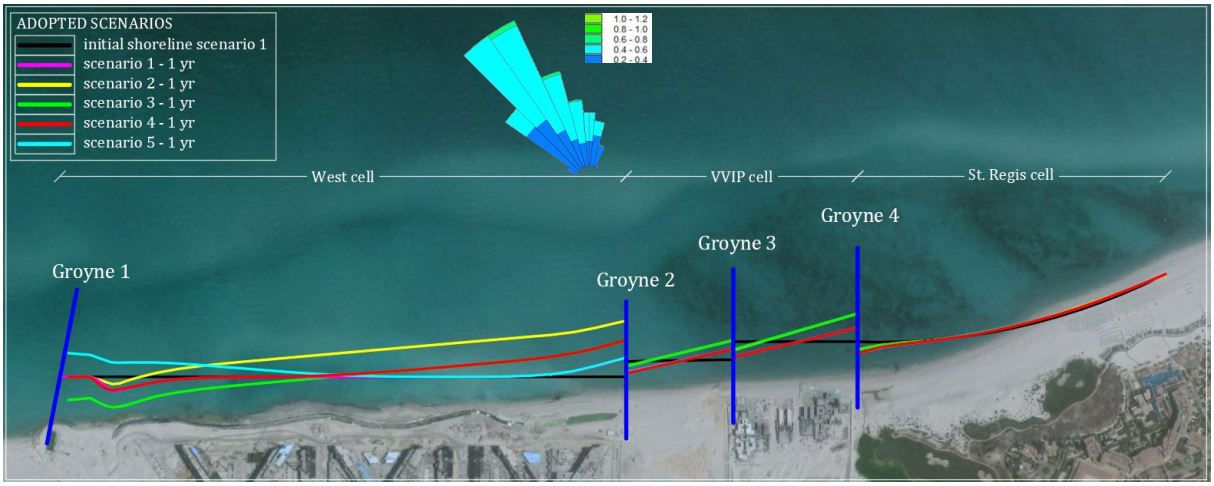

Figure A.7 - Evolution of the initial shoreline after 1 year, for the different considered the scenarios simulated (Hamza et al. 2019)

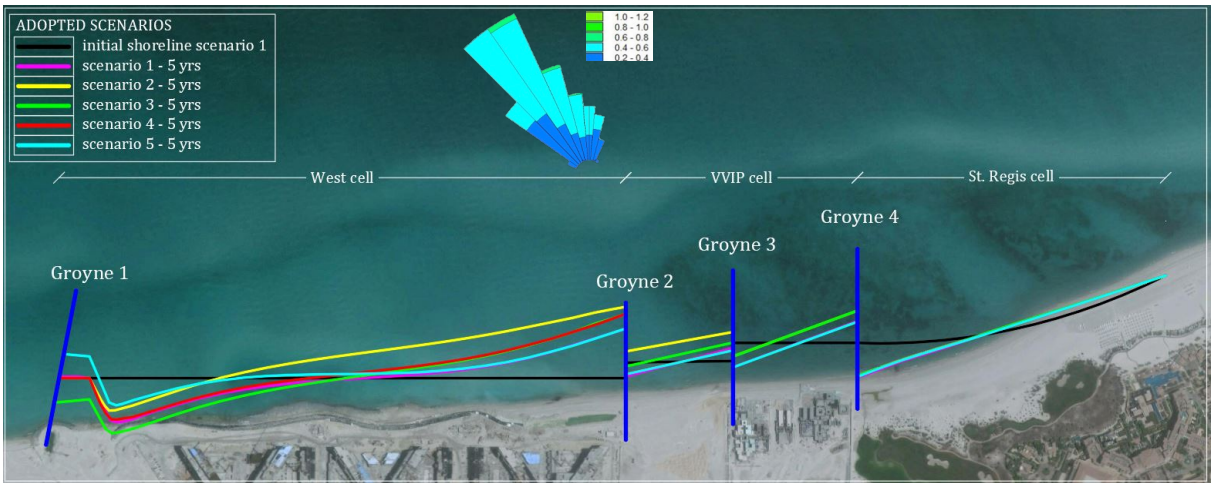

Figure A.8 - Evolution of the initial shoreline after 5 years, for the different considered scenarios (Hamza et al. 2019)

The maximum accretion/recession volumes, i.e. the new beachline dry area as resulting from the shoreline shifts multiplied by the closure depth, in relation to the sand volume of the initial nourishment in the 6 sectors along the analysed shoreline, were calculated. The shoreline shifts are calculated considering the new beach shoreline position as resulting after a fixed amount of time from the end of the intervention and the "as built shoreline after the nourishment intervention". The results are shown in Table A.4 and Table A.5.

Table A.4 - Maximum accretion/erosion occurred after 1 year, for the proposed scenarios

Scenarios	Sand volume (x 10^3 m^3)			Max recession after 1 year (m)			Max accretion after 1 year (m)		
	W cell	VVIP cell	St. Regis cell	S1	S2	S3	S4	S5	S6
1	600	240	180	26	20	21	20	25	4
2	830	270	180	20	13	31	44	16	4
3	600	270	180	20	13	31	30	16	4
4	650	240	180	26	20	21	30	25	4
5	650	270	180	10	20	21	20	25	4

Table A.5 - Maximum accretion/erosion occurred after 5 years, for the proposed scenarios

Scenarios	Sand volume (x 10^3 m^3)			Max recession after 5 years (m)			Max accretion after 5 years (m)		
	W cell	VVIP cell	St. Regis cell	S1	S2	S3	S4	S5	S6
1	600	240	180	80	27	62	75	39	14
2	830	270	180	65	22	77	71	29	14
3	600	270	180	63	22	77	79	24	14
4	650	240	180	79	27	62	79	39	14
5	650	270	180	85	27	61	76	39	14

Table A.6 shows the initial sand volume *W*, necessary for the nourishment intervention and the beach area that will be eroded 1 year or 5 years after the intervention, simulated with the GSb numerical model. This area is calculated as the area enclosed by the simulated shoreline after 1/5 years from the intervention and the corresponding initial shoreline for each scenario separately.

Table A.6 - Recession values at Saadiyat beach

	West cell		*VVIP cell*		*St. Regis cell*	
Scenarios (1 year)	*Sand volume x10³ (m³)*	*Recession (m²)*	*Sand volume x10³ (m³)*	*Recession (m²)*	*Sand volume x10³ (m³)*	*Recession (m²)*
1	600	2227	240	2685	180	1110
2	830	2394	270	1707	180	638
3	600	1944	270	1338	180	693
4	650	2368	240	2712	180	962
5	650	874	270	2708	180	1140
Scenarios (5 years)	*Sand volume x10³ (m³)*	*Recession (m²)*	*Sand volume x10³ (m³)*	*Recession (m²)*	*Sand volume x10³ (m³)*	*Recession (m²)*
1	600	15450	240	3643	180	6175
2	830	13920	270	1642	180	5625
3	600	13017	270	1958	180	5737
4	650	14106	240	3615	180	5683
5	650	13798	270	3769	180	5856

The optimal intervention scenario among the 5 proposed ones has to be individuated on the basis of the Nourishment Performance Index (NPI), proposed by (Hamza et al., 2019), considering the maximum recession that will occur after 1/5 years from the nourishment intervention related to the initial volume of sand necessary for the nourishment, according to:

$$NPI = \frac{W}{S_{1yr} \cdot h_c} \tag{A.2}$$

where W is the initial design volume necessary for the nourishment, S_{1yr} is the area in recession in the emerged beach after 1 year, with respect to the initial shoreline and h_c the closure depth.

Table A.7 shows the calculated NPI values and the increase in percentage of NPI in the beach longevity, calculated with respect to scenario 1, assumed as a reference.

Table A.7 - NPI for Saadiyat beach

	West cell		*VVIP cell*		*St. Regis cell*	
Scenarios (1 year)	*NPI*	*NPI increase (%)*	*NPI*	*NPI increase (%)*	*NPI*	*NPI increase (%)*
1	75	reference	25	reference	45	reference
2	96	29	44	77	78	74
3	86	15	56	126	72	60
4	76	2	25	-1	52	15
5	207	176	28	12	44	-3
Scenarios (5 years)	*NPI*	*NPI increase (%)*	*NPI*	*NPI increase (%)*	*NPI*	*NPI increase (%)*
1	11	reference	18	reference	8	reference
2	17	54	46	150	9	10
3	13	19	38	109	9	8
4	13	19	18	1	9	9
5	13	21	20	9	9	5

Results show that the NPI value depends mainly on the as built nourishment shoreline. The scenario that offers the overall best nourishment performance is scenario 2, representing a solution economically acceptable and its durability is sounding from the environmental sustainability prospective.

REFERENCES

Abbott, M. B. (1979). Computational Hydraulics: elements of the theory of free surface flows. Pitman Pub.

Amante, C., Eakins, B. W. (2009). ETOPO1 1 Arc-Minute Global Relief Model: Procedures, Data Sources and Analysis. In NOAA Technical Memorandum NESDIS; NGDC-24; National Geophysical Data Center: Boulder, CO, USA; p. 19.

Amourdy, L. (2008). A review on coastal sediment transport modelling. Liverpool, Proudman Oceanographic Laboratory. Internal Document No.189.

Bagnold, R. A. (1966). An approach to the sediment transport problem from general physics. US government printing office.

Bagnold, R. A., (1963). An approach of marine sedimentation. In: The Sea. Vol. 3. M. N. Hill, Interscience, New York, pp. 507-528.

Bailard J. A. (1981). An energetics total load sediment transport model for a planesloping beach, J. Geophys. Res., 86(C11), 10938–10954.

Bailard, J. A. (1982). Modeling on-offshore sediment transport in the surf zone. In Coastal Engineering 1982 (pp. 1419-1438).

Bailard, J. A. (1984). A simplified model for longshore sediment transport, Proceedings of the 19th International Conference on Coastal Engineering, ASCE, 1454-1470.

Bailard, J. A., Inman, D. L. (1981). An energetics bedload model for a plane sloping beach: local transport. Journal of Geophysical Research, 86(C3): 2035–2043.

Bakker, W. T. (2013). Coastal Dynamics (Vol. 34). World Scientific.

Bakker, W. T. J. N. P., Edelman, T. (1965). The coastline of river-deltas. In Coastal Engineering 1964 (pp. 199-218).

Bakker, W.T. (1968). The dynamics of a coast with a groyne system. Proc. 11th Intl. Conf. Coast. Eng., Am. Soc. Civil Eng., 492–517.

Balsillie, J. H. (1984). A multiple shore-breaking wave transformation computer model, Florida department of natural resources, beaches and shores technical and design. Memorandum, No. 84-4, Tallahassee, Florida.

Bascom, W. (1964). Waves and beaches: the dynamics of the ocean surface (No. 34). Garden City: Anchor Books.

Battjes, J. A., Janssen, P. F. M. (1978). Energy loss and set-up due to breaking of random waves. In Proc. 16th Int. Conf. on Coastal Eng., ASCE, Hamburg, pp. 569–587.

Bayram, A., Larson, M., Hanson, H. (2007). A new formula for the total longshore sediment transport rate. Coastal Engineering 54 (9), 700–710.

Bernabeu, A. M., Medina, R., Vidal, C. (2003). Wave reflection on natural beaches: An equilibrium beach profile model. Estuarine, Coastal and Shelf Science, 57: 577 – 585.

Bijker E. W. (1971). Longshore transport computations, J. Waterway. Harbour.Coast. Eng. Div.-ASCE, 97(WW4), 687–701.

Blaas, M., Dong C., Marchesiello P., McWilliams J., Stolzenbach K. (2007). Sediment-transport modeling on Southern Californian shelves: A ROMS case study, Cont. Shelf Res., 27(6), 832–853.

Blanco, B. (2003). Beachplan (Version 04.01) User manual. HR Wallingford report IT508.

Boak, E. H., Turner, I. L. (2005). Shoreline definition and detection: a review. Journal of coastal research, 688-703.

Boczar-Karakiewicz, B., Davidson-Arnott, R. G. D. (1987). Nearshore bar formation by non-linear wave processes– a comparison of model results and field data. Mar. Geol., 77: 287–304.

Bodge, K. R. (1986). Short term impoundment of longshore sediment transport. PhD Thesis, University of Florida and U.S. Army Corps of Engineers, Coastal Engineering Research Centre, Vicksburg.

Bodge, K. R. (1992). Representing equilibrium beach profiles with an exponential expression. Journal of coastal research, 47-55.

Bodge, K. R., Dean G. D. (1987). Short- term impoundment of longshore sediment transport report. Miscellaneous paper CERC-87-7. Coastal Engineering Research Center, U.S. Corps of Eng.

Booij, N., Holthuijsen, L. H., Ris, R. C. (1997). The "SWAN" wave model for shallow water. In Coastal Engineering 1996 (pp. 668-676).

Bowen, A. J. (1981). Simple models of nearshore sedimentation: beach profiles and longshore bars. In McCann, S.B. (ed.), The Coastline of Canada: littoral processes and shore morphology. Geological Survey of Canada, Special Paper: 80–10, pp. 1–11.

Briand, M. H. G., Kamphuis, J. W. (1993). Sediment transport in the surf zone: a quasi 3-D numerical model. Coastal Engineering, 20(1-2), 135-156.

Bruun, P. (1954). Coast erosion and the development of beach profiles. Technical Memorandum No. 44, Beach Erosion Board, Coastal Engineering Research Center, US Army Engineer Waterways Experiment Station, Vicksburg, MS.

Bruun, P. (1962). Sea-level rise as a cause of shore erosion. Journal of the Waterways and Harbors division, 88(1), 117-132.

Burcharth, H. F., Frigaard, P. (1987). On the stability of berm breakwater roundheads and trunk erosion in oblique waves. Seminar on Unconventional Rubble Mound Break- waters. Ottawa, Ontario.

Burcharth, H. F., Frigaard, P. (1988). On 3-dimensional stability of reshaping breakwaters. Proceedings 21st International Conference on Coastal Engineering. ASCE, Malaga, pp. 2284–2298.

Canovas Losada, V., Medina Santamaría, R. (2012). A long-term equilibrium beach planform model for coastal work design.

CERC (1973). Shore protection manual (Vol. 1). Coastal Engineering Research Center, Corps of Engineers., U. S. Government Printing Office, Washington, DC.

CERC (1984). Shore protection manual (Vol. 2), Coastal Engineering Research Center, Corps of Engineers., U. S. Government Printing Office, Washington, DC.

Chadwick, A. J., (1989). Field measurements and numerical model verification of coastal shingle transport. BHRA, The Fluid Engineering Centre, UK, pp. 381–402. Chapter 27.

Chadwick, A.J. (1989). Field measurements and numerical model verification of coastal shingle transport. BHRA, The Fluid Engineering Centre, UK, pp. 381–402. Chapter 27.

CIRIA (1996). Beach management manual. CIRIA Report 153.

Courant, R., Friedrichs, K., Lewy, H. (1967). On the partial difference equations of mathematical physics. IBM journal of Research and Development, 11(2), 215-234.

Crank, J., Nicolson, P. (1947). A practical method for numerical evaluation of solutions of partial differential equations of the heat-conduction type. In Mathematical Proceedings of the Cambridge Philosophical Society (Vol. 43, No. 1, pp. 50-67). Cambridge University Press.

Dabees, M. A. (2000). Efficient modeling of beach evolution. Ph. D. Thesis, Queen's University.

Dabees, M., Kamphuis, J. W. (1999). ONELINE, a numerical model for shoreline change. In Coastal Engineering 1998 (pp. 2668-2681)

Dally, W. R. (1980). A numerical model for beach profile evolution. Unpubl. Master's Thesis, University of Delaware, Newark, DE.

Dally, W. R., Dean, R. G. (1984). Suspended sediment transport and beach profile evolution. Jour. Waterway Port Coast. Ocean, Eng., 110: 15–33.

Dang, V. T. (2006). Development of a Mathematical N-line Model for Simulation of Beach Changes. University of New South Wales.

De Vriend, H. J., Capobianco, M., Chesher, T., De Swart, H. D., Latteux, B., Stive, M. J. F. (1993). Approaches to long-term modelling of coastal morphology: a review. Coastal engineering, 21(1-3), 225-269.

De Vriend, H. J., Ribberink, J. S. (1989). A quasi-3D mathematical model of coastal morphology. In Coastal Engineering 1988 (pp. 1689-1703).

Dean, R. G. (1977). Equilibrium Beach Profiles: US Atlantic and Gulf Coasts. Ocean Engineering Report No. 12, Department of Civil Engineering, University of Delaware, Newark, DE.

Dean, R. G. (1987). Coastal Sediment Processes, Toward Engineering Solutions. In Coastal Sediments' 87, Specialty Conference on Advances in Understanding of Coastal Sediment Processes, ASCE, New Orleans, LA, 1987 (Vol. 1, pp. 1-24).

Dean, R. G. (1990). Equilibrium beach profiles: characteristics and applications. Journal of coastal research, 53-84.

Dean, R. G. (1991). Equilibrium beach profiles: Characteristics and applications. Journal of Coastal Research, 7(1): 53-84.

Dean, R. G. (2003). Beach nourishment: theory and practice (Vol. 18). World Scientific Publishing Company.

Dean, R. G., Berek, E. P., Gable, C. G., Seymour, R. J. (1982). Longshore transport determined by an efficient trap. In Coastal Engineering 1982 (pp. 954-968).

Dean, R. G., Dalrymple, R. A. (2004). Coastal processes with engineering applications. Cambridge University Press.

Del Valle, R., Medina, R., Losada, M. A. (1993). Dependence of coefficient K on grain size, Technical Note No. 3062, Journal of Waterway, Port, Coastal, and Ocean Engineering, 119 (5) 568-574.

Delft3D website. https://oss.deltares.nl/web/delft3d. Deltares, NL (accessed on 17 September 2019).

Deltares (2011). UNIBEST-CL+ Manual: Manual for Version 7.1 of the Shoreline Model UNIBEST-CL+. 13 January 2011, draft.

Dey S. (2014). Bed-Load Transport. In: Fluvial Hydrodynamics. GeoPlanet: Earth and Planetary Sciences. Springer, Berlin, Heidelberg

DHI (2003). An integrated modeling system for littoral processes and coastline kinetics, short introduction and tutorial, Danish Hydraulic Institute, Copenhagen.

DHI (2005). Litpack: Noncohesive Sediment Transport in Currents and Waves—User Guide, Danish Hydraulic Institute, Copenhagen.

DHI (2009a). LITPACK: An Integrated Modeling System for Littoral Processes and Coastline Kinetics (Short Introduction and Tutorial). Delft Hydraulics Institute. Published by DHI.

DHI (2009b). LITLINE: Coastline Evolution (LITLINE User Guide). Delft Hydraulics Institute. Published by DHI. Jan 2009.

DHI (2009c). LITDRIFT: Longshore Current and Littoral Drift (LITDRIFT User Guide). Delft Hydraulics Institute. Published by DHI.

DHI (2009d). LITSTP: Noncohesive Sediment Transport in Currents and Waves (LITSTP User Guide). Delft Hydraulics Institute. Published by DHI. Jan 2009.

DHI (2017). Littoral processes FM. Mike 17. DHI Software, Danish Hydraulic Institute, Copenhagen.

DHI. (1995). EU MAST II Berm Breakwater Structures. Report on Three-Dimensional Model Tests. Draft Report. Danish Hydraulic Institute.

Dingler, J. R. (2005). Beach processes. Encyclopedia of Coastal Science, 161-168.

Dolan, R., Hayden, B. P., May, P., May, S. (1980). The reliability of shoreline change measurements from aerial photographs. Shore and beach, 48(4), 22-29.

Eaton, R. O. (1951). Littoral processes on sandy coasts. Coastal Engineering Proceedings, 1(1), 15.

Elfrink, B., Baldock, T. (2002). Hydrodynamics and sediment transport in the swash zone: a review and perspectives. Coastal Engineering 45: 149-167

Engelund, F., Fredsøe, J. (1976). A sediment transport model for straight alluvial channels. Hydrology Research, 7(5), 293-306.

Fang, H., Rodi W. (2003). Three-dimensional calculations of flow and suspended sediment trans- port in the neighborhood of the dam for the Three Gorges Project (TGP) reservoir in the Yangtze River., Journal of Hydraulic Research, 41(4), 379–394.

Faye, I. (2010). Dynamique du trait de côte sur les littoraux sableux de la Mauritanie à la Guinée-Bissau (Afrique de l'Ouest): Approches régionale et locale par photo-interprétation, traitement d'images et analyse de cartes anciennes (Doctoral dissertation).

Felder, W. N. (1978). Simulation modeling of offshore bars. Depart. Environ. Sci., Unpub. Ph.D. thesis, University of Virginia, Charlottesville, VA.

Felder, W. N., Fisher, J. S. (1980). Simulation model analysis of seasonal beach cycles. Coast. Eng., 3: 269–282.

Field, J. C., Boesch, D. F., Scavia, D., Buddemeier, R., Burkett, V. R., Cayan, D., Pietrafesa, L. J. (2001). Potential consequences of climate variability and change on coastal areas and marine resources. Climate Change Impacts on the United States: The Potential Consequences of Climate Variability and Change, Report for the US Global Change Research Program. Cambridge University Press, Cambridge, UK, 461-487.

Fleming, C. A. (1990). Principles and Effectiveness of Groynes. Coastal Protection, Balkema Press, Rotterdam, 121-156.

Folk, R. L. (1954). The distinction between grain size and mineral composition in sedimentary-rock nomenclature. The Journal of Geology, 62(4), 344-359.

Folk, R. L. (1974), The petrology of sedimentary rocks: Austin, Tex., Hemphill Publishing Co., 182 p.

Folk, R. L., Ward, W. C. (1957). Brazos River bar [Texas]; a study in the significance of grain size parameters. Journal of Sedimentary Research, 27(1), 3-26.

Francone, A., D'Alessandro, F., Musci, F., Tomasicchio, G. R. (2018). Resistenza e resilienza di una spiaggia in sabbia: uno studio in campo e numerico. Proceedings 36th IDRA - Convegno Nazionale di Idraulica e Costruzioni Idrauliche, Ancona.

Francone, A., Lusito, L., D'Alessandro F., Frega, F., Tomasicchio, G. R. (2019). Influence of hard structures on beach morphodynamics. Proceedings 40° Edition of Italian Conference on Integrated River Basin Management, Guardia Piemontese, 285-295.

Fredsoe, J., Andersen, O. H., Silberg, S. (1985). Distribution of suspended sediment in large waves. Journal of waterway, port, coastal, and ocean engineering, 111(6), 1041-1059.

Fredsøe, J., Deigaard, R. (1992). Mechanics of coastal sediment transport, Adv. Ser. Ocean Eng, 3, 369.

Frey, A. E., Connell, K. J., Hanson, H., Larson, M., Thomas, R.C., Munger, S., Zundel A. (2012). GenCade Version 1 Model Theory and User's Guide. Tech. Report ERDC/CHL TR-12-25, U.S. Army Engineer Res. and Development Center, Vicksburg, MS.

GenCade website, http://cirp.usace.army.mil/products/gencade.php. U.S. Army Corps of Engineers (accessed on 17 September).

Gessler, D., Hall B., Spasojevic M., Holly F., Pourtaheri H., Raphelt N. (1999). Application of 3 D Mobile Bed, Hydrodynamic Model, Coastal Eng., 125(7), 737–749.

GIOC (2003). Coastal Modelling System (SMC). Reference and User Manual. State Coastal Office Spanish Environmental Ministry and University of Cantabria, 82

Goda, Y. (2010). Random Seas and Design of Maritime Structures, 3rd ed. Singapore: World Scientific, Advanced Series on Ocean Engineering.

González, M., Medina, R., González-Ondina, J., Osorio, A., Méndez, F. J., García, E. (2007). An integrated coastal modeling system for analyzing beach processes and beach restoration projects, SMC. Computers & geosciences, 33(7), 916-931.

Graham, D., Sault, M., Bailey, C. J. (2003). National ocean service shoreline - Past, present, and future. Journal of Coastal Research, 14-32.

Gravens, M. B. (1991). Development of an Input Data Set for Shoreline Change Modeling. Proceedings, Coastal Sediments '91, American Society of Civil Engineers, pp 1800-1813.

Gravens, M. B. (1992). User's Guide to the Shoreline Modeling System (SMS). Instruction Report CERC-92-1, U.S. Army Engineer Waterways Experiment Station, Vicksburg, MS.

Gravens, M. B., Kraus, N. C., Hanson, H. (1991). GENESIS: Generalized Model for Simulating Shoreline Change. Instruction Report CERC-89-19, U.S. Army Engineer Waterways Experiment Station, Vicksburg, MS.

Gravens, M. B., Wang P. (2007). Data report: laboratory testing of longshore sand transport by waves and currents; morphology change behind headland structures. Technical Report, ERDC-CHL TR-07-8, U.S. Army Engineer Research and Development Center, Vicksburg, MS.

Gravens, M., Rosati, J. (1994). Numerical Model Study of Breakwaters at Grand Isle, Louisiana. 83.

Grijm, W. (1961). Theoretical forms of shorelines. Proc. 7th Coastal Eng. Conf., ASCE: 197-202.

Güner, H. A. A., Yüksel, Y., Çevik, E. Ö. (2011). Determination of Longshore Sediment Transport and Modelling of Shoreline Change. Sediment Transport, 117.

Hallermeier, R. J. (1978). Uses for a calculated limit depth to beach erosion. In Coastal Engineering 1978 (pp. 1493-1512).

Hallermeier, R. J. (1983). Sand Transport Limits in Coastal Structure Design, Proceedings, Coastal Structures '83, American Society of Civil Engineers, pp. 703-716.

Hallermeier, R.J. (1981). A Profile Zonation for Seasonal Sand Beaches from Wave Climate. Coastal Engineering, 4, 253-277.

Hamilton, D. G., Ebersole, B. A., Smith, E. R., Wang P. (2001). Development of a large-scale laboratory facility for sediment transport research. Technical Report ERDC/CHL-TR-01-22, U.S. Army Engineer Research and Development Center, Vicksburg, MS.

Hamza, W., Tomasicchio, G. R., Ligorio, F., Lusito, L., Francone, A. (2019). A Nourishment Performance Index for Beach Erosion/Accretion at Saadiyat Island in Abu Dhabi. Journal of Marine Science and Engineering, 7(6), 173.

Hamza, W., Lusito, L., Ligorio, F., Tomasicchio, G.R., D'Alessandro, F. (2018). Wave Climate at Shallow Waters along the Abu Dhabi Coast. Water, 10(8), 985, https://doi.org/10.3390/w10080985.

Hanson, H. (1987). GENESIS, A Generalized Shoreline Change Model for Engineering Use. Report No. 1007, Department of Water Resources Engineering, University of Lund, Lund, Sweden.

Hanson, H. (1989). GENESIS: a generalized shoreline change numerical model. Journal of Coastal research, 1-27.

Hanson, H., Kraus, N. (1989). GENESIS – generalized model for simulating shoreline change. Report TR-CERC 89-19 (Report 1), Coastal and Hydraulic Laboratory, US Army Corps of Engineers.

Hanson, H., Kraus, N. C. (1990). Shoreline response to a single transmissive detached breakwater. Proceedings 22nd Coastal Engineering Conference, ASCE, pp. 2034–2046.

Hanson, H., Kraus, N. C. (2004). Advancements in one-line modeling of T-head groins:(Genesis-T). Journal of Coastal Research, 315-323.

Hanson, H., Kraus, N. C. (2011). Long-term evolution of a long-term evolution model. Journal of Coastal Research, 118-129.

Hanson, H., Larson, M., Kraus, N. C., Gravens, M. B. (2006). Shoreline response to detached breakwaters and tidal current: Comparison of numerical and physical models. Proceedings of 30th International Coastal Engineering Conference, World Scientific, 3,630-3,642.

Hedegaard, I. B., Deigaard, R., Fredsøe, J. (1991). Onshore/offshore sediment transport and morphological modelling of coastal profiles. In Coastal Sediments (pp. 643-657). ASCE.

Hess, K. W. (2003). Tidal datums and tide coordination. Journal of Coastal Research, 33-43.

Horikawa, K., Harikai, S., Kraus, N.C. (1979). A physical and numerical modeling of waves, current and sediment transport near a breakwater. Ann. Rep. of the Eng. Res. Inst., Fac. of Eng., University of Tokyo, 38: 41-48.

Horikowa, K. (1988). Nearshore Dynamics and Coastal Processes: Theory, Measurement, and Predictive Models. University of Tokyo Press, Japan

Hydroqual (2002). A primer for ECOMSED. Version 1.3. Users Manual.

Inman, D. L. (1952). Measures for describing the size distribution of sediments. Journal of Sedimentary Research, 22(3), 125-145.

Inman, D. L., Bagnold, R. A. (1963). Beach and nearshore processes Part II: Littoral processes, in The Sea: Ideas and Observations, 3, M.N. Hill (ed.), Interscience, New York, 529-553.

Jayaratne, M. P. R. (2004). Modelling of Suspended Sediment Concentration and Cross-Shore Beach Deformation Model, PhD thesis, Yokohama National University, Japan.

Kamphuis, J. W. (1975). Friction factor under oscillatory waves. Journal of the Waterways, Harbors and Coastal Engineering Division, 101(2), 135-144.

Kamphuis, J. W. (1991). Alongshore sediment transport rate. Journal of Waterways, Port, Coastal and Ocean Engineering, ASCE, 117(6), 624-641.

Kamphuis, J. W. (1991). Littoral transport rate. In Coastal Engineering 1990 (pp. 2402-2415).

Kamphuis, J. W. (1999). Marketing uncertainty. In Proceedings International Conference on Coastal and Port Engineering in Developing Countries (COPEDEC) (pp. 2088-2099).

Kamphuis, J. W. (2002). Alongshore transport of sand, Proceedings of the 28th International Conference on Coastal Engineering, ASCE, 2478-2490.

Kamphuis, J. W. (2010). Introduction to Coastal Engineering and Management, 2nd Edition, World Scientific Publishing Co. Pte. Ltd., ISBN-13 978-981-283-484-3, Singapore.

Kamphuis, J. W. Davies, M. H. Nairn, R. B., Sayao, O. J. (1986). Calculation of littoral sand transport rate, Coastal Engineering, 10, 1-21.

Kamphuis, J. W., Readshaw, J. S. (1978). A model study of alongshore sediment transport rate, Proceedings of the International Conference on Coastal Engineering, ASCE press, 1656-1674.

Kobayashi, N., Payo, A., Schmied, L. (2008). Cross-shore suspended sand and bed load transport on beaches. J. Geophys. Res. 113(C07001), 1–17.

Komar, P. D. (1971). The mechanics of sand transport on beaches. Journal of Geophysical Research, 76(3), 713-721.

Komar, P. D. (1977). Beach sand transport: distribution and total drift. Journal of the Waterway Port Coastal and Ocean Division, 103(2), 225-239.

Komar, P. D. (1998). The modeling of processes and morphology in the coastal zone - reflections on the maturity of our science. Shore and Beach, 66(1): 10-22.

Komar, P. D., Gaughan, M. K. (1972). Airy wave theory and breaker height prediction. Proceedings of the 13th International Conference on Coastal Engineering. ASCE, Vancouver, pp. 405–418.

Komar, P. D., Inman, D. L. (1970). Longshore sand transport on beaches, Journal of Geophysical Research, 75(30), 5514-5527.

Komar, P. D., McDougal, W. G. (1994). The analysis of exponential beach profiles. Journal of Coastal Research, 10(1): 59-69.

Kraus N. C. (2005). Shore Protection Structures. In: Schwartz M.L. (eds) Encyclopedia of Coastal Science. Encyclopedia of Earth Science Series. Springer, Dordrecht

Kraus, N. C. (1981). One-Line Development and Simulation for Oarai Beach. NERC Report No. 13, Cooperative Research of Surf Zone Dynamics, Part 3, Beaches Near Breakwaters and Rocky Coasts, Nearshore Environment Research Center, Tokyo, Japan, pp 155-192.

Kraus, N. C. (1983). Applications of Shoreline Prediction Model, Proceedings of Coastal Structures 83, American Society of Civil Engineers, pp. 632-645.

Kraus, N. C. Harikai, S., (1983). Numerical Model of the Shoreline Change at Oarai Beach, Coastal Engineering, Vol. 7, No. 1, pp. 1-28.

Kraus, N. C., (1984). Estimate of Breaking Wave Height Behind Structures. Journal of Waterway, Port, Coastal and Ocean Engineering, Vol 110, No. 2, pp 276-282.

Kraus, N. C., Isobe, M., Igarashi, H., Sasaki, T. O., Horikawa, K. (1982). Field experiments on longshore transport in the surf zone, Proceedings of the 18th International Conference on Coastal Engineering, ASCE, 969-988.

Kriebel, D. L. (1982). Beach and dune response to hurricanes. Master's Thesis, University of Delaware, Newark, DE.

Kriebel, D. L., Dean, R. G. (1984). Beach and dune response to severe storms. Proc. 19th Coast. Eng. Conf., Am. Soc. Civil Eng., 1584–1599.

Kriebel, D. L., Dean, R. G. (1985). Numerical simulation of time-dependent beach and dune erosion. Coastal Engineering, 9: 221-245.

Krumbein, W. C., Sloss, L. L. (1963). Stratigraphy and Sedimentation, Ch. 4, Properties of Sedimentary Rocks, W. H. Freeman & Company, pp 93-149.

Kuroiwa, M., Noda, H., Son, C. B., Katoh, K., Taniguchi, S. (2001). Numerical prediction of bottom topographical change around coastal structures using quasi-3D nearshore current model. In Coastal Engineering 2000 (pp. 2914-2927).

Lamberti, A., Tomasicchio, G. R. (1997). Stone mobility and longshore transport at reshaping breakwaters. Coastal Engineering 29 (3), 263–289.

Larson M. (2005). Numerical Modeling. In: Schwartz M.L. (eds) Encyclopedia of Coastal Science. Encyclopedia of Earth Science Series. Springer, Dordrecht

Larson, M., Hanson, H., Kraus, N. C. (1987). Analytical Solutions of the One-Line Model of Shoreline Change, Technical Report CERC-87-15, U.S. Army Engineer Waterways Experiment Station, Vicksburg, MS.

Larson, M., Kraus, N. C. (1989). SBEACH. Numerical model for simulating storm- induced beach change; report 1. Empirical foundation and model development. Tech Rep. CERC-89-9. US Army Corps of Engineers, CERC. Vicksburg, Miss.

Larson, M., Kraus, N. C. (1995). Prediction of cross-shore sediment transport at different spatial and temporal scales. Marine geology, 126(1-4), 111-127.

Larson, M., Kraus, N. C. (2000). Representation of non-erodible (hard) bottoms in beach profile change modeling. Journal of Coastal Research, 16(1): 1-14.

Larson, M., Kraus, N. C., Hanson. H. (2002). Simulation of regional longshore sediment transport and coastal evolution - the "CASCADE" model. Coastal Engineering 2002, 2612-2624, https://www.worldscientific.com/doi/abs/10.1142/9789812791306_0218

Larson, M., Kraus, N. C., Sunamura, T. (1988). Beach profile change: Morphology, transport rate and numerical simulation. In Proc. 21st Int. Conf. on Coastal Eng., ASCE, Torremolinos, pp. 1295–1309.

Le Mehaute, B., Soldate, M. (1977). Mathematical Modeling of Shoreline Evolution, Miscellaneous Report 77-10, U.S. Army Engineer Waterways Experiment Station, Vicksburg, MS.

Le Mehaute, B., Soldate, M. (1980). A Numerical Model for Predicting Shoreline Changes (No. TETRAT-TC-831A).

Leatherman, S. P. (2003). Shoreline change mapping and management along the US East Coast. Journal of Coastal Research, 5-13.

Leontyev, I. O. (1996). Numerical modelling of beach erosion during storm event. Coastal Engineering, 29(1-2): 187-200.

Lesser, G., J. Roelvink, van Kester J., Stelling G. (2004). Development and validation of a three- dimensional morphological model, Coastal Eng., 51(8-9), 883–915.

Lesser, G., van Kester J., Roelvink J. A. (2000). On-line sediment within DELFT3D-FLOW, Tech. rep., WL Delft Hydraulics.

Lincoln, R. J. (1998). A dictionary of ecology, evolution and systematics (No. C/574.5 L5).

Longuet-Higgins, M. S. (1970). Longshore currents generated by obliquely incident sea waves: 1. Journal of geophysical research, 75(33), 6778-6789.

Lumborg, U. (2005). Modelling the deposition, erosion, and flux of cohesive sediment through Øresund, Journal of Marine Systems, 56(1-2), 179–193.

Lumborg, U., Windelin A. (2003). Hydrography and cohesive sediment modelling: application to the Rømø Dyb tidal area, Journal of Marine Systems, 38(3-4), 287–303.

Madsen, O. S., Grant, W. D., (1976). Sediment transport in the coastal environment. Tech. Rep. 209, M. I. T., Cambridge, Massassuchetts, USA.

Maloney, F. E., Ausness, R. C. (1974). The use and legal significance of the mean high water line in coastal boundary mapping. North Carolina L.Review, 53: 185–273.

Mangor, K. (2004). Shoreline Management Guidelines. DHI Water and Environment, 294pg.

Mangor, K., Drønen, N. K., Kaergaard, K. H., Kristensen, N. E. (2017). Shoreline management guidelines. DHI. https://www.dhigroup.com/marine-water/ebook-shoreline-management-guidelines

Martin-Grandes, I. (2014). Understanding Longshore Sediment Transport on a Mixed Beach. Master of Philosophy Thesis, Plymouth University

Martin-Grandes, I., Hughes, J., Simmonds, D. J., Chadwick, A. J., Reeve, D. E. (2009). Novel methodology for one line model calibration using impoundment on mixed beach. *Coastal Dynamics* - Impacts of Human Activities on Dynamic Coastal Processes, DOI: 10.1142/9789814282475_0106.

MathWorks (2019). MATLAB, The MathWorks, Inc., Natick, Massachusetts, United States.

McCall, R. T., Masselink, G., Poate, T. G., Roelvink, J. A., Almeida, L. P. (2015). Modelling the morphodynamics of gravel beaches during storms with XBeach-G. Coastal Engineering, 103, 52-66.

McCammon, R. B. (1962). Efficiencies of percentile measures for describing the mean size and sorting of sedimentary particles. The Journal of Geology, 70(4), 453-465.

Medellín, G., Torres-Freyermuth, A., Tomasicchio, G. R., Francone, A., Tereszkiewicz, P. A., Lusito, L., Palemón-Arcos, L., López, J. (2018). Field and Numerical Study of Resistance and Resilience on a Sea Breeze Dominated Beach in Yucatan (Mexico). Water 2018, 10, 1806.

Mil-Homens, J., Ranasinghe, R., van Thiel de Vries, J. S. M., Stive, M. J. F. (2013). Re-evaluation and improvement of three commonly used bulk longshore sediment transport formulas. Coastal Engineering 75, 29-39.

Miller, H. C. (1998). Comparison of storm longshore transport rates to predictions, Proceedings of the 26th International Conference on Coastal Engineering, ASCE, 2954-2967.

Miller, J. K., Dean, R. G. (2004). A simple new shoreline change model. Coastal Engineering, 51(7), 531-556.

Mimura, N., Shimizu, T., Horikawa, K. (1983). Laboratory study on the influence of detached breakwater on coastal change. In Coastal Structures' 83 (pp. 740-752). ASCE.

Ming D., Chiew Y. M. (2000). Shoreline changes behind detached breakwater, Journal of Waterway, Port, Coastal, and Ocean Engineering, Vol. 126, No. 2, 63-70.

Mizuguchi, M. (1980). A heuristic model of wave height distribution. In Proc. 17th Int. Conf. on Coastal Eng., ASCE, Sydney, pp. 278–289.

Moore, B. D. (1982). Beach profile evolution in response to changes in water level and wave height. Master's Thesis, University of Delaware, Newark, DE.

Nairn, R. B., Roelvink, J. A., Southgate, H. N. (1990). Transition zone width and implications for modelling surfzone hydrodynamics. In Coastal Engineering 1990 (pp. 68-81).

Natesan, U. (2009). Shoreline Dynamics of Dhanushkodi, Rameswaram Using Gis. In Advances in Water Resources and Hydraulic Engineering (pp. 1294-1298). Springer, Berlin, Heidelberg.

Nguyen, N. T., Luong, P. H. (2007). Studying shoreline change by using LITPACK mathematical model (case study in Cat Hai Island, Hai Phong City, Vietnam).

Nilsson, H. D. (1979). Multiple longshore sand bars: Environments of deposition and a model for their generation and maintenance. Unpubl. Ph.D. Thesis, University of Massachusetts, Amherst, MA.

NOOA (2017). The Economic Importance of Our Coasts. Available from https://celebrating200years.noaa.gov/. [accessed on 23-11-2019]

O'Connor, B. A., Pan, S., Nicholson, J., MacDonald, N., Huntley, D. A. (1999). A 2D model of waves and undertow in the surf zone. In Coastal Engineering 1998 (pp. 286-296).

Oertel, G. F. (2005). Coasts, coastlines, shores, and shorelines. Encyclopedia of Coastal Science, 323-327.

Otto, G. H. (1939). A modified logarithmic probability graph for the interpretation of mechanical analyses of sediments. Journal of Sedimentary Research, 9(2), 62-76.

Overeem, J. V. (1978). Numerical model for the computation of coastal changes caused by waves and currets. Delft University of Technology; Dept. of Civil Eng.; Sect. Coastal Eng.

Ozasa, H., Brampton, A. H. (1980). Mathematical modelling of beaches backed by seawalls. Coastal Engineering, 4, 47-63.

Ozhan, E. (1982). Laboratory study of breaker type effect on longshore sand transport, in Proceedings, Euromech 156: Mechanics of Sediment Transport; July, 1982, B.M. Sumer and A. Muler, (ed.), A. A. Balkema, Rotterdam, The Netherlands.

Pajak, M. J., Leatherman, S. (2002). The high-water line as shoreline indicator. Journal of Coastal Research, 329-337.

Pechon, P., Teisson, C. (1996). Numerical modelling of bed evolution behind a detached breakwater. In Coastal Engineering 1996 (pp. 2050-2062).

Pelnard-Considere, R. (1956). Essai de Theorie de l'Evolutio des Form de Rivage en Plage de Sable et de Galets. 4th Journees de l'Hydaulique, Les Energies de la Mer, Question III, No. 1, 289-298.

Perlin, M. (1979). Predicting beach planforms in the lee of a breakwater. In Coastal Structures' 79 (pp. 792-808). ASCE.

Perlin, M., Dean R. G. (1979). Prediction of Beach Planforms with Littoral Controls, Proceedings of 16th Coastal Engineering Conference, ASCE, pp. 1818- 1838.

Perlin, M., Dean, R. G. (1983). A Numerical Model to Simulate Sediment Transport in the Vicinity of Coastal Structures. Coastal And Offshore Engineering And Research Inc Newark De.

Polidoro, A., Pullen, T., Eade, J., Mason, T., Blanco, B., Wyncoll, D. (2018). Gravel beach profile response allowing for bimodal sea states. In Proceedings of the Institution of Civil Engineers-Maritime Engineering (Vol. 171, No. 4, pp. 145-166). Thomas Telford Ltd.Pope, J., Dean, J. L. (1987). Development of design criteria for segmented breakwaters. In Coastal Engineering 1986 (pp. 2144-2158).

Price, W.A., Tomlinson, K.W., Willis, D.H. (1973). Predicting changes in the plan shape of beaches. Proc. 13th Coastal Eng. Conf., ASCE: 1321-1329.

Qiu, L. I. J. I. E. (2013). Analysis of Model Performance Related to Uncertainty in the Model BEACHPLAN for the Simulation of Shoreline Evolution.

Rakha, K. A. (1998). A Quasi-3D phase-resolving hydrodynamic and sediment transport model, Coastal Eng., 34(3-4), 277–311.

Ranasinghe, R., Pattiaratchi, C., Masselink, G. (1999). A morphodynamic model to simulate the seasonal closure of tidal inlets. Coastal Engineering, 37(1), 1-36.

Rattanapitikon, W., Shibayama, T. (1996). Cross-shore sediment transport and beach deformation model. In Proc. 25th Int. Conf. on Coastal Eng., ASCE, Orlando, pp. 3062–3075.

Rea, C. C., Komar, P. D. (1975). Computer simulation models of a hooked beach shoreline configuration. Journal of Sedimentary Research, 45(4), 866-872.

Reeve, D. E., Valsamidis, A. (2014). On the stability of a class of shoreline planform models. Coastal Engineering, 91, 76-83.

Rivero, F., Rodriguez, M., Sánchez-Arcilla, A. (1993). Propagación del Oleaje sobre Fondos variables en Presencia de Corrientes. II Jornadas Españolas de Ingeniería de Costas, 187-204.

Roelvink, D. (2011). A guide to modeling coastal morphology (Vol. 12). world scientific.

Roelvink, D., Reniers, A. J. H. M., Van Dongeren, A., Van Thiel de Vries, J., Lescinski, J., McCall, R. (2010). XBeach model description and manual. Unesco-IHE Institute for Water Education, Deltares and Delft University of Tecnhology. Report June, 21, 2010.

Roelvink, J. A., Stive, M. J. F. (1989). Bar-generating cross-shore flow mechanisms on a beach, Journal of Geophysical Research: Oceans (1978–2012)94(C4): 4785–4800.

Ruggiero, P., Kaminsky, G. M., Gelfenbaum, G. (2003). Linking proxy-based and datum-based shorelines on a high-energy coastline: implications for shoreline change analyses. Journal of Coastal Research, 57-82.

Saha, S., Moorthi, S., Pan, H.L., Wu, X., Wang, J., Nadiga, S., Tripp, P., Kistler, R., Woollen, J., Behringer, D. (2010) The NCEP Climate Forecast System Reanalysis. Bull. Am. Meteorol. Soc. 2010, 91, 1015–1057.

Samaras, A. G., Koutitas, C. G. (2014). Comparison of three longshore sediment transport rate formulae in shoreline evolution modeling near stream mouths. Ocean Engineering, 92, 255-266.

Sasaki, T. (1973). Simulation of shoreline and nearshore current. Civil Eng. Oceans, 3: 179–196.

Schlee, J.S. (1973). Atlantic continental shelf and slope of the United States–Sediment texture of the northeastern part. US Geological Survey Professional Paper 529-L.

SCOPAC (2003). Sediment transport study: Hengistbury Head to Hurst Spit. Standing Conference on Problems Associated with the Coastline. http://www.Scopac.org.uk/

Seymour, R. J. (2005). Cross-shore sediment transport. Encyclopedia of Coastal Science, 352-353.

Shalowitz, A. (1962). Shore and Sea Boundaries, Vol. 1. Washington: U.S. Government Printing Office.

Shepard, F. P. (1954). Nomenclature based on sand-silt-clay ratios. Journal of Sedimentary Research, 24(3), 151-158.

Shibayama, T., Horikawa, K. (1980). Bed load measurement and prediction of two-dimensional beach transformation due to waves. Coast. Eng. Japan, 23: 179–190.

Shibayama, T., Horikawa, K. (1985). Numerical model for two-dimensional beach transformation. In Proc. JSCE, No. 357/II–3 (Hydraulic and Sanitary), pp. 167–176.

Shore Protection Manual (1977). 3rd ed., 2 Vol, U. S. Army Engineer Waterways Experiment Station, U. S. Government Printing Office, Washington, DC.

Shore protection manual (Vol. 1). Coastal Engineering Research Center, Corps of Engineers.

Shore Protection Manual. (1984). 4th ed., 2 Vol, U. S. Army Engineer Waterways Experiment Station, U. S. Government Printing Office, Washington, DC.

Skou, A., Hedegaard, I. B., Fredsoe, J., Deigaard, R. (1991). Applications of mathematical models for coastal sediment transport and coastline development. 3rd Intl. Conf. Coast. Port Eng. Develop. Countries, COPEDEC, Mombasa (Kenya), 227–236.

Southgate, H. N., Nairn, R. B. (1993). Deterministic profile modelling of nearshore processes. Part 1. Waves and currents. Coastal Engineering, 19(1-2), 27-56.

Stive, M. J. F., Battjes, J. A. (1984). A model for offshore sediment transport. in Proc. 19th Int. Conf. on Coastal Eng., ASCE, Houston, pp. 1420–1436.

Stive, M.J.F. (1987). A model for cross-shore sediment transport. in Proc. 20th Coast. Eng. Conf., Am. Soc. Civil Eng., 1550–1564.

Sunamura, T. (1983). A predictive model for shoreline changes on natural beaches caused by storm and post-storm waves. Trans. Jap. Geomorphol. Union, 4: 1– 10.

Sutherland J. (2019). Process-based modelling. Available from http://www.coastalwiki.org/wiki/Process-based_modelling [accessed on 12-11-2019]

Sutherland, J., Harper, A., Bolster, M. (2013). Beachplan as an Open-MI composition. In Proceedings of the 35th IAHR World Congress, Chengdu, China.

Swart, D. H. (1974). Offshore sediment transport and equilibrium beach profiles. Laboratory Publications no. 131 Delft hydraulics. The Netherlands, 302p.

Swart, D. H. (1976). Coastal sediment transport: computation of longshore transport. Report R0968. Pt. 1. Delft Hydraul. Lab.

Swart, D. H. (1977). Predictive equations regarding coastal transports. In Coastal Engineering 1976 (pp. 1113-1132).

Thornton, E. B. (1973). Distribution of sediment transport across the surf zone. In Coastal Engineering 1972 (pp. 1049-1068).

Tolman, H. L., (1997). User manual and system documentation of WAVEWATCH-III version 1.15. NOAA / NWS / NCEP / OMB Technical Note 151, 97 pp. (0.74MB PDF file).

Tolman, H. L., (2009). User manual and system documentation of WAVEWATCH III version 3.14. NOAA / NWS / NCEP / MMAB Technical Note 276, 194 pp.+ Appendices (0.83Mb pdf file).

Tomasicchio G. R., Lamberti A., Guiducci F. (1994). Stone movement on a reshaped profile. Proceedings of the 24th International Conference on Coastal Engineering, ASCE, Kobe, 1625-1640.

Tomasicchio, G. R., Archetti, R., D'Alessandro, F., Sloth, P. (2007). Long-shore transport at berm breakwaters and gravel beaches. Proceedings of the International Conference Coastal Structures '07, Venice, World Scientific, Singapore, pp. 65–76.

Tomasicchio, G. R., D'Alessandro, F., Barbaro, G., Malara, G. (2013). General longshore transport model. Coastal Engineering, 71, 28-36.

Tomasicchio, G. R., D'Alessandro, F., Barbaro, G., Ciardulli, F., Francone, A., Mahmoudi Kurdistani, S. (2016). General model for estimation of longshore transport at shingle/mixed beaches. Proceedings 35th International Conference on Coastal Engineering, Instanbul.

Tomasicchio, G. R., D'Alessandro, F., Barbaro, G., Malara, G. (2013). General longshore transport model. Coast. Eng., 71, 28-36.

Tomasicchio, G. R., D'Alessandro, F., Barbaro, G., Musci, E., De Giosa, T. M. (2015). Longshore transport at shingle beaches: an independent verification of the general model. Coast. Eng., 104, 69-75.

Tomasicchio, G. R., Francone, A., D'Alessandro, F., Barbaro, G., Frega, F. (2018). Morphodynamic model to simulate shoreline evolution at any coastal mound. Proceedings 36th International Conference on Coastal Engineering, Baltimore.

Tomasicchio, G. R., Lamberti, A., Guiducci, F. (1994). Stone movement on a reshaped profile. Proceedings of the 24th International Conference on Coastal Engineering, 2, 1625–1640.

Toure, S., Diop, O., Kpalma, K., Maiga, A. S. (2019). Shoreline Detection using Optical Remote Sensing: A Review. ISPRS International Journal of Geo-Information, 8(2), 75.

Townsend, K. E., Thomas, R. C., Frey, A. E. (2014). Shoreline Change Modeling Using One-Line Models: Application and Comparison of GenCade, Unibest, and Litpack (No. ERDC/CHL CHETN-IV-102). Army corps of engineers vicksburg ms engineer research and development center.

Trinder, J., Liu, Q. (2018). Sub-Pixel Technique for Time Series Analysis of Shoreline Changes Based on Multispectral Satellite Imagery. In Advanced Remote Sensing Technology for Coastal Environment, Disasters, and Infrastructure. IntechOpen.

USACE (1984). Shore protection manual, SPM, U.S. Army Coastal Engineering Research Center, Department of the Army, US Corps of Engineers, DC, USA.

USACE (1992). Coastal Engineering Manual, CEM. Coastal Groins and Nearshore Breakwaters.

USACE (2003a). Coastal Engineering Manual, CEM. Chapter III-1-2, Classification of Sediment by Size. Engineer Manual 1110-2-1100, U.S. Army Corps of Engineers, Washington, DC.

USACE (2003b). Coastal Engineering Manual, CEM. Chapter III-2-2, Longshore sediment transport processes. Engineer Manual 1110-2-1100, U.S. Army Corps of Engineers, Washington, DC.

Valentin, H. (1952). Die Küsten der Erde.Petermanns Geogr. Mitteilungen. Ergänzungsband 246, 118 pp.

Van der Meer, J. W. (1990). Static and dynamic stability of loose material. Coastal Protection, Balkema, pp. 157–195.

Van der Meer, J. W., Pilarczyk, K. W. (1987). Dynamic stability of rock slopes and gravel beaches. In Coastal Engineering 1986 (pp. 1713-1726).

Van der Meer, J. W., Veldman, J. J. (1992). Singular points at berm breakwaters: scale effect, rear, round head and longshore transport. Coastal Engineering 17 (3–4), 153–171.

Van der Meer, J.W., (1988). Rock Slopes and Gravel Beaches under Wave Attack. Delft University of Technology, Delft, The Netherlands, Ph.D. Thesis.Van Hijum, E. (1976). Equilibrium profiles and longshore transport of coarse material under oblique wave attack. Delft Hydraulics Laboratory, Netherlands. Publication no 174.

Van Hijum, E. (1976). Equilibrium profiles and longshore transport of coarse material under oblique wave attack. In Coastal Engineering 1976 (pp. 1258-1276).

Van Hijum, E., Pilarczyk, K. W., (1982). Equilibrium profile and longshore transport of coarse material under regular and irregular wave attack. Delft Hydraulics Laboratory, Netherlands. Publication no 274.

Van Overeem, J. (1978). Numeriek model voor de berekening van kustlijnveranderinen tgv golven en getij.

Van Rijn L. C. (1993). Principles of sediment transport in rivers, estuaries andcoastal seas, Aqua Publ., Amsterdam, 614 pp.

Van Rijn, L. C. (1993). Principles of sediment transport in rivers, estuaries and coastal seas (Vol. 1006). Amsterdam: Aqua publications.

Van Rijn, L. C. (2002). Longshore sand transport. Proceedings of the 28th International Conference on Coastal Engineering, pp. 2439–2451. Cardiff.

Van Rijn, L. C. (2005-2017). Principles of sedimentation and erosion engineering in rivers, estuaries and coastal seas. www.leovanrijn-sediment.com

Van Rijn, L. C. (2007). Unified View of Sediment Transport by Currents and Waves. I: Initiation of Motion, Bed Roughness, and Bed-Load Transport. Journal of Hydraulic Engineering, (June), pp. 649–667.

Van Rijn, L. C. (2014). A simple general expression for longshore transport of sand, gravel and shingle. Coastal Engineering, 90, 23-39.

Van Rijn, L. C. (2014). A simple general expression for longshore transport of sand, gravel and shingle. Coastal

Van Rijn, L. C. (2018). Detached breakwaters. Taken from: www.leovanrijn-sediment.com.

Van Rijn, L. C. V., Ribberink, J. S., Werf, J. V. D., Walstra, D. J. (2013). Coastal sediment dynamics: recent advances and future research needs. Journal of hydraulic research, 51(5), 475-493.

Van Rijn, L. C., Walstra D. J. R. (2003). Modelling of sand transport in delft3d, Tech. Rep. Z3624, WL Delft Hydraulics.

Van Rijn, L. C., Walstra, D. J. R., Grasmeijer, B., Sutherland, J., Pan, S., Sierra, J. P. (2003). The predictability of cross-shore bed evolution of sandy beaches at the time scale of storms and seasons using process-based Profile models. Coastal Engineering 47: 295 – 327.

Van Rijn, L. C., Wijnberg, K. M. (1996). One-dimensional modelling of individual waves and wave-induced longshore currents in the surf zone. Coastal Engineering, 28(1-4), 121-145.

Van Rijn, L.C. (1998). Principles of Coastal Morphology. Aqua Publications, The Netherlands (www.aquapublications.nl)

Van Wellen, E., Chadwick, A. J., Mason, T. (2000). A review and assessment of longshore sediment transport equations for coarse-grained beaches. Coastal Engineering 40 (3), 243–275.

Vellinga, P. (1982). Beach and dune erosion during storm surges. Coastal Engineering, 6: 361-387.

Villaret, C. (2010). Sisyphe user manual, EDF R&D Report NH-P73-2010-01219.

Villaret, C., Hervouet, J. M., Kopmann, R., Merkel, U., Davies, A. G. (2013). Morphodynamic modeling using the Telemac finite-element system. Computers & Geosciences, 53, 105-113.

Vos K., Harley M. D., Splinter K. D., Simmons J. A., Turner I. L. (2019b). Sub-annual to multi-decadal shoreline variability from publicly available satellite imagery. Coastal Engineering. 150, 160–174.

Vos, K., Splinter, K. D., Harley, M. D., Simmons, J. A., Turner, I. L. (2019a). CoastSat: A Google Earth Engine-enabled Python toolkit to extract shorelines from publicly available satellite imagery. Environmental Modelling & Software, 104528.

Vrijling, J. K., Smith, E. S. P., De Swart, P. F. (1991). Berm breakwaters design – the longshore transport case: a probabilistic approach. Coastal Structures and Break- waters, London.

Wai, O., Chen Y., Li Y. (2004). A 3-D wave-current driven coastal sediment transport model, Coastal Engineering Journal, 46(4), 385–424.

Walton Jr, T. L., Bruno, R. O. (1989). Longshore transport at a detached breakwater, phase II. Journal of coastal Research, 679-691.

Wang, P., and Kraus, N. C. (1999). Longshore sediment transport rate measured by short-term impoundment, Journal of Waterway, Port, Coastal and Ocean Engineering 125 (3), 118-126.

Wang, P., Kraus, N. C., (1999). Longshore sediment transport rate measured by short-term impoundment, *J. Waterway, Port, Coastal, Ocean Eng. 125*, No. 3, 118-126.

Wang, P., Kraus, N.C., Davis, R. A., (1998). Total rate of longshore sediment transport in the surf zone: field measurements and empirical predictions. Journal of Coastal Research, 14(1), 269-283.

Warner, J. C., Sherwood C. R., Signell R. P., Harris C. K., Arango H. G. (2008). Development of a three-dimensional, regional, coupled, wave, current and sediment transport model, Computers and Geosciences.

Warner, J., Sherwood C., Arango H., Signell R. (2005). Performance of four turbulence closure models implemented using a generic length scale method, Ocean Modelling, 8(1-2), 81–113.

Watanabe, A. (1982). Numerical model of nearshore currents and beach deformation model. Coastal Eng. Jpn., JSCE 25, 147–161.

Watanabe, A. (1985). Three-dimensional predictive model of beach evolution around a structure. Proc. Intl. Symp. Water Wave Res., University of Hannover, Germany, 121–142.

Watanabe, A., Riho, Y., Horikawa, K. (1980). Beach profiles and on-offshore sediment transport. In Coastal Engineering 1980 (pp. 1106-1121).

Watts, G. M. (1953). A study of sand movement at South Lake Worth Inlet, Florida. US Army Corps of Engineers, Beach Erosion Board Technical Memo 42.

Wentworth, C. K. (1922). A scale of grade and class terms for clastic sediments. The journal of geology, 30(5), 377-392.

Willis, D. H. (1977). Evaluation of alongshore transport models. In Coastal Sediments (pp. 350-365). ASCE.

WL | Delft Hydraulics (1999). Unibest - TC; A generic tool to investigate the morphodynamic behaviour of cross-shore profiles, User manual V2.02. WL | Delft Hydraulics report 8.6520.00.

Wu, W., Rodi W., Wenka T. (2000). 3D Numerical Modeling of Flow and Sediment Transport in Open Channels, J. Hydraul. Eng., 126(1), 4–15.

Zenkovich, V. P. (1967). Processes of coastal development. Editor: J.A. Steers. Edinburgh: Oliver and Boyd, 738p.

Zheng, J., Dean, R. G. (1997). Numerical models and intercomparisons of beach profile evolution. Coastal Engineering, 30(3-4), 169-201.

Zyserman, J. A., Ronberg J. K. (2001). Model intercomparison - morwin project: 2d morphological modelling and 3d modelling of flow in the area of bock inlet, Tech. Rep. 50848-01, DHI